Office of Naval Research

Contract Nonr-1866 (32) NR 371-016

ELECTROMAGNETIC FIELD PROBES

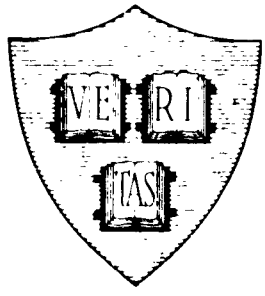

By

Haven Whiteside

October 25, 1962

Technical Report No. 377

Cruft Laboratory
Harvard University
Cambridge, Massachusetts

Office of Naval Research

Contract Nonr-1866(32)

NR - 371 - 016

Technical Report

on

ELECTROMAGNETIC FIELD PROBES

by

Haven Whiteside

October 25, 1962

The research reported in this document was made possible through support extended Cruft Laboratory, Harvard University, jointly by the Navy Department (Office of Naval Research), the Signal Corps of the U. S. Army, and the U. S. Air Force, under ONR Contract Nonr-1866 (32). Reproduction in whole or in part is permitted for any purpose of the United States Government.

Technical Report No. 377

Cruft Laboratory

Harvard University

Cambridge, Massachusetts

TR377 ERRATA

"Electromagnetic Field Probes. "
by Haven Whiteside

October 25, 1962
Contract Nonr-1866(32)/NR-371-016

- - - - - - -

Page or Fig.

I-17 line 16 for $\pm$ arctan read $\pm$ arc sin

I-19 line 26 for $\pm$ 0.3 cm read $\pm$ 0.03 cm

I-22 line 19 for $I_S \doteq I_E$ read $I_S \doteq I_{FL}$

II-5 line 11 numerical interpretation

III-1 Eq. III-5 should read $Y_n = \frac{1}{j\pi\zeta_0} \left(\frac{2}{2n}\right)$

III-2 line 10 should read (Fig. III-1b)

III-21 next to last line should read 0.1 db and 1 degree

V-4 third from last line should read closely-spaced dipoles

Fig. VI-1 (a) Read $I_L \propto E_\theta$ instead of E_ϕ

Fig. VI-1 (b) Read $I_L \propto B_\theta$ instead of B_ϕ

VII-18 line 16 should read:the probe of Fig. VII-7b (see Fig. III-9) .

Preface

The author wishes to express his thanks to the many individuals without whose assistance this work would not have been accomplished.

To Mr. Neil Whitman, Mr. Charles Sampson, Mr. James Meehan, Mr. Olaf Gustavson, Mr. John Doyle, and Mr. Joseph Lanza for the construction of much of the experimental apparatus.

To Mrs. Susheela Seshadri, Miss Jennifer Smith, Miss Josephine Hanlon, and Mrs. Richard Mack for many of the computations.

To Mr. Paul Donaldson and his assistants for the photographic work, to Miss Margo Burrell for drafting the figures, to Mrs. Paul Campanis for the typing, and to Miss Josephine Hanlon for proofreading the entire manuscript.

To the Office of Naval Research for extending financial support under contract number Nonr-1866(32).

To Mrs. Frederick Tingley, Dr. Keigo Iizuka, Dr. Edward E. Altshuler, Mrs. William B. Cormack, and Mr. Henry LeGault for valuable general assistance.

To Professor Tai T. Wu, Mr. Richard Mack, and Dr. William Pickard for stimulating technical discussions.

To his wife, Rose, for her understanding and encouragement, as well as for her assistance in a variety of tasks; to his son, Matthew, for adding joy to the most tedious days; and to the Cambridge prayer group for their faithful prayer support.

To Professor H. J. Schmitt and Dr. S. R. Seshadri for their advice at many points and their review of the manuscript.

And finally, to Professor Ronold W. P. King, who has been a willing and helpful advisor at every step of the way.

Table of Contents

List of Figures*

- - - - - - -

*The figures for each chapter immediately follow the text for that chapter.

List of Tables*

- - - - - - -

*The tables for each chapter follow the figures for that chapter.

Synopsis

The purpose of this investigation is to study the behavior of various probes used in the measurement of time-varying electromagnetic fields on a macroscopic scale. Both theoretical and experimental treatments of the subject are included.

The ideal probes for this purpose would be an infinitesimal electric dipole and an infinitesimal magnetic dipole. The former can be physically approximated very well by a finite electric dipole, that is, a linear receiving antenna. The latter, on the other hand, should be approximated by a finite magnetic dipole, and this is only approximately formed by a receiving loop antenna. The deviation is caused by the presence of modes of oscillation other than the circulating loop-current mode for a loop of finite size.

In both cases, a field-averaging effect is present which depends on the size of the loop relative to the shortest wavelength required in the representation of the incident field by a Fourier integral of plane waves.

In both cases, a transmission line is customarily used to take the probe current to a distant receiver for measurement. Since the line usually lies in the incident field, currents will be excited on its outer surface, and these may be coupled electromagnetically to the probe currents, thereby causing an error.

In both cases, a probe-loading effect may be present if the probe is too large or too close to the source, so that the presence of the probe significantly alters the current distribution on the source itself.

Each of these effects is studied here to some degree, but the major emphasis is placed upon the study of the effect of higher-order modes in a loop probe. The other effects are, at least qualitatively, generally known and understood, but the errors peculiar to the loop have usually been ignored.

In a receiving loop of fairly small size (less than one wavelength in circumference), there is a constant circulating current proportional to the average magnetic field normal to the plane of the loop. The magnetic sensitivity can be defined as the ratio of this current to the magnetic field that produces it. There are also currents for which two halves of the loop oscillate separately and in phase, with maximum currents at the centers and zero current at the ends of the halves, much like the currents in a folded dipole antenna. These currents are proportional to the average electric field parallel to the two sides of the loop. The electric sensitivity can be defined as the ratio of this current to the electric field that produces it. Higher-order currents, with more zeros around the loop are also present, but they are small, and may be combined with the magnetic and electric dipole currents in the final evaluation of the magnetic and electric sensitivities. A probe-error ratio can then be defined as the ratio of the (undesired) electric sensitivity to the (desired) magnetic sensitivity.

The magnetic and electric sensitivities were measured for a variety of loops, with varying shape, size, and load configuration. These values were compared with the theoretically-predicted values in each case.

The principal contribution of this study is the evaluation of the probe errors to be expected for various loops. On the basis of this discussion, certain recommendations are made for the limitation of these errors in various measurement situations. In fact, one probe is developed which utilizes the electric mode currents to allow measurement of the electric field in one circuit, while these currents are canceled out in another circuit to obtain an output that is proportional purely to the desired magnetic field. A further improvement is presented which somewhat reduces the effect of transmission-line coupling.

Finally, these effects are illustrated in connection with particular measurements of radiation fields, near-zone fields, transmission-line fields, and linear-antenna currents. It is shown in each case what the deviations are in the measured results and how they may be reduced.

Abstract

It is well known that the behavior of probes in the electromagnetic field is limited by the averaging of the measured field over the finite size of the probe. This is the major restriction on the use of the receiving dipole as an electric probe.

The usual magnetic probe, a shielded loop, suffers in addition from a less well-known source of error. Such a loop, even for moderate size, will sustain currents that are proportional to the tangential electric field, not to the normal magnetic field as desired. These electric mode currents are studied in some detail, and methods of avoiding or reducing them are proposed and tested. In addition, the behavior of loop probes is studied in general, both theoretically and experimentally, varying all the relevant parameters such as loop size, shape, wire size, and load.

CHAPTER I. EXPERIMENTAL SETUP

Section A. Mechanical Equipment

1. Free-space room

In order to conduct field measurements indoors it was found necessary to construct a free-space room. The advantages of an indoor setup were two: experiments can be performed at any time of year without regard to the vagaries of New England weather, and it was possible to use existing space with a minimum of new construction. The disadvantages are obvious: the need for constant conditions despite the movements of other people and their equipment nearby, and the need to reduce even constant interactions between the field and the surroundings to a minimum in order to simulate the theoretically assumed conditions of free space.

The conventional image plane technique was used, whereby the associated equipment is placed behind a perfectly conducting ground screen and isolated from the field region. The field in front of the image plane is identical to that which would be present if the metal screen were removed, and the electrical images of all objects in the field region introduced. This restricts the problems that can be studied to those with suitable symmetry, but possible configurations are quite adequate for our purposes.

It was hoped that a suitable placement of a few absorbing sheets would provide the required isolation, at least within a small region, but this was far from the case. In fact, the sensitivity of the equipment was such that even the motion of people walking by in the hall outside produced noticeable fluctuations, so the construction of a complete free-space room was necessary. The free-space room ideally should have perfectly absorbing boundaries in order that no reflected waves be present; however, absorbing materials available for 50 cm

wavelength reflect about 2% of the incident power.* Since we could not have an ideal room, it was designed for minimum reflections in a limited region, the measurement region (Figs. I-1a, b). In the interest of economy the room was made as small as consistent with a small reflected field in this region.

The room is built against a vertical aluminum ground plane 12 feet wide by 10 feet high. An absorbing floor and ceiling are mounted against the floor and ceiling of the room, giving an interior height of about 8 feet. The floor was raised and lowered to determine the optimum position for reduction of standing waves, and it was found that simply laying it on the existing floor was adequate, if the section nearest the ground plane, and directly under the source, was raised and tilted downward at an angle of 20 degrees. This directed any reflected rays out beyond the measurement region. The floor was strong enough for walking, but a Styrofoam plank 1 foot thick was used to allow the operator to reach his equipment better, and paper was used to keep the walkway clean. Above the measurement region it was necessary to recess the ceiling to allow for the probe-positioning mechanism. Furthermore, lack of space prevented canting the ceiling near the ground plane, and a large beam necessitated a step in it. It is not known specifically how much reflection these factors introduced, but it seems likely that they are slightly larger than reflections from other sources.

The side walls are built near the ends of the ground plane, and again the sections nearest to the ground plane were canted outward at a 20 degree angle. One wall was placed in position first, and then the other tuned in and out to find the position for minimum standing waves in the measurement region for the

- - - - - - -

*This is a nominal figure deduced from the manufacturer's specifications and applies to all types of absorber used, for angles of incidence up to 60 degrees from normal. Tests conducted, although not precise, confirmed this.

chosen source position. Then the front wall (which is in the null direction from a broadside source) was placed parallel to the image plane about 7 feet out. By moving the wall in and out and observing the standing-wave ratio of the field at various points in the measurement region this distance was found to be adequate. The entrance is constructed in an open labyrinth style which is much more convenient to use than a closing door, and which was found to be equally good with respect to reflections in the region of interest.

The absorber used was mainly type BL-8 manufactured by the McMillan Industrial Corporation, although a few sheets of type FR-350* were obtained from Emerson and Cuming, Incorporated and a few sheets of B. F. Goodrich Spongex† were also used. Type BL-8 is shown in position in Fig. I-2. It is made by boring conical holes from the back in an 8-inch thick sheet of Styrofoam and then spraying them with a lossy compound of graphite. From the front surface, an incident wave "sees" the graphite loading increase smoothly from zero to a high value per unit area. The front surface is painted white for convenience in lighting.

In order to provide complete isolation from the outside a conducting screen was built of aluminum window screening outside the walls. The floor and ceiling were up against the reinforced concrete of the building and needed no additional screening. By locating the screening about one-quarter wavelength

- - - - - - -

*FR-350 is essentially the same as BL-8 except that it has an extra rubber backing sheet. The choice of type BL-8 over type FR-350 was governed only by price.

†Spongex is a spongy horsehair mat which is loaded with graphite in a manner that increases with depth. It is black in color and its open construction picks up dust, although it has the advantage of mechanical flexibility and was used where this was needed.

behind the back of the absorber it was found possible to enhance somewhat its operation. This is due to the standing-wave pattern produced, which places an electric field maximum in the region of greatest dissipation and thus gains the greatest possible absorption of power.

Dimensional drawings of the room are shown in Fig. I-1, and photographs in Figs. I-3, 4. Test results showed a standing-wave ratio of less than 1.13 in the region within 50 cm of the source and at least 10 degrees off the null axis. When referred to the field near the source in the direction of maximum field, the SWR drops to 1.06 or less. Therefore, the field approximated the free-space field within 7% over a region within a wavelength of the source and within 4% over a region within a radius of one-half wavelength.

2. Probe mount for image method

The probes themselves can conveniently be studied against the image plane, in which case there is no need for a transmission line in the incident field. This was the primary method of determining the probe parameters, although free-space measurements were used for comparison in certain cases.

To do this, half probes were mounted on a disc which could be rotated in place in the image plane (Figs. I-5, 6). Two coaxial lines were connected at the back of the disc, and the ends of the probe could be connected to the center conductors or short-circuited to ground at the image plane. A method of construction using eccentric placement of the lines in two rotatable internal discs allowed a single probe mount to be used for a variety of probe sizes.

3. Probe-positioning mechanism

The probe-positioning mechanism used for "free-space" measurements is illustrated in Figs. I-7, 8. It consists of a radial arm with one end mounted

with a ball bearing at the top of the image plane directly above the source antenna, and the other end free to swing horizontally through 90 degrees, riding on a wooden supporting arc. Along the arm travels a sliding carriage, from which is hung a rigid section of transmission line with the probe at the end. A universal joint connecting the line and carriage allows the probe position to be adjusted slightly without moving the carriage. By means of a system of strings and pulleys, the operator standing below can move the probe in azimuth and radius anywhere within a quadrant-shaped region.

The probe rotates freely through about 380 degrees about its vertical axis and stops are provided to prevent rotating further and twisting the cable. An angle scale is attached to the carriage to indicate the amount of rotation, and a magnifier and a vernier are provided to allow reading it from a distance of 5 feet. In addition, there is a probe-rotating gear drive in the carriage which may be attached to a flexible shaft and operated remotely from behind the image plane. The advantage of this for determining the rotation angle for maximum or minimum output is great, since it allows continuous reading of the output while the probe is being rotated. The angle can be read to $\pm$ 0.4 degree, but backlash and bending of the entire mechanism in use limit the angular accuracy to about 2 degrees in absolute value and about 1 degree in angular difference at a single probe position.

It was found absolutely essential to avoid resonant lengths of metal in this system. Many of the parts of the probe-positioning mechanism are made of wood to minimize the scattered field, but the radial arm itself is made of metal, since the metal transmission line lies along its length anyway. It is, however, made with an open and narrow construction to minimize the backscattering cross section. Various methods of reducing the backscattering from

the arm were tried, such as covering with Spongex absorber, applying a coating of resistive paint, and hanging quarter-wave wedges of resistive Nikon cloth from it, but none seemed to make much difference once all resonant pieces of metal had been detected and removed. An auxiliary probe was used to study the scattering effects, and it was concluded that at typical points in the region of measurement the scattered field was at least 30 db below the direct incident field for the system finally adopted. A dummy transmission line with detuning sleeves identical to those on the actual transmission line was in place during this test, showing that radiative scattering from the feed line was also negligible.

4. Coordinate table

For "free-space" measurement a means of measuring the probe location is required, so a set of coordinates* is plotted on the surface of a table lying a fraction of an inch below the probe (Fig. I-9). Because it was required that the table have a minimal electromagnetic effect it was made of Styrofoam HD-2, manufactured by Dow Chemical Company. This has a higher density than ordinary Styrofoam and a sheet 1 inch thick (.05λ) was rigid enough for the table top. It has a relative dielectric constant of 1.07, so its wave impedance and propagation constant differ by only 3.5% from those of free space. For such a thin sheet, this produces a phase error of less than 1 degree in the transmitted wave, and a field reflection coefficient of less than 2% (.04% of the power). The legs are of thin-walled polystyrene tubing and are well away from the source.

When the probes are rotated they should not change location, so pivot pins are used in holes tapped in the table top at convenient intervals (Fig. I-10).

- - - - - - -

*For the near-zone field of a dipole, confocal coordinates were used, but rectangular coordinates were also available.

These pins are also made of Styrofoam HD-2, and they are threaded by pressing in a die. They have a pointed top which engages a Styrofoam fitting at the center of the probe and holds it in position, and they can be withdrawn in order to move the probe to a new location.

Section B. Transmitting System

(Figures I-11, 12)

5. Transmitter

The transmitter is a military type T85/APT-5, which uses a 2C39 lighthouse triode oscillator in a mechanically tunable cavity. It was operated at a fixed frequency of 600 mc in the CW mode, and provided about 20 watts output into a 50 ohm load. Using the wavemeter, no measurable frequency drift was found after a warm up of four hours.

6. Choice of frequency

A frequency of about 600 mc (wavelength 50 cm) was chosen as a compromise between the requirement of a long wavelength to allow mechanical construction of electrically small probes and the need for a short wavelength so that the ground plane and the free-space room would be electrically large. At this wavelength it was possible to construct probes with reasonable accuracy down to a diameter of 0.01 λ, and the free-space room was 5 wavelengths wide by 4.5 wavelengths high.

7. Frequency measurement

The transmitter signal was sampled by a 30 db directional coupler and then fed to a cavity wavemeter, type AN/UPM-2. This has a diode detector and DC micrometer together with a reactive network and a micrometer-tuned cavity to measure wavelength. Although the cavity is only 4 inches long, it is still possible to detect wavelength changes of the order of .02 cm. The wavemeter was calibrated by comparison with wavelengths measured in a standard slotted line, Hewlett Packard type 805A, with a short-circuit termination, in which wavelength can be measured to $\pm$ .01 cm.

8. Filter

A coaxial low-pass filter manufactured by Cruft Laboratory was tested and found to cut off at 800 mc and have 20 db insertion loss at 900 mc and essentially zero insertion loss at 600 mc. This was used for the elimination of harmonics in the transmitted signal.

9. Transmitter power measurement

The transmitter signal was sampled by a 30 db directional coupler and then fed to a General Radio signal sampler, type 874-VQ, which is terminated in a matched load, and uses a crystal detector and a type 874-VI voltmeter indicator to sample the signal voltage. This indicator has only about 5% accuracy, but was convenient as a continuous relative signal-level monitor.

For a measurement of absolute transmitted power, a Hewlett Packard Model 430-B power bridge with a thermistor detector was used in place of the signal sampler, but the long-term instability of the bridge made it unsuitable for continuous monitoring purposes.

10. Source antenna

The source antenna was a quarter-wave unipole extending through the image plane, with a length, h, of 12.5 cm and a diameter, $2a$, of 0.159 cm (1/16 inch), which gives a value of the thickness parameter, $\Omega = 2\ln\frac{2h}{a}$, of 11.4. It is constructed by extending the center conductor of a type N coaxial connector through the image plane. The connector is mounted on the image plane using a flanged plate, and may be readily connected to a flexible cable (Fig. I-13). The field of such a source is discussed in detail in Appendix A.

Section C. Receiver System

(Figures I-14, 15, 16)

11. Receivers

There are two superheterodyne receivers, General Radio type DNT-3, one in the sum circuit, and one in the difference circuit. They are tunable from 250 to 920 mc and have a half-power bandwidth of 0.7 mc. The sensitivity is such that 25 microvolts behind a 50 ohm source produces 0 db meter indication. This is the lowest reading for which the system is linear, although readings may be obtained down to -10 db. The useful range is from 0 to 80 db.

This receiver has a 1N21B mixer crystal in a broadband coaxial holder, type 874-MR, with a local oscillator, type 1209-B, using a Sylvania type RT-434 disc-seal triode in a butterfly tuning circuit. The IF amplifier, type 1216-A, is a four-stage high-gain linear amplifier, operating at 30 mc, with a 70 db precision step attenuator at the input. The output meter is calibrated in linear units and in decibels, and can be read within 0.1 db.

The long-term drift of the entire system produces less than 0.5 db change in output indication over a 6 hour period after warm up. Normally, the drift is much less than this, of the order of 0.1 db, and fairly frequent calibration checks were made to ensure accuracy. The receiver linearity was adjusted and the scale calibrated from time to time by using a slotted line with a short-circuit termination, assuming that its probe current followed the theoretical cosine distribution. Since the residual standing-wave ratio of this line was 1.01, this was a reasonable assumption. With this calibration, the receiver system was accurate to $\pm$ 0.1 db, over any 30 db range, but there is 0.1 db switching error in the attenuator switch, so a stability figure of 0.1 db gives over-all receiver accuracy of $\pm$ 0.3 db.

12. Cables and accessories

For the most part, double-shielded, 50 ohm coaxial cable type RG-9/U was used, and where single shielded cable was used, an extra layer of braided shielding was pulled over it to minimize leakage. This was found to be absolutely essential in the sensitive receiver circuits, although not particularly important in the transmitter circuits with their higher signal levels. All cables were clamped in position to avoid flexing. Type N connectors were generally used because of their low leakage, low standing-wave ratio, and mechanical stability.

Various double-stub tuners and attenuator pads, such as those manufactured by Microlab Incorporated, were used. Directional couplers and hybrid junctions were standard wide-band types made by Norda Microwave Corporation.

Some of the components in the receiver circuit had General Radio connectors, which have notably high leakage even with their metal retainer rings, so it was found desirable to place all the receiver circuitry in a shielded metal box with feed-through connectors for signal, phase reference, and local oscillator inputs and for IF output.

13. Balun detector

The "balun detector" [1] is a device with a shielded-pair input, which couples the balanced mode to one output port and the unbalanced mode to the other output port. In our application, the input is adapted from two single coaxial lines, and the outputs are the sum and the difference of the two input currents.

The construction of the "balun detector" is shown in Fig. I-17. It is seen to be a shielded-pair transmission line with a short circuit across the end.

The two inner conductors are also short-circuited together by a conducting bridge located one-quarter wavelength from the end, where the unbalanced voltage has a maximum. The output terminal for the sum circuit is connected by a symmetrically placed post to the center of this bridge. A second bridge, with a gap in the center, is one-half wavelength from the end, where the balanced voltage has a maximum. This voltage appears across the gap and drives a miniature coaxial line connected to the gap and traveling within one inner conductor to the outside terminal for the difference output. The other inner conductor contains a short-circuiting piston which is also connected to the gap and which may be tuned to maximize the difference output.

For an idealized balun detector with matched terminations, we can write a simplified scattering-matrix equation:

$$\begin{pmatrix} I_\Sigma \\ I_\Delta \end{pmatrix} = \begin{pmatrix} S_{\Sigma 1} & S_{\Sigma 2} \\ S_{\Delta 1} & S_{\Delta 2} \end{pmatrix} \begin{pmatrix} I_1 \\ I_2 \end{pmatrix} \tag{I-1}$$

where I_Σ and I_Δ are the two output currents and I_1 and I_2 the two input currents. This idealization is simply a reduction of the general scattering matrix where all the other coefficients are assumed to vanish. This can be rewritten:

$$\begin{pmatrix} I_\Sigma \\ I_\Delta \end{pmatrix} = \frac{1}{2} \begin{pmatrix} S_{\Sigma U} & S_{\Sigma B} \\ S_{\Delta U} & S_{\Delta B} \end{pmatrix} \begin{pmatrix} I_1 + I_2 \\ I_1 - I_2 \end{pmatrix} \tag{I-2}$$

where

$$\begin{aligned} S_{\Sigma U} &= 1/2\,(S_{\Sigma 1} + S_{\Sigma 2}) \\ S_{\Delta U} &= 1/2\,(S_{\Delta 1} + S_{\Delta 2}) \\ S_{\Sigma B} &= 1/2\,(S_{\Sigma 1} - S_{\Sigma 2}) \\ S_{\Delta B} &= 1/2\,(S_{\Delta 1} - S_{\Delta 2})\,. \end{aligned} \tag{I-3}$$

For a perfect balun detector, $|S_{\Sigma U}| = |S_{\Delta B}| = 1$ and $S_{\Sigma B} = S_{\Delta U} = 0$, so that

one output equals half the sum and the other half the difference of the input currents.

It was only necessary to measure these coefficients approximately, since a later test of the over-all balance of the system was to be made. To do this the output currents were measured under four different driving conditions: $I_1 \approx I_2$ and $I_1 \approx -I_2$, interchanging the input leads in each case. This gave

$$|S_{\Sigma U}| = 0.97$$

$$|S_{\Delta U}| = 0.013$$

$$|S_{\Sigma B}| = 0.020$$

$$|S_{\Delta B}| = 0.92$$

which implies that the sum and the difference currents are separated to an accuracy of better than 30 db. For equal sum and difference signals this will give 3% accuracy in the output circuit.

14. Balance adjustment

The balun detector is connected by various transmission lines and other components to the probe under study, and the probe itself may not be mechanically exactly symmetrical. Therefore, a variable attenuator and phase shifter were placed in each of the coaxial input lines in order to make adjustments for accurate sum and difference output.

For a loop probe, the balance adjustment is made as follows.* The probe is placed in a position where it will only be excited symmetrically, which can be

- - - - - - -

*This discussion is written in general terms so as to apply to either the free-space or the image method. For the image method, all reference to the feed line should be omitted.

done mechanically by locating it symmetrically with respect to the source. Any reading in the difference output is then due to either coupling from the symmetric input or to a residual antisymmetric excitation, so we can write an expression for the difference output:

$$I_\Delta = c_1 I_A + c_2 I_S \tag{I-4}$$

where I_A is the antisymmetric probe excitation

I_S is the symmetric probe excitation

c_1 , c_2 are complex constants of the balun detector system.

But the symmetric excitation itself may come from two sources: the incident electric field in the plane of the loop, or electromagnetic coupling to the current on the outside of the feed line. Hence, it can be written:

$$I_S = I_E + I_{FL} \tag{I-5}$$

and

$$I_\Delta = c_1 I_A + c_2 I_E + c_2 I_{FL} . \tag{I-6}$$

By decoupling the feed line, I_{FL} can be made small compared to I_E.* Then the balance adjustments are made for minimum I_Δ . Next the probe is rotated 180 degrees and the balance adjusted until the difference output is constant under this rotation. The difference output in the 180 degree position is

$$I'_\Delta = c_1 I_A - c_2 I_E + c_2 I_{FL} . \tag{I-7}$$

Since the antisymmetric excitation depends on the normal component of B , it is invariant under this rotation, as is I_{FL} , which depends on coupling to a feed line which lies along the axis of rotation. On the other hand, I_E reverses sign under 180 degree rotation, since it depends on the electric vector in the plane of rotation.

- - - - - - -

*For the method of decoupling, see below under Transmission Line.

The condition $I_\Delta = I'_\Delta$ is the desired condition of balance since it requires

$$c_1 I_A + c_2 I_E + c_2 I_{FL} = c_1 I_A - c_2 I_E + c_2 I_{FL} \tag{1-8}$$

which can only be satisfied for finite I_E at $c_2 = 0$, and this does imply zero coupling of the symmetric excitation to the difference output.*

If interest is primarily in the sum output a similar method can be devised. It is to be noted that unless separate balun detectors are provided for the sum and difference circuits, only one of these can be optimized at a time, since no balun detector will be perfect. Nevertheless, one that is carefully made will perform fairly well in both modes at once.

It is important to know how accurate the balance adjustment is in a given field measurement, and this is readily determined. The error in the difference current due to asymmetry and imbalance combined is simply half the change in this difference current under a rotation of the probe of 180 degrees in its own plane. Typically, this error was found to be less than 2% in magnitude and 1 degree in phase. This is as good or better than the balun detector alone, and is quite satisfactory.

- - - - - - -

*Another method of balance adjustment that was sometimes used consisted of placing the probe in the same symmetrically excited position and then measuring individually the currents $I_{\Delta 1}$ and $I_{\Delta 2}$ in the difference output due to line 1 and line 2 from the probe. Then the probe is rotated 180 degrees and the new currents $I'_{\Delta 1}$ and $I'_{\Delta 2}$ are measured. Adjustment is made for the condition

$$\frac{I_{\Delta 2}}{I_{\Delta 1}} = \frac{I'_{\Delta 1}}{I'_{\Delta 2}}$$

which implies a correct balance adjustment if the (symmetrical) excitation of the probe by the feed line is negligible compared to its excitation by the symmetrical electric field. Although this is a reasonable assumption which can easily be checked, it is not needed for the preferred method described in the text.

15. Phase measuring system

The phase of the probe signal was measured in the conventional way, by cancellation against a reference signal of variable and measurable (relative) phase. The two signals are added in a hybrid junction and the reference phase adjusted for minimum output in each case. The reference signal is obtained by using a 10 db directional coupler coupled to the forward wave at the transmitter output. It is brought to the receiver by a cable of electrical length approximating that in the signal circuit to minimize errors due to frequency drift.

Since the sharpness of the null thus obtained depends on the relative magnitudes of signal and reference, it is necessary to provide amplitude adjustment in the reference circuit. This was done in two different ways. A variable turret attenuator with 10 db steps was placed in the reference circuit, so that the reference amplitude could always be set within 5 db of the signal amplitude. The phase difference due to a change in the attenuator was measured for each value of attenuation and used as a correction. Because of the variations in phase shift due to switching the attenuator, these corrections vary over a range $\pm$ 2.5 degrees from the mean value. The second method was to use a continuously variable waveguide-beyond-cutoff attenuator, which allows setting the reference level for an exact null whenever desired. Theoretically, for a single cutoff mode, such an attenuator has a constant phase shift (the propagation constant in the cutoff guide is purely imaginary). In practice, the presence of other modes and of mechanical imperfections causes some deviation from this ideal. By comparison with the current in a short-circuited coaxial line, which has varying amplitude and constant phase over each half wave section, it was found that for the General Radio type 874-GA

attenuator used, the phase error is less than 1 degree for any 20 db range of attenuation beyond 2 db on the scale. Because of the sharper nulls available, this method has less error due to residual SWR in the phase line than does the method with the step attenuator. Unfortunately, this was not discovered until after many of the measurements had been taken, so the poorer figure must be assumed throughout Chapters II, III, and IV.

The phase of the reference signal is varied by using two constant-impedance trombone-type line stretchers, General Radio type 874-LT, mounted with a rack and pinion for precise adjustment and a vernier scale for measurement. These are very well made and show a variation in transmitted signal of $\pm$ 0.5%, which implies a phase error less than $\pm$ 0.3 degree. The vernier scale can be read to $\pm$ .01 cm, implying a reading uncertainty of $\pm$ 0.15 degree ($\pm$ 0.3 degree for two trombone lines in series). The over-all accuracy of the phase shifter is $\pm$ 0.6 degree, which is much better than that of the available phase lines using a matched termination and a traveling probe, which have a residual SWR of 1.05 and thus a phase error of $\pm \arctan \frac{SWR - 1}{2} = \pm 1.5$ degrees [2].

As the sharpness of the null increases, the slope of the output current becomes steeper and the effect of the reading uncertainty of the output meter has less and less effect on the accuracy of adjusting the phase shifter. The null was normally located by taking two points with equal amplitude on either side of it and averaging their positions. It can be shown that points about 3 db above the minimum give the greatest accuracy for standing-wave ratios greater than 10 db so these were normally used except for very sharp nulls where any convenient level was used, and for shallow nulls when the 3 db points became too far apart.*

As a result of these considerations, accuracy of phase measurement was $\pm$ 3 degrees in Chapters II, III, and IV, and $\pm$ 1.5 degrees later.

- - - - - - -

*Ginzton [3] gives a graph of equal response points for minimum error in location of voltage minimum as a function of the voltage standing-wave ratio.

Section D. Probe System

16. Probes

Half-probes for use against the image plane were made of solid copper rod and required no feed line since the load was effectively located at the image plane itself. Pointed tips were soldered to their ends for insertion in the ends of the coaxial lines in the probe mount. The wire sizes chosen were the same as the diameter of 1/2 watt resistors, the tubing used for free-space probes, and the center conductor of Microdot cable. For the study of variable load resistance, ordinary 1/2 watt fixed composition resistors were inserted in these tips (Fig. I-6). The reflection and transmission coefficients of the resistors were measured, using a Deschamps method, and the measured load impedance was used in calculations. It may be seen from Fig. III-7 that for increasing resistance the measured impedances show increasing departure from the nominal DC values, and that this departure may be as great as 40%.

The free-space probes are made of coaxial tubing with teflon dielectric and a silver-plated, solid copper center conductor. The specifications are:

Type 1 — O.D. = .078 in. Z_o = 56.2 ohm λ_g/λ_o = .741
center conductor 29 gauge
outer conductor .078 in. O.D., .018 in. wall
center conductor and dielectric from Microdot cable No. 50-3902

Type 2 — O.D. = .032 in. Z_o = 50 ohm λ_g/λ_o = .696
center conductor 34 gauge
outer conductor .032 in. O.D., .004 wall
manufactured to order by Wirecraft Products Incorporated West Brookfield, Massachusetts, and Precision Tube Company, North Wales, Pennsylvania.

They are bent and soldered in aluminum jigs and can be built accurately within $\pm$ 0.3 cm in sizes down to 0.5 cm diameter. Circular loops are readily made, but square loops have somewhat rounded corners since they were made by bending. All free-space probes have a short perpendicular section of feed line for

attachment to the main feed line. They are also mounted on a thin wafer of Styrofoam with a hole in the center to engage the pivot pins. Their "load" is simply a gap or gaps in the outer conductor, and the load impedance is the impedance looking into the internal coaxial line at the gap.* The feed line is connected at various points on the loop, but the effect of this is negligible on the antisymmetric current. The effect on the symmetric current is discussed under the measurements themselves. Various sets of probes are illustrated in Figs. I-18 - 24.

17. Probe connector

The probes are connected to the transmission line by a specially designed connector (Fig. I-25), which allows easy interchange of probes. A jig is provided to hold the parts in alignment while the center conductors are soldered together. The jig is then removed and the connector, which is split in half, is placed over the joint and clamped in place by a tapered retaining sleeve. To match the transmission line, the impedance of the connector is 56.2 ohms, except in the central section where it lies between 63 and 69 ohms for a distance of $.016\lambda_g$ (less than 6 electrical degrees). Such a small change in characteristic impedance over such a short length produces no significant transformation of the load impedance through the connector except for a rotation of $.016\lambda_g$ on the Smith chart. The load impedance presented to the probes was measured at the input plane of the connector and transformed mathematically along the internal line to the probe gap, so that the effect of the probe connector was taken into account.

- - - - - - -

*This is discussed further in Section V-1.

18. Transmission line (Fig. I-26)

The transmission line from the probe serves two purposes: to conduct the current back to the receiver, and to connect the probe mechanically to the positioning mechanism. It is erected perpendicular to the plane of the probe to minimize coupling between them. Electrically it consists simply of two 56.2 ohm miniature coaxial lines with a solid outer conductor for the first few feet and double shielding the rest of their length. These are contained in a steel tube that runs from the probe to the positioning carriage and provides the desired mechanical support. They then continue as flexible cable along the positioning arm to the back of the image plane where they are connected to the receiver.

Since much of the line lies in the primary field, there are currents on its surface which may be large. These currents produce a scattered field which must be made small in the region of the probe. This may be discussed in three parts. First, the radiation from the horizontal portion was negligible, since (for a non-resonant line) its field equals approximately the incident field at the line times a/r (about .02) where a is the average radius of the conductor and r is the distance to the probe. Secondly, the radiation from the vertical portion of the line was neglected since it has an electric field parallel to the vertical axis and therefore normal to the plane of the probe, and can excite no currents in the probe itself.* Thirdly, the conductive and capacitive coupling from the near portion of the line to the probe may be quite large.

- - - - - - -

*These effects were experimentally checked and found negligible in connection with the probe-positioning mechanism.

Currents on the surface of the transmission line can be minimized by placing tuners at intervals along it in order to prevent resonant currents from building up to large values [4]. The tuners are coaxial sleeves filled with polystyrene with one end closed and the other open (Fig. I-27). They slide on the outside of the transmission line, and may be tuned in both length and position. There are twelve tuners in all, and it was impossible to find a method of tuning them individually, so all except the bottom one were placed with open ends at intervals somewhat less than a quarter wavelength (actually .196λ) along the line and set for an internal length of .25λ_g so that they present a high reactance (ideally an open circuit) at the open end. The general effect of these is to make the outside of the line look broken up into a series of short (non-resonant) lengths of conductor connected at the ends by very large impedances so that each short section is excited somewhat independently of the others.

The bottom tuner, nearest the probe, can be adjusted more precisely, so it is made with a threaded construction (Fig. I-28). The adjustment is made experimentally by considering the output of the sum circuit from the probe. It is known that $I_S = I_E + I_{FL}$ (Eq. I-5), and that for a reasonably good balance adjustment* $I_\Sigma \propto I_S$. Therefore, the probe is placed in a position where the parallel electric field is very small†, so that $I_S \doteq I_E$, and the feed line is detuned for minimum I_Σ, which then implies that the probe current I_{FL} due to feed line coupling is a minimum. Equation I-5 also shows

- - - - - - -

* This adjustment is made before the final balance adjustment.

†Such a region is on the axis of a quarter-wave unipole with the load sides of the probe perpendicular to the axis and parallel to the tangential electric field which theoretically vanishes there. The normal magnetic field is also ideally zero there, so there is negligible coupling from the antisymmetric mode, as it is only residually excited.

that any error in a particular measurement due to this source may be detected by a change in the sum current other than a change in sign when the probe is rotated 180 degrees.

In practice, I_{FL} was compared to the excitation I_E due to the radial electric field on the axis of the unipole source, and found to be 10 to 30 db below it. Small probes were considerably poorer in this respect than larger ones, mainly because their response to the E field decreases rapidly with size while I_{FL} decreases relatively slowly with size. This produced errors in the sum current I_Σ ranging from 1% to 18% in a typical field region, and even greater errors in regions of small E field. However, the balance adjustment was good enough to prevent feed line coupling from producing a measurable error in the difference current I_Δ, which was the output of primary interest.

Bibliography, Chapter I

1. Matthews, Edgar W., Jr., "A UHF Impedance Bridge for Shielded Two Wire Lines," Cruft Laboratory Technical Report No. 184, Harvard University, pp. 2-11 (March 1954).

2. King, Donald D., Measurements at Centimeter Wavelengths, p. 234, D. Van Nostrand, New York (1952).

3. Ginston, Edward L., Microwave Measurements, p. 270, McGraw-Hill, New York (1957).

4. Hatch, R. M., Jr., "Current Distributions on Conducting Sheets Excited by Arrays of Slot Antennas," Cruft Laboratory Technical Report No. 103, Harvard University, pp. 8, 9 (July 1950).

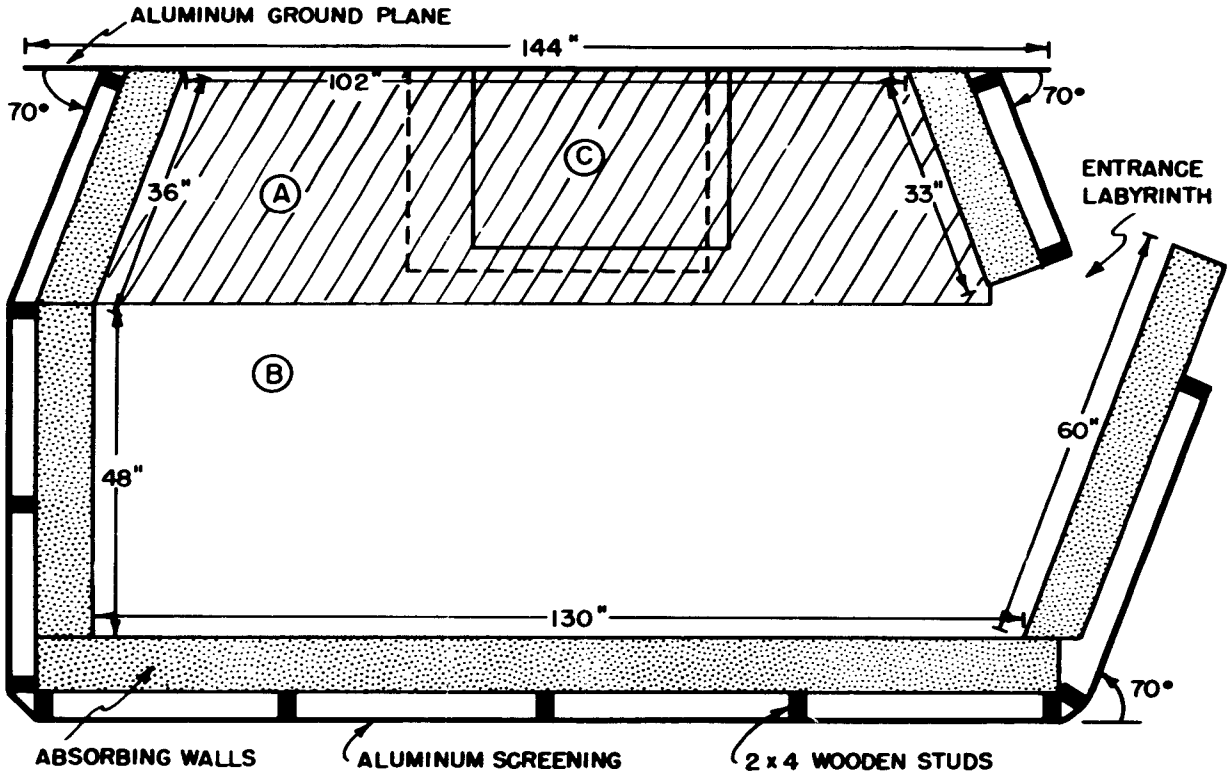

---- MEASUREMENT REGION

(A) ABSORBING FLOOR IN THIS REGION RISES AT AN ANGLE OF 20° ABOVE THE HORIZONTAL TOWARD THE GROUND PLANE.

(B) ABSORBING FLOOR LIES FLAT ON CONCRETE FLOOR.

(C) CEILING RECESSED ABOVE THIS REGION.

I-1a FLOOR PLAN, FREE SPACE ROOM

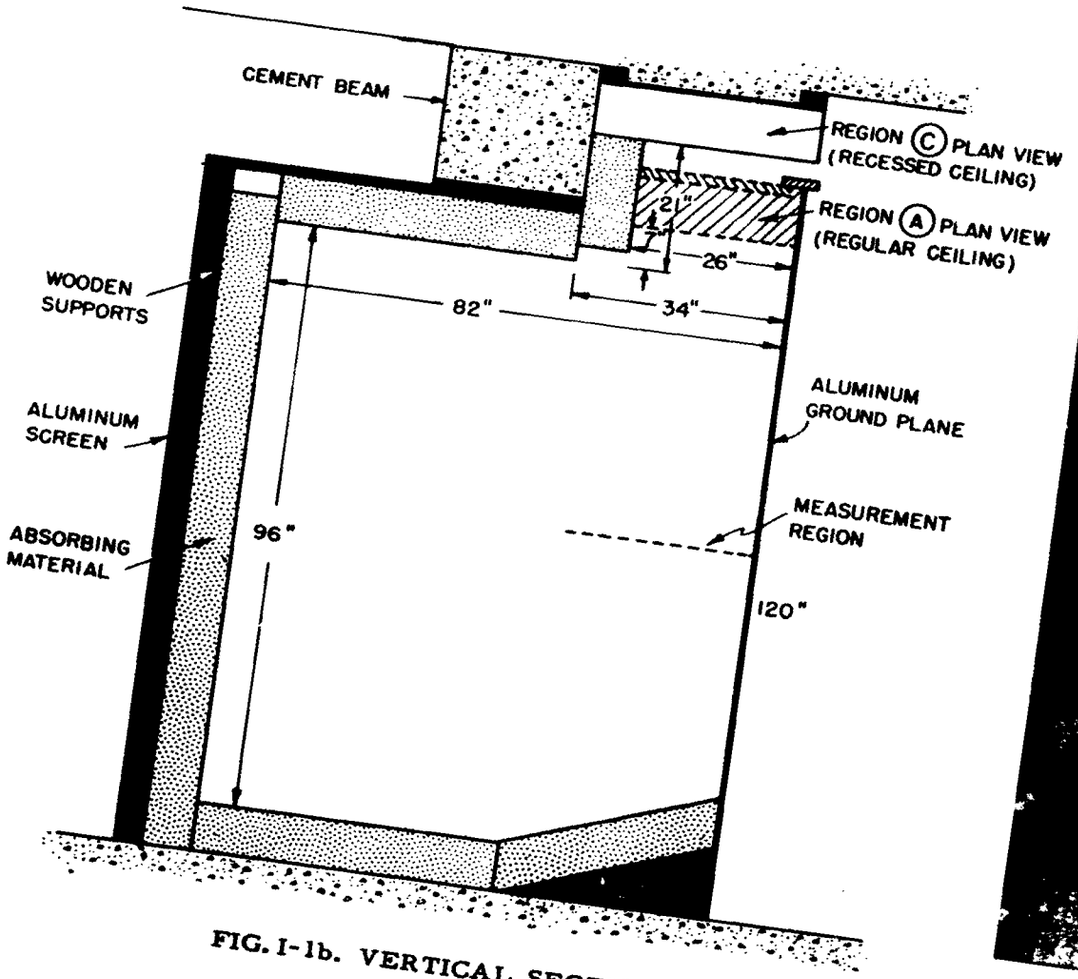

FIG. I-1b. VERTICAL SECTION
FREE SPACE ROOM

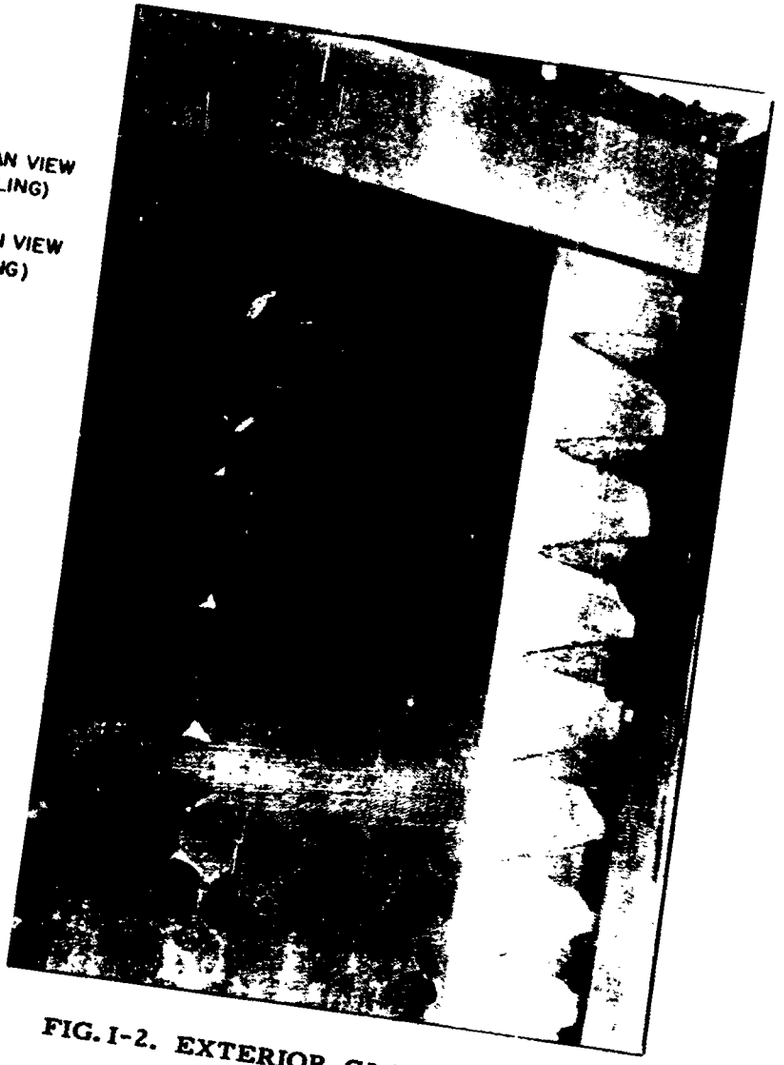

FIG. I-2. EXTERIOR CLOSEUP
FREE SPACE ROOM
SCREENING PARTIALLY REMOVED

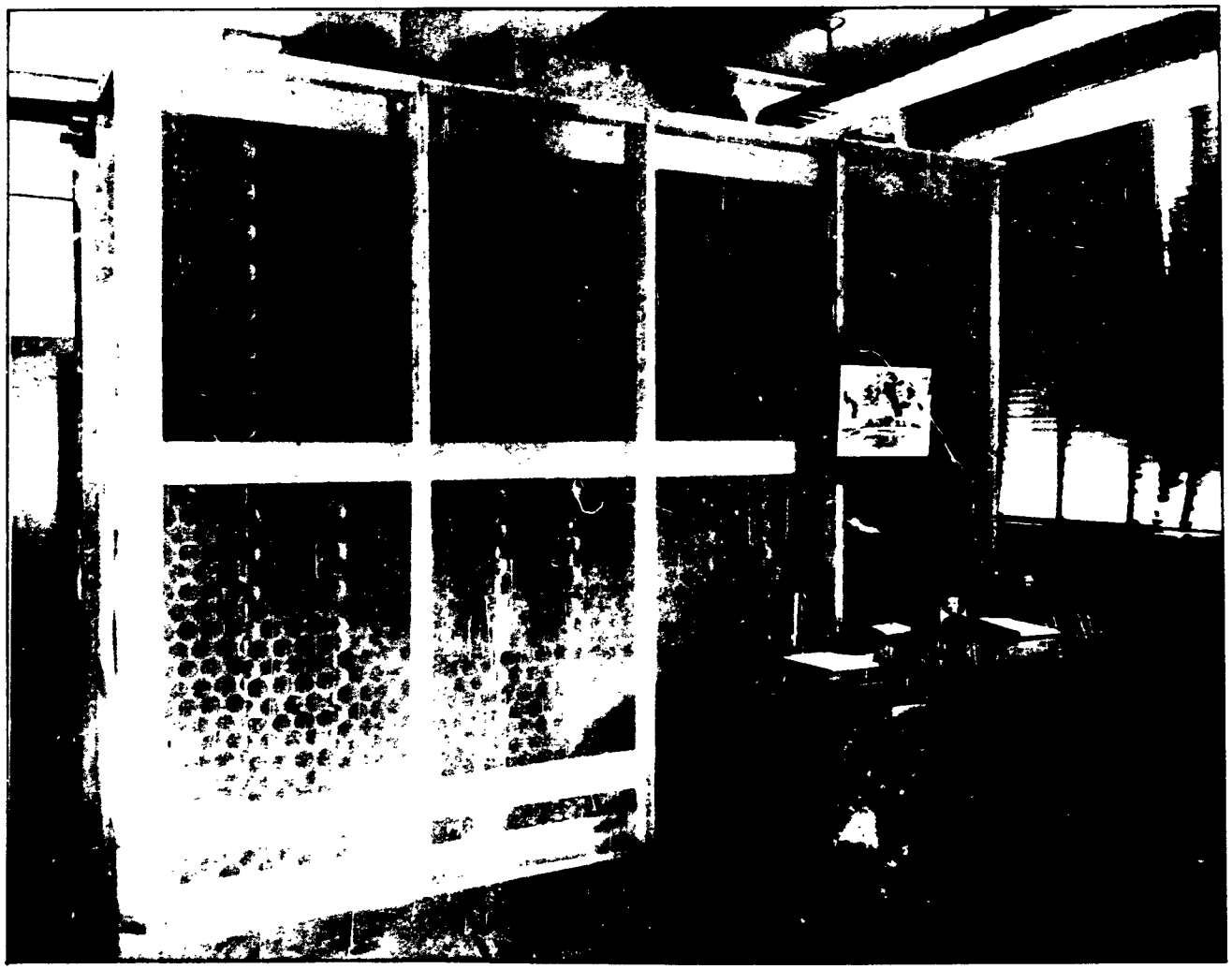

FIG. I-3. EXTERIOR, FREE SPACE ROOM

FIG. I-4a. INTERIOR
FREE SPACE ROOM

FIG. I-4b. FREE SPACE ROOM
IN OPERATION

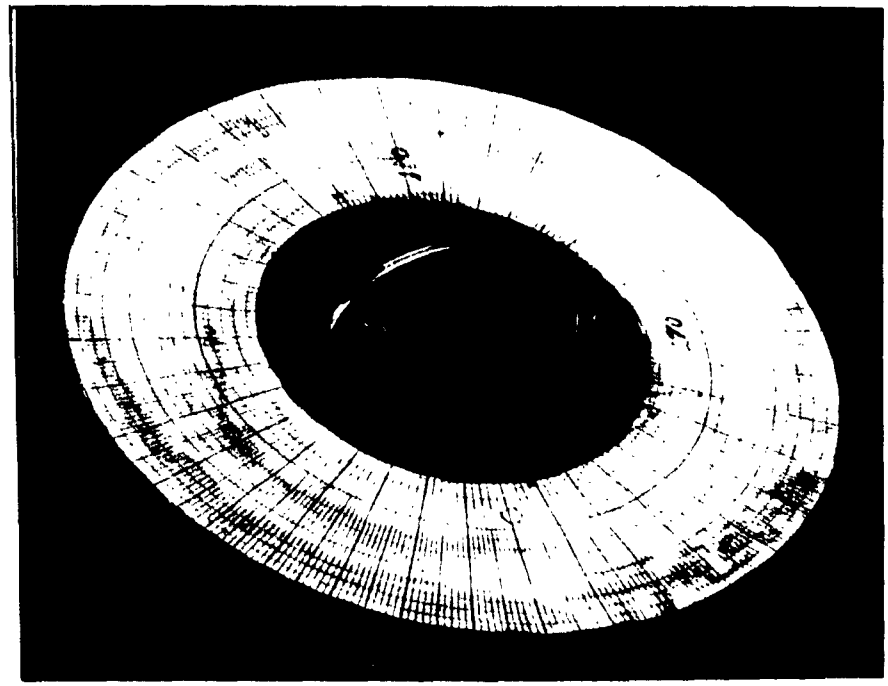

FIG. I-5. HALF PROBE IN POSITION AGAINST IMAGE PLANE

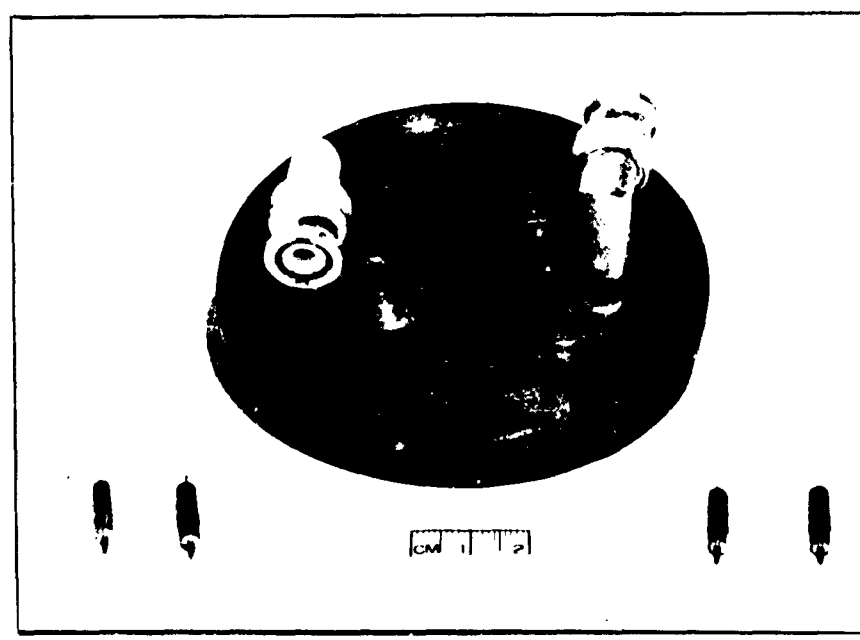

FIG. I-6. MOUNTING DISC AND RESISTOR INSERTS

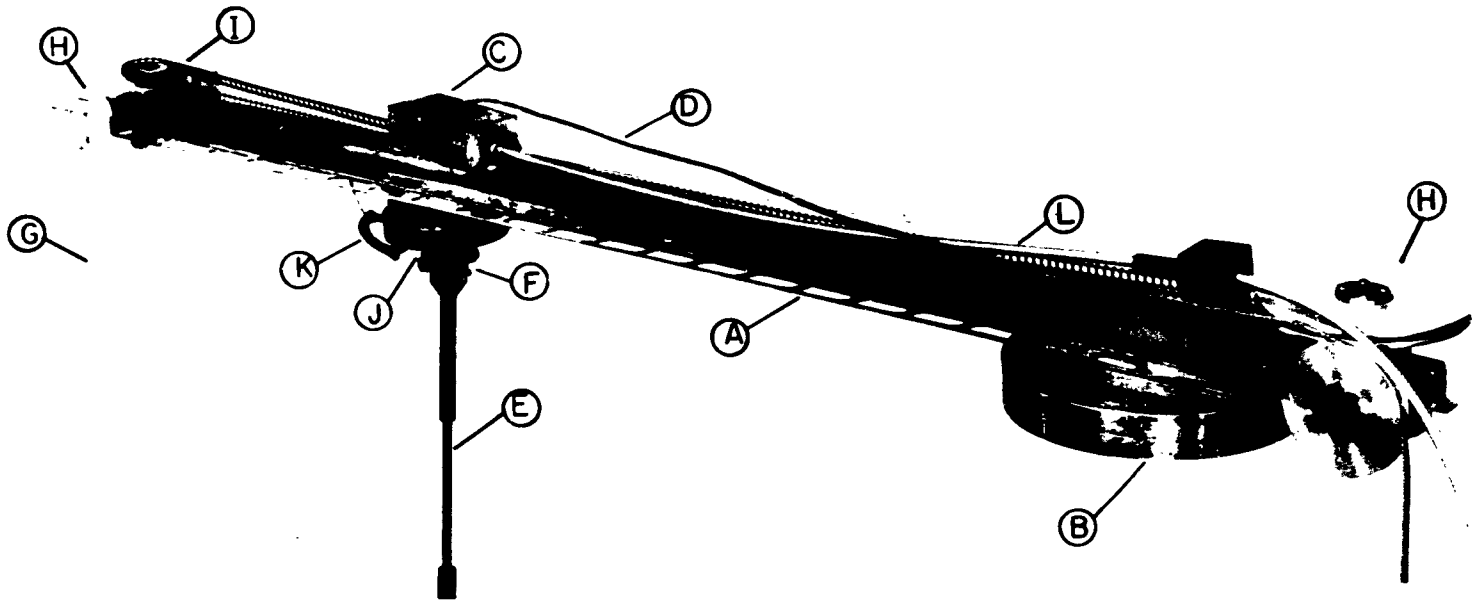

I-7 SCHEDULE OF PARTS

(A) RADIAL ARM	(G) RADIUS ADJUSTMENT STRING
(B) BALL BEARING AZIMUTH MOUNT	(H) PULLEYS (2 VISIBLE)
(C) SLIDING CARRIAGE	(I) CHAIN & SPROCKET RADIAL DRIVE
(D) FLEXIBLE TRANSMISSION LINE	(J) ROTATION ANGLE SCALE
(E) RIGID TRANSMISSION LINE	(K) MAGNIFIER
(F) UNIVERSAL JOINT	(L) FLEXIBLE SHAFT FOR ROTATION

FIG. I-8a. PROBE POSITIONING MECHANISM IN PLACE

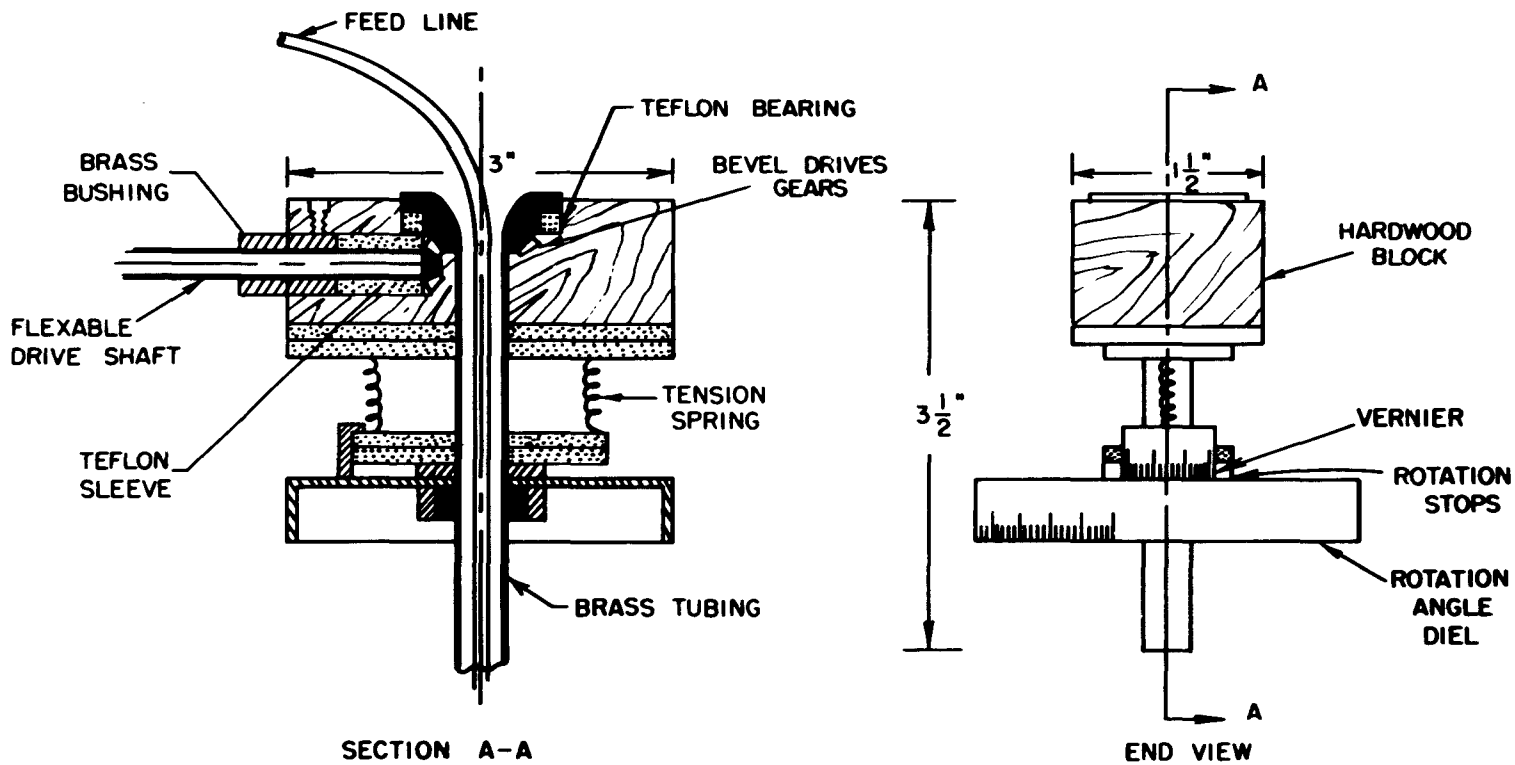

I-8b PROBE POSITIONING MECHANISM DETAIL OF SLIDING CARRIAGE

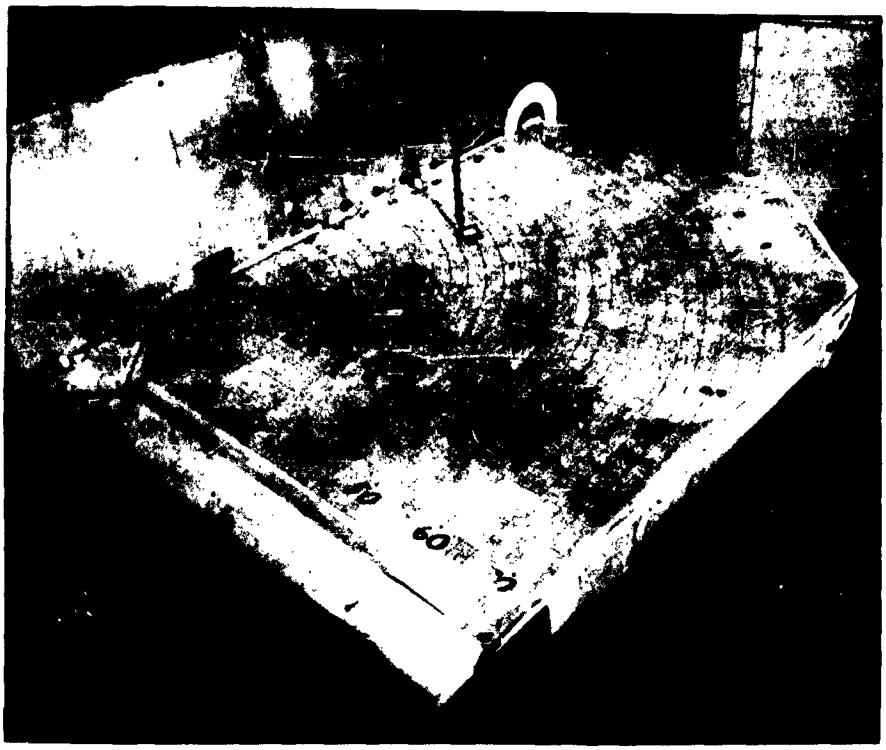

FIG. I-9. COORDINATE TABLE WITH SOURCE ANTENNA AND PROBE

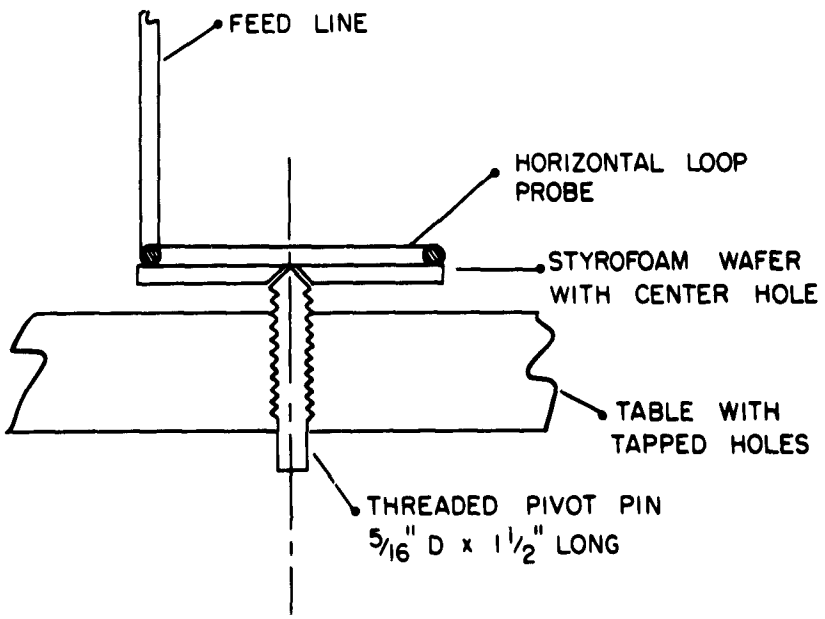

FIG. I-10. COORDINATE TABLE DETAIL SHOWING PROBE PIVOT

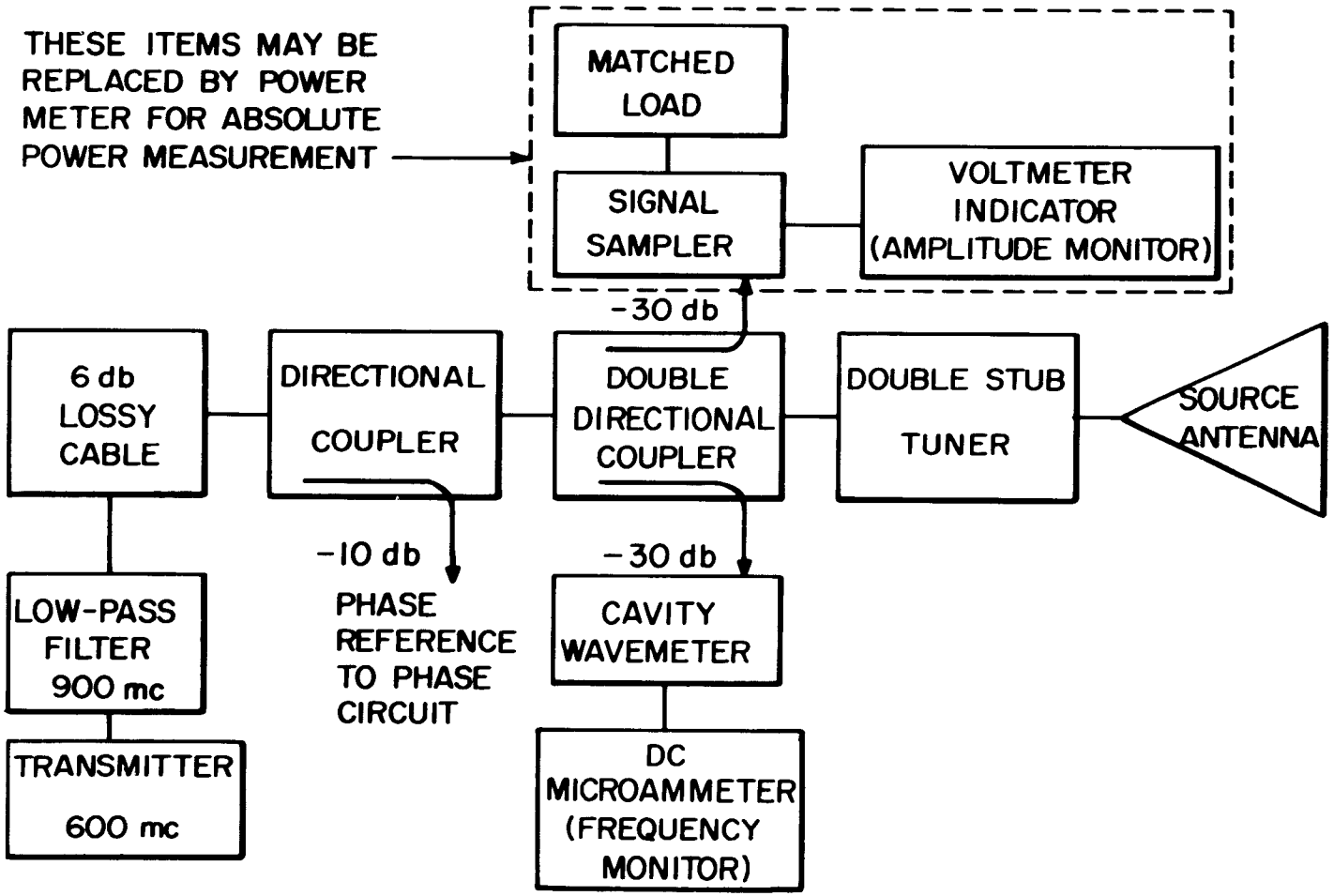

BLOCK DIAGRAM OF TRANSMITTING SYSTEM

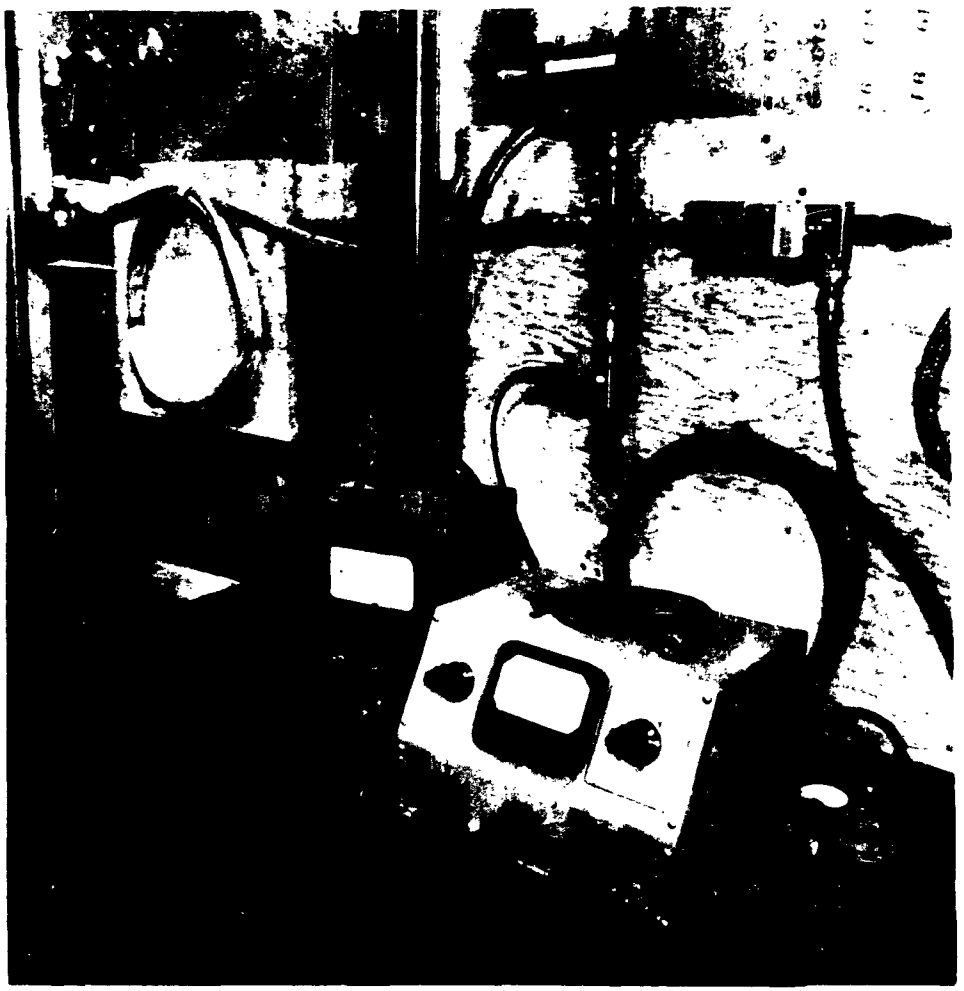

FIG. I-12. TRANSMITTING SYSTEM
FROM BEHIND IMAGE PLANE

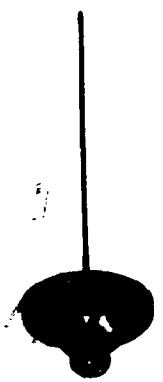

FIG. I-13. QUARTER-WAVE UNIPOLE
SOURCE ANTENNA

I-14 BLOCK DIAGRAM OF RECEIVER SYSTEM

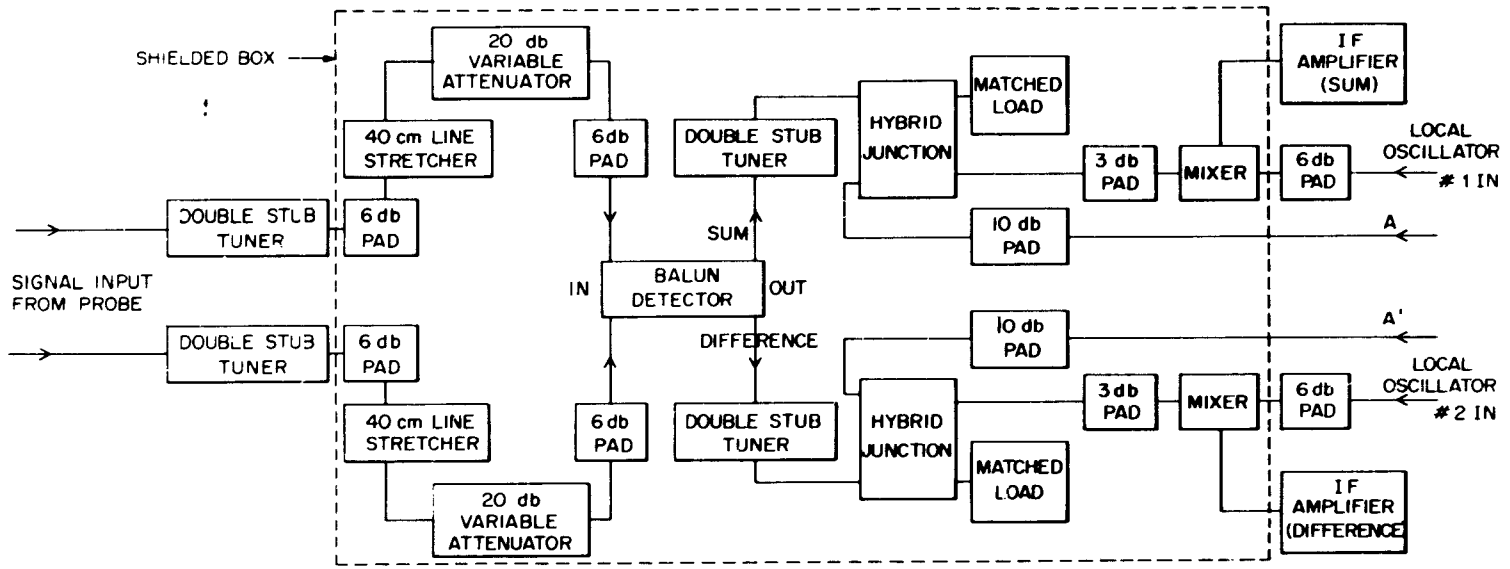

PHASE CIRCUIT

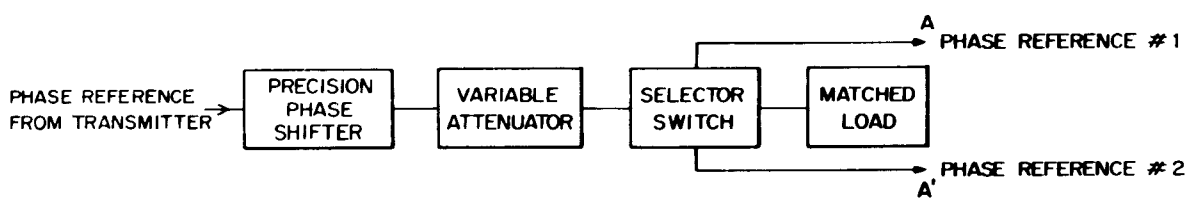

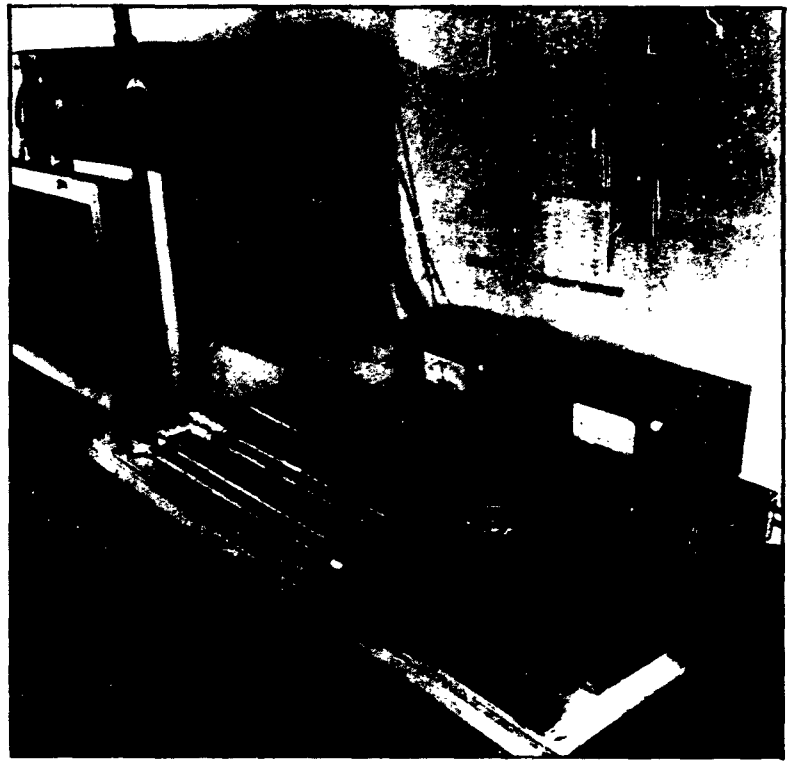

FIG. I-15. RECEIVER AND PHASE MEASURING SYSTEM

FIG. I-16. SHIELDED BOX COVER REMOVED

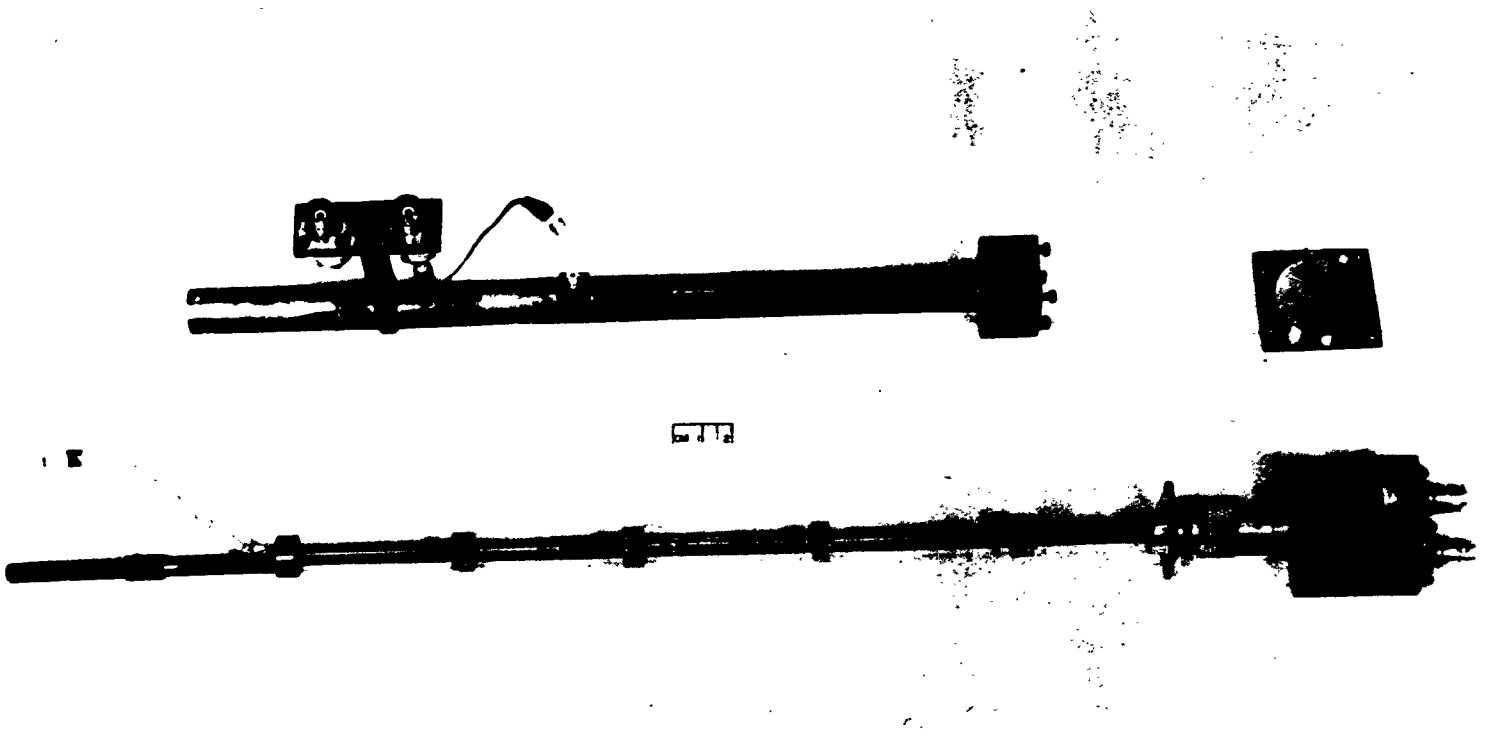

FIG. I-17. BALUN DETECTOR, SHELL AND INTERIOR

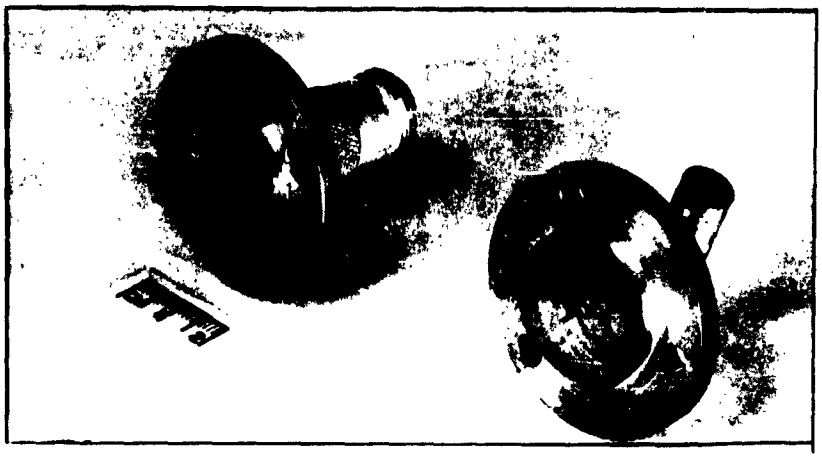

FIG. I-18. IMAGE PROBES
UNIPOLES IN MOUNTING FLANGES

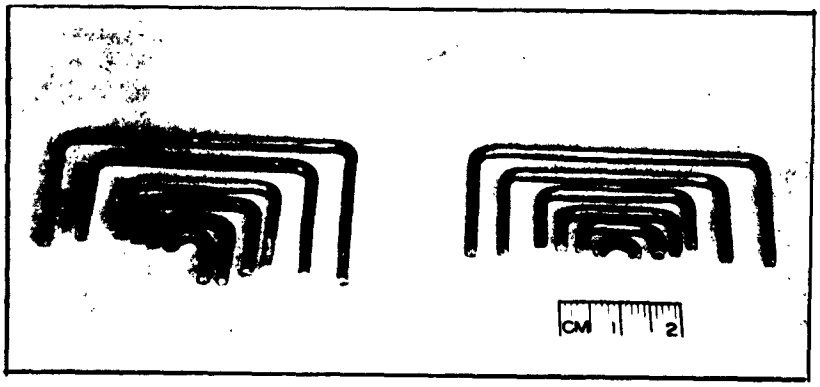

FIG. I-19. IMAGE PROBES, SQUARE HALF-LOOPS

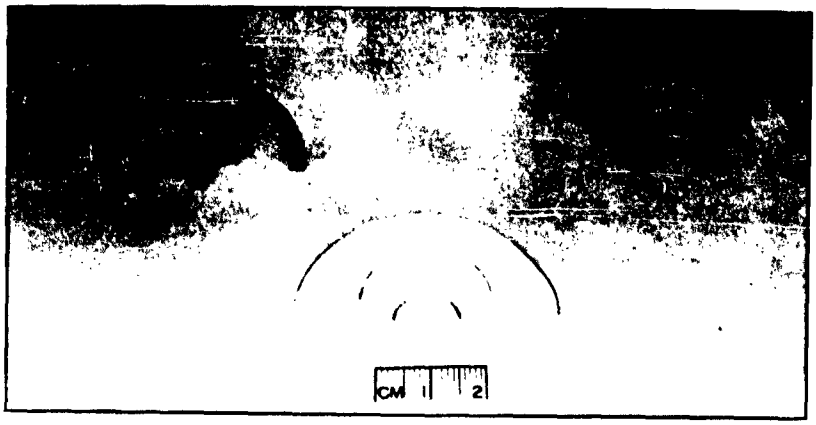

FIG. I-20. IMAGE PROBES, CIRCULAR HALF-LOOPS

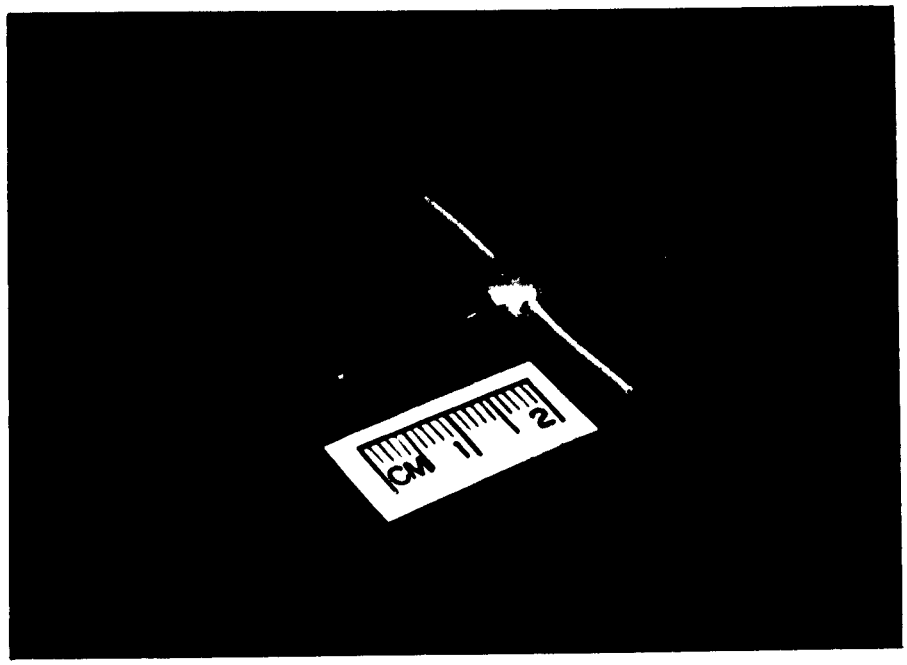

FIG. I-21. FREE SPACE PROBE, ELECTRIC DIPOLE

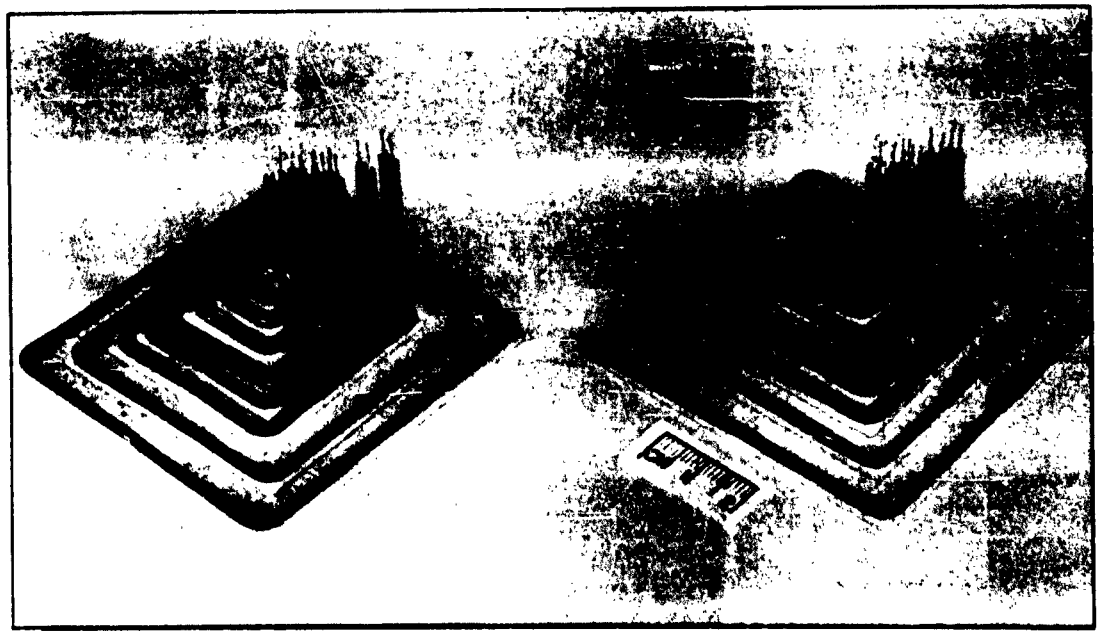

FIG. I-22. FREE SPACE PROBES, SQUARE LOOPS,
SINGLE AND DOUBLE LOADS

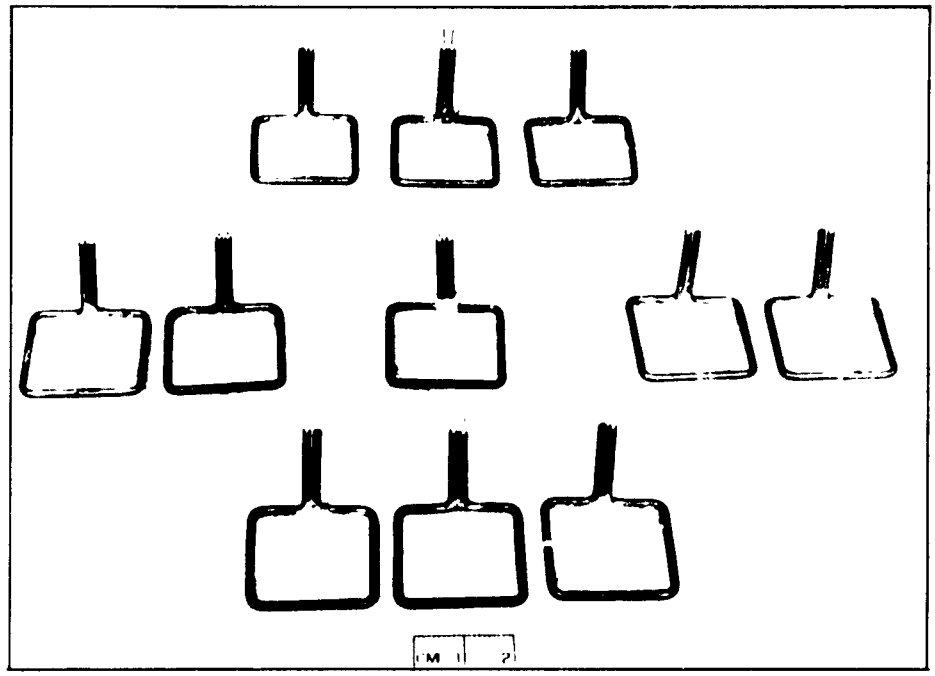

FIG. I-23. FREE SPACE PROBES
VARIABLE LOAD PLACEMENT

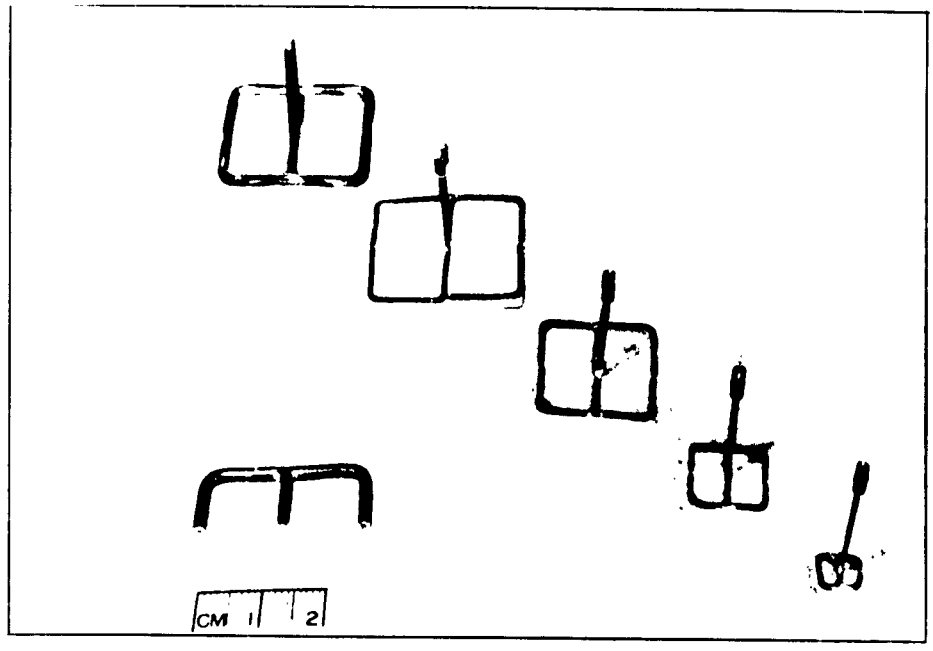

FIG. I-24. BRIDGED LOOPS
FREE SPACE AND IMAGE TYPE

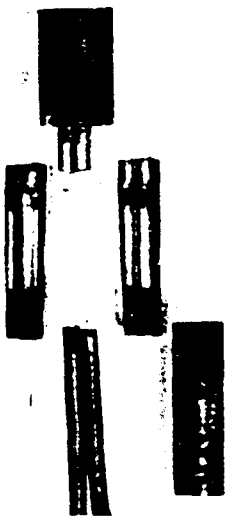

FIG. I-25a. PROBE CONNECTOR DISASSEMBLED

FIG. I-25b. PROBE CONNECTOR PARTIALLY ASSEMBLED

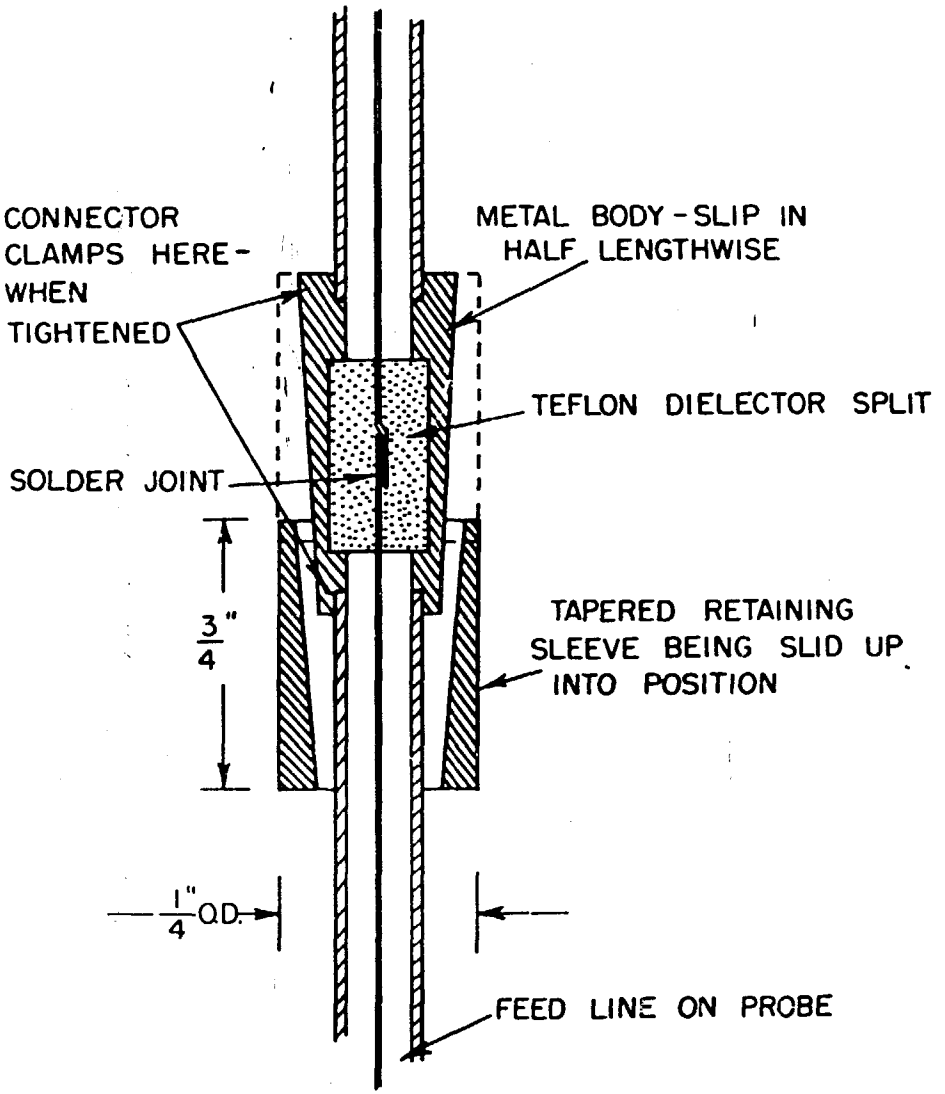

FIG. I-25c. PROBE CONNECTOR SCHEMATIC

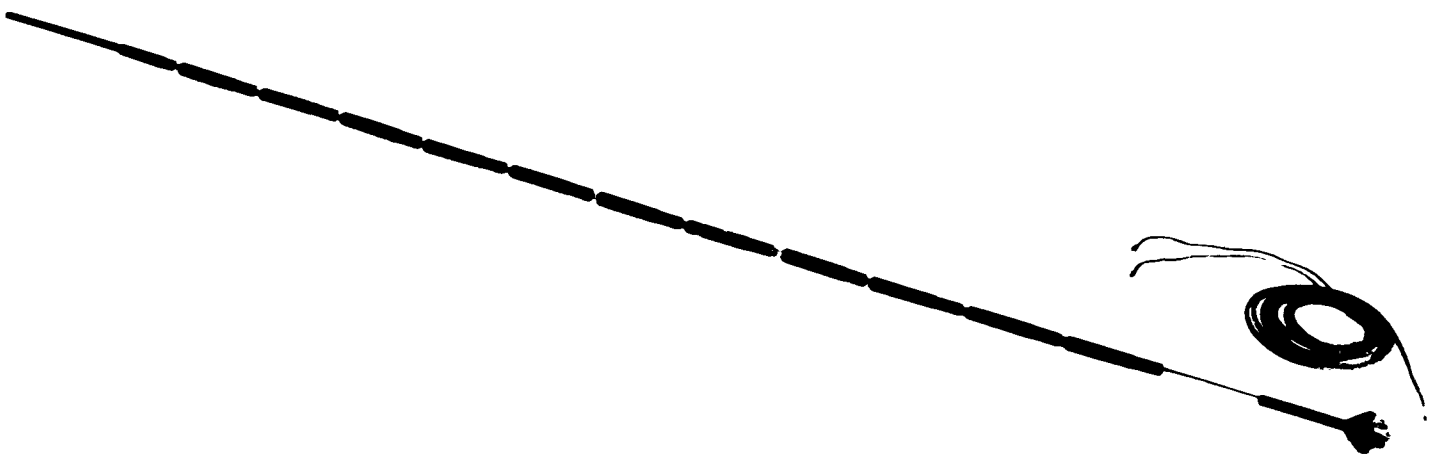

FIG. I-26. TRANSMISSION LINE, DISMOUNTED

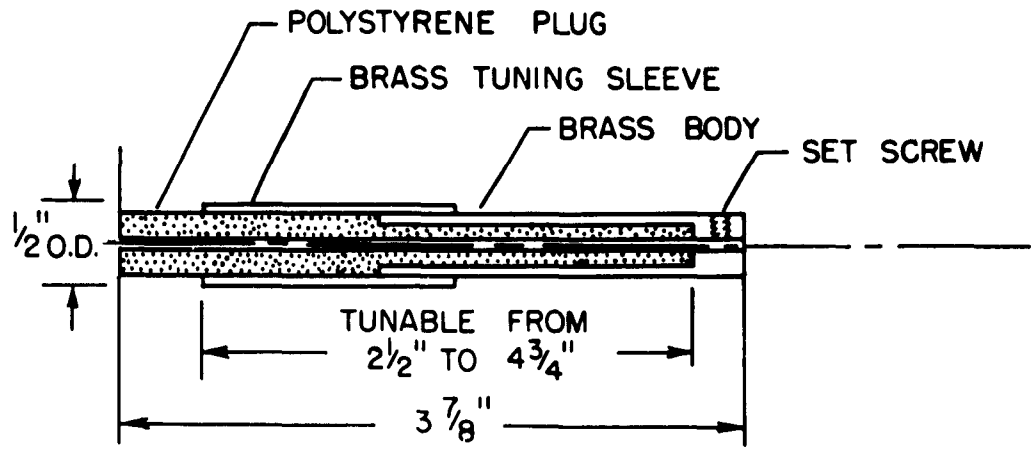

I-27a CROSS SECTION OF TYPICAL TRANSMISSION LINE TUNER

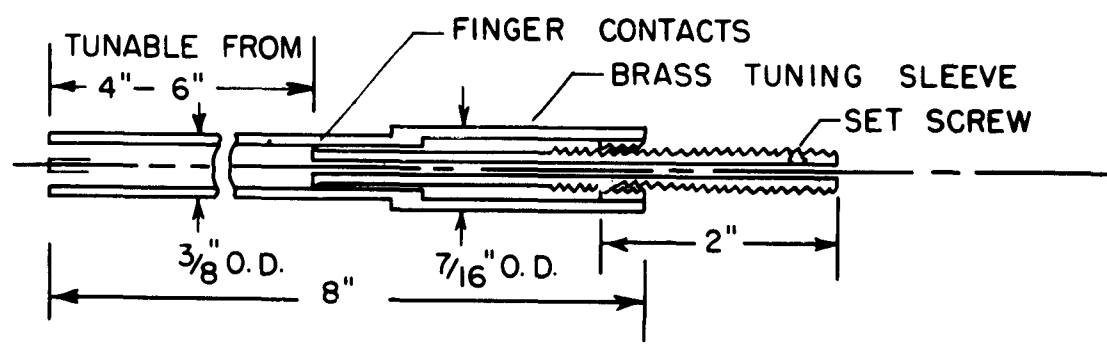

I-27b CROSS SECTION OF BOTTOM TRANSMISSION LINE TUNER

CHAPTER II. THE ELECTRIC DIPOLE AS A PROBE

Section A. Theory

It was convenient to begin the study of probes with an examination of the electric dipole, even though its behavior is relatively well understood, because it is the simplest probe, and the procedures used give some insight into the more complicated ones.

1. Equivalent circuit

Consider a linear antenna of length $2h$ and diameter $2a$, center loaded by a transmission line terminated in its characteristic impedance Z_L (Fig. II-1a). The component of the incident field parallel to the antenna, $E_{\parallel}$, excites a current in the load. On the other hand, it may be seen by symmetry that the component of the incident field perpendicular to the antenna, $E_{\perp}$, induces no current in the load. The current I_L in the load Z_L is to be determined.

The actual system can be replaced by an idealized antenna coupled with a passive terminal-zone network into an idealized transmission line [1] terminated in Z_L. Referring to Fig. II-1b, the impedance looking into the antenna at terminals A-B is Z_0, the input impedance of the antenna when driven. The impedance looking toward the load at these terminals is Z'_L. By Thevenin's theorem, the antenna can be replaced by an ideal voltage generator with the same open-circuit voltage, V_0, in series with the impedance Z_0 (Fig. II-1c) [2]. From the equivalent circuit we see at once that the base current in the antenna is:

$$I'_L = \frac{V_0}{Z_0 + Z'_L} \,. \qquad \text{(II-1a)}$$

This can be written in terms of admittances:

$$I'_L = \frac{Y'_L}{Y'_L + Y_0} Y_0 V_0 . \qquad \text{(II-1b)}$$

This can be normalized to unit incident field:

$$i'_L = \frac{Y'_L}{Y'_L + Y_0} Y_0 v_0 \qquad \text{(II-1c)}$$

where

$$i'_L = I'_L / E_{\|} \quad \text{and} \quad v_0 = V_0 / E_{\|} .$$

The normalized base current in the unloaded receiving antenna is:

$$i_0 = Y_0 v_0 . \qquad \text{(II-2)}$$

For a passive terminal-zone network the current entering the load is:

$$i_L = c_z i'_L \qquad \text{(II-3)}$$

where c_z is a constant dependent only on the geometry of the terminal zone. The probe sensitivity in amperes per volt per meter can now be defined:

$$S = i_L = \frac{I_L}{E_{\|}} . \qquad \text{(II-4)}$$

By substitution in the above:

$$S = c_z \frac{Y'_L}{Y'_L + Y_0} i_0 . \qquad \text{(II-5)}$$

2. Admittance Y_0

The input admittance of the driven linear antenna has been the subject of intensive theoretical studies. King [3] uses an iteration method to solve the integral equation for the current in such an antenna, and obtains as a result the ratio of two power series in the reciprocal of the expansion parameter

Ψ.* Evaluating the current at the driving point and dividing out the voltage leaves an expression for the desired admittance. The analytical expressions involved are rather formidable, but, fortunately, he has prepared rather complete tables of the second-order impedance for antennas of half lengths greater than $h = .08\lambda$ and various thicknesses. For $\Psi = 5$,† these values are accurate to about 4%, with accuracy increasing for larger values of Ψ.

King also shows that for short antennas with $h \leq .03\lambda$ the first-order impedance is adequate, and he derives a particularly simple expression for it. However, in the range $.03\lambda \leq h \leq .08\lambda$, a second-order expression is still needed. A more recent study [5] of the short antenna provides this by again using the iterative procedure, but with an improved trial current. This leads to an expression accurate to 3% in the range $0 \leq h \leq .08\lambda$ for $\Omega \geq 6$:

$$Y_0 = \frac{jkh\,(1 + \frac{1}{3}k^2 h^2)}{60\,\Psi} \tag{II-6}$$

where

$$\Psi = \Omega - 3.39. \tag{II-7}$$

Here it is seen that the numerator is just the first two terms in the power series for tan kh and that the next term can be neglected to the order of 1%. Therefore

$$Y_0 \doteq j\,\frac{\tan kh}{60\,\Psi}. \tag{II-8}$$

The substitution of tan kh in the numerator seems reasonable when it is noted that the final expression has the form of the zeroth-order admittance, although it uses an improved value for Ψ.

- - - - - - -

*An approximate expression is $\Psi \doteq \Omega - 2$, where $\Omega = 2\ell n \frac{2h}{a}$.

†This is a rather thick antenna, with $\frac{h}{a} \doteq 16.6$.

3. Short-circuit current i_0

The problem of the linear receiving antenna in a plane-wave field has been solved in terms of two simultaneous integral equations by an iteration method similar to that used for the transmitting antenna [6]. For the short-circuited case, this gives for the zeroth-order current at the center:

$$[I_0]_0 \doteq E_{\parallel} \left(\frac{\tan kh}{-j\,60\,\Psi}\right) \frac{2 \tan \frac{1}{2} kh}{k}. \qquad \text{(II-9)}$$

The quantity in parenthesis is recognized as the zeroth-order admittance $[Y_0]_0$. The zeroth-order induced voltage per unit field is v_0.*

$$[v_0]_0 = \frac{2}{k} \tan \tfrac{1}{2} kh. \qquad \text{(II-10)}$$

Then the zeroth-order current per unit field is:

$$[i_0]_0 \doteq [Y_0]_0 [v_0]_0 . \qquad \text{(II-11)}$$

This is the same as the actual current for an infinitely thin antenna, but higher order values are required for thicker antennas. In general, the calculation of higher order values of induced voltage is just as involved as that of impedances, and extensive tables do not exist. The accuracy of the zeroth-order values will therefore be examined by comparison with the available first-order values.

The first-order current distribution on the unloaded receiving antenna differs very little from the zeroth-order distribution [7], and since the solution is obtained by iteration, it may be concluded that it is quite accurate and may be used with the second-order admittance to give accuracy comparable to second order in determining the induced voltage. A new formulation of the first-

- - - - - - -

*v_0 is a quantity often referred to as effective length, $2 h_e$.

order current is convenient [8].

$$[i_0]_1 = j \frac{1}{30k} \frac{(1 - \cos kh)}{\Psi_{ku} \cos kh - \Psi_{uk}(h)} \doteq [Y_0]_2 [v_0]'_1 . \qquad \text{(II-12)}$$

The Ψ functions can be expanded in terms of the integrals $C_a(h, z)$ and $E_a(h, z)$ which have recently been tabulated [9] for certain values of the parameters a and h. Using these, it was possible to compute $[i_0]_1$ and $[v_0]'_1$, for $h = .125\lambda$. A comparison of $[v_0]'_1$ for this length with $[v_0]_0$ shows the zeroth-order value to be less than 3% too high for $\Omega \geq 8.6$ and about 9% too high for $\Omega = 7.8$. Consideration of the general behavior of v_0 indicates that this result is typical of antennas of moderate length ($0.1 \leq h/\lambda \leq 0.2$). $[v_0]_0$ can then be used in this region, provided $\Omega \geq 8.6$, with 3% accuracy.

For short antennas ($h \leq .08\lambda$) a numerical interpretation of Reference [10] shows that at least for $\Omega = 10$ the accuracy of the 0^{th}-order approximation improves slightly as shorter lengths are approached. Therefore $[v_0]_0$ will be used over the entire range ($0 \leq h \leq 0.2\lambda$), with estimated accuracy of at least 3% for $\Omega \geq 8.6$. It is not known how poor an approximation this is for smaller Ω values, but the entire analysis is expected to break down at $\Omega \leq 6$ where a^2/h^2 is not $<<$ 1 and the thin-wire approximations used throughout are not valid.

For antennas near resonance ($0.2 \leq h/\lambda \leq 0.3$) first-order values for the effective length are available [10] as a function of kh and Ω. The desired numerical values for the induced voltage can be found by linear interpolation from these.

Using these values of v_0 and the previously discussed values of Y_0, the desired short-circuit current i_0 can be computed with an accuracy of better than 5% over most of the region.

Section B. Experiment

4. Image method

Rather than study the dipole probe directly, it is more convenient to investigate a unipole over a conducting screen. By the theorem of images this is equivalent to a dipole in the actual field plus the image field, and the same current will flow in the apparent load Z'_L in both cases (Fig. II-1). This method has the advantage of removing the transmission line from the incident field and making it possible to study the effect of the probe alone, although it is obviously useful for only a selected group of situations.

5. End effect

Referring to Eq. II-3, it is seen that the end effect constant c_z must be evaluated for the specific situation before the experimental current i_L, measured in the actual load Z_L, and the theoretical current i'_L, evaluated in the apparent load Z'_L, can be related. For the unipole over a conducting screen, the terminal-zone network is simply a capacitance C_T in shunt with the load [11], with an admittance given by:

$$Y_E = j\omega C_T = -j C_K \frac{6.28}{Z_G} \frac{b}{\lambda_g} \qquad \text{(II-13)}$$

where b is the outer diameter of the dielectric, Z_G is the characteristic impedance, λ_g is the guide wavelength in the coaxial line, and $C_K = -C_T/C_0 b$ is a constant which has been theoretically determined and plotted in Reference [11] (Fig. II-10.9). From Fig. II-1d, it is seen that:

$$Y'_L = Y_L + Y_E \,. \qquad \text{(II-14)}$$

Two different coaxial lines were used, both with a characteristic admittance of 20 millimhos and with matched terminations. The end effect admittances

calculated from Eq. II-13 are -j 0.17 and -j 0.54 millimhos, so it is seen at once that $Y'_L \doteq Y_L$ within 2%, and end effect can be neglected in this case, at least from the receiving point of view.*

In some cases it was experimentally convenient to introduce a step in the diameter of the center conductor where it emerges from the screen in order to obtain various antenna diameters. The effect of such a step is to place a shunt capacitance across the load [12], but its value is an order of magnitude smaller than that from end effect and it may be totally neglected.

Therefore, the current in the load can be measured for the experimental (unipole) case and compared directly with the theoretical current computed for a dipole with half the load admittance of the actual unipole (Fig. II-2e).

6. Experimental setup

The experiment is set up in the free-space room against the image plane with a quarter-wave unipole source and receiving unipole probes of various diameters (Fig. II-2a-e). The probe length is varied by starting with a long antenna and cutting it back, step by step. The frequency used was 600 mc, and the distance from source to probe 70 cm, which is necessarily short to avoid any effect of standing waves in the room.

The loading effect of the probe on the primary antenna is readily estimated for the worst case, when both are $\lambda/4$ long, and even in this case the error introduced is no more than 1.4%†, while for the shorter probes, which are more interesting for measuring purposes, it is much less.

- - - - - - -

* Note that from the transmitting point of view, Y_E is seen in shunt with the antenna admittance Y_0, which varies from about 10 down to 0.2 millimho for the antennas used. Y_E is clearly not negligible for the transmitting case.

† The input impedance to the transmitting antenna in the presence of the probe

A worse effect with the probe so near the source is the curvature of the incident wave front. Even for the longest probe, this only produces a variation of 1% in the magnitude of $E_{\|}$ along its length, but there may be an appreciable phase lag towards the end of the antenna, so a correction must be made. This is done by assuming an incident field of uniform phase equal to the mean value of the phase along the antenna. Since the largest correction obtained in this manner was 3.4 degrees, this estimated correction was deemed adequate.

7. Normalization

In order to get an absolute measurement of the magnitude of probe sensitivity $|S|$ the experimental data must be normalized to $E_{\|} = 1$ volt/meter incident field and also normalized for the absolute receiver calibration constant.

The theoretical electric field at the probe position ($k_h = 0$, $k_e = 5.8$), is $E_{\|} = 38.3$ db above 1 volt/meter for a current of amplitude 1 amp. and a

- - - - - - - -

becomes equal to [13] $Z_{10} = Z_{S1}\left(1 - \frac{Z_{12}^2}{Z_{S1}^2}\right)$ where the self impedance Z_{S1} equals approximately the impedance with no parasite, $Z_{S1} \doteq 73 + j\,42$, and according to a zeroth-order calculation the mutual impedance $Z_{12} \doteq 6 - j\,12$. Therefore, the change in impedance is:

$$\left|\frac{Z_{10} - Z_0}{Z_0}\right| = \left|\frac{Z_{12}}{Z_0}\right|^2 \doteq .027$$

and the reflected voltage in a feed line matched to the isolated antenna is:

$$|V^r| = |V^i| \left|\frac{Z_{10} - Z_0}{2Z_0}\right| \doteq .014\,|V^i|,$$

which would produce 1.4% error in the measured current.

cosine distribution* on the source antenna. If the maximum current on a transmitting antenna is I_m, the total radiated power is $I_m^2 R_m^e$. But $R_m^e = 73.13$ ohm† for a linear dipole of half length $h = \lambda/4$ and a cosine distribution of current, and half this for a unipole, so that in the theoretical calculations a total radiated power $P_A = 36.57$ watts has been assumed. The actual power incident on the transmitting antenna can be measured using a thermistor power bridge and a calibrated directional coupler. Since the VSWR looking into this antenna was only 1.02, only .01% of the power is reflected, and the radiated power P_R is essentially equal to the measured incident power P_T. Therefore, the experimental current can be normalized to the theory by multiplying by a transmitter normalization constant:

$$C_T = \frac{E_{assumed}}{E_{actual}} = \sqrt{\frac{P_A}{P_R}} = \sqrt{\frac{36.57}{P_T}} \quad . \tag{II-15}$$

To calibrate the receiver in terms of current in the 50 ohm line at the probe, loss in the connector between the probe and the coaxial cable to the receiver is assumed negligible.‡ Then a known calibration power input into this cable, P_c, implies a calibration current $I_c = \sqrt{P_c/50}$, and if the output meter reads $M_{cal.}$ the receiver calibration constant is:

$$C_R = \frac{I_c}{M_{cal.}} = \frac{1}{M_{cal.}} \sqrt{\frac{P_c}{50}} \quad . \tag{II-16}$$

- - - - - - -

*For a discussion of the current distribution of the source and its effect on the field see Appendix A.

†This value is found by integration of the far-zone field (Reference [14]).

‡The loss through two such connectors placed back to back was measured as less than 0.1 db.

The combined calibration factor to be applied to the receiver meter readings to obtain the normalized probe current is the product of C_T and C_R or

$$K_{(db)} = C_T\,(db) + C_R\,(db)\ . \qquad \text{(II-17)}$$

If the calibration power is taken from a 28.6 db directional coupler in the transmitter circuit, $P_c = .01380\ P_T$, and:

$$K_{(db)} = -\,M_{cal.}\ (db) - 30.1\ (db)\ . \qquad \text{(II-18)}$$

$K_{(db)}$ must be added to the meter readings to get I_{probe} (db/1 amp.), and then the theoretical field $E_{\|} = 38.3$ (db/1 volt/meter) must be subtracted from this to get the probe sensitivity $|S|$ (db/1 meter/ohm).* It is felt that the over-all accuracy of normalization is within 0.5 db.

No attempt was made to make an absolute measurement of phase, so the experimental values of arg S were normalized for each† of the probe diameters used to agree with the theory in the range $.05 \leq h/\lambda \leq .10$ where both theory and experiment are expected to be quite good.

8. Results

The experimental measurements of probe sensitivity S for a unipole with 50 ohm resistive load are plotted in Fig. II-3 against h/λ for six different values of probe radius a/λ. On the same graphs are plotted the theoretical values of S as determined above, and the general agreement in both magnitude (absolute) and phase (relative) is very good, excluding the region where $\Omega < 6$

- - - - - - -

*1 meter/ohm is equivalent to 1 ampere/volt/meter.

†The reason for normalizing for each diameter separately is that they were measured at different times, with two different adapters, and with the adapters sometimes resoldered. Even so, the variation for a single adapter was less than $\pm$ 2 degrees for the various runs.

and the theory is definitely inaccurate. In order to illustrate better the effect of varying a/λ, the theoretical curves are all replotted together in Fig. II-4.

For ($.02 < h/\lambda < .15$), the main region of interest for probes, the mean deviation is 0.4 db in magnitude and 0.5 degree in phase, and the maximum deviation is 0.8 db and 1 degree.

For $.15 < h/\lambda < .23$ the measured magnitudes average 0.8 db too large, and the phases lag by an average of 4 degrees, which is a greater discrepancy than can be attributed to mutual coupling or curvature of the wave front. It may be that part of this is due to error in normalization of the magnitudes, but the phase error and at least half the magnitude error must be attributed to the approximate nature of the theory used.

For ($.23 < h/\lambda < .28$), the region near resonance, two theoretical curves are presented for the magnitude, one using the zeroth-order effective length, and the other using an estimated first-order value. They differ by an amount ranging from 1-2 db, and the experimental points lie between. The phase curves do not include a first-order estimate, which would make use of a complex effective length, and the experimental points lag the theoretical by an average of 7 degrees.

For the very shortest probes ($h/\lambda = .01$), phase agreement is good within 2 degrees for $\Omega > 6$, but the experimental magnitudes are 2 db below the theory. This is not surprising since neither the theory nor the experiment is designed for exceedingly short antennas.

The expected accuracy of the theory is better than 5% ($\pm$ 4 db in magnitude and $\pm$ 3 degrees in phase) over the region ($.02 \leq h/\lambda \leq .23$) for $\Omega > 6$. The relative accuracy of the experiment is $\pm$ 0.2 db and $\pm$ 3 degrees, and the absolute accuracy (used for magnitudes only) $\pm$ 0.7 db, so that agreement between theory and experiment is quite satisfactory.

A comparison with the results of Morita and Taylor is interesting [15]. They measured the relative power into a matched line from a receiving antenna of variable length in a constant field, and also the input impedances of the same antennas when driven. From this they computed an experimental effective length which was then normalized near anti-resonance and compared with the first-order theory. In the region $h/\lambda < 0.25$, their experimental values lie considerably above the theoretical curve, even if allowance is made for the changes in Ω, but the present measurements suggest that this result is in error and that the theory is verified by experiment in this region. It seems quite likely that this error is due to the use of the measured impedance Z_{SA} as the antenna impedance Z_0 in computing the effective length from the received power. As discussed above (Section II-5), the measured impedance in the transmitting case may differ considerably from the antenna impedance because of end effect, but it is the antenna impedance itself that must be used as the source impedance in the receiving case, with the end effect shunting the load. Since all parameters of their measurements are not available, a quantitative check cannot be made, but it is precisely in the region where R_{SA} is small and $|Z_{SA}|$ will differ most from $|Z_0|$ due to end effect that the deviation is largest, and the direction of disagreement is correct for this hypothesis.

Section C. Conclusions

Only general conclusions were drawn for the dipole antenna as an electric probe, since it was mainly used for a check on the experimental procedures.

The dipole is indeed a suitable electric probe, responding only to the tangential component of $\mathbf{E}$. The sensitivity S is a maximum for a resonant length, slightly less than $2h = 0.5\lambda$, but such a long probe responds to an average field, not the field at a point. Thick antennas are more sensitive than thin, but it is more difficult to determine the polarization of $\mathbf{E}$ with them.

Finally, the agreement between experiment and theory was seen to be good enough to verify both and allow the use of similar procedures in further investigations.

Bibliography, Chapter II

1. King, Ronold W. P., The Theory of Linear Antennas, pp. 50-55, Harvard University Press, Cambridge (1956). (Hereafter referred to as King, Antennas,)

2. King, Antennas, pp. 466-468.

3. King, Antennas, pp. 141-193.

4. King, Antennas, Chapter II, Tables 30.3-30.10.

5. King, Ronold, C. W. Harrison, Jr., and D. H. Denton, Jr., "The Electrically Short Antenna as a Probe for Measuring Free Electron Densities and Collision Frequencies in an Ionized Region," Journal of Research of the National Bureau of Standards, Section D, Vol. 65, No. 4, pp. 377, 378 (July-August 1961).

6. King, Antennas, pp. 456-478.

7. King, Antennas, p. 487 and p. 475.

8. King, Ronold W. P., and Charles W. Harrison, Jr., Electromagnetic Radiation, Chapters III and VIII (book to be published).

9. Mack, Richard B., and Evelyn W. Mack, "Tables of E (h, z), C (h, z), S(h, z)," Cruft Laboratory Technical Report No. 331, Harvard University (November 1960).

10. King, Antennas, Fig. IV-9.6b.

11. King, Antennas, pp. 65-69.

12. Moreno, Theodore, Microwave Transmission Design Data, pp. 286-289, Dover, New York (1958).

13. King, Antennas, pp. 286-289.

14. King, Antennas, p. 561.

15. Cited in King, Antennas, pp. 494-495.

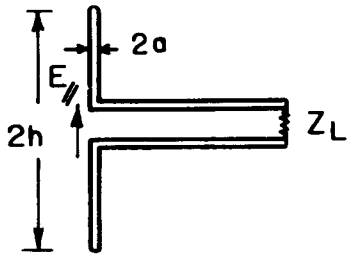

(a) ACTUAL DIPOLE

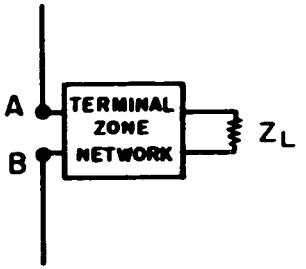

(b) IDEALIZED DIPOLE

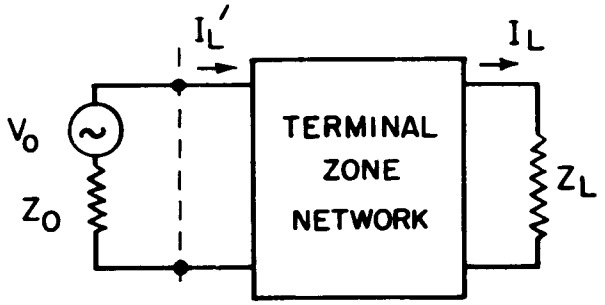

(c) THEVENIN EQUIVALENT CIRCUIT

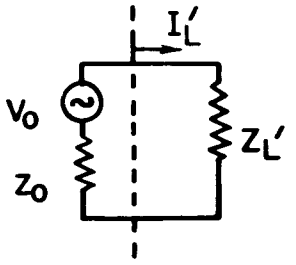

(d) SIMPLIFIED EQUIVALENT CIRCUIT

II-1 RECEIVING DIPOLE

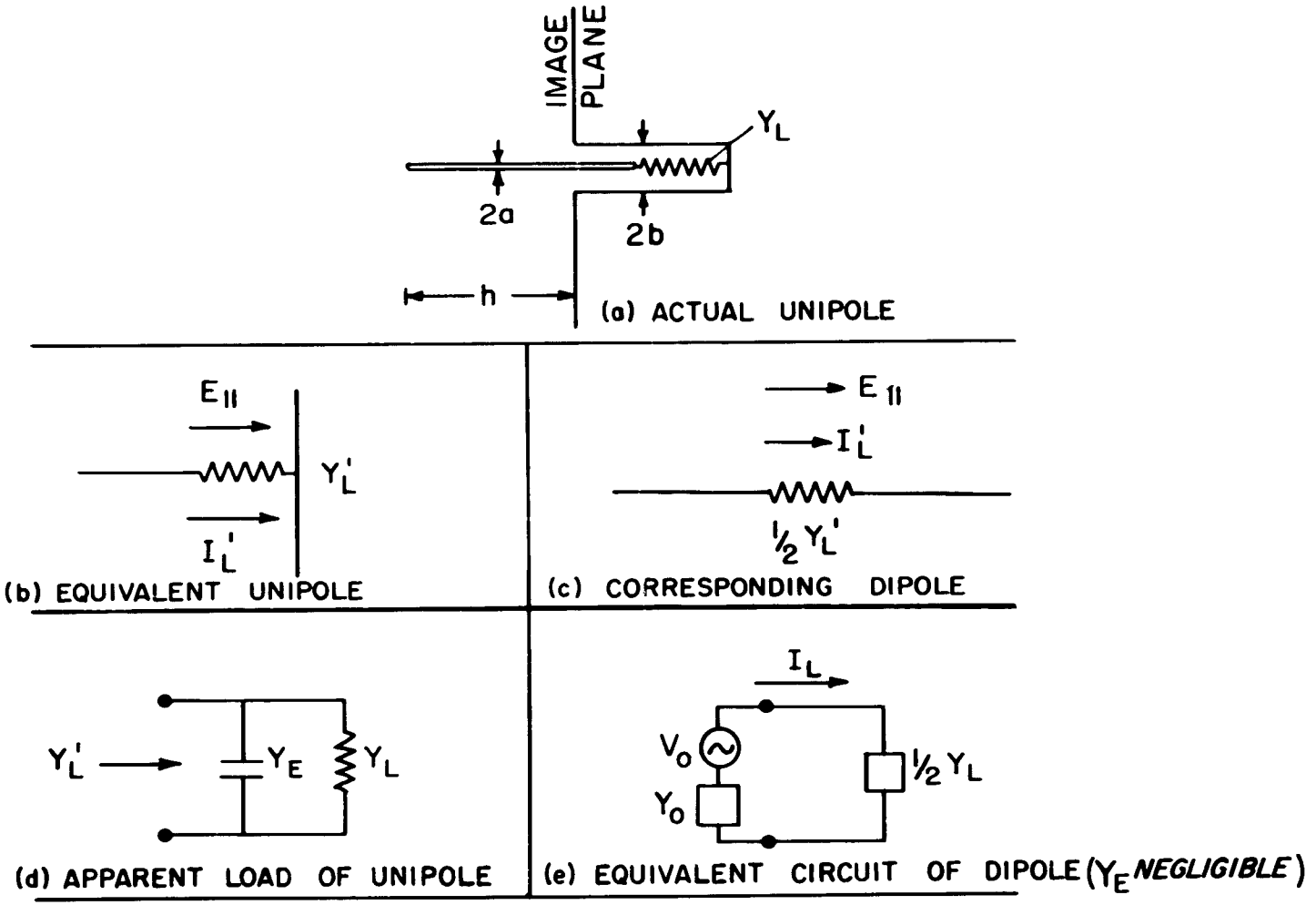

II-2 RECEIVING UNIPOLE

II-3 UNIPOLE SENSITIVITY THEORY AND EXPERIMENT

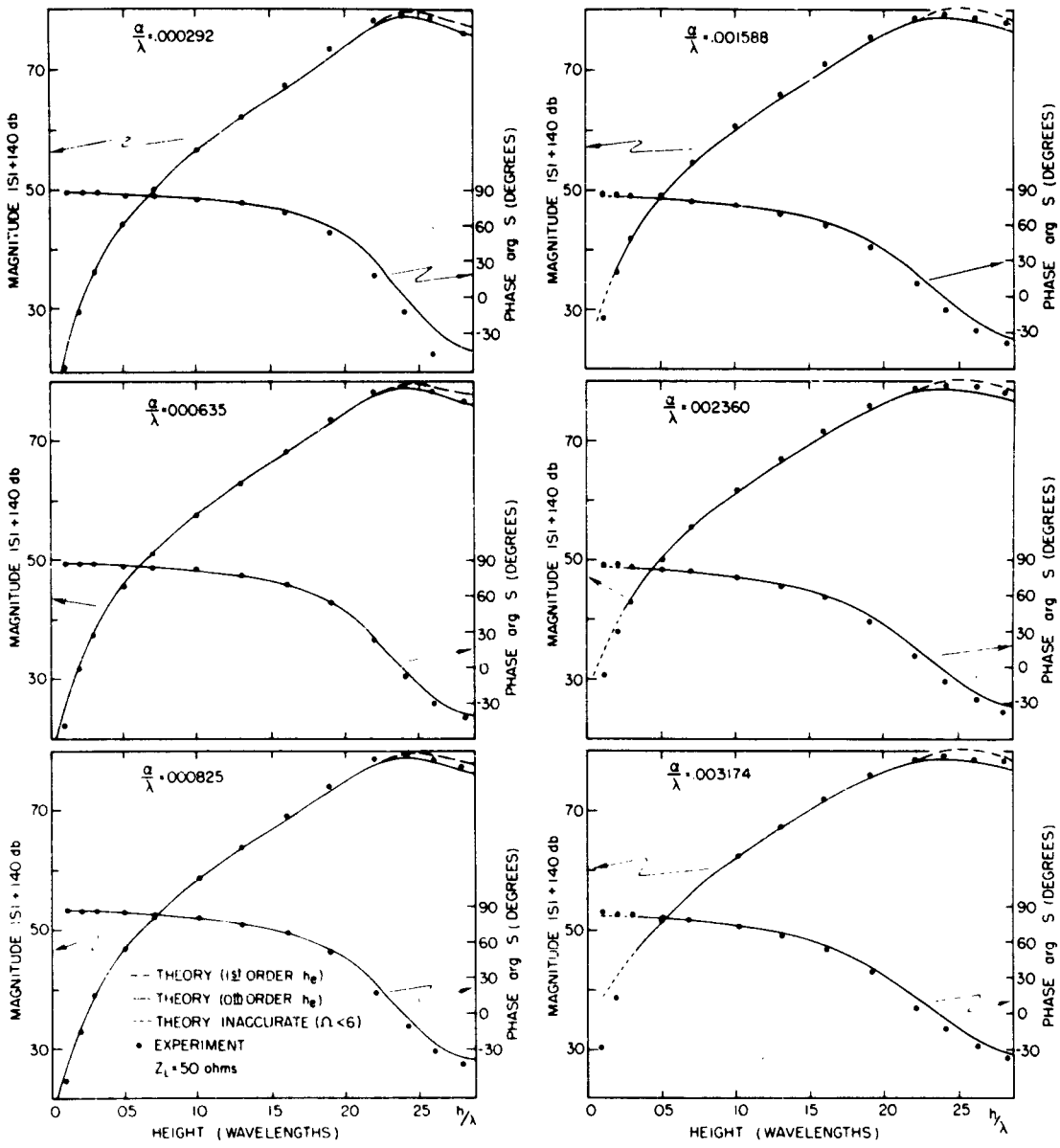

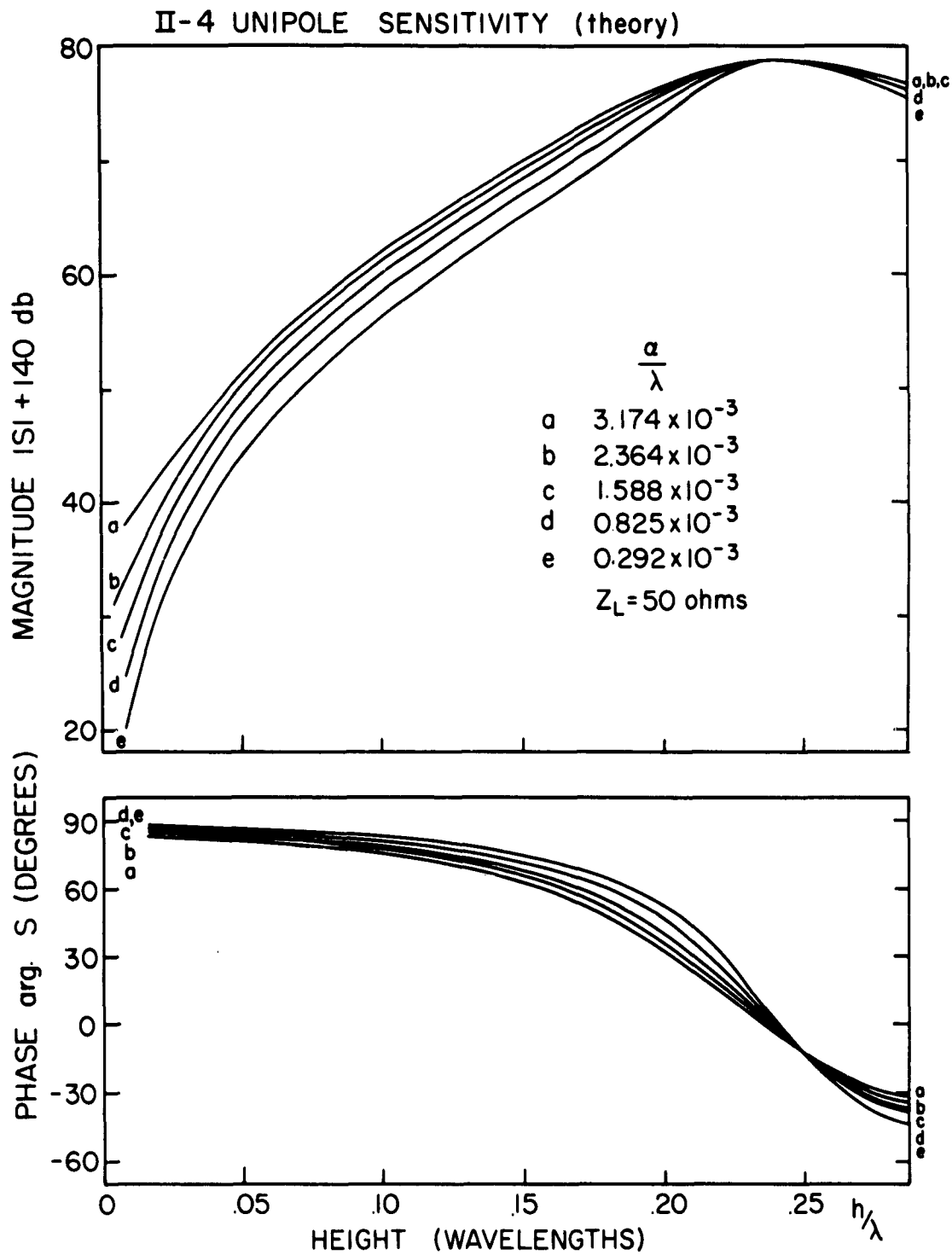
II-4 UNIPOLE SENSITIVITY (theory)
MAGNITUDE |S| + 140 db
80
60
40
20
a,b,c
d
e
a
b
c
d
e
α/λ
a 3.174 x 10⁻³
b 2.364 x 10⁻³
c 1.588 x 10⁻³
d 0.825 x 10⁻³
e 0.292 x 10⁻³
Z_L = 50 ohms
PHASE arg. S (DEGREES)
90
60
30
0
-30
-60
d,e
c
b
a
0
.05
.10
.15
.20
.25
h/λ
HEIGHT (WAVELENGTHS)

CHAPTER III. THE CIRCULAR LOOP AS A PROBE

Section A. Theory

The second type of probe studied was the circular loop, which is the easiest shape to build, and the one for which the best theory was available [1].

1. The unloaded circular loop in a plane wave field*

Consider first the simplest case, an unloaded loop in a plane wave field as shown in Fig. III-1a. The incident electric field lies in the z direction in a plane of the loop, is traveling in the x direction, and its value at the center of the loop is $E^i_{z\theta}$. Then:

$$I(\theta) = E^i_{z0}\, i(\theta) \tag{III-1}$$

where $I(\theta)$ is the total current at a point in the loop and $i(\theta)$ is a current distribution function which may be expanded in a Fourier series.†

$$i(\theta) = \sum_0^\infty v_n Y_n \cos n\theta \tag{III-2}$$

where:

$$v_n = 2\pi d f_n = (-j)^{n-1} (\pi d) (J_{n-1}(kd) - J_{n+1}(kd)) \tag{III-3}$$

$$Y_0 = \frac{1}{j\pi\zeta_0} \left(\frac{1}{a_0}\right) \tag{III-4}$$

$$Y_n = \frac{1}{j\pi\zeta_0} \left(\frac{1}{a_n}\right) \qquad n = 1, 2, 3, \cdots \tag{III-5}$$

- - - - - - -

*The theory summarized here is adapted from the work of King and Harrison [1].

†For an incident plane wave in a given direction $i(\theta) = i(-\theta)$ and the sine terms are not necessary.

and: v_n is the excitation voltage per unit field of the n^{th} mode in King's formulation. These have the dimensions of length and are often called effective lengths $2h_{en}$ for each mode.

$J_n(x)$ is the Bessel function of order n.

Y_n is the input admittance for the n^{th} current mode.

$\zeta_0 = 120\pi$ ohms is the impedance of free space.

a_n is the n^{th} coefficient in Storer's formulation of impedance [2].

It is convenient to separate the loop currents into two types according to their symmetry with respect to the z axis*: a symmetric current I_S and an antisymmetric current I_A (Fig. III-16):

$$I_S(\pi - \theta) = -I_S(\theta) \qquad \text{(III-6a)}$$

$$I_A(\pi - \theta) = I_A(\theta) . \qquad \text{(III-6b)}$$

Therefore

$$I_S(\theta) = E^i_{z0} \sum_{n\ \text{odd}} v_n Y_n \cos n\theta . \qquad \text{(III-7a)}$$

$$I_A(\theta) = E^i_{z0} \sum_{n\ \text{even}} v_n Y_n \cos n\theta \qquad \text{(III-7b)}$$

$$I(\theta) = I_S(\theta) + I_A(\theta) . \qquad \text{(III-7c)}$$

The appearance of the electric field in both expressions is somewhat arbitrary, and due to the assumption of a particular incident field for which $E^i_z = c\, B^i_y$. This obscures the fact that the antisymmetric current is basically due to the normal component of magnetic field. An antisymmetric current can only be

- - - - - - -

*Note that symmetric currents at image points in the loop are directed in the same sense with respect to z, but opposite with respect to θ.

maintained by an antisymmetric electric field. Therefore:

$$I_A \propto E^i_{zA}. \tag{III-8}$$

But the antisymmetric field is half the field difference between image points:

$$E^i_{zA} = \frac{1}{2}\left(E^i_z(x) - E^i_z(-x)\right) . \tag{III-9}$$

By Taylor's theorem:

$$E^i_{zA} = x\left[\frac{\partial E^i_z(x)}{\partial x}\right]_{x=c} + \cdots . \tag{III-10}$$

But:

$$-j\omega B^i_y = \hat{y} \cdot \nabla \times \vec{E}^i = \frac{\partial E^i_z}{\partial x} . \tag{III-11}$$

And the first term in the expansion of E^i_{zA} is proportional to B^i_y. Therefore, since to the first order I_A is proportional to the magnetic field itself at the center of the loop, but only to a derivative of the electric field, Eq. III-7b can be rewritten more logically:*

$$I_A(\theta) = c\, B^i_{y0} \sum_{n \text{ even}} v_n Y_n \cos n\theta . \tag{III-12}$$

Equation III-7a on the other hand is in the best form already since I_S is dependent to the first order on the electric field at the center of the loop.

2. The unloaded circular loop in an arbitrary field

Equations III-7a and III-12 can be reduced to:

- - - - - - -

*This may be illustrated as follows. Addition of a field with constant E_z in the xz plane and $B_y = 0$ will change only the symmetric current, but addition of a field with B_y constant in the xz plane and $E_z = 0$ will change only the antisymmetric current. Therefore, it is reasonable to relate the symmetric current to the electric field and the antisymmetric current to the magnetic field even though the two are never strictly independent.

$$I_A(0) = S_B\,(c\,B^i_{y0}) \qquad \text{(III-13a)}$$

$$I_S(0) = S_E\,(E^i_{z0}) \qquad \text{(III-13b)}$$

where S_B and S_E are magnetic and electric sensitivity constants for the incident plane wave, indicating the possible use of $I_A(0)$ and $I_S(0)$ for field measurement.† In order to use the loop as a probe it must be shown that these relations hold in an arbitrary field, with the proportionality constants S_B and S_E dependent on the probe geometry alone.

An arbitrary incident field can be expressed as a Fourier integral of plane waves:

$$\vec{E}(\vec{r}) = E_0 \int_{-\infty}^{\infty} \vec{g}(\vec{k})\, e^{-i\vec{k}\,\cdot\,\vec{r}}\,\cdot\,\overrightarrow{dk}\,. \qquad \text{(III-14)}$$

A general direction of incidence has not been considered here, but it is in reference [1], and the linearity of Maxwell's equations implies that Eq. III-14 can be combined with a modification of Eq. III-1 giving:

$$I(\theta) \propto E(\vec{r}) \qquad \text{(III-15)}$$

which can at least formally be broken up into I_S and I_A as before. However, it is obvious that the proportionality constants required will be functions of $\vec{k}$ and not independant of either the wavelength or the direction of propagation of each plane-wave component in the incident field. Therefore, the probe equations, III-14, cannot be extended to a general field, but are indeed restricted to constant $\vec{k}$, a single plane wave.

- - - - - - -

†In most equations it is convenient to write the magnetic field as cB rather than B , where c is the velocity of light in a vacuum, in order to give the magnetic field the dimensions volts/meter, the same as E .

Fortunately, the situation is better than it seems. First, assume that only B_y and E_z are significant in determining $I(0)$ and $I(\pi)$ for the given probe orientation.* Three situations may be distinguished. In the situation illustrated in Fig. III-1 the plane wave travels in the x direction, the electric field is E_z, and $c\,B_y = E_z$. A second situation would be a plane wave traveling in the y direction, with the electric field in the z direction and with $B_y = 0$. A third would be a plane wave traveling in the z direction, with the magnetic field in the y direction and with $E_z = 0$. If attention is restricted to the currents at $I = 0$ and $I = \pi$ it is only necessary to consider these three types of fields. It will be noted that their Fourier integral can still represent an arbitrary distribution of B_y and E_z.

For any field the Taylor series can be written in the plane $y = 0$:

$$E_z = E_{z0} + \left[x\left(\frac{\partial E_z}{\partial x}\right)_0 + z\left(\frac{\partial E_z}{\partial z}\right)_0\right]$$

$$+ \frac{1}{2}\left[x^2\left(\frac{\partial^2 E_z}{\partial x^2}\right)_0 + z^2\left(\frac{\partial^2 E_z}{\partial z^2}\right)_0 + 2xz\left(\frac{\partial^2 E_z}{\partial x \partial z}\right)_0\right]$$

$$+ \frac{1}{6}\left[x^3\left(\frac{\partial^3 E_z}{\partial x^3}\right)_0 + z^3\left(\frac{\partial^3 E_z}{\partial z^3}\right)_0 + 3x^2z\left(\frac{\partial^3 E_z}{\partial x^2 \partial z}\right)_0 + 3xz^2\left(\frac{\partial^3 E_z}{\partial x \partial z^2}\right)_0\right]$$

$$+ \cdots . \qquad \text{(III-16)}$$

Terms with an odd power of z in the coefficient will produce a current such that $I(-\theta) = -I(\theta)$, which implies $I(0) = I(\pi) = 0$ and they may be ignored here.

- - - - - - -

*This is a reasonable assumption in that E_y, B_x and B_z clearly do not affect $I(0)$. E_x produces two types of currents: those that are symmetrical with respect to the x axis and thus are zero at $\theta = 0, \pi$, and those that are antisymmetrical, of which the first term is related to B_y in a manner similar to the relation between I_A and B_y in Eqs. III-9 - 12. The higher order antisymmetrical terms in the Taylor series for E_x must be negligible as in Eq. III-17 for this assumption to be valid.

Furthermore, for small loops, terms of second and higher orders can be neglected. The criterion for an electrically small loop is dependent on the field:

$$\frac{1}{2} k_{max}^2 d^2 << 1 \qquad \text{(III-17)}$$

where $k_{max} = \frac{2\pi}{\lambda_{min}}$ for the shortest wavelength required in the Fourier representation of the field. That is $g(k) \doteq 0$ for $|k| > k_{max}$ in Eq. III-14. Then for the small probe the effective electric field is entirely included in:

$$E_z \doteq E_{z0} + x\left(\frac{\partial E_z}{\partial x}\right)_0 \qquad \text{(III-18)}$$

which can be written as the sum of two plane waves:

$$E_z = \left[E'_{z0} + x\left(\frac{\partial E'_z}{\partial x}\right)_0\right] + \left[E''_{z0}\right] . \qquad \text{(III-19)}$$

The wave including E'_{z0} is a plane wave traveling in the x direction as shown in Fig. III-1 and for which Eqs. III-7a, b and III-12 give the induced currents. The wave including E''_{z0} is a plane wave traveling in the y direction with E''_z constant over the xz plane. It is readily shown that for this wave $I''_A(\theta) = 0$ and:

$$I''_S(\theta) = E''_{z0} \sum_{n\ \text{odd}} v_n Y_n \cos n\theta \qquad \text{(III-20)}$$

to the same order of approximation as Eq. III-17.

In summary, the currents due to E'_z and E''_z can be superposed, giving for a <u>general</u> incident field:

$$I_A(0) = S_B(c B^i_{y0}) \qquad \text{(III-13a)}$$

$$I_S(0) = S_E(E^i_{z0}) \qquad \text{(III-13b)}$$

and

$$I_A(\pi) = S_B(c B^i_{y0}) \qquad \text{(III-13c)}$$

$$I_S(\pi) = -S_E(E^i_{z0}) \qquad \text{(III-13d)}$$

from Eqs. III-6 so that:

$$I(0) = I_A(0) + I_S(0) \qquad \text{(III-13e)}$$

$$I(\pi) = I_A(0) - I_S(0) \qquad \text{(III-13f)}$$

as required by the definitions of I_A and I_S, and subject to the restriction $\frac{1}{2} k^2_{max} d^2 << 1$, and where S_B and S_E are sensitivity constants* dependent on probe geometry alone:

$$S_B = \sum_{n \text{ even}} v_n Y_n \qquad \text{(III-21a)}$$

$$S_E = \sum_{n \text{ odd}} v_n Y_n \qquad \text{(III-21b)}$$

3. Evaluation of constants

In order to evaluate the sensitivity constants S_B and S_E it is first necessary to determine the v_n and Y_n from Eqs. III-3 - 5. The Bessel functions can be expanded in a truncated series valid within .01% for $2d \leq 0.13\lambda$:

$$J_p(kd) \doteq \frac{1}{p!} \left(\frac{kd}{2}\right)^p \left[1 - \frac{1}{(p+1)} \left(\frac{kd}{2}\right)^2\right] \qquad \text{(III-22)}$$

which gives:

$$v_o \doteq -j \frac{1}{4} (k2d) \left[1 - \frac{1}{32} (k2d)^2\right] (2\pi d) \qquad \text{(III-23a)}$$

$$v_2 \doteq -j \frac{1}{8} (k2d) \left[1 - \frac{1}{24} (k2d)^2\right] (2\pi d) \qquad \text{(III-23b)}$$

- - - - - - -

*i_A and i_S may be written for S_B and S_E since they are the currents per unit field induced at $\theta = 0$.

$$|v_4| \leq .0004\,|v_0| \qquad \text{(III-23c)}$$

$$v_1 \doteq \frac{1}{2}\left[1 - \frac{3}{32}(k2d)^2\right](2\pi d) \qquad \text{(III-23d)}$$

$$v_3 \doteq -\frac{1}{64}(k2d)^2\,(2\pi d) \qquad \text{(III-27e)}$$

$$|v_5| \leq .004\,|v_1| \quad . \qquad \text{(III-27f)}$$

Storer [2] gives the relations:

$$a_n = \frac{1}{4}(k2d)\,(K_{n+1} + K_{n-1}) - \frac{2n^2}{k2d}\,K_n \qquad \text{(III-24)}$$

$$K_{n+1} = K_n + \Omega_{2n+1}(k2d) + j\,J_{2n+1}(k2d) \qquad \text{(III-25)}$$

$$K_o = \frac{1}{\pi}\ln\frac{8d}{a} - \frac{1}{2}\int_0^{k2d}\Omega_0(x)\,dx - j\,\frac{1}{2}\int_0^{k2d} J_0(x)\,dx \qquad \text{(III-26)}$$

where $\Omega_p(x)$ is the Lommel-Weber function [3] of order p. The Bessel functions can be expanded as before and the Lommel functions can be expanded with 1% accuracy as:

$$\Omega_p(x) \doteq \begin{cases} -\frac{2}{\pi}\,\frac{1}{p}\left(1 - \frac{x^2}{4 - p^2}\right) & p \text{ odd} \\ \\ \frac{2}{\pi}\,\frac{x}{1 - p^2}\left(1 - \frac{x^2}{9 - p^2}\right) & p \text{ even}\,. \end{cases} \qquad \text{(III-27)}$$

This leads to the following expressions for the admittances Y_n accurate to 1% in magnitude and 1 degree in phase for $2d \leq .13\lambda$:

$$Y_0 \doteq \left\{j\zeta_0\,\frac{1}{4}(k2d)\left[\Omega - 3.52 + 0.33\,(k2d)^2\right]\right\}^{-1} \qquad \text{(III-28a)}$$

$$Y_2 \doteq \left\{-j\zeta_0\left[2\left(\frac{1}{k2d}\right)(\Omega - 4.85) + \frac{1}{8}(k2d)\,(\Omega - 5.65)\right]\right\}^{-1} \qquad \text{(III-28b)}$$

$$Y_1 \doteq \left\{-j\zeta_0\left[\frac{1}{2}\left(\frac{1}{k2d}\right)(\Omega - 3.52) - \frac{1}{8}(k2d)\,(\Omega - 3.52)\right]\right\}^{-1} \qquad \text{(III-28c)}$$

$$Y_3 \doteq \left\{-j\zeta_0 \left[\frac{1}{2}\left(\frac{9}{kZd}\right)(\Omega - 5.65)\right]\right\}^{-1} \qquad \text{(III-28d)}$$

where* $\Omega = \partial ln \frac{2\pi d}{a}$. Higher-order admittances could also be calculated, but they remain small, and when combined with the negligibly small higher-order values of the excitation voltages v_n do not add appreciably to the current in the unloaded receiving loop. They do, however, combine to change the input admittance of the driven loop, which will be discussed below.

The total current in a driven circular loop is [2]:†

$$I(\theta) = V \sum_{0}^{\infty} Y_n \cos n\theta \qquad \text{(III-29)}$$

which can be rewritten:

$$I(\theta) = V \left[\sum_{0}^{3} Y_n \cos n\theta + Y_4 \cos 4\theta + Y_\psi g(\theta)\right] \qquad \text{(III-30)}$$

where Y_ψ is an admittance representing the higher-order modes and $g(\theta)$ is the normalized distribution function for the higher-order currents, which is small except near $\theta = 0$ where it equals 1. The terms under the sum have already been expressed in Eqs. III-28, and Y_ψ can be computed in the same manner from:

$$Y_4 \doteq \left\{-j\zeta_0 \left[16\left(\frac{1}{kZd}\right)(\Omega - 6.22)\right]\right\}^{-1} . \qquad \text{(III-31)}$$

- - - - - - -

* This Ω must be distinguished from Ω for the dipole and from the $\Omega_p(x)$ above.

† A very recent paper by Wu [4] examines this problem more rigorously, but unfortunately, since the results are not in a form ready for computation, it was not possible to use them. There is, however, no reason to suspect that they will change the results very much for the very small loops used here.

Storer derives an expression for $Y_\psi\, g(\theta)$ in integral form by various manipulations valid for $2d \leq 0.8\lambda$:

$$Y_\psi\, g(\theta) = \frac{1}{-j\zeta_0} \frac{2(\frac{kd}{4.5})}{\ell n \frac{n_0}{4.5}} [J_1(\theta) + (\frac{kd}{4.5})^2 J_2(\theta)] \qquad \text{(III-32a)}$$

where $J_1(\theta)$ and $J_2(\theta)$ are somewhat complicated definite integrals which he has calculated and plotted. Only the following values are needed:

$$J_1(0) = \frac{\ell n\, N_0}{N_0} \int_{-\infty}^{\ell n\, N_0} \frac{e^x}{x}\, dx \qquad \text{where } N_0 = \frac{2d}{4.5a} e^{-.5772} \qquad \text{(III-32b)}$$

$$J_1(\pi) = -.071 \qquad \text{(III-32c)}$$

$$J_2(0) = .333 \qquad \text{(III-33a)}$$

$$J_2(\pi) = -.023. \qquad \text{(III-33b)}$$

Using these, $Y_\psi\, g(0)$ and $Y_\psi\, g(\pi)$ can be computed for each loop size. For the single loaded loop, Eq. III-30 gives:

$$Y = \sum_0^3 Y_n + Y_4 + Y_\psi \qquad \text{(III-34)}$$

for the input admittance. For $\Omega \doteq 10$, direct computation shows that the error involved in Y by neglecting $Y_4 + Y_\psi$ is less than 20% for $2d \leq 0.13\lambda$ and drops rapidly to 2% for $2d = 0.06\lambda$.

Since $g(0) = 1$ and $g(\pi) \doteq 0$, the symmetrical and antisymmetrical parts of Y_ψ are equal, and for the doubly-loaded loop:*

$$Y_A = (Y_0 + Y_2) + Y_4 + \frac{1}{2} Y_\psi \qquad \text{(III-35a)}$$

- - - - - - -

*See below, Eq. III-47.

$$Y_S = (Y_1 + Y_3) + \frac{1}{2} Y_\psi . \qquad \text{(III-35b)}$$

Here computations show that for $\Omega \geq 10$ the error involved in Y_A by neglecting $Y_4 + \frac{1}{2} Y_\psi$ is less than 8% for $2d \leq 0.13\lambda$ and drops to 2% for $2d \leq 0.06\lambda$. The error involved in Y_S by neglecting $\frac{1}{2} Y_\psi$ is about 30% and does not vary much with loop diameter.

Y_ψ was evaluated for the various loops actually used, and because it only enters in a sum with Y_L, it was necessary only to include it in the resistive loaded case, when Y_L had relatively small values, and then only in the computation of Y_S, since the largest loop used had $2d = .05\lambda$.

4. Singly-loaded circular loop

The series equivalent circuit of the receiving loop with a single load at $\theta = 0$ is similar to that of the dipole, discussed in Section II-1 above, and is shown in Fig. III-1d. End effect must again be included, and its actual values will be given below in Section III-7. However, for simplicity in the following discussion it will be neglected. It may be included in any equation here by replacing load quantities I_L, Y_L, etc., by apparent load quantities I'_L, Y'_L. The relationship between a full loop in free space and a half loop against an image plane is essentially the same as that between the dipole and unipole which has been discussed fully in Section II-4, so the discussion here will be in terms of the complete loop although it actually applies to both situations.

From the point of view of the current in the load it is permissible to use the shunt equivalent circuit of Fig. III-1e. This gives the current in the load Y_L:

$$I_{L0} = \frac{Y_L}{Y + Y_L} I_0 \qquad \text{(III-36)}$$

where Y is the input admittance of the loop when driven and I_0 is the short-circuit current at $\theta = 0$ from Eq. III-1. Noting Eq. III-13a, b, and defining the load admittance ratio for the singly-loaded loop as:

$$r^{(1)} = \frac{Y_L}{Y + Y_L} . \tag{III-37}$$

Equation III-36 can be replaced by:

$$I_{L0} = r^{(1)} S_B(c B^i_{y0}) + r^{(1)} S_E(E^i_{z0}) \tag{III-38a}$$

$$= S^{(1)}_B (c B^i_{y0}) + S^{(1)}_E(E^i_{z0}). \tag{III-38b}$$

This is the basic probe equation for the singly-loaded loop with load Y_L. It shows that the load current is made up of two components, one proportional to B_y, and the other to E_z. It shows also that a magnetic and an electric sensitivity constant can be defined for the loaded probe by multiplying the unloaded sensitivity constants of Eqs. III-21 by the load admittance ratio of Eq. III-37.

$$S^{(1)}_B = r^{(1)} S_B \tag{III-39a}$$

$$S^{(1)}_E = r^{(1)} S_E . \tag{III-39b}$$

The effectiveness of the loop as a magnetic probe depends upon the relative size of these constants, so it is convenient to define an error ratio:

$$\epsilon^{(1)} = \frac{S^{(1)}_E}{S^{(1)}_B} \tag{III-40}$$

which should be minimized for best operation.

If the loop is rotated 180 degrees, placing the load at $\theta = \pi$, Eqs. III-13e, f show that:

$$I_{L\pi} = S^{(1)}_B (c B^i_{y0}) - S^{(1)}_E (E^i_{z0}) . \tag{III-41}$$

Comparison of Eq. III-41 with Eq. III-38b suggests that $S_B^{(1)}$ and $S_E^{(1)}$ may be measured by measuring I_{L0} and $I_{L\pi}$ consecutively in a known field and adding and subtracting the results, the method which was in fact used. It further suggests that a pure magnetic or a pure electric response might be obtained by measuring I_{L0} and $I_{L\pi}$ simultaneously and adding or subtracting them electrically.

5. Doubly-loaded circular loop

The above considerations lead naturally to the concept of the loop with two loads, one at $\theta = 0$ and one at $\theta = \pi$. However, because the current at more than one point must be considered, a somewhat different analysis must be used. Only the case of equal loads will be studied since there appears to be no advantage in using unequal loads over using a single load.*

- - - - - - -

* The use of arbitrary loads leads to currents of the form:

$$I_A = S_{11}\, c\, B^i_{y0} + S_{12}\, E^i_{z0}$$

$$I_S = S_{21}\, c\, B^i_{y0} + S_{22}\, E^i_{z0}$$

where $S_{12} = S_{21} = 0$ only in the special case of equal loads. It is seen at once that I_A and I_S are not useful as measures of B and E in the general case. The total current in the load at $\theta = 0$ may be written:

$$I_{L0} = \frac{c\, B^i_{y0}(Y_{L\pi} + 2Y_S)\, S_B + E^i_{z0}(Y_{L\pi} + 2Y_A)\, S_E}{Y_{L\pi} + Y_A + Y_S + \frac{1}{Y_{L0}}(Y_{L\pi} Y_A + Y_{L\pi} Y_S + 4 Y_A Y_S)} .$$

Inspection shows that a particular choice of load can be made to eliminate the response to E or that to B. For example, setting $Y_{L\pi} = -2Y_A$ leads to

$$I_{L0} = \left[\frac{Y_{L0}(Y_{L\pi} + 2Y_S)}{(Y_S - Y_A)(Y_{L0} + 2Y_A)}\, S_B\right] c\, B^i_{y0}$$

from which it can be seen that I_{L0} is indeed a measure of B alone, as desired for a magnetic probe. The limitations of this method are purely practical: the accurate measurement of Y_A for a particular loop and the accurate production of $Y_{L\pi} = -2Y_A$. It might be possible to start with an estimated value

In Fig. III-2a, the doubly-loaded loop is indicated schematically, and in Fig. III-2b the loads have been replaced by equivalent generators, using the compensation theorem. This leads to an equation for the current at any point in the loop as the sum of the currents due to the unloaded receiving distributions and the transmitting distribution due to the two generators:

$$I(\theta) = E^i_{z0}\, i(\theta) - I_{L0}\, Z_L\, w(\theta) - I_{L\pi}\, Z_L\, w(\theta + \pi) \qquad \text{(III-42)}$$

where $i(\theta)$ is the unloaded receiving distribution given in Eq. III-2 and the transmitting distribution is given by a Fourier series in Storer's formulation [2]:

$$w(\theta) = \frac{1}{j\pi\zeta_0}\left\{\frac{1}{a_0} + \sum_1^\infty \frac{2}{a_n}\cos n\theta\right\} \qquad \text{(III-43)}$$

which can be rewritten in terms of admittances as:

$$w(\theta) = \sum_0^\infty Y_n \cos n\theta\ . \qquad \text{(III-44)}$$

Therefore:

$$I_{L0} = E^i_{z0} \sum_0^\infty v_n\, Y_n - I_{L0}\, Z_L \sum_0^\infty Y_n - I_{L\pi}\, Z_L \sum_0^\infty (-1)^n\, Y_n \qquad \text{(III-45a)}$$

$$I_{L\pi} = E^i_{z0} \sum_0^\infty (-1)^n\, v_n\, Y_n - I_{L0}\, Z_L \sum_0^\infty (-1)^n\, Y_n - I_{L\pi} Z_L \sum_0^\infty Y_n . \qquad \text{(III-45b)}$$

- - - - - - -

of $Y_{L\pi}$ and then make adjustments using a procedure similar to that for balancing the balanced loop, but if this is done, the method has no advantage over the use of balanced loads, and the disadvantage of being somewhat more difficult to achieve physically. This is because it is easier to adjust line stretchers and attenuators to balance two currents than it is to adjust tuners to present a particular impedance at a remote point with a (possibly lossy) length of line intervening.

These can be combined to give:

$$I_A = \frac{1}{2}(I_{L0} + I_{L\pi}) = \frac{Y_L}{Y_L + 2\sum_{n\ even} Y_n} \sum_{n\ even} v_n Y_n E^i_{z0} \qquad \text{(III-46a)}$$

$$I_S = \frac{1}{2}(I_{L0} - I_{L\pi}) = \frac{Y_L}{Y_L + 2\sum_{n\ odd} Y_n} \sum_{n\ odd} v_n Y_n E^i_{z0} \,. \qquad \text{(III-46b)}$$

Recalling the substitution of $c\,B^i_{y0}$ for E^i_{z0} in the antisymmetric current, Eq. III-12, using Eqs. III-13, and defining:

$$Y_A = \sum_{n\ even} Y_n \qquad \text{(III-47a)}$$

$$Y_S = \sum_{n\ odd} Y_n \qquad \text{(III-47b)}$$

and

$$r^{(2)}_A = \frac{Y_L}{Y_L + 2Y_A} \qquad \text{(III-48a)}$$

$$r^{(2)}_S = \frac{Y_L}{Y_L + 2Y_S} \qquad \text{(III-48b)}$$

the antisymmetric and symmetric currents can be written:

$$I_A = r^{(2)}_A S_B (c\,B^i_{y0}) \qquad \text{(III-49a)}$$

$$I_S = r^{(2)}_S S_E (E^i_{z0}) \qquad \text{(III-49b)}$$

and

$$I_A = S^{(2)}_B (c\,B^i_{y0}) \qquad \text{(III-50a)}$$

$$I_S = S^{(2)}_E (E^i_{z0}) \,. \qquad \text{(III-50b)}$$

The similarity between these and Eq. III-39 is obvious. Again magnetic and electric sensitivity constants are obtained by multiplying the unloaded sensitivities by the load admittance ratios, but here the two load admittance ratios are not equal.

$$S_B^{(2)} = r_A^{(2)} S_B \tag{III-51a}$$

$$S_E^{(2)} = r_S^{(2)} S_E \,. \tag{III-51b}$$

Again a loop error ratio is defined:

$$\epsilon^{(2)} = \frac{S_E^{(2)}}{S_B^{(2)}} \,. \tag{III-52}$$

It is to be remembered that the current in either load alone still contains both electric and magnetic components with their relative sizes governed by $\epsilon^{(2)}$, but, using an external circuit to add or subtract I_{L0} and $I_{L\pi}$, it is possible to obtain $2I_A$, which depends on the magnetic field alone, or $2I_S$, which depends on the electric field alone. Thus, although the error ratio of the probe is still finite*, the error of the entire system can be theoretically zero. In practice it is, of course, limited by the accuracy of the adder (or subtracter) circuit.† Furthermore, it is quite possible to use both the adder and the subtracter at once and have one output dependent only on B_y and another dependent only on E_z simultaneously.

A summary of the probe constants for very small circular loops is given in Table III-1.

- - - - - - -

*In fact $|\epsilon^{(2)}| > |\epsilon^{(1)}|$ in most cases as will be seen below.

†This is discussed in Chapter I, Sections 13 and 14.

Section B. Experiment

6. Experimental setup

The circular loop probes were studied by the image method as was the electric dipole. Half loop probes were mounted against the image plane in the free-space room with a quarter-wave unipole source at a distance of 1.4λ. Despite the closeness of the source, a test of probe loading by moving the source showed that even the largest probe does not load the source antenna measurably. The effect of curvature of the wavefront was less than 1% on the magnitude and 0.5 degree on the phase of $E_{\parallel}$ and $c\,B_N$. The wave differed from a plane wave in that $|E_{\parallel}|$ is 2% smaller than $|c\,B_N|$, and there is a radial electric field $E_{\perp}$ with a magnitude of 3% of $E_{\parallel}$. For the smaller probes, the plane-wave approximation was even better, so the only account taken of these effects was the use of the actual (near-zone) theoretical values of both $E_{\parallel}$ and $c\,B_N$ for normalization of the measured currents.

In order to measure the probe sensitivities, the probe current was measured with the load towards the source, and with it rotated to the opposite position as shown in Figs. III-3 and discussed in Section III-4 for the singly-loaded case. This procedure was also followed in the doubly-loaded case as shown in Fig. III-4 to obviate the need of balancing the two outputs for each new probe. A check for one probe showed that this gave identical results to the slower method of using the balance circuits for this measurement.

7. End effect

End effect is considered in essentially the same way as for the unipole (Section II-5), but here it must be considered more thoroughly because of the larger values of load resistance used.

The theoretical probe constants for comparison must now be calculated using the modified load admittance:

$$Y'_L = Y_L + Y_E \qquad \text{(II-14)}$$

where Y_E is the end effect admittance given by Eq. II-13. Calculation shows that Y_E is negligible within 1% in Y'_L for all loops using a 50 ohm line as load. When the load resistance is increased by using resistors in the line, Y_E becomes as large as 8% of Y_L if the value of Y_E calculated without the resistors present is accepted. The shape of the resistor is too complex to allow the end effect to be computed exactly in its presence, but a qualitative examination of the effects present (thinner center conductor and higher dielectric constant) indicates that it will not differ in order of magnitude, and that it will be smaller if anything. Nevertheless, this seemed too nebulous for calculation, so no end effect correction was made, and it remains a possible source of error for the larger loads.

In the calculation of sensitivity constants the admittance ratio is calculated from an equation of the type:

$$r_n = \frac{Y_L}{Y_L + Y_n} . \qquad \text{(III-53)}$$

If the sensitivity constants are defined in the presence of end effect so that they refer to the current delivered to the actual load and not the current at the base of the antenna, Eq. III-53 must be replaced by an equation of the type:

$$r'_n = \frac{Y_L}{Y_L + Y_E} \; \frac{Y_L + Y_E}{Y_L + Y_E + Y_n} \qquad \text{(III-54a)}$$

$$= \frac{Y_L}{Y_L + Y_E + Y_n} \qquad \text{(III-54b)}$$

where it is seen that the only difference is the presence of Y_E in the denomi-

nator. Since Y_L is predominantly real and Y_n is imaginary, the maximum error in using r_n instead of r'_n is 1% in magnitude and 4 degrees in phase, so that the error in neglecting Y_E is less than it seemed at first, and quite comparable with other errors in the experiment.

8. Normalization

The normalization was carried out in the same manner as for the unipole (Section II-7) with the addition that the theoretical value of $c\,B_N$ is assumed as 3.8 db/1 volt/meter while $E_{\|}$ is still assumed as 38.3 db/1 volt/meter as discussed in Section III-6. The over-all accuracy of normalization remains at 0.5 db.

9. Load resistors

In order to study the effect of varying load resistance on the probe sensitivity constants, various resistors were inserted in series with the center conductor of the coaxial line where it joins the loop (Fig. I-6). The resistors used were ordinary Ohmite 1/2 watt fixed composition resistors.

Since their high-frequency operation may differ greatly from that at low frequencies, it was necessary to measure the input impedance and the transmission coefficient of each resistor when mounted in operating position. Since two similar coaxial fittings were used to mount the image loops, these were removed from the mounting disc, one used as an adapter and the other, with a resistor inserted and the coaxial line to the receiver as load, was used as the unknown load. A variable short circuit was made to fit the open end of the first adapter which allowed the determination of its scattering matrix by Deschamps' method [5] (Fig. III-6a). Then the impedance of the resistor and the line were measured through the adapter junction [6] (Fig. III-6b). The

measured resistance and reactance are plotted in Fig. III-7 against the nominal resistance of the resistor plus 50 ohm line.

The transmission coefficient K of the resistor treated as a two-port network was also measured using the setup of Fig. III-6b, where $K = I_m / I_o$. Redrawing the circuit as in Fig. III-6c, the equations can be written:

$$I_m = I^i S_{21} \sum_0^\infty (S_{11} U_{22})^n \qquad \text{(III-55a)}$$

$$I_o = I^i \sum_0^\infty (S_{11} U_{22})^n - I^i S_{11} \sum_0^\infty (S_{11} U_{22})^n \qquad \text{(III-55b)}$$

where: I_m is the total current in the matched load,

I_o is the total current at the input to the resistor,

I^i is the current in the first incident wave,

S_{ij} are the elements of the scattering matrix of the resistor,

U_{22} is the reflection coefficient looking back toward the source.

Therefore, the transmission coefficient is independent of U_{22}:

$$K = \frac{S_{21}}{1 - S_{11}} . \qquad \text{(III-56)}$$

First, I_m was measured with no resistor, in which case $S_{21} = 1$, $S_{11} = 0$, giving:

$$I_{m0} = I^i . \qquad \text{(III-57)}$$

Second, I_m was measured with the resistor present, giving:

$$I_{m1} = I^i S_{21} \sum_0^\infty (S_{11} U_{22})^n . \qquad \text{(III-58)}$$

A fairly well matched source is required, in which case higher order terms in

U_{22} can be neglected. In the present case $|U_{22}| = .06$, so to a good approximation:

$$I_{m1} = I^i S_{21} (1 + S_{11} U_{22}) \quad , \tag{III-59}$$

or, combining with Eq. III-57 and solving for S_{21} :

$$S_{21} = \frac{I_{m1}}{I_{m0}} (1 + S_{11} U_{22})^{-1} \quad . \tag{III-60}$$

S_{11} is known by measurement of the load impedance of the resistor and line and U_{22} is known from the scattering matrix of adapter junction number 1, since the circuit ahead of that is matched. Using these values, Eq. III-56 can be solved for K .

Actually, $K' = 1/K$ was used as a correction factor to apply to the output meter readings to give the current flowing into the resistor, which is the current that would flow in a load attached directly to the loop.

10. Results

The experimental points fall on smooth curves with very few exceptions, so random errors due to probe construction and variations in experimental details were negligible. For loops with ($.02 \leq 2d/\lambda \leq .10$) the theoretical sensitivities are expected to be accurate to 0.1 db and 1 degree, but for smaller loops the one dimensional analysis breaks down since Ω becomes too small.* The experimental values may have systematic errors of 1 db and 5 degrees made up of: error in load resistance, 1 db and 1 degree; error in phase measurement, 3 degrees; error in amplitude measurement, 0.3 db; error due to

- - - - - - -

*See this effect for the unipole, Fig. II-3.

incident field variations, 0.1 db and 1 degree; and normalization error, 0.5 db in magnitude only.*

The experimental measurements of probe sensitivities S_B and S_E for a circular loop with 100 ohm load† and $a/\lambda = 1.984 \times 10^{-3}$ are plotted in Fig. III-8 against loop diameter, $2d/\lambda$, for both singly and doubly-loaded loops. The theoretical values as determined above are plotted on the same graphs, and the general agreement between theory and experiment is fairly good. The phases showed a mean deviation of 3 degrees or less and a maximum deviation of 6 degrees, about what is expected from the possible errors. The measured magnitudes of electric sensitivity are uniformly low by about 0.6 db except for the smallest doubly-loaded loops. Considering the very close agreement between theory and experiment for the sensitivity of an electric unipole under similar circumstances it seems likely that this is due to error in the absolute normalization. The magnetic sensitivities, on the other hand, show experimental magnitudes that are uniformly low by about 1.4 db for the singly-loaded and 1.1 db for the doubly-loaded loops. About 0.6 db could be attributed to normalization again, but 0.5-0.8 db discrepancy remains. This discrepancy occurred in measurements of S_B in general, and appears to be inherent in the theory or in the assumptions of the experiment. Various possible explanations were explored, but none was found adequate. The plot of the error ratios in Fig. III-9 shows essentially the same discrepancies, except that no normalization error is present, since it cancels out.

- - - - - - -

*There is no observable normalization error in phase since these were only relative measurements.

†Note that these were taken using a half loop with 50 ohm load over an image plane.

The effect of varying wire radius is shown in Figs. III-10, 11 and very little change is seen in the agreement between theory and experiment as a function of wire size. For the thickest wire and the smallest loops used, the experimental points diverge from the theory somewhat more than for the thinnest wire and moderate sized loops. This is to be expected since the one dimensional theory is less accurate for thicker antennas.

Figures III-12-14 show the effect of increasing load resistance, with probe sensitivity and error ratio plotted against nominal load resistance. Figure III-7 gives the actual load impedance for a half loop as a function of nominal load resistance. The values must be doubled for the complete loops. The measurements were made using loops with thick wire of the same diameter as the resistors. Measured magnetic sensitivity averages 1 db below the theory, but deviates from this considerably as the load resistance is increased, with values for small loops dropping as much as 2.3 db below the theory and values for larger loops increasing even to 0.5 db above the theory. The phase of $S_B^{(2)}$ for the doubly-loaded loop consistently leads the theoretical values by 5 degrees, but the measured phase of $S_B^{(1)}$ for the singly-loaded loops shows a variable behavior between lagging the theoretical phase by 3 degrees and leading it by 5 degrees. The electric sensitivity agrees closely in magnitude with the theory for small loads, but shows variable and increasing deviation for the larger loads, reaching as much as 0.5 db above and 1.5 db below the theory. The phase of $S_E^{(2)}$ agrees within 1 degree with the theory for small loads, but shows a steady increase in deviation with increasing resistance until it leads by 5 degrees for R_L = 800 ohm. For the singly-loaded loop, arg $S_E^{(1)}$ shows variable behavior, but the deviation tends to be greatest for large loops and the experimental value leads the theory by as much as 12 degrees in one case. The measurements of

the error ratio ϵ shown in Fig. III-11 show that $\epsilon^{(1)}$ is essentially independent of R_L as expected. On the other hand, $\epsilon^{(2)}$ does not show a constant difference from the theoretical curve, but one that varies systematically in a way that increases with the size of the loop and with the size of the load. This is clearly due to the variation in $S_E^{(2)}$. A look at the curves narrows down the source of error to the admittance ratio $r_S^{(2)}$, but it is not Y_S, since that would affect $\epsilon^{(1)}$, and it is not Y'_L as that would affect $S_B^{(2)}$ and $S_E^{(2)}$ in almost the same way. Furthermore, it is not due to end effect, which would be worse for small loops than large. The size of this deviation is within the tolerance of the experiment, but it is unfortunate that its source cannot be specifically named. Possibly it is due to some of the assumptions made in correcting for the transmission from the resistor to the receiver. The phase of $\epsilon^{(2)}$ varies with R_L as expected.

Section C. Conclusions

11. Conclusions

A look at Figs. III-7, 9, and 11 leads to several conclusions about the loop as a probe, since operation as a magnetic probe is enhanced by a low error ratio $|\epsilon|$.

For a singly-loaded loop, the error ratio $\epsilon^{(1)}$ is independent of load impedance, and for convenient wire radii, it is independent of wire size as well. However, the error ratio decreases markedly with loop diameter, going from about 80% at $2d = 0.1\lambda$ to about 8% at $2d = 0.01\lambda$. From this it is concluded that a singly-loaded probe should be smaller than 0.01λ in diameter if it is in a position where the electric dipole mode may be excited.

For a doubly-loaded loop, there is a minimum error ratio of about 55% for a loop diameter of about 0.04λ. The error ratio $\epsilon^{(2)}$ is a function of the load impedance and the wire size, with small wire and small loads reducing the value of $\epsilon^{(2)}$. The measurement error in a system using the doubly-loaded loop is much less than $\epsilon^{(2)}$, by an amount dependent upon the isolation between modes in the balun detector system. If this is accurate to 20 db, the over-all error ratio would be 6% for a probe of optimum size, $2d = 0.04\lambda$, as good as a singly-loaded probe of diameter $2d = 0.005\lambda$. If the balun detector can be made accurate to 30 db, the over-all error ratio drops to 2%, as good as a singly-loaded probe of diameter $2d = 0.002\lambda$, very small indeed!

Bibliography, Chapter III

1. King, Ronold W. P., and Charles W. Harrison, Jr., Electromagnetic Radiation, Chapter X (book to be published).

2. Storer, James, E., "Impedance of Thin Wire Loop Antenna," Cruft Laboratory Technical Report No. 212, Harvard University, p. 9 (May 1955).

3. Jahnke, Eugene, and Fritz Emde, Tables of Functions, pp. 211-217, Dover, New York (1945).

4. Wu, Tai Tsun, "Theory of the Thin Circular Loop Antenna," Cruft Laboratory Technical Report No. 361, Harvard University (April 1962).

5. Deschamps, G. A., "Determination of Reflection Coefficient and Insertion Loss of a Waveguide Junction," Journal of Applied Physics, Vol. 24, pp. 1046-50 (August 1953).

6. King, Ronold W. P., Transmission Line Theory, pp. 314-317, McGraw-Hill, New York (1955).

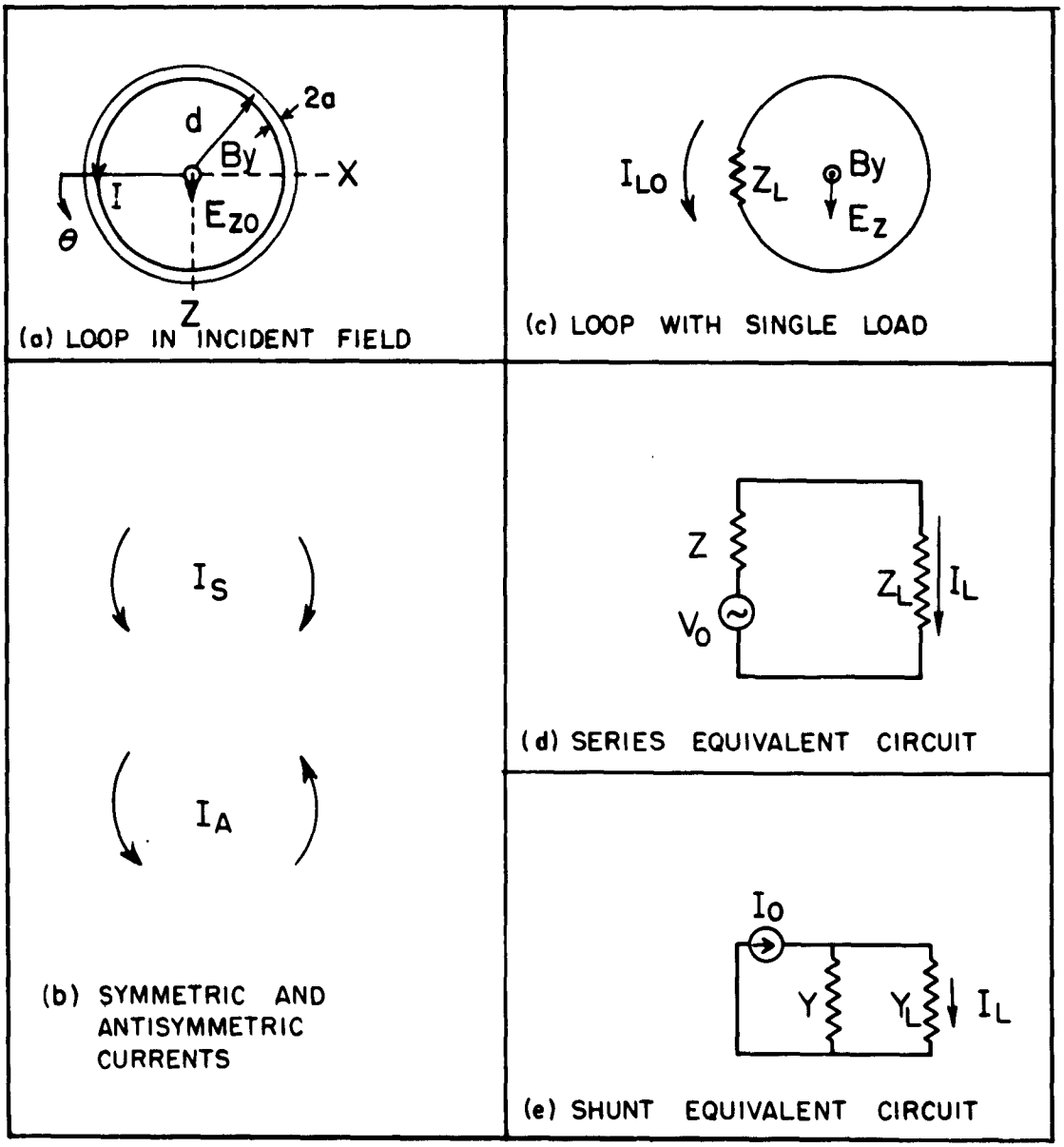

III-1 CIRCULAR RECEIVING LOOP

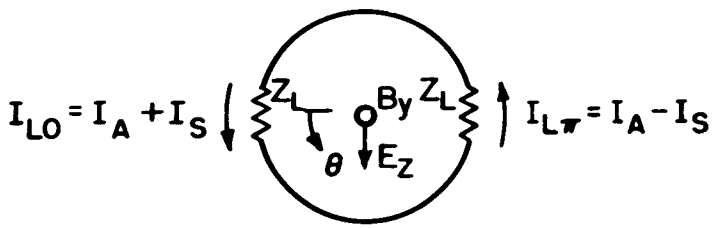

III-2a CIRCULAR LOOP WITH DOUBLE LOAD

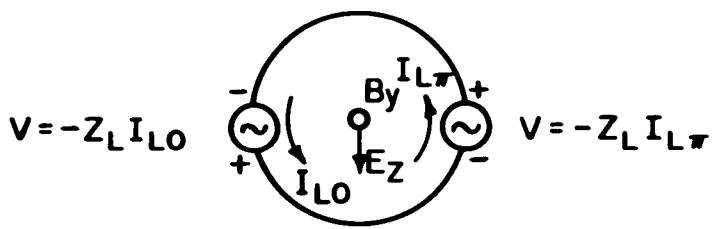

III-2b CIRCULAR LOOP WITH EQUIVALENT GENERATORS

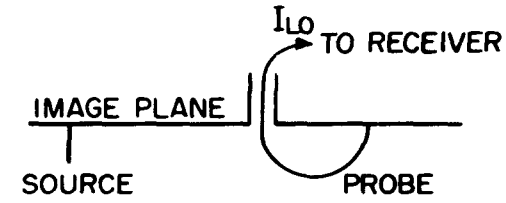

(a) PROBE ANGLE 0°

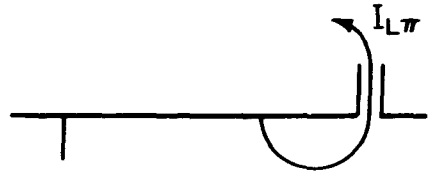

(b) PROBE ANGLE 180°

III-3 *SINGLE LOADED IMAGE LOOP*

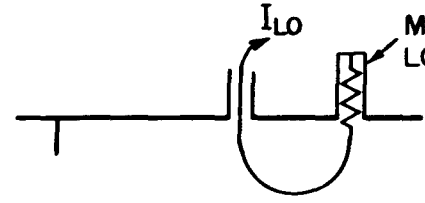

(a) PROBE ANGLE 0°

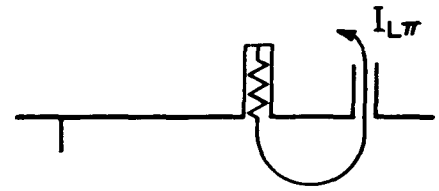

(b) PROBE ANGLE 180°

III-4 *DOUBLE LOADED IMAGE LOOP*

(a) SINGLE LOAD

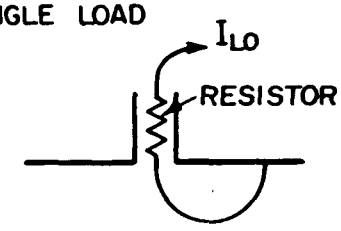

(b) DOUBLE LOAD

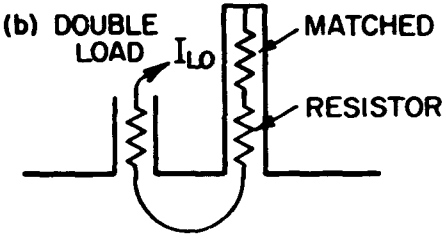

III-5 *IMAGE LOOPS WITH RESISTORS INSERTED*

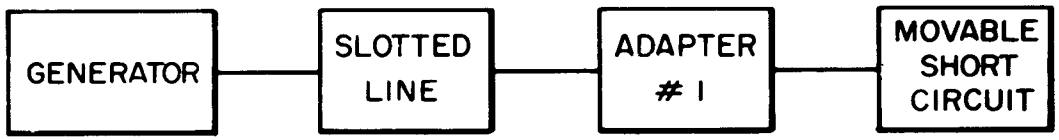

III-6a MEASURING SCATTERING MATRIX OF ADAPTER

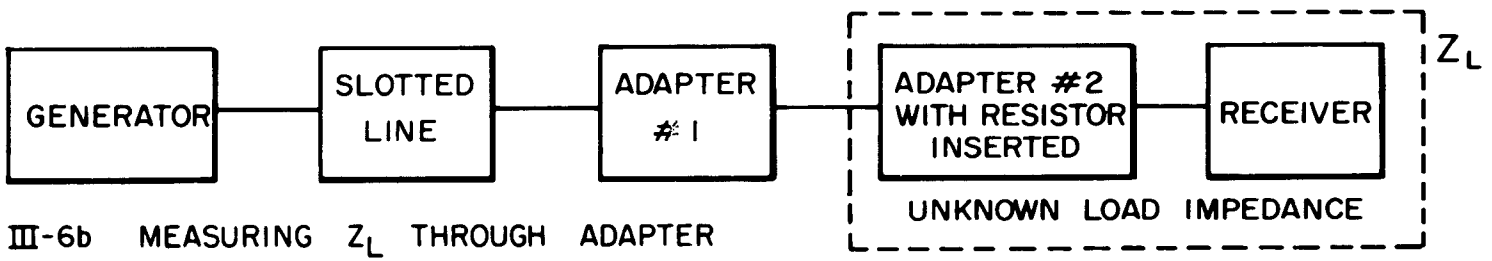

III-6b MEASURING Z_L THROUGH ADAPTER

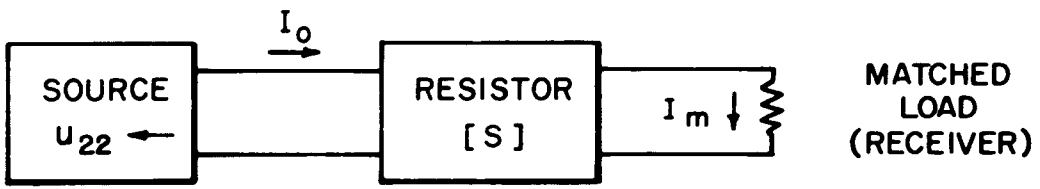

III-6c MEASURING TRANSMISSION COEFFICIENT OF RESISTOR

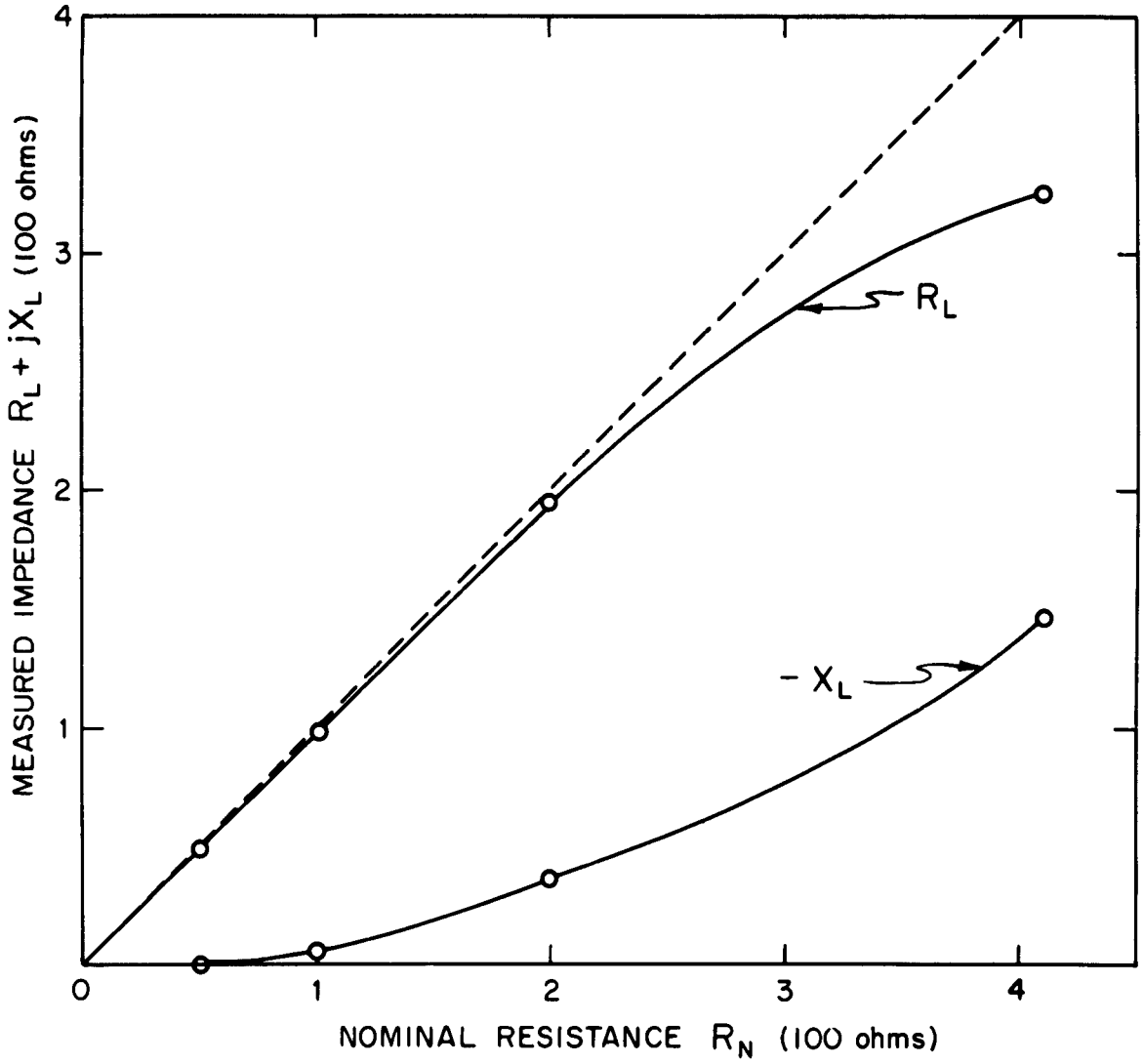

III-7 IMPEDANCE OF RESISTORS TERMINATED IN A MATCHED LINE

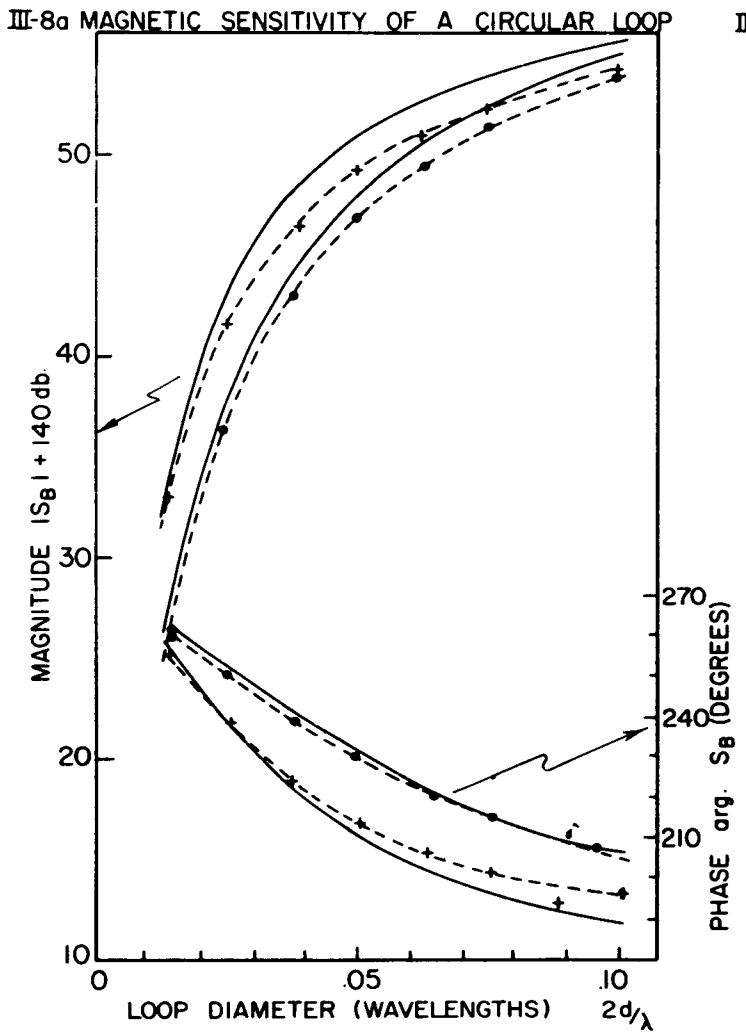
III-8a MAGNETIC SENSITIVITY OF A CIRCULAR LOOP
MAGNITUDE $|S_B| + 140$ db
PHASE arg. S_B (DEGREES)
LOOP DIAMETER (WAVELENGTHS) $2d/\lambda$
50
40
30
20
10
0
.05
.10
270
240
210

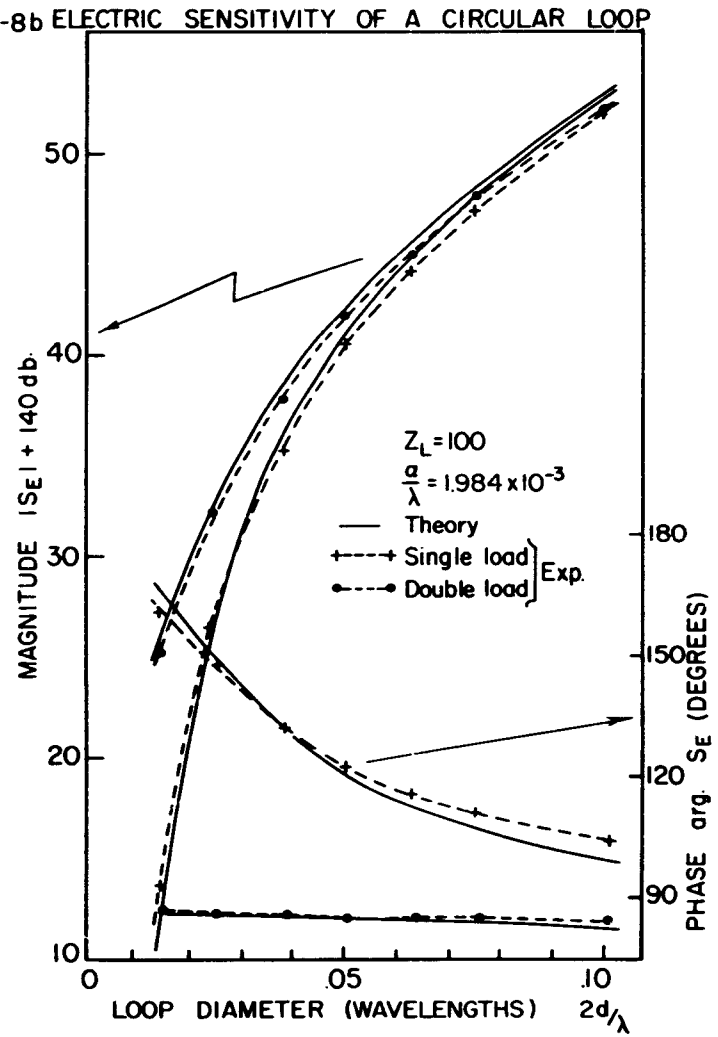
III-8b ELECTRIC SENSITIVITY OF A CIRCULAR LOOP
MAGNITUDE $|S_E| + 140$ db
PHASE arg. S_E (DEGREES)
LOOP DIAMETER (WAVELENGTHS) $2d/\lambda$
$Z_L = 100$
$\frac{a}{\lambda} = 1.984 \times 10^{-3}$
Theory
Single load
Double load
Exp.
50
40
30
20
10
0
.05
.10
180
150
120
90

III-9 ERROR RATIO OF A CIRCULAR LOOP

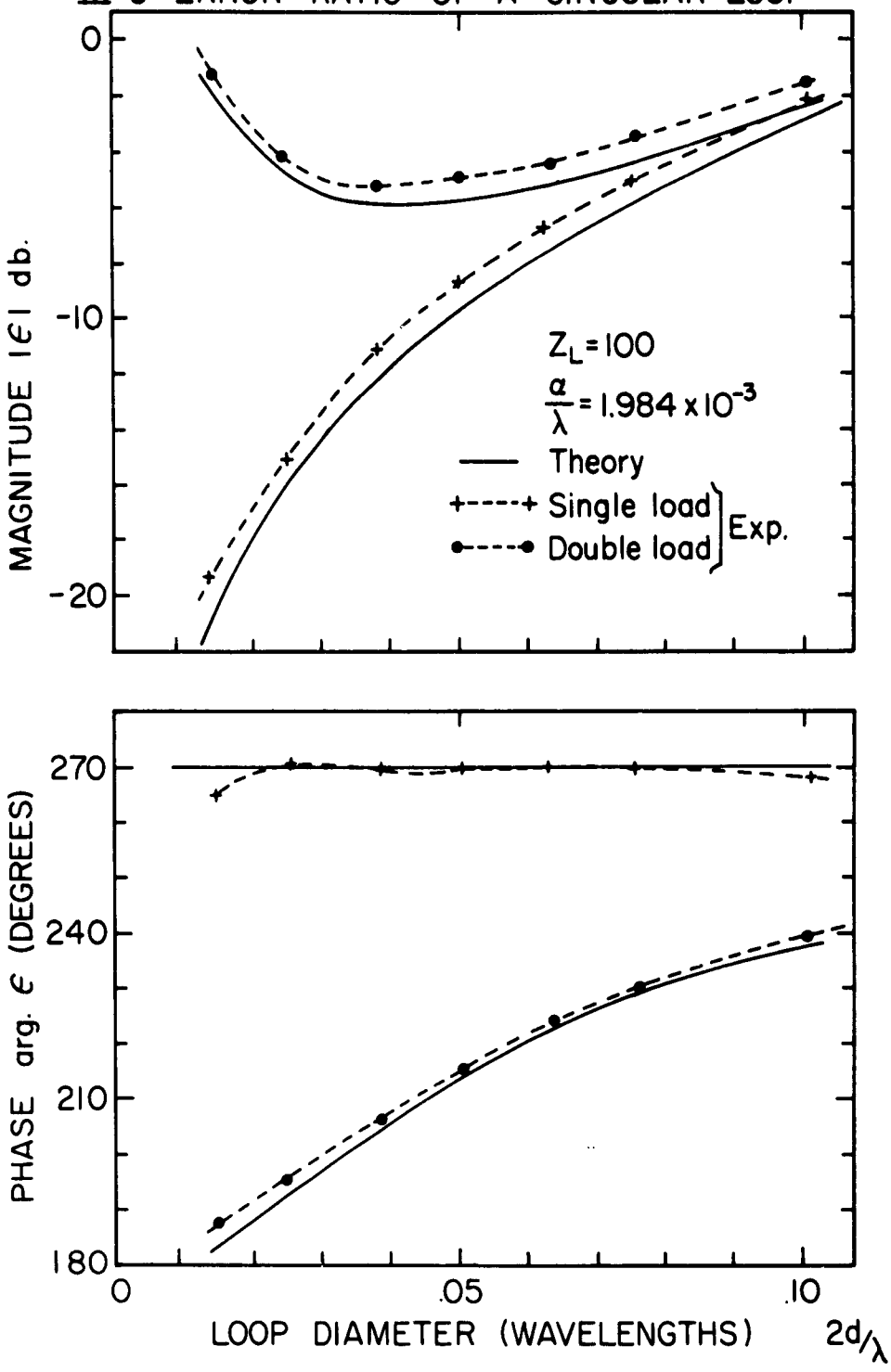

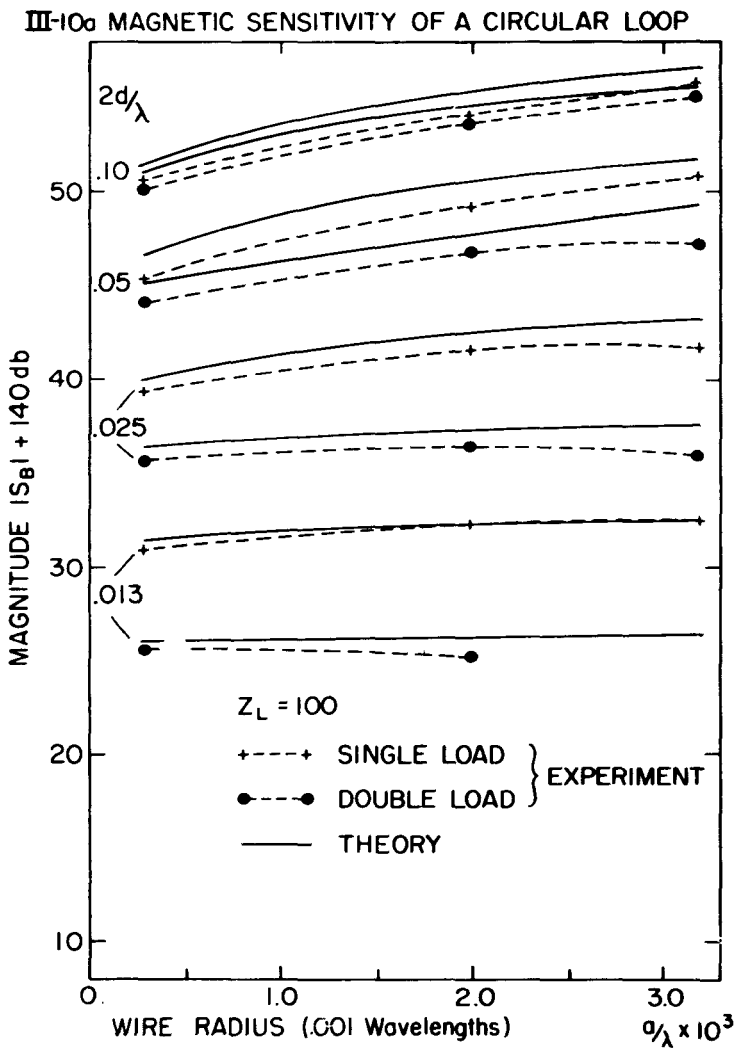
III-10a MAGNETIC SENSITIVITY OF A CIRCULAR LOOP
2d/λ
.10
.05
.025
.013
MAGNITUDE |S_B| + 140 db
50
40
30
20
10
0
1.0
2.0
3.0
WIRE RADIUS (.001 Wavelengths)
a/λ x 10^3
Z_L = 100
SINGLE LOAD
DOUBLE LOAD
EXPERIMENT
THEORY

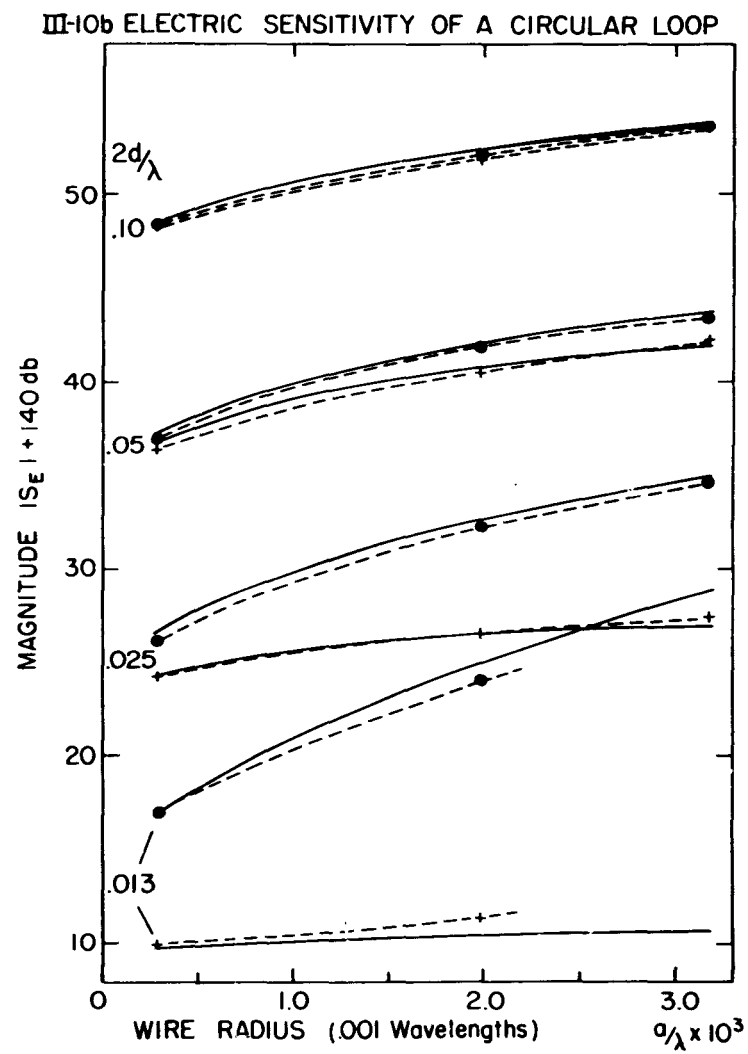
III-10b ELECTRIC SENSITIVITY OF A CIRCULAR LOOP
2d/λ
.10
.05
.025
.013
MAGNITUDE |S_E| + 140 db
50
40
30
20
10
0
1.0
2.0
3.0
WIRE RADIUS (.001 Wavelengths)
a/λ x 10^3

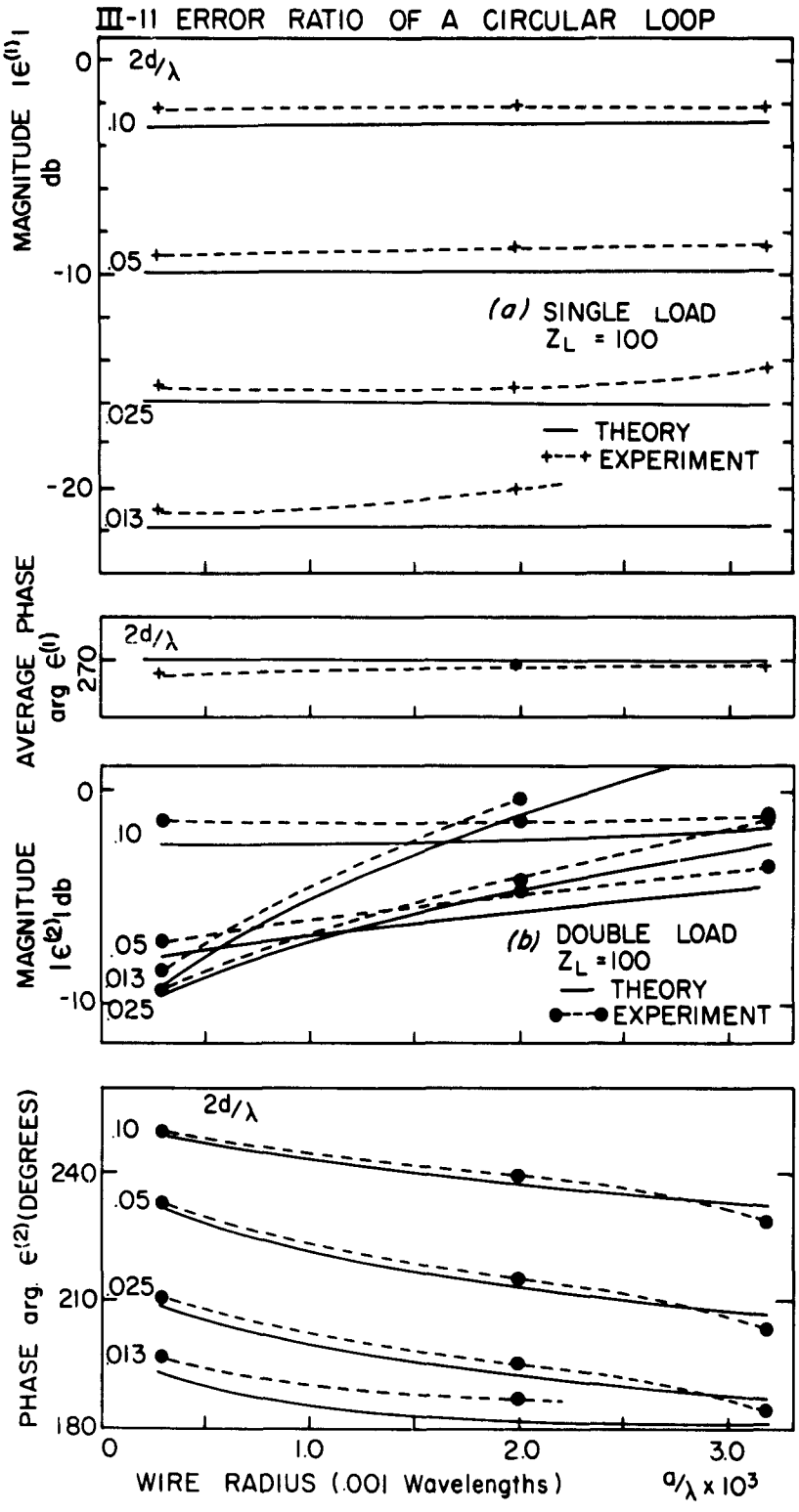
III-11 ERROR RATIO OF A CIRCULAR LOOP
MAGNITUDE $|\epsilon^{(1)}|$ db
0
-10
-20
2d/λ
.10
.05
.025
.013
(a) SINGLE LOAD
Z_L = 100
THEORY
EXPERIMENT
AVERAGE PHASE arg $\epsilon^{(1)}$
270
2d/λ
MAGNITUDE $|\epsilon^{(2)}|$ db
0
-10
.10
.05
.013
.025
(b) DOUBLE LOAD
Z_L = 100
THEORY
EXPERIMENT
PHASE arg. $\epsilon^{(2)}$ (DEGREES)
240
210
180
2d/λ
.10
.05
.025
.013
0
1.0
2.0
3.0
WIRE RADIUS (.001 Wavelengths)
$a/\lambda \times 10^3$

III-12 MAGNETIC SENSITIVITY OF A CIRCULAR LOOP

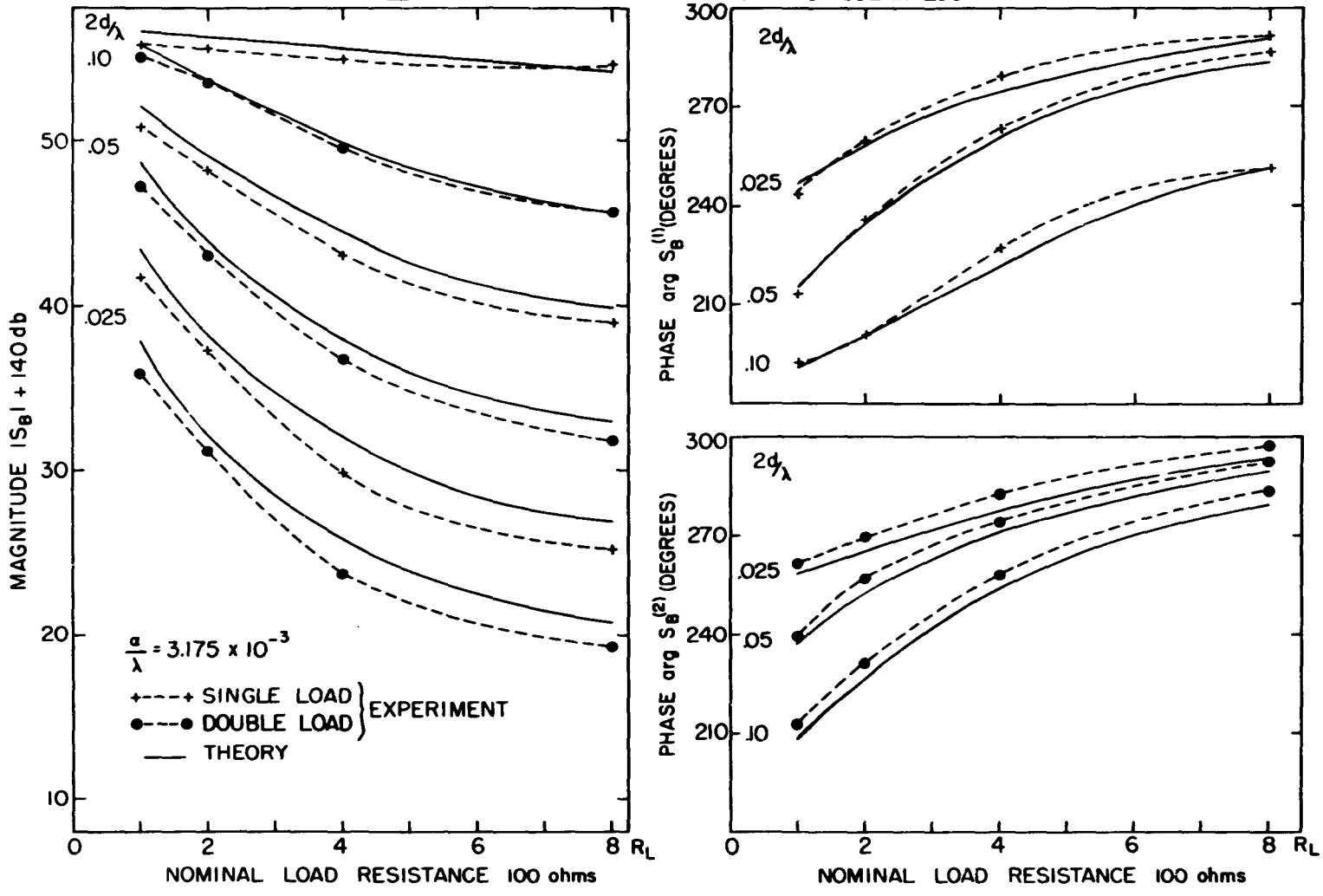

III-13 ELECTRIC SENSITIVITY OF A CIRCULAR LOOP

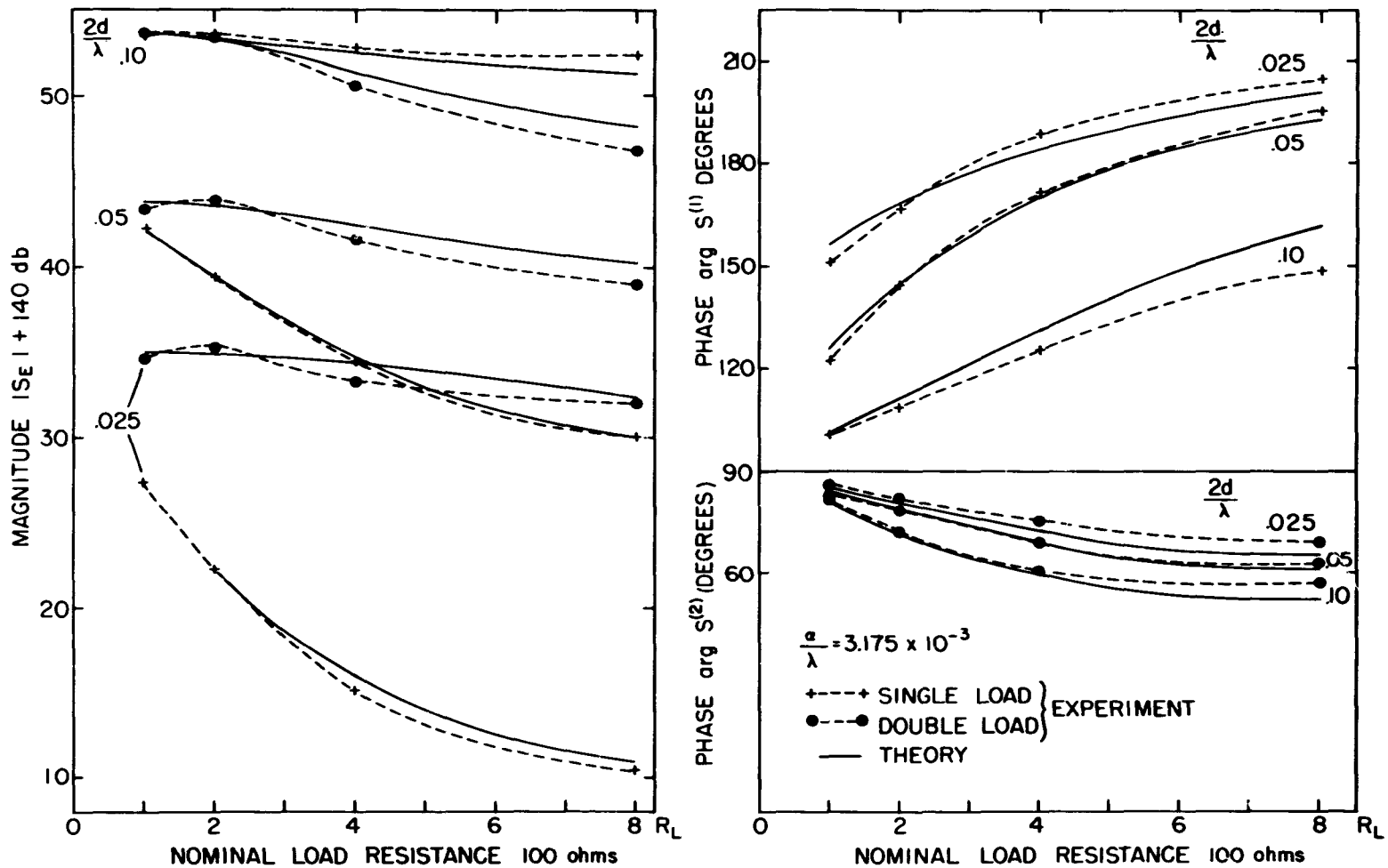

III-14 ERROR RATIO OF A CIRCULAR LOOP

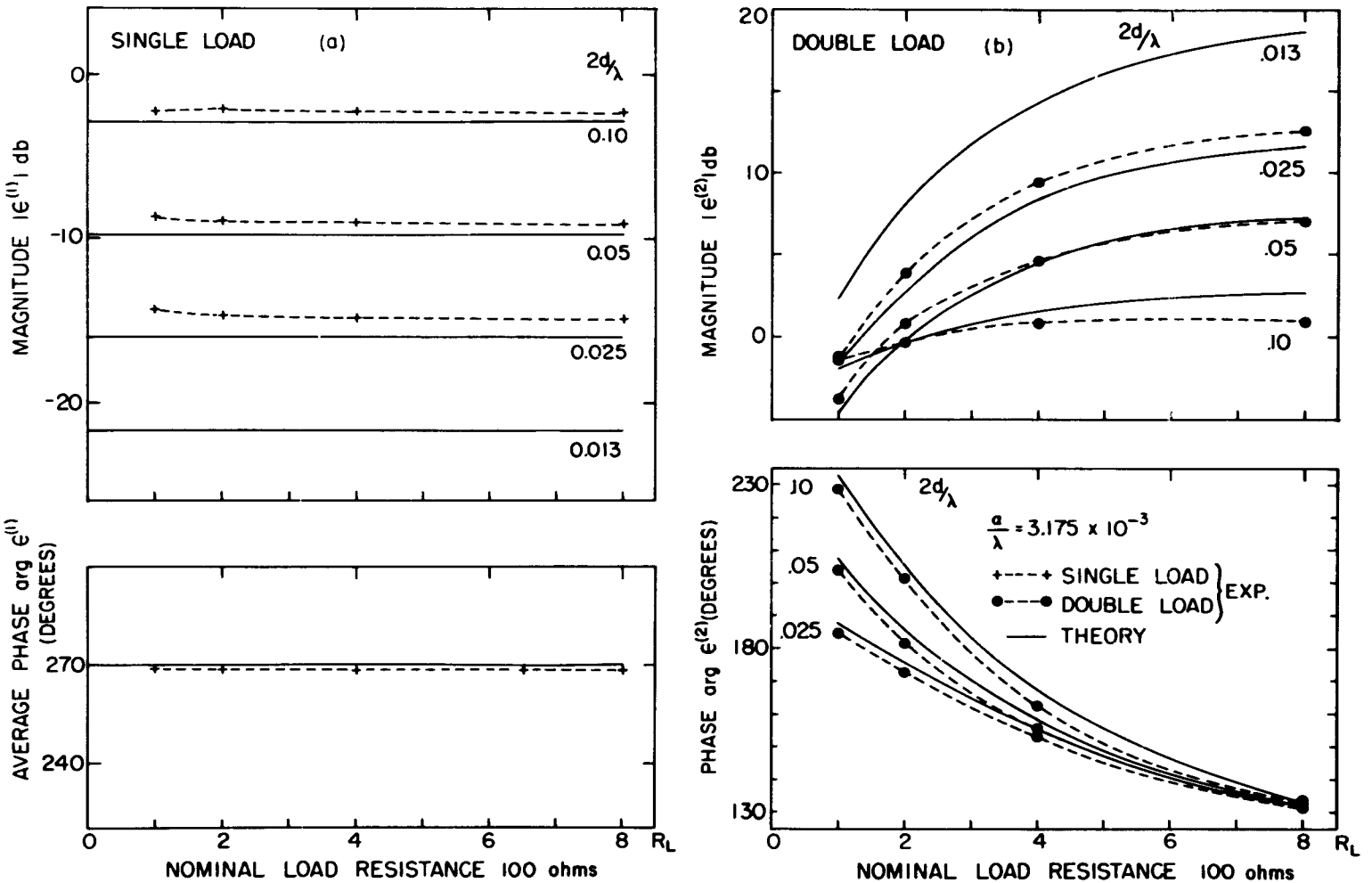

TABLE III-1

Probe Constants for Small Circular Loops

(Approximate Expressions for $a^2 << d^2$, $4k^2d^2 << 1$)

Single Load, Y_L

$$S_B^{(1)} \doteq \frac{Y_L}{Y_L - j\,[30k\,(2\pi d)\,(\Omega - 3.5)]^{-1}} \cdot \frac{(-2\pi d)}{\zeta_0(\Omega - 3.5)}$$

$$S_E^{(1)} \doteq \frac{Y_L}{Y_L - j\,[30k\,(2\pi d)\,(\Omega - 3.5)]^{-1}} \cdot \frac{j\,2\,(2\pi d)^2}{\lambda\,\zeta_0(\Omega - 3.5)}$$

$$\epsilon^{(1)} \doteq -j\,\frac{2}{\lambda}\,(2\pi d)$$

Double Load, Y_L each

$$S_B^{(2)} \doteq \frac{Y_L}{Y_L - j.\,2\,[30k\,(2\pi d)\,(\Omega - 3.5)]^{-1}} \cdot \frac{(-2\pi d)}{\zeta_0(\Omega - 3.5)}$$

$$S_E^{(2)} \doteq \frac{Y_L}{Y_L + j\,2\,[30\pi\,(\Omega - 3.5)\,\frac{\lambda}{2\pi d}]^{-1}} \cdot \frac{j\,2\,(2\pi d)^2}{\lambda\,\zeta_0(\Omega - 3.5)}$$

$$\epsilon^{(2)} \doteq [1 - j\,\frac{Z_L}{15k\,(2\pi d)\,(\Omega - 3.5)}] \cdot [-j\,\frac{2}{\lambda}\,(2\pi d)]$$

CHAPTER IV. THE SQUARE LOOP AS A PROBE

Section A. Theory

1. Rectangular loops

The square loop is only a special case of the rectangular loop, but as previous studies [1] have shown, it is the optimum shape for minimizing the averaging error for a given magnetic sensitivity in a general incident field. The criterion for negligible averaging error in a rectangular loop with sides 2c and 2d is the criterion for an electrically small loop in both dimensions, and is similar to the one for the circular loop, Eq. III-17:

$$\frac{1}{2} k_{1\max} c^2 << 1 \quad \text{and} \quad \frac{1}{2} k_{2\max} d^2 << 1 . \qquad \text{(IV-1)}$$

It will be shown below that for small loops, the magnetic sensitivity is proportional to the loop area:

$$S_B \propto cd . \qquad \text{(IV-2)}$$

Therefore, if $k_{1\max} = k_{2\max}$, that is, if the highest frequency required in the Fourier expansion of the field along one side of the loop is equal to the highest frequency required along the perpendicular side, a square provides maximum S_B with minimum averaging in both directions at once. It is obvious that if, for example, $k_{1\max} > k_{2\max}$, the rectangle should have $c^2 < d^2$ in the same ratio for optimum operation. In this analysis only the square loop is discussed, but extension to the rectangular loop is straightforward.

2. The unloaded loop in a plane wave field (Fig. IV-1a)

For the square loop, the Fourier expansion used for the circular loop does not apply since the tangential electric field is discontinuous at the corners. However, the current can be separated again into symmetric and antisymmetric

modes with respect to the z direction as in Fig. IV-1b:

$$I_S\left(\tfrac{1}{2}s_t - s\right) = -I_S(s) \qquad \text{(IV-3a)}$$

$$I_A\left(\tfrac{1}{2}s_t - s\right) = I_A(s) \qquad \text{(IV-3b)}$$

$$I(s) = I_S(s) + I_A(s) \qquad \text{(IV-3c)}$$

where s_t is the total loop perimeter. The symmetric current is again due to the symmetric electric field E^i_{ZS} and the antisymmetric current to the antisymmetric field E^i_{ZA} and therefore to the normal magnetic field c B^i_y. Therefore:

$$I_S(0) = S_E(E^i_{Z0}) \qquad \text{(IV-4a)}$$

$$I_A(0) = S_B(c\ B^i_{y0}) \qquad \text{(IV-4b)}$$

defining the probe sensitivity constants as before.

3. The unloaded loop in an arbitrary incident field

As written in Eqs. IV-4, S_E and S_B are functions of the incident field configuration, but they may be considered constants of the probe geometry alone for electrically small loops with:

$$\tfrac{1}{2}k^2_{max}\,d^2 << 1\ . \qquad \text{(IV-5)}$$

The justification for this is the same as in Section III-2 for the circular loop.

4. Evaluation of constants

The probe sensitivity constants S_E and S_B must now be derived. From Maxwell's equations and the definition of vector potential, an integral equation can be written for the contour of the loop, where a is the area and s is the perimeter:

$$-j\omega \int_{a} \vec{B} \cdot d\vec{a} = \oint \vec{E} \cdot d\vec{s} \,. \qquad \text{(IV-6)}$$

The magnetic field is the sum of the incident field and the reradiated field due to current in the wire:

$$\vec{B} = \vec{B}^{i} + \vec{B}^{r} \qquad \text{(IV-7)}$$

from which:

$$-j\omega \int_{a} \vec{B}^{i} \cdot d\vec{a} = \oint \vec{E} \cdot d\vec{s} + j\omega \oint \vec{B}^{r} \cdot d\vec{a} \,. \qquad \text{(IV-8)}$$

In the integral formulation any contribution of I_S vanishes, and Ohm's law for the antisymmetric current gives:

$$E_A = I_A Z^{i} \,. \qquad \text{(IV-9)}$$

From Helmholtz's integral and the definition of the vector potential:

$$\vec{B}^{r} = \nabla \times \vec{A}^{r} = \nabla \times \frac{\mu_0}{4\pi} \oint I \frac{e^{-jkR}}{R} d\vec{s} \qquad \text{(IV-10)}$$

and by substitution in Eq. IV-8:

$$-j\omega \int \vec{B}^{i} \cdot d\vec{a} = \oint I_A Z^{i} \, ds + \frac{j\omega\mu_0}{4\pi} \oint\oint I_A \frac{e^{-jkR}}{R} d\vec{s} \cdot d\vec{s} \,. \qquad \text{(IV-11)}$$

For a small enough loop the current around the loop is a constant, and for the small circular loop the dominant antisymmetric term in the Fourier series for the current is a constant current. Therefore, the zeroth-order antisymmetric current in the square loop is also assumed to be a constant so that I_A can be brought out from under the integral sign in Eq. IV-11. When this is done, the remaining integrals are by definition the (low frequency) input impedance of the loop when driven:

$$\frac{1}{Y_0} = Z_0 = \oint Z^{i} \, ds + j \frac{\omega\mu_0}{4\pi} \oint\oint \frac{e^{-jkR}}{R} d\vec{s} \cdot d\vec{s} \,. \qquad \text{(IV-12)}$$

For small loops, as has already been shown from the Taylor series expansion for the incident field in Section III-2:

$$B^i \doteq B_0^i + x\left[\frac{\partial B^i}{\partial x}\right]_0 + z\left[\frac{\partial B^i}{\partial z}\right]_0 \quad , \tag{IV-13}$$

and Eq. IV-11 may be solved for I_A :

$$I_A \doteq -j\omega \, a \, Y_0 \, B_{y0}^i \, . \tag{IV-14}$$

Comparison with Eq. IV-4b gives:

$$S_B = -j \, k \, a \, Y_0 \, . \tag{IV-15}$$

This is the first term of an expansion similar to Eq. III-21a. There, for the circular loop with $2d \leq .13\lambda$, the next term in the series produces less than a 4% correction. Presumably, Eq. IV-15 is also accurate to about 4%.

The evaluation of Eq. IV-12 is straightforward [2] when the exponential is approximated by $(1 - jkR - \frac{1}{2}k^2 R^2)$. The internal impedance and the radiation resistance are found to be negligible compared to the external self inductance, leaving:

$$Y_0 \doteq \left\{ j \, \zeta_0 \, \frac{1}{\pi} (k2d) \left[\Omega - 4.32 + 0.37 \, (k2d)^2 \right] \right\}^{-1} \tag{IV-16}$$

where $\Omega = 2\ell n \, \frac{8d}{a}$.

Comparison with Eq. III-21a shows that the excitation voltage per unit field for the zero mode is

$$v_0 = -j \, k \, a \tag{IV-17}$$

and

$$S_B \doteq v_0 \, Y_0 \, . \tag{IV-18}$$

This formulation gives no information whatsoever about the symmetrical current I_S , which vanishes in the line integrals of Eq. IV-11. For this purpose

the loop can be broken at the two points $x = 0$ where $I_S = 0$ and considered as an array of two U-shaped antennas as in Fig. IV-1c.

The excitation voltage per unit field (effective length) of this receiving array may be found from the characteristics of the same array when transmitting, using a formula obtained by application of the Rayleigh-Carson reciprocal theorem to a two-port passive system consisting of the given array with a short dipole antenna in the far zone field [3]:

$$v_S = \frac{2}{k} F_{0S} \tag{IV-19}$$

where F_{0S} is the far-zone field function evaluated at $\theta = \pi/2$ for the array driven by symmetric currents only (Fig. IV-1d). By definition:

$$F_{0S} = \frac{2\pi R_0}{j \zeta_0 I_{z0} e^{-jkR_0}} [E_\theta^r]_{\theta = \pi/2} \tag{IV-20}$$

but

$$[E_\theta^r]_{\pi/2} = \frac{-jk \zeta_0}{4\pi} \int_{\text{both halves}} \frac{e^{-jkR}}{R} I_z \, dz \tag{IV-21}$$

from the Helmholtz integrals and the definitions of the potential functions, since only currents parallel to the z axis contribute to the tangential field at $\theta = \pi/2$. These three equations combine to give:

$$v_S = \frac{2 \cos kd}{I_{z0}} \int_{-d}^{d} I_z \, dz \, . \tag{IV-22}$$

In order to solve Eq. IV-22, the transmitting distribution of current $I_z(z)$ must be known. The problem of the symmetrically driven loop has been solved by iteration of the integral equations for the current [4] in a manner similar to that used for the single dipole. The solution gives the current as the quotient

of two series in inverse powers of the expansion parameter Ψ_S . For calculation of the far-zone field along the midplane the zeroth-order current distribution should be adequate. This is:

$$I_S(s) = I_S(0) \frac{\sin k\,(2d - |s|)}{\sin k\,2d} \qquad \text{(IV-23)}$$

which is substituted into Eq. IV-22, leading to an expression for the symmetric excitation voltage for the entire loop:

$$V_S = \frac{2}{k} \frac{\cos kd - \cos k\,2d}{\sin kd} . \qquad \text{(IV-24)}$$

The same theory gives the first-order symmetric admittance of the entire loop:

$$Y_S = \left\{ \frac{-j\,\zeta_0\,\Psi_S\,(\cos k\,2d + D_1/\Psi_S)}{\pi\,(\sin k\,2d + B_1(0)/\Psi_S)} \right\}^{-1} \qquad \text{(IV-25)}$$

where, assuming that $a^2 << d^2$:

$$\Psi_S = \Big| C_a(2d,\,0) + C_{2d}(2d,\,0) - 2\,C_{2d}(d,\,0) - \frac{2}{k}\left[\left(\frac{e^{-jk2d}}{2d} + \frac{e^{-jk2\sqrt{2d}}}{2\sqrt{2d}}\right)\sin k\,2d - 2\,\frac{e^{-jk\sqrt{5d}}}{\sqrt{5d}}\sin kd\right]\Big| \qquad \text{(IV-26)}$$

with

$$C_i(h_i\,0) = \int_{-h}^{h} \frac{e^{-jk\sqrt{Z^2 + i^2}}}{\sqrt{Z^2 + i^2}} \cos kZ\, dZ . \qquad \text{(IV-27)}$$

Integrals of this form must be evaluated by numerical methods, and have not been tabulated for the small values of h involved here. For small kd , these integrals and the other functions in Eq. IV-26 can be expanded in power series. Examination of the second and third-order terms shows that they may be neglected within 6% for $2d/\lambda \leq 1.25$. The first-order term is zero, and the zeroth-order value of Ψ_S is:

$$\Psi_S \doteq 2 \sinh^{-1} \frac{2d}{a} - 1.786 \qquad \text{(IV-28a)}$$

which may be rewritten for $a << d$ as:

$$\Psi \doteq \Omega - 3.172 . \qquad \text{(IV-28b)}$$

Calculation shows that the numerical values of Ψ_S are rather small, ranging from about 3 for small loops to about 8 for the largest loops used. For this reason it would be necessary to evaluate D_1 and $B_1(0)$ in Eq. IV-25 to get better than 25% accuracy in the impedance. Unfortunately, these are very complex functions involving small differences of large quantities, which are mostly integrals that must be integrated numerically. Since this study was not concerned with the input impedance of a symmetrically driven loop as such, but with its over-all behavior as a probe, it was not felt that undertaking such a large problem in numerical analysis would give results of value in proportion to the effort involved. Therefore, it was decided to use the zeroth-order symmetric impedance. In this case, a small loop approximation could again be made, leaving:

$$Y_S = j \frac{\pi k 2d}{\zeta_0 \Psi_S} \qquad \text{(IV-29)}$$

with 25% accuracy, and where Ψ_S is to be evaluated using Eq. IV-28b. The electric sensitivity of the square loop can now be written,*

$$S_E = v_S Y_S \qquad \text{(IV-30)}$$

where v_S is given by Eq. IV-24 and Y_S by Eq. IV-29.

5. Singly-loaded square loop

The use of a single load with a square loop may be dealt with in the

- - - - - - -

*Note that this analysis has formally included all the symmetric modes of the Fourier series approach, although the use of zeroth-order approximations is no doubt equivalent to neglecting most of the higher modes.

same way as for the circular loop, using the same equivalent circuit. The current in the load is again:

$$I_L = S_B^{(1)} \, c \, B_{y0}^i + S_E^{(1)} \, E_{z0}^i \qquad \text{(III-38b)}$$

where the loaded loop sensitivities are given by the products of the load admittance ratio and the unloaded loop sensitivities:

$$S_B^{(1)} = r^{(1)} \, S_B \qquad \text{(III-39a)}$$

$$S_E^{(1)} = r^{(1)} \, S_E \qquad \text{(III-39b)}$$

and where the load admittance ratio is given by:

$$r^{(1)} = \frac{Y_L}{Y + Y_L}. \qquad \text{(III-37)}$$

Since Y is the total input admittance of the loop when driven, it is the sum of the admittances of all the individual modes connected in parallel:

$$Y \doteq Y_0 + Y_S. \qquad \text{(IV-31)}$$

The error ratio for the singly-loaded loop is again independent of the load impedance

$$\epsilon^{(1)} = \frac{S_E^{(1)}}{S_B^{(1)}}. \qquad \text{(III-40)}$$

6. Doubly-loaded square loop

In this case the analysis could, in principle, be carried out using the Fourier series for the current as was done for the circular loop. However, the complete Fourier series has not actually been derived, nor is it needed, for the results depend only on the unloaded loop sensitivities which have been obtained by other means, the symmetric and antisymmetric admittances, for

which at least zeroth-order approximations have been derived, and the load admittance. The results are:

$$I_A = \frac{1}{2}(I_{L1} + I_{L2}) = S_B^{(2)}\, c\, B_{y0}^i \tag{IV-32a}$$

$$I_S = \frac{1}{2}(I_{L1} + I_{L2}) = S_E^{(2)}\, E_{z0}^i \tag{IV-32b}$$

where

$$S_B^{(2)} = r_A^{(2)}\, S_B \tag{III-51a}$$

$$S_E^{(2)} = r_S^{(2)}\, S_E \tag{III-51b}$$

$$r_A^{(2)} = \frac{Y_L}{Y_L + 2Y_A} \tag{III-48a}$$

$$r_S^{(2)} = \frac{Y_L}{Y_L + 2Y_S}\,. \tag{III-48b}$$

The symmetric admittance Y_S is determined by Eq. IV-29, and the antisymmetric admittance Y_A is approximated by Y_0, the admittance of the zeroth-order mode, from Eq. IV-16.

The error ratio for the doubly-loaded loop is a function of the load admittance:

$$\epsilon^{(2)} = \frac{r_S^{(2)}\, S_E}{r_A^{(2)}\, S_B} = \frac{Y_L + 2Y_A}{Y_L + 2Y_S}\,\epsilon^{(1)}. \tag{IV-33}$$

The same remarks as in Section III-5 apply to the system error ratio as distinct from the loop error ratio.

A summary of the probe constants for very small square loops is given in Table IV-1.

Section B. Experiment

7. Experimental setup

The square-loop probes were studied by both the image method and the free-space method.* The discussion of the image method for the circular loop applies, and this was the basic method for determination of the sensitivity constants of the probes, since it best duplicates the theoretically assumed conditions. However, in both cases the probes actually used were not exactly square, but had rounded corners, which required some modifications to the theory, as discussed below. The image loops could have been made with square corners, but since the free-space loops could not,† they were both made the same shape for better comparison. The free-space probes have the additional complication of the exposed transmission line, which will also be discussed below.

8. Normalization, free-space method

The free-space measurements were made in two separate runs using the near-zone field of a dipole as the incident field. A continuous run used all the probes at a given point, and a second series of runs used a single probe at various points. The first run was normalized absolutely by calibrating the system in a manner similar to that used for the unipole (Section II-7). The balance

- - - - - - -

*It may be wondered why only the square, and not the circular loop was studied by the free-space method. The answer lies in the fact that the square loop could be aligned more readily with a given direction, and that no additional information was to be expected from doing both types of loops.

†The image loops are solid wire connected through a hole in the ground plane to the load, while the free-space loops use an internal coaxial line to connect the gap (load) to the external line. This internal line must be bent to shape in order to avoid internal discontinuities.

circuits were adjusted for the most symmetrical loop (the next to largest), and then left unchanged during the run so as to preserve the normalization constant. This introduces no error for the singly-loaded loops, but a small unbalance error for the doubly-loaded loops. The mean error is 0.1 db and 1 degree and the maximum error is 0.3 db and 7 degrees as estimated from the change in balanced current under 180 degree rotation.

The runs using a single probe at various points were all normalized using a constant obtained by comparison with the first run. Although the balance circuits were adjusted for each loop, only one side (one attenuator and one line stretcher) was actually changed in the process. The normalization can then be considered to apply to the other side of the balance circuits, while the adjustments merely correct for mechanical asymmetries in probe manufacture. This method of normalization is as accurate as the mechanical tolerances of the probe allow. The purpose of these runs was to verify (relatively) the results of the first run, which only used measurements at one field point to allow its accomplishment in a reasonable length of time.

9. Incident field, free-space method

The most reliable points for the free-space method were quite near the source (on the $k_e = 2.0$ and $k_e = 4.4$ ellipses) because of the low value of scattered fields in proportion to the desired incident field. Despite the extreme nearness of the source, the presence of the probe produced negligible change in the input impedance of the source antenna. In fact, it was only for $k_e \leq 1.6$ that probe loading was appreciable.

The field in this region is not very much like a plane wave, but could be expanded in terms of plane waves with a degree of accuracy as described in the

theory. From a practical standpoint this means that the values obtained where the field is slowly changing (off the axis of the antenna) are the most reliable.

An additional complication is the response of a practical probe to the cross-polarized component of electric field. This has been studied in some detail by Dunn [5] and was not the subject of the present investigation, but it did prove to be a limiting factor in probe accuracy. The sensitivity to the cross-polarized component of $E_{\perp}$ was estimated as 20 db below the sensitivity to the parallel-polarized component $E_{\parallel}$ and this limited the depth of null which could be measured.

10. End effect

High values of load impedance were not used with the square loops, so end effect was negligible for the receiving situation.

11. Effect of image plane, free-space method

The use of a probe near but not against an image plane is an interesting problem which remains to be investigated. Some theoretical work has been done [6], but an order of magnitude calculation is sufficient for use here.

The current induced in a short receiving dipole of half length h is approximately:

$$I_0 \doteq j \frac{kh^2}{60\,(\Omega - 3.4)}\, E^i_{\parallel}. \qquad \text{(IV-34)}$$

The reradiated field along the midplane polarized parallel to the axis is:

$$E^r_{\theta = \pi/2} \doteq I_0 \left(\frac{-j\,60}{kh}\right)\left(\frac{1}{\sqrt{h^2 + 4z^2}} - \frac{1}{2z}\right) \qquad \text{(IV-35a)}$$

and along the axis it is:

$$E_{\theta}^{r} = 0 \pm I_0 \left(\frac{60}{k}\right) \left(\frac{1}{4z^2 - h^2}\right) . \qquad \text{(IV-35b)}$$

From these equations it can be deduced directly that the field at a probe due to reradiation from its image is less than 2% of the directly incident field if the nearest point of the probe is at least a distance h from the image plane, for any probe orientation. Therefore, it is assumed that the coupling to the image can be neglected for any simple probe with its center at least one probe "diameter" away from the image plane.

12. Probes with rounded corners

Rounding the corners of the square loop changes the unloaded loop sensitivities by changing both the excitation voltages and the impedances.

The discussion of excitation voltage in Section IV-4 was actually not restricted to any particular loop shape, so the same equation may be used:

$$v_0 = -j\,k\,\boldsymbol{a} . \qquad \text{(IV-17)}$$

Letting s_t be the perimeter of the loop, Eq. III-28a for the circular loop can be written as:

$$Y_0 = \left\{ j\,30k\,s_t(\Omega - 3.52 + 0.33\,(k2d)^2) \right\}^{-1} \qquad \text{(IV-36a)}$$

and Eq. II-E-16 for the square loop as:

$$Y_0 = \left\{ j\,30k\,s_t(\Omega - 4.32 + 0.37\,(k2d)^2) \right\}^{-1} . \qquad \text{(IV-36b)}$$

This suggests that for any intermediate-shaped loop:

$$Y_0 = \left\{ j\,30k\,s_t(\Omega - N + 0.35\,(k2d)^2) \right\}^{-1} \qquad \text{(IV-36c)}$$

where N is a shape constant. N is assumed to be a linear function of the ratio $s_t/2d$ which takes the limiting values 3.52 and 4.32 for a circle and a square, respectively. This assumption gives:

$$N = 0.93 \frac{s_t}{2d} + 0.60 \qquad \text{(IV-37)}$$

and allows Eq. IV-36c to be used for the square loop with rounded corners.

The modified symmetric excitation voltage is calculated from:

$$v_S = \frac{2 \cos kd}{I_{Z0}} \int_{-2d}^{2d} \vec{I}_S \cdot d\vec{Z} \qquad \text{(IV-38)}$$

which is Eq. IV-22 generalized to use only the z component of current from a wire lying in an arbitrary direction. This must be done because it is only the z component of current that contributes to the tangential electric field along the midplane, $[E_\theta^r]_{\pi/2}$ of Eq. IV-21. This integral leads to:

$$v_S = \frac{4 \cos kd}{k} \left[\sin k(d - r) - (1 - \cos k(d - r)) \operatorname{ctn} k\frac{s_t}{4} + k^2 rd \csc k\frac{s_t}{4}\right] \qquad \text{(IV-39)}$$

where r is the radius of curvature of the corners of the loop.

Since the symmetric admittance is only given to a fair approximation by Eq. IV-29, the only change made* for rounding the corners was replacing $8d$ by s_t so that

$$Y_S = j \frac{\pi k \frac{s_t}{4}}{\zeta_0 \Psi_S} \qquad \text{(IV-40a)}$$

where

$$\Psi_S = 2\ell n \frac{s_t}{a} - 3.17 . \qquad \text{(IV-40b)}$$

- - - - - - -

*A more elaborate correction was originally applied to the calculation of Ψ_S, but it produced only a 2% change in the result, and in view of the approximations already made in the impedance Z_S, it was dropped as negligible.

13. Effect of transmission line

For the doubly-loaded loop in the free-space measurement the external transmission line can have an appreciable effect on the symmetric current. This can be seen from Fig. IV-2. In Fig. IV-2a there is no transmission line, and the symmetric current vanishes at points A and B . In Fig. IV-2b with the transmission line present, the symmetric current no longer vanishes at point A but at point C instead, at the first high impedance point on the vertical line, the entrance to the detuning sleeve. This will alter the current distribution on the loop and make a change in the symmetric excitation voltage which can be estimated by using:

$$I_S(s) = I_S(0) \frac{\sin k (2d + h - |s|}{\sin k (2d + h)} \qquad \text{(IV-41)}$$

instead of Eq. IV-23 for the current in the left half of the loop. This gives an increase in v_S ranging from 1.1 db for the smallest to 0.4 db for the largest loop, as computed from the measured value of h . There will also be an increase in the admittance Y_S , which can only be obtained by solving the problem completely, but which is likely to be of the same order of magnitude.

For the singly-loaded loop, the symmetry of load placement with respect to the transmission line cancels out this effect at the load (Fig. IV-3).

14. Results; image method

These results are plotted in Figs. IV-4, 5, where it can be seen that the experimental points lie on smooth curves, with the possible exception of those for the very smallest probes, showing that random errors were negligible.

The theoretical values for S_B are expected to be about 4% less accurate than those for the circular loop, because only the zeroth-order mode impedance has been used here. There is a further uncertainty introduced by the approximate

method of dealing with rounded corners, especially for the smaller loops. The error due to this is less than 10% for $2d = .013\lambda$ and 5% for $2d = .05\lambda$. The over-all accuracy of S_B is expected to be within 0.7 db and 5 degrees in the range $.02 \leq 2d/\lambda \leq .10$.

The theoretical values for S_E are expected to be considerably poorer than those for S_B because of the approximate nature of Z_S. This affects mainly the magnitude of S_E, leaving an expected accuracy of 2 db and 5 degrees over the same range.

Both experimental values are expected to be accurate within 1 db and 5 degrees just as in the case of the circular loop. The actual agreement between theory and experiment is somewhat better than expected. The phases showed a mean deviation of less than 2 degrees and a maximum deviation of 3 degrees. The measured magnitudes of electric sensitivity S_E show a slightly steeper rise with $2d/\lambda$ than the theory predicts, but the mean deviation is only 0.7 db, and the maximum deviation 1.2 db, despite the rough approximations used in the theory. The magnetic sensitivity S_B shows experimental amplitudes that are uniformly low by about 1.7 db for the singly-loaded and 1.2 db for the doubly-loaded loop. This behavior is almost identical to that for the circular loop, and is no doubt due to the same (unknown) cause. The plots of error ratio in Fig. IV-5 show the combination of the discrepancies due to S_E and S_B, except that no normalization error is present.

15. Results; free-space method

The expected accuracy of the theory for the free-space method is essentially the same as for the image method, but the experimental accuracy is reduced. In particular, the presence of the transmission line will produce changes in v_S and Z_S for the doubly-loaded loop which may change $S_E^{(2)}$ by as much

as 20% for small loops and 10% for large loops. In addition, probe manufacture was less accurate and unbalance error sometimes was present. The problems of normalization have already been discussed.

The results plotted in Figs. IV-6, 7 refer to the measurements in which all probes were placed consecutively at a given field point. Comparison with the series of runs using each probe at various points gave a measure of the experimental errors. A mean deviation of 0.4 db in amplitude and 4 degrees in phase was found for the normalized results.

In Fig. IV-6 it is seen that the phases have some points scattered by as much as 10 degrees from the smoothed curves. This is believed to be due to the difficulty of correcting exactly for the differing lengths of internal transmission line in the various sizes of loop. This is borne out by the disappearance of this random scattering in the phases in the plot of arg ϵ in Fig. IV-7. In addition to this scattering, there is a certain amount of systematic deviation in phase which averages about 4 degrees and is somewhat greater than in the image method, as was expected.

The measured magnitudes of the magnetic sensitivity $|S_B|$ are again uniformly low, by 1.5 db for the singly-loaded loop, and 1.0 for the doubly-loaded loop, essentially the same behavior as in the image method, although these points do scatter somewhat more about the smoothed curve.

For the singly-loaded loop the electric sensitivity $|S_E^{(1)}|$ follows the theoretical curve very closely, with a mean deviation of 0.3 db. For the doubly-loaded loop, however, the experimental values all lie above the theoretical curve, by an amount equal to 3.0 db for the smallest loop, and decreasing to about 1.8 db for the large loops. This is in marked contrast to the results from the image method, for which $|S_E^{(2)}|$ lies very close to the theoretical curve for small

loops and deviates by less than 1 db for the large ones. It is believed that this is due to the alteration of the loop parameters in the presence of the transmission line. In Section IV-13 this was discussed and an increase in S_E ranging from 2 db to 1 db was justified semi-quantitatively.

The theoretical dependence of the magnitude of the error ratio $|\epsilon|$ upon the wire radius, a/λ, is shown in Fig. IV-8 for both singly and doubly-loaded loops. In Fig. IV-9, the dependence of $|\epsilon^{(2)}|$ upon the load resistance, R_L, is shown. The curve for $R_L = 0$ applies also to $|\epsilon^{(1)}|$ for the singly-loaded loop with arbitrary load resistance. Experimental data were not taken for either of these cases since the variation of $|\epsilon|$ with a/λ and with R_L does not differ significantly from that for the circular loop.

Section C. Conclusions

16. Conclusions

The conclusions which may be drawn about the square loop are practically the same as those for the circular loop in Section III-11.

Figure IV-10a gives a comparison of the magnitudes of the error ratios for circular and square loops of the same diameter. It is seen that, in general, a square loop has an error ratio about 1.2 db larger than a circular loop of the same diameter. The only exception comes for doubly-loaded square loops of diameter $2d \leq .025\lambda$, for which the error ratio actually becomes smaller than that for the circular loop. However, a comparison of the error ratios of circular and square loops with the same magnetic sensitivity, as in Fig. IV-10b, shows for singly-loaded loops that the square shape gives a lower error ratio for a given magnetic sensitivity than the circular shape. For doubly-loaded loops, the square loop gives smaller $|\epsilon|$ for small diameters but larger $|\epsilon|$ for large diameters compared to the circular loop, although the two differ by less than 0.5 db everywhere.

For convenience in probe design, Figs. IV-11a, b give curves for the maximum loop diameter which can be used if the error ratio must be kept below a certain value. These are shown for the square loop, in both doubly and singly*-loaded cases, for various values of the load resistance R_L and the wire thickness parameter Ω. The circular loop will have very similar behavior. It must be noted again that the doubly-loaded loop is to be used within a balun detector, so that the system error ratio will be below the probe error ratio by a factor dependent on the degree of balance, as discussed in Sections

- - - - - - -

*Notice the change of scale on the ordinate of the singly-loaded case.

III-5, 10. Typically, this factor will be 0.03 to 0.10, so that a probe error ratio $|\epsilon^{(2)}| = 1$ implies a system error ratio of 0.03 to 0.10. The error ratio of the singly-loaded loop, however, is identical with the system error ratio.

Another conclusion which is reached by comparison of the free-space loops with the image loops is that the presence of the transmission line significantly increases the error ratio. This leads to the discussion of load placement and bridged loops in Chapter V.

Bibliography, Chapter IV

1. Dunn, Beverly C., Jr., "Microwave Field Measurements I," Cruft Laboratory Technical Report No. 71, Harvard University, p. 18 (September 1949).

2. King, Ronold W. P., Electromagnetic Engineering, pp. 427-430, McGraw-Hill, New York (1945).

3. King, Ronold W. P., The Theory of Linear Antennas, pp. 568-570 and 690-693, Harvard University Press, Cambridge (1956).

4. King, Ronold W. P., "The Rectangular Loop Antenna as a Dipole," Cruft Laboratory Technical Report No. 263, Harvard University (May 1957).

5. Dunn, Beverly C., Jr., "Microwave Field Measurements III," Cruft Laboratory Technical Report No. 73, Harvard University, pp. 23-27 (October 1949).

6. Hsu, Hwei-Piao, "Analysis of the Interaction between a Measuring Probe and a Reflector," Scientific Report No. 22, Case Institute of Technology (February 1961).

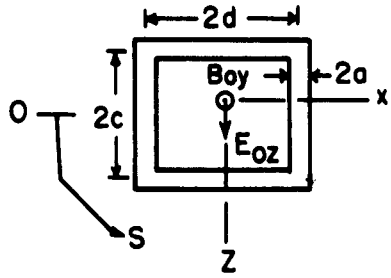

(a) LOOP IN INCIDENT FIELD

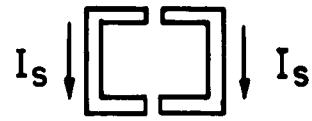

(c) SYMMETRIC EQUIVALENT ARRAY

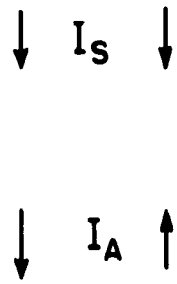

(b) SYMMETRIC AND ANTISYMMETRIC CURRENTS

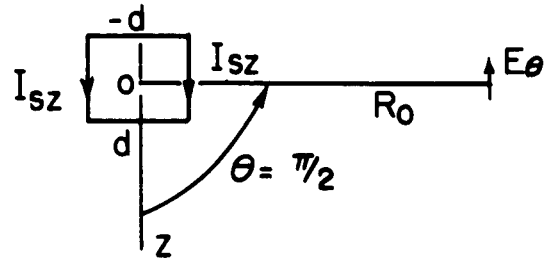

(d) ARRAY WHEN TRANSMITTING

IV-1 SQUARE LOOP

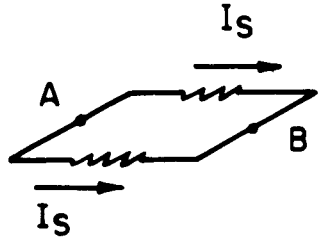

IV 2(a)

DOUBLE LOADED LOOP
WITHOUT TRANSMISSION LINE

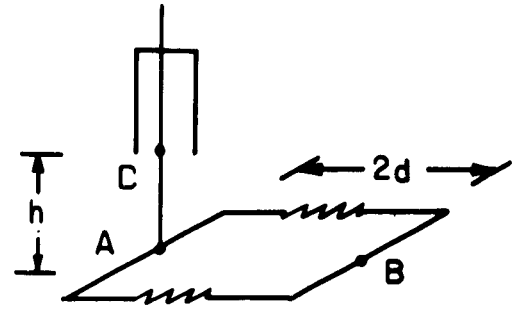

IV 2(b)

DOUBLE LOADED LOOP WITH
TRANSMISSION LINE

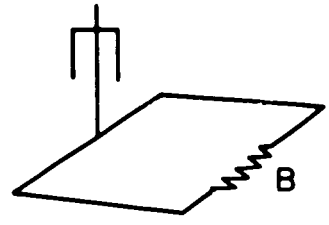

SINGLE LOADED LOOP WITH
TRANSMISSION LINE

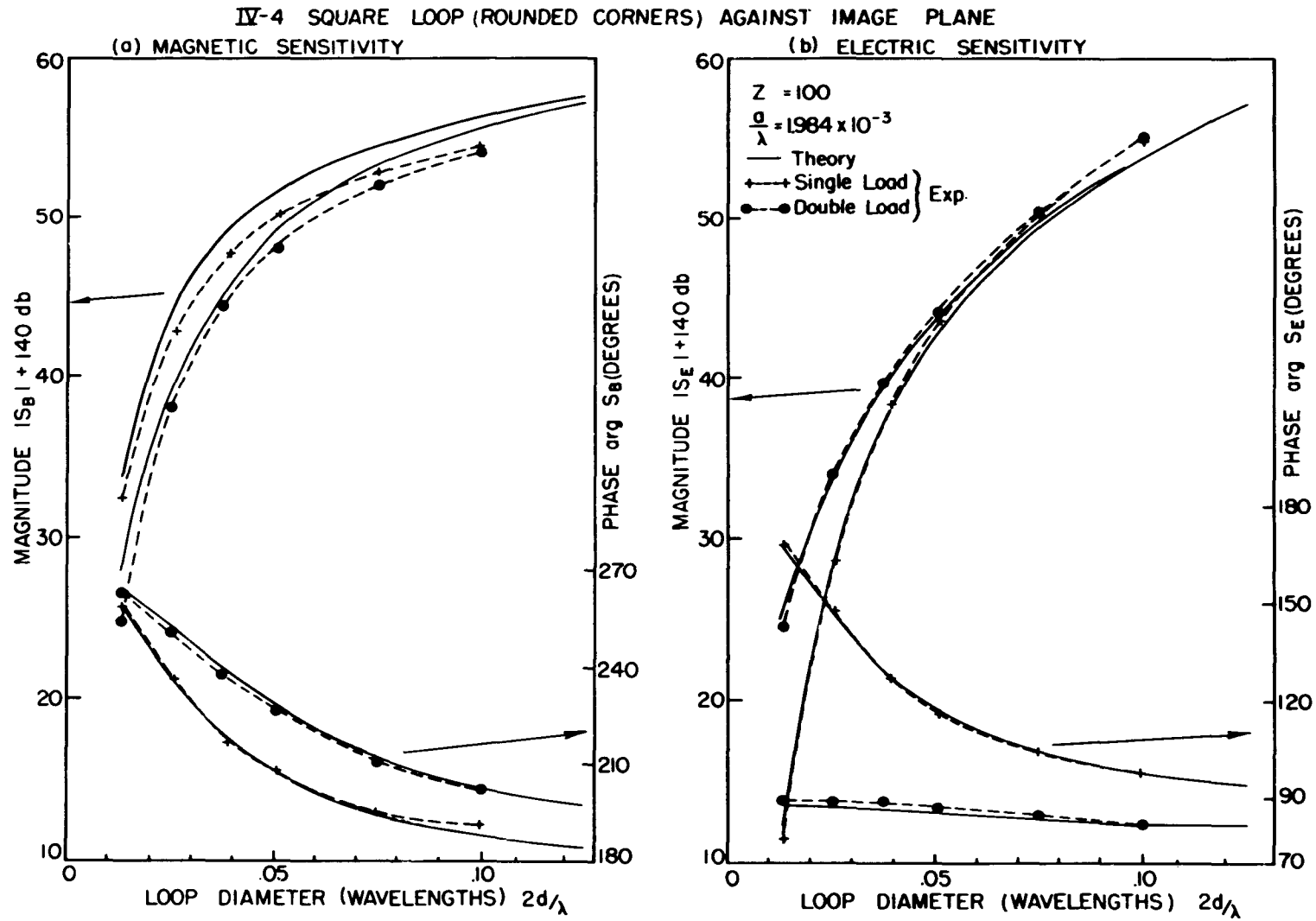
IV-4 SQUARE LOOP (ROUNDED CORNERS) AGAINST IMAGE PLANE
(a) MAGNETIC SENSITIVITY
(b) ELECTRIC SENSITIVITY
Z = 100
a/λ = 1.984 x 10⁻³
Theory
Single Load
Double Load
Exp.
MAGNITUDE |SB| + 140 db
PHASE arg SB (DEGREES)
MAGNITUDE |SE| + 140 db
PHASE arg SE (DEGREES)
LOOP DIAMETER (WAVELENGTHS) 2d/λ
LOOP DIAMETER (WAVELENGTHS) 2d/λ

IV-5 SQUARE LOOP (ROUNDED CORNERS) AGAINST IMAGE PLANE, ERROR RATIO

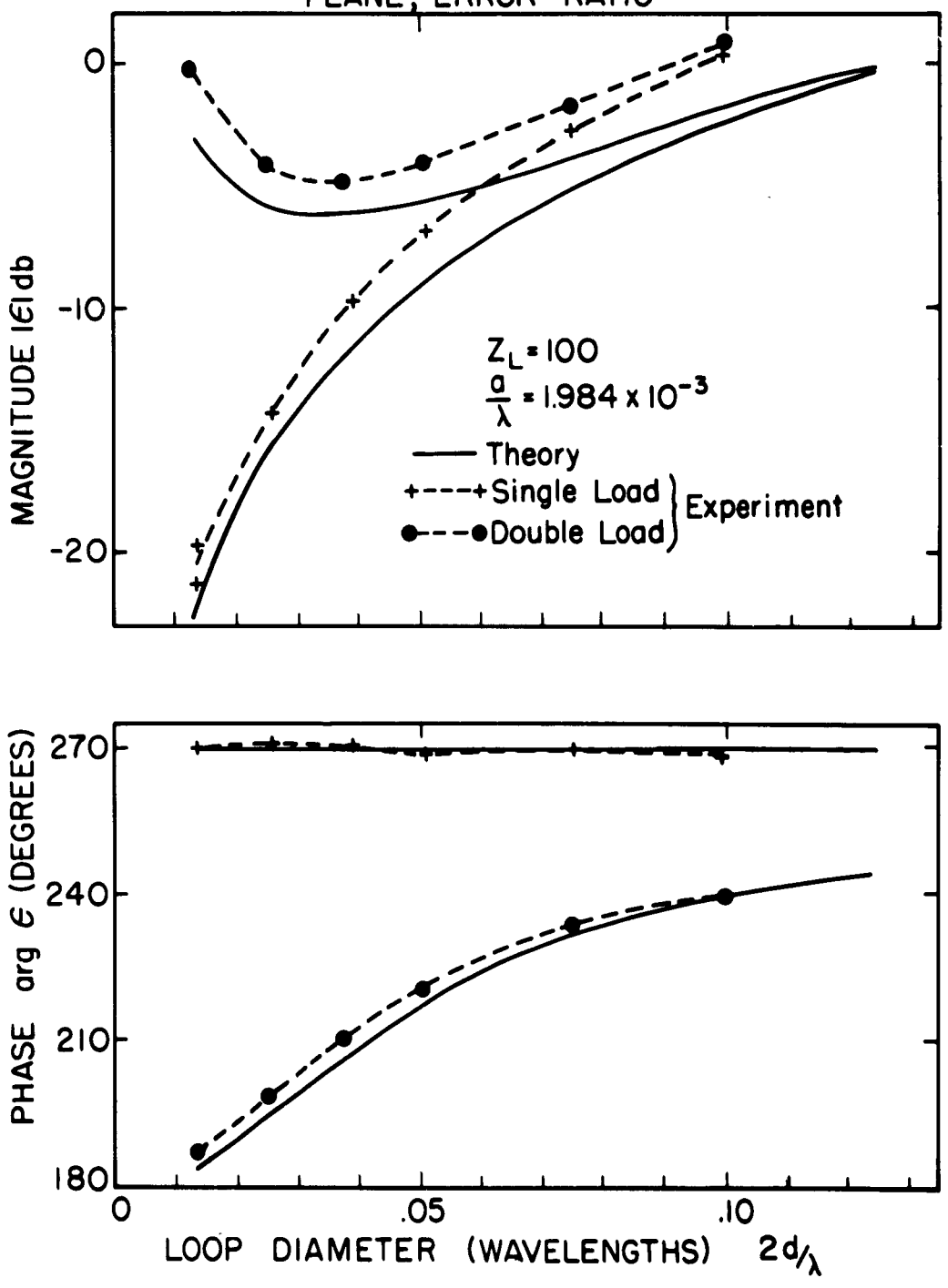

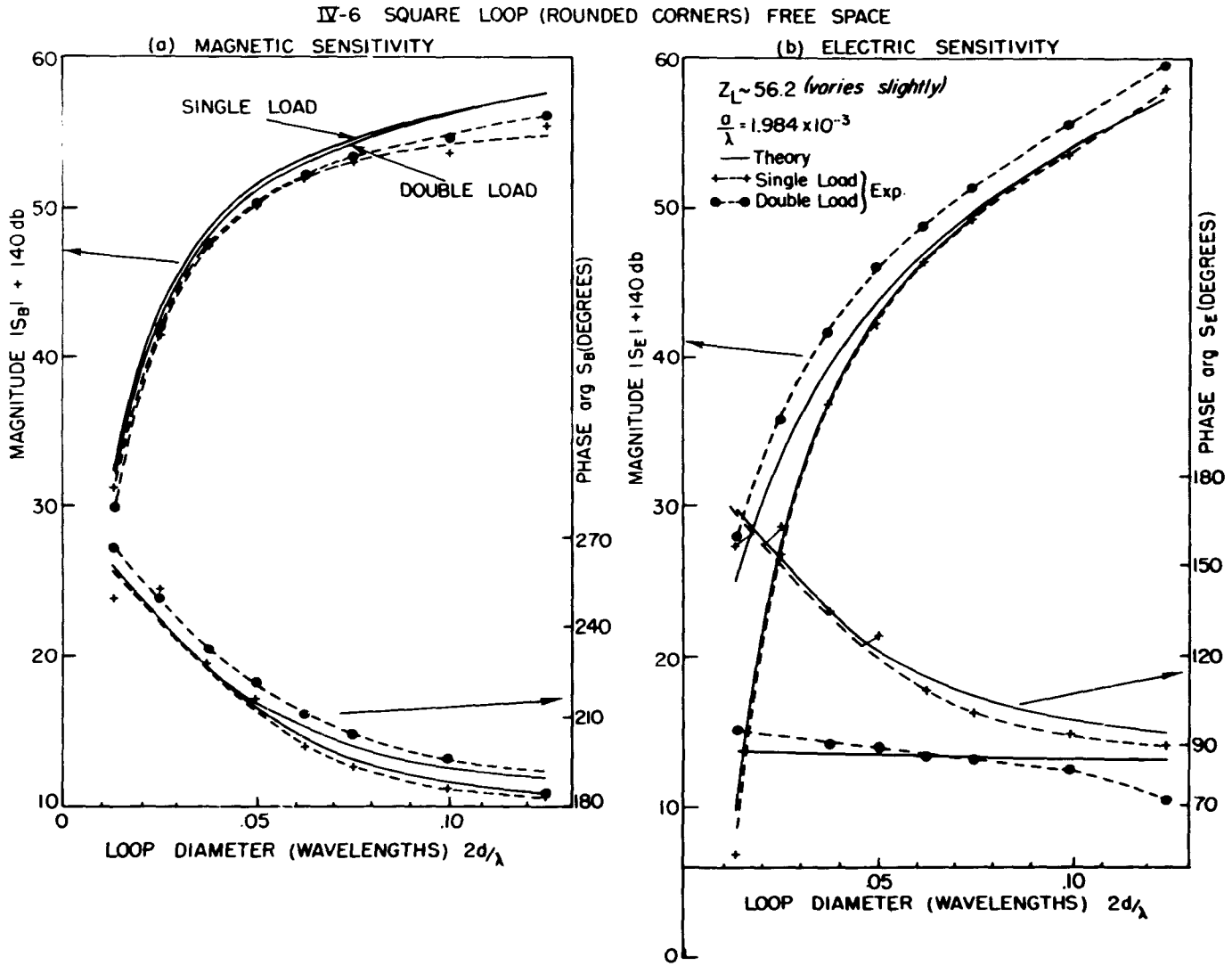
IV-6 SQUARE LOOP (ROUNDED CORNERS) FREE SPACE
(a) MAGNETIC SENSITIVITY
SINGLE LOAD
DOUBLE LOAD
MAGNITUDE |SB| + 140 db
PHASE arg SB(DEGREES)
LOOP DIAMETER (WAVELENGTHS) 2d/λ
(b) ELECTRIC SENSITIVITY
ZL~56.2 (varies slightly)
a/λ = 1.984 x 10⁻³
Theory
Single Load
Double Load
Exp.
MAGNITUDE |SE| + 140 db
PHASE arg SE(DEGREES)
LOOP DIAMETER (WAVELENGTHS) 2d/λ

IV-7 SQUARE LOOP (ROUNDED CORNERS) FREE SPACE, ERROR RATIO

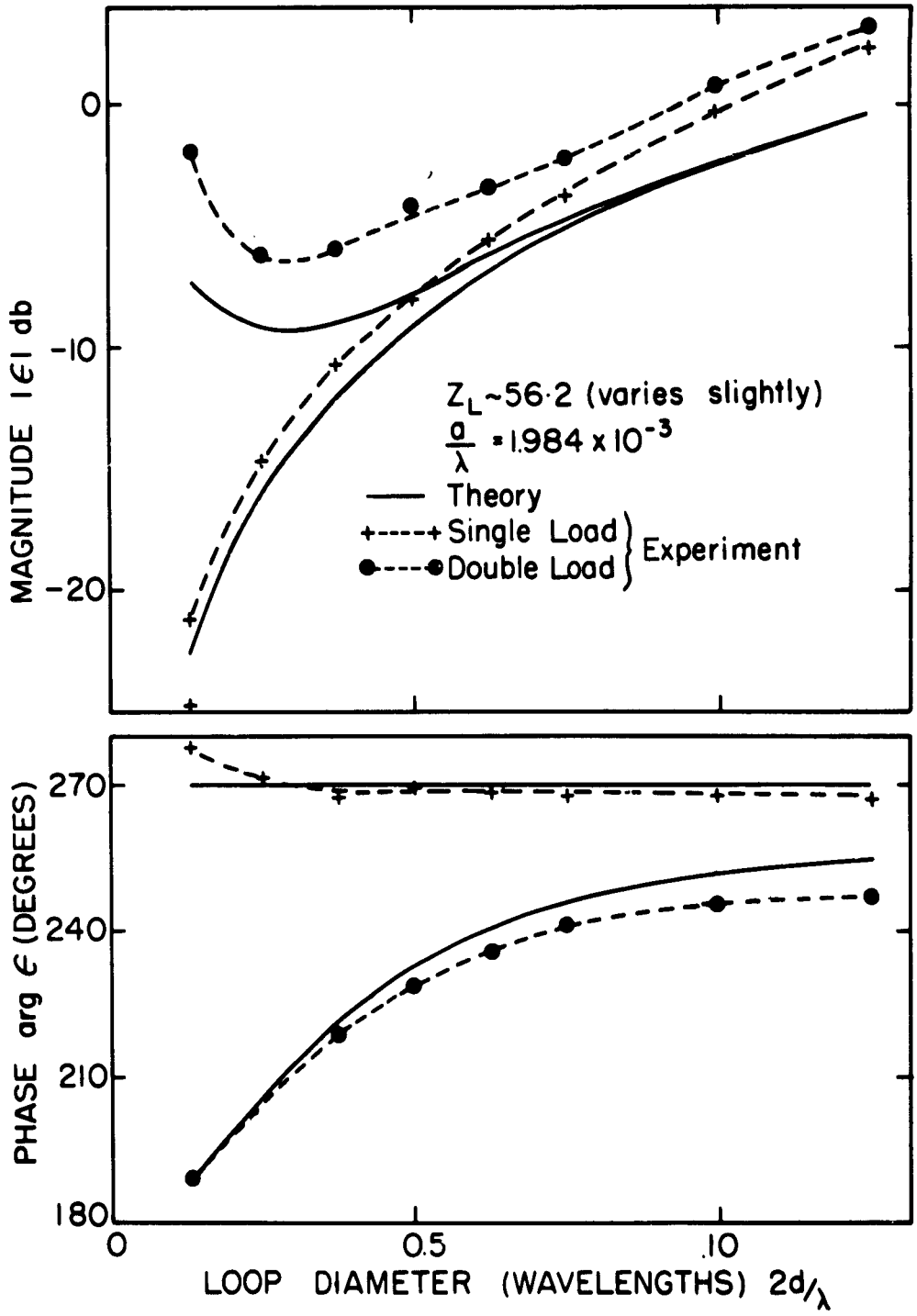

IV-8 SQUARE LOOP, THEORETICAL ERROR RATIO

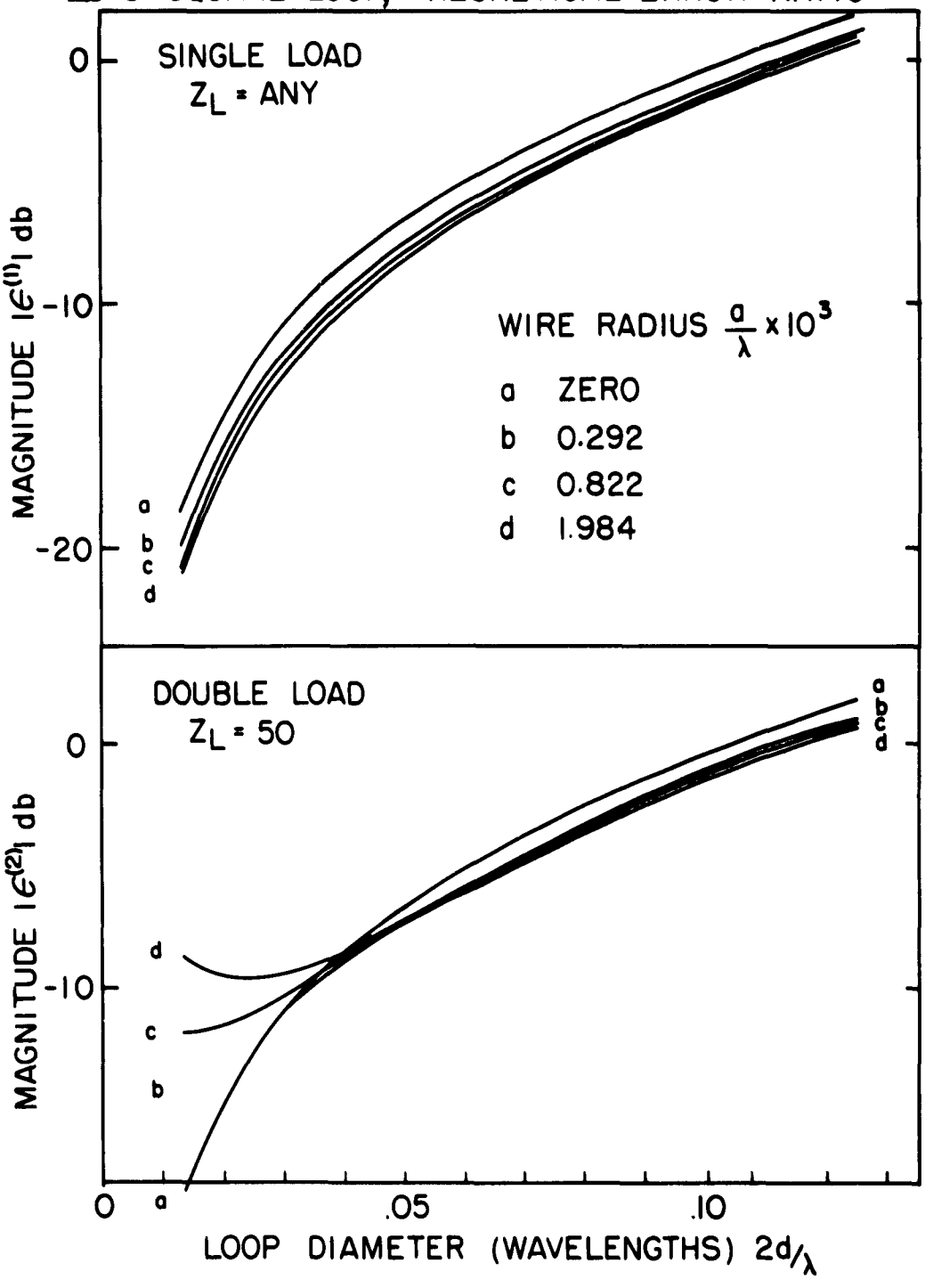

IV-9 SQUARE LOOP, THEORETICAL ERROR RATIO

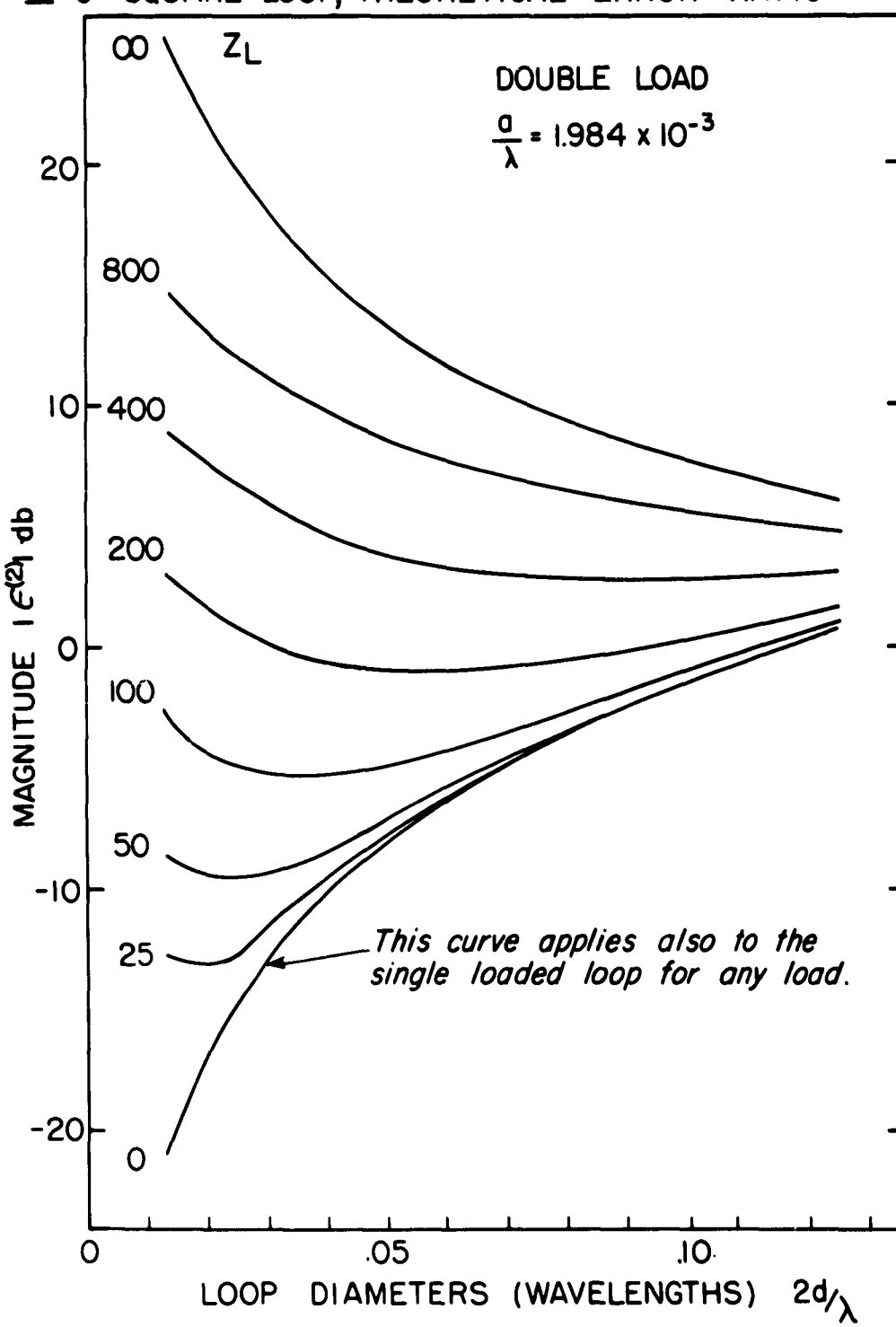

IV-10 THEORETICAL ERROR RATIO, SQUARE AND CIRCULAR LOOPS

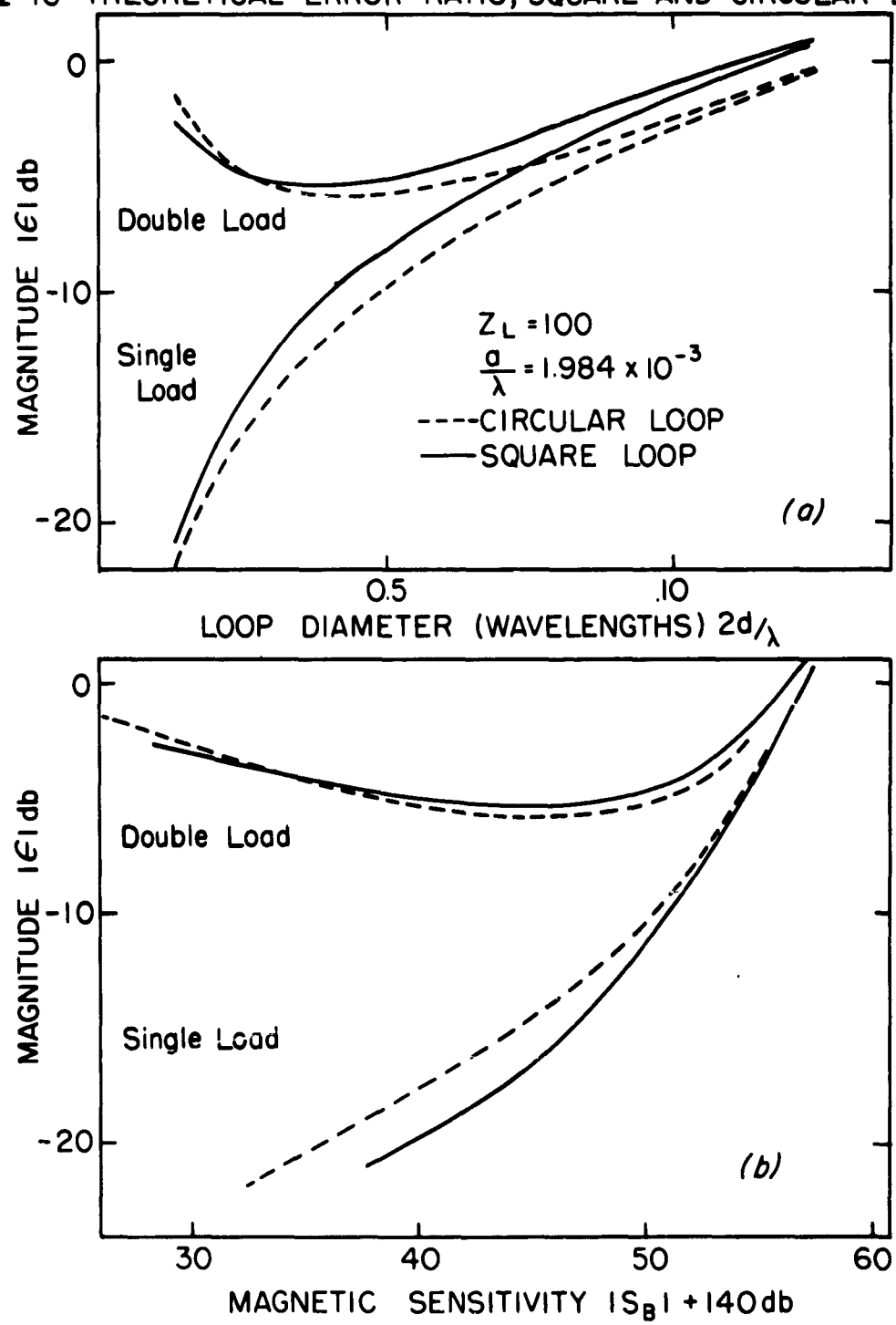

IV-11a SQUARE LOOP, DOUBLE LOAD, MAXIMUM DIAMETER FOR $|\epsilon^{(2)}| \leq 1$

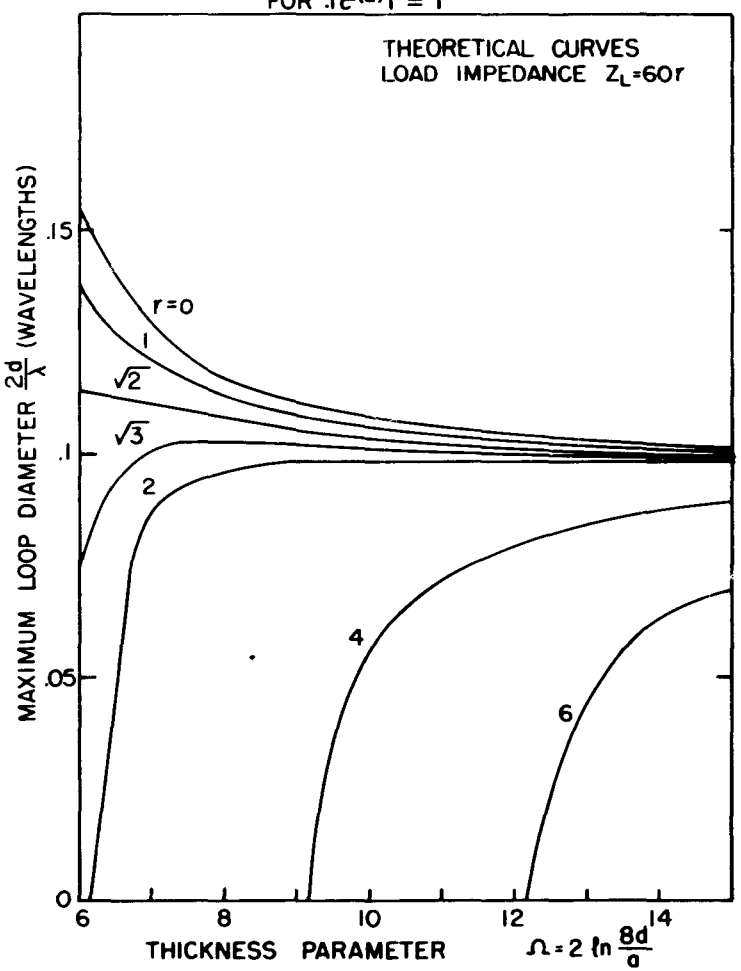

IV-11b SQUARE LOOP, SINGLE LOAD, MAXIMUM DIAMETER FOR GIVEN $|\epsilon^{(1)}|$

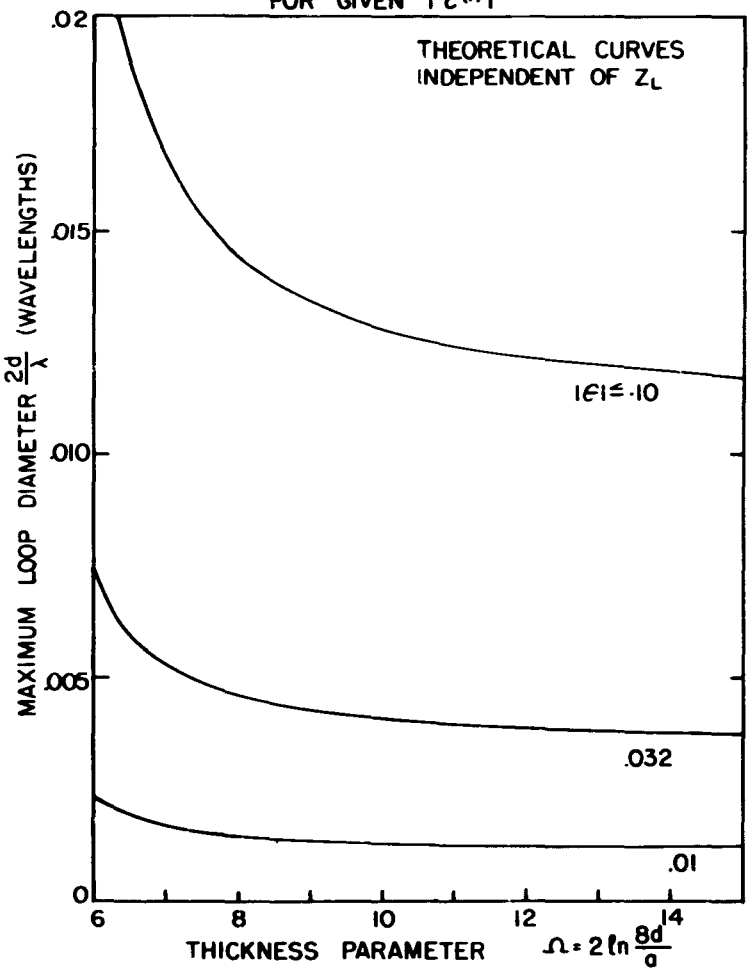

TABLE IV-1

Probe Constants for Small Square Loops

(Approximate Expressions for $a^2 << d^2$, $4k^2d^2 << 1$)

Single Load, Y_L

$$S_B^{(1)} \doteq \frac{Y_L}{Y_L - j\,[30k\,(8d)\,(\Omega - 4.3)]^{-1}} \cdot \frac{(-2\pi d)}{\zeta_0(\Omega - 3.5)}$$

$$S_E^{(1)} \doteq \frac{Y_L}{Y_L - j\,[30k\,(8d)\,(\Omega - 4.3)]^{-1}} \cdot \frac{j\,3\,(2\pi d)^2}{\lambda\,\zeta_0(\Omega - 3.2)}$$

$$\epsilon^{(1)} \doteq -j\,\frac{2}{\lambda}\left(\frac{\Omega - 4.3}{\Omega - 3.2}\right)(3\pi d)$$

Double Load, Y_L each

$$S_B^{(2)} \doteq \frac{Y_L}{Y_L - j\,2\,[30k\,(8d)\,(\Omega - 4.3)]^{-1}} \cdot \frac{(-2\pi d)}{\zeta_0(\Omega - 3.5)}$$

$$S_E^{(2)} \doteq \frac{Y_L}{Y_L + j\,2\,\left[30\,(\Omega - 3.2)\,\frac{\lambda}{\pi d}\right]^{-1}} \cdot \frac{j\,3\,(2\pi d)^2}{\lambda\,\zeta_0(\Omega - 3.2)}$$

$$\epsilon^{(2)} \doteq \left[1 - j\,\frac{Z_L}{15k\,(8d)\,(\Omega - 4.3)}\right] \cdot \left[-j\,\frac{2}{\lambda}\left(\frac{\Omega - 4.3}{\Omega - 3.2}\right)(3\pi d)\right]$$

CHAPTER V. PLACEMENT OF PROBE LOAD

Section A. Effect of Load Placement

1. Introductory discussion

It was suggested in Section IV-13 that the external transmission line couples to currents in the loop that are symmetric with respect to the plane through the transmission line and the center of the loop. If a load is connected opposite the transmission line it will be at a null of such currents, but if it is anywhere else, the line will alter the load current. A deviation in the measured electric sensitivity of the doubly-loaded loop was attributed to this cause (Section IV-15).

The response of a series of singly-loaded loops differing from one another only in the load position was studied in order to test this hypothesis. Referring to Fig. V-1a, three load positions are distinguished, with position No. 2 directly opposite the transmission line, and position Nos. 1 and 3 on sides adjacent to it.

The use of shielded loops facilitates the placement of the load, since the probe consists of the outer surface of the loop, loaded at the gap by the internal transmission line. The internal transmission line is completely isolated from external fields at the driving gap, and the antenna currents on the outside surface of the loop behave as if there were no internal line, but only a lumped load Z_L at the position of the gap. The load currents, I_2 in Figs. V-1b and V-1c are equal.

2. Experiment

The loops used had a diameter $2d = .05\lambda$, wire radius $a = 1.984 \times 10^{-3}\lambda$ and a load impedance $Z_L \doteq 56$ ohms. The load gap was located in different

positions, and correction was made for the corresponding change in transmission-line length between the gap and the remote detector. Figure I-23 shows the actual probes used.

The relative probe sensitivities, S_E and S_B (unnormalized), and the absolute error ratio ϵ, were measured using the mean value from several points in the near-zone dipole field just as in previous free-space measurements (Section IV-9).

3. Results

The mean values of S_B were constant in both magnitude and phase within the limits of experimental error for all three load positions. The mean values of S_E were equal for load positions Nos. 1 and 3, but for load position No. 2 the magnitude of S_E was lower by 2 db (Table V-1). This is approximately the same effect observed in Chapter IV with doubly-loaded loops. Since load placement here only has meaning with respect to the transmission line, the change in S_E must be due to coupling to the line.

A second question can also be answered from the same set of measurements. Does the error in measurement due to transmission line coupling cause the effective (observed) value of S_E or S_B to vary from point to point within the field? Table V-2 gives the mean deviation of these constants from their mean values for measurements at a variety of field points. It is seen that there is no significant dependence of these mean deviations on load position.

4. Conclusions

It has been shown experimentally that the presence of the transmission line normal to the plane of the probe has no effect on the magnetic sensitivity S_B of a loop, but that it does increase the electric sensitivity S_E unless the load is symmetrically placed.

It was also shown that this is not a source of error in relative field measurements, since the new value of S_E is still independent of the field. For absolute measurements of E, the new value of S_E would have to be determined. The only other adverse effect is an increase of the order of 2 db in the error ratio ϵ, so that in a critical situation where ϵ was rather large anyway it would be especially desirable to locate the load symmetrically with respect to the line.

Section B. Bridged Loops

5. Introductory discussion

From the consideration of load placement it is clear that for a singly-loaded loop, the load gap should be placed directly opposite the transmission line. With the doubly-loaded loop this is impossible, but in order that the error ratio be minimized the line should enter symmetrically with respect to both loads. This can be done by means of a conducting bridge, as shown in Fig. V-2b.

6. Theory

It is evident that the bridge allows the line to be connected in such a way that currents coupled from it have zeros at both loads. This removes the transmission-line coupling, but at the expense of complicating the probe antenna by adding the bridging element.

Consider the square loop first, and then add the bridge. In the square loop the zero mode current I_0 is simply a circulating current that is constant at all points. When the bridge is added, it is seen from symmetry that I_0 is unchanged because any current entering the bridge at point A will be canceled by an equal and opposite current entering at point B, as shown in Fig. V-3b.

The symmetric currents, however, will definitely couple to the bridge as to a parasitic antenna, causing a current I_B in the bridge, and changing the symmetric current to I'_S (but keeping it symmetric) (Fig. V-4). The complete solution of this problem involves three coupled integral equations and has not been solved. An estimate of the direction and magnitude of the effect can be made by considering the behavior of closely-shaped dipoles. King [1] shows that two symmetrically-driven parallel dipoles of radius a and spacing b are equivalent to a single antenna with an effective radius

$$a_e = \sqrt{ab} \, . \qquad \text{(V-1)}$$

This results in an increase in the total current carried by the two antennas, but a decrease in the current carried by one, compared to its isolated state. The ratio of the admittance of an antenna in the presence of a second coupled antenna to its admittance when isolated is

$$\gamma = \frac{Y_2}{Y_1} = \frac{\Psi_1}{2\,\Psi_1 - 2\ln\frac{b}{a}} \qquad \text{(V-2)}$$

where Ψ_1 is the expansion parameter for the single antenna.

The previous analysis of the receiving loop in Section IV-4 shows that the electric sensitivity is proportional to the excitation voltage v_S and the symmetric admittance Y_S. The excitation voltage is not changed by the presence of the bridge, but Y_S is. Therefore, the change in S_E is proportional to the change in Y_S. As an estimate, it was assumed that the new value of Y_S has the same ratio to the old value as Y_2 has to Y_1 for coupled dipoles. Therefore, the new value of electric sensitivity is approximately:

$$S'_E \approx \gamma\, S_E \, . \qquad \text{(V-3)}$$

For probes with $2d \leq .05\lambda$ and a typical value of a, it was estimated that S_E should decrease by 0.5 - 1 db, depending on loop size.

An alternative point of view would be to treat the bridged loop as two closely-spaced rectangular loops, each with a single load. This would indicate only a very small change in S_B when the bridge is added, but the decrease in S_E could be substantial since $S_E^{(1)}$ is considerably less than $S_E^{(2)}$ for the smaller loops (Fig. IV-4b).

7. Experiment

The experiment was conducted in the usual way, using both the image

and the free-space techniques. The first part of the experiment was designed to compare the sensitivities of a bridged loop with those of a square loop. The second part was a study of the accuracy of the two types of loops as probes, and the third was a study of a series of bridged loops themselves. In all cases the loops actually had rounded corners, and corrections were made for this and for the internal transmission line as in Chapter IV.

8. Results

Table V-3 gives a comparison of the sensitivities of square and bridged loops with and without a transmission line (free-space and image methods). It is seen that for the image loop, the bridge changes only the phase of S_E, increasing it by 30 degrees, while for the free-space loop the same phase change occurs but there is also a drop of 4 db in the magnitude of S_E. Therefore, transmission line coupling is seen to increase S_E for the the square loop by about 4 db. Use of the bridge removes this effect and produces an increase of 30 degrees in the phase of S_E.

The mean deviations of the sensitivities S_B and S_E for various positions in the field are a measure of probe accuracy. These are presented in Table V-4, where it is seen that there is no appreciable difference between the square and the bridged types.

For the study of the bridged loops themselves a smaller wire, with $a = .822 \times 10^{-3}\lambda$, was used to allow manufacture of the bridge for very small loops. The probes are shown in Fig. I-24 and the results are plotted in Figs. V-5, 6. For comparison, theoretical curves are plotted for the square loop with single and with double loads. The magnitudes are absolute measurements and the phases are relative measurements. The magnetic sensitivity is seen to lie about 1 db below the theoretical curve for the small loops, just as in the

case of the square loops (Fig. IV-6a), but for $2d \doteq .05\lambda$ the experimental and theoretical magnitudes agree. The experimental phase, arg S_B, agrees with the theory throughout. The electric sensitivity, however, behaves quite differently from that of the square loop. In both magnitude and phase it lies between the theoretical curves for double and single loads. This has been discussed qualitatively in Section V-2 above. The error ratio also lies between the two theoretical curves in both magnitude and phase.

9. Conclusions

It has been determined that the bridged loop represents an improvement over the square loop in magnetic field measurements for two reasons. Firstly, it allows symmetrical connection of the transmission line, with a corresponding reduction in the effective value of S_E. Secondly, it decreases the symmetric admittance of the probe and thus reduces S_E still further. The reduction in S_E reduces the error ratio by a few db, and therefore, may improve measurements of B in critical situations where the cross coupling of modes is significant. The improvement is less than 1 db for large probes or for image probes, but may reach 4 db for small free-space probes.

Bibliography, Chapter V

1. King, Ronold W. P., The Theory of Linear Antennas, p. 275, Harvard University Press, Cambridge (1956).

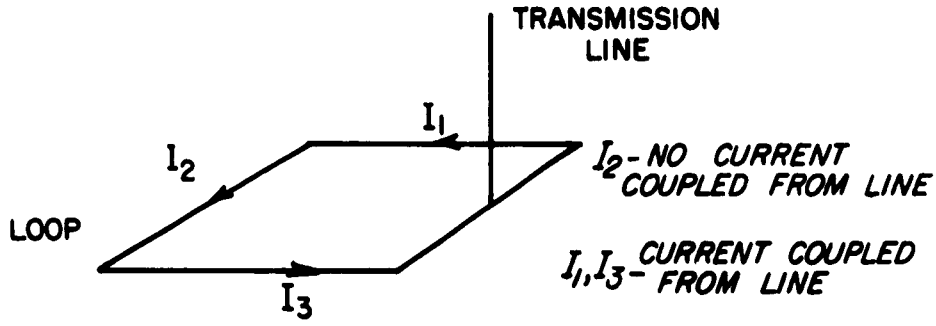

V-1a COUPLING OF TRANSMISSION LINE TO LOOP

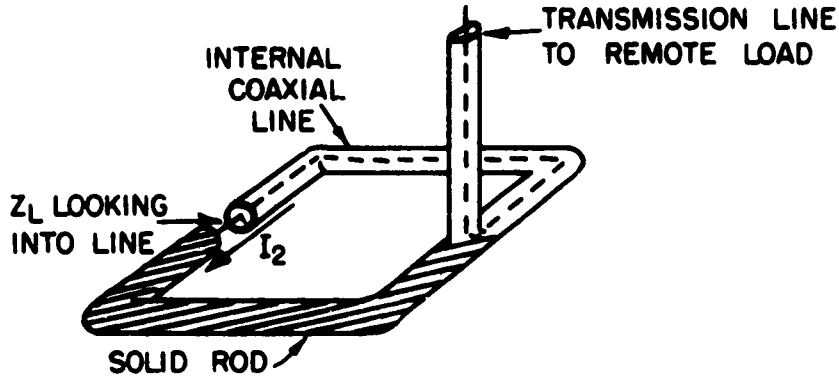

V-1b SHIELDED LOOP

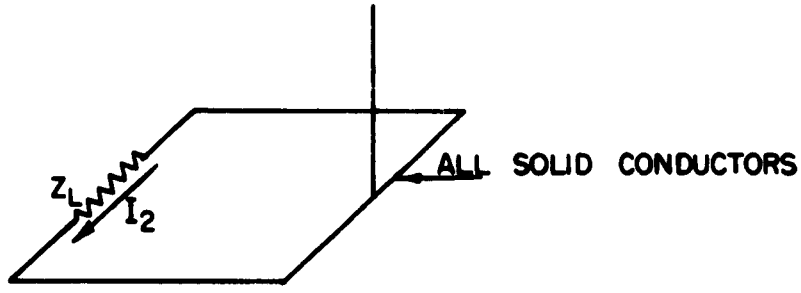

V-1c EQUIVALENT LOOP

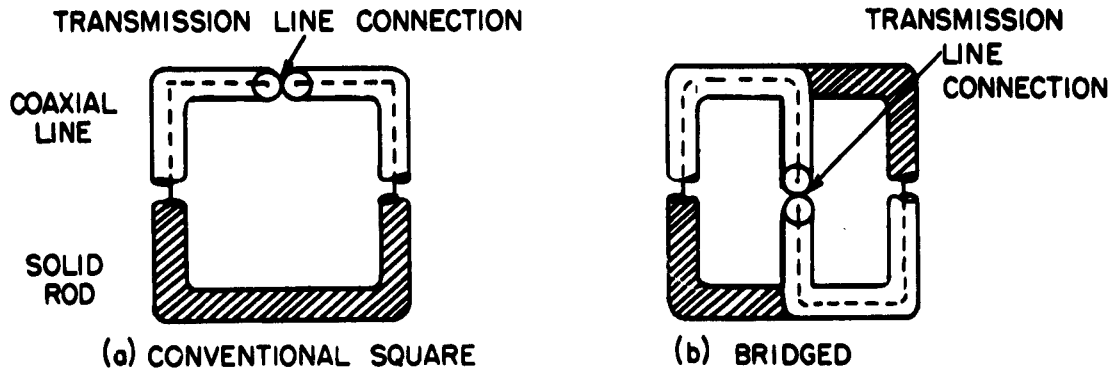

V-2 DOUBLE LOADED LOOPS, TOP VIEW, WITH VERTICAL TRANSMISSION LINE

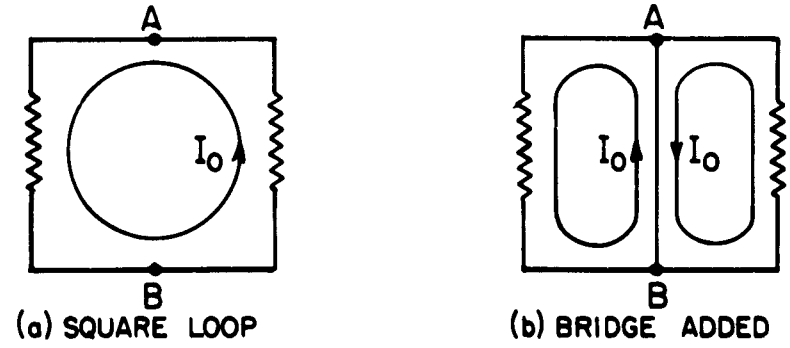

V-3 ZERO MODE CURRENTS

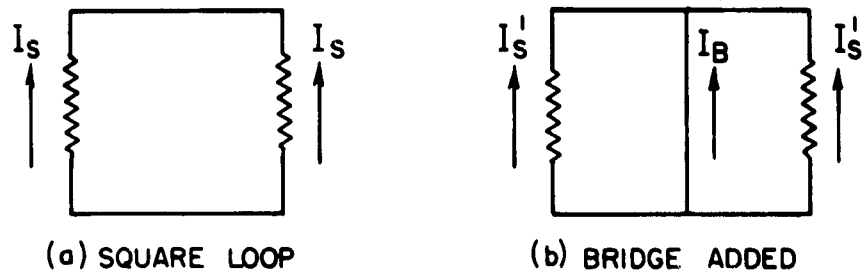

V-4 SYMMETRIC CURRENTS

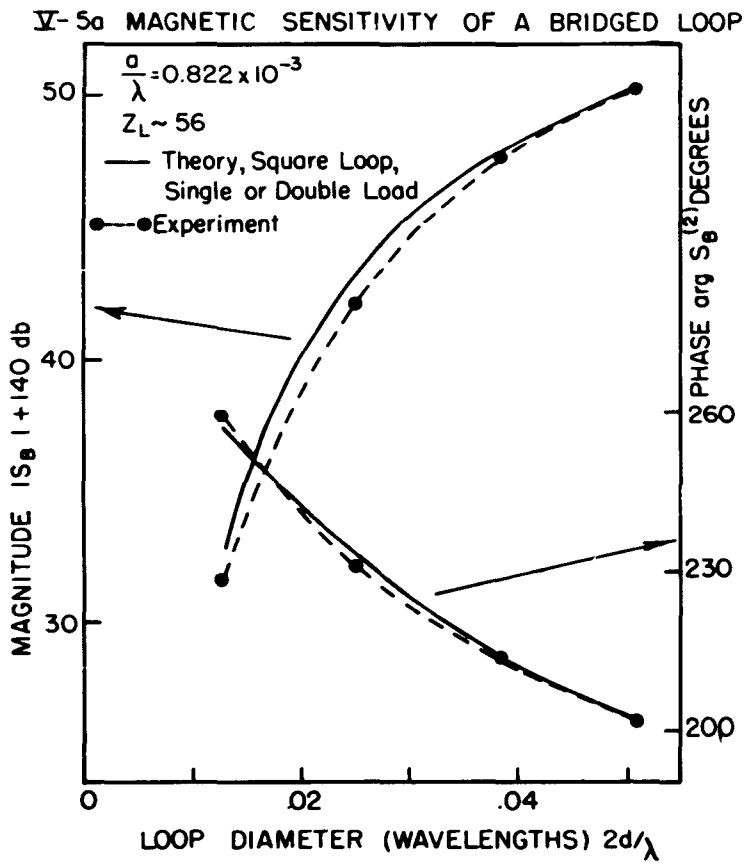
V-5a MAGNETIC SENSITIVITY OF A BRIDGED LOOP
a/λ = 0.822 x 10^-3
Z_L ~ 56
Theory, Square Loop, Single or Double Load
Experiment
MAGNITUDE |S_B| + 140 db
PHASE arg S_B^(2) DEGREES
50
40
30
260
230
200
0
.02
.04
LOOP DIAMETER (WAVELENGTHS) 2d/λ

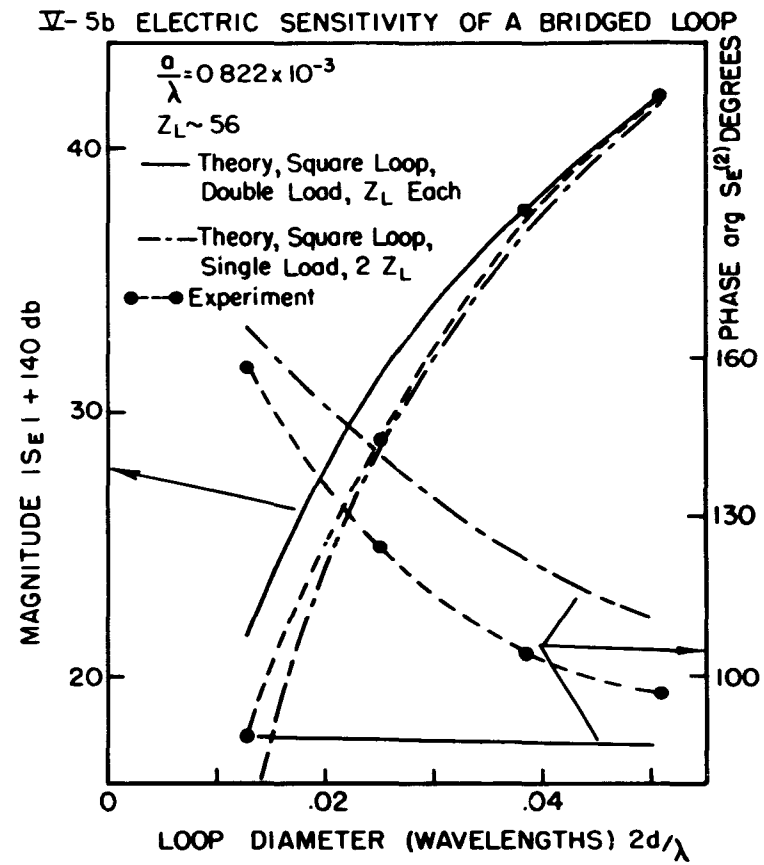
V-5b ELECTRIC SENSITIVITY OF A BRIDGED LOOP
a/λ = 0.822 x 10^-3
Z_L ~ 56
Theory, Square Loop, Double Load, Z_L Each
Theory, Square Loop, Single Load, 2 Z_L
Experiment
MAGNITUDE |S_E| + 140 db
PHASE arg S_E^(2) DEGREES
40
30
20
160
130
100
0
.02
.04
LOOP DIAMETER (WAVELENGTHS) 2d/λ

V-6 ERROR RATIO OF A BRIDGED LOOP

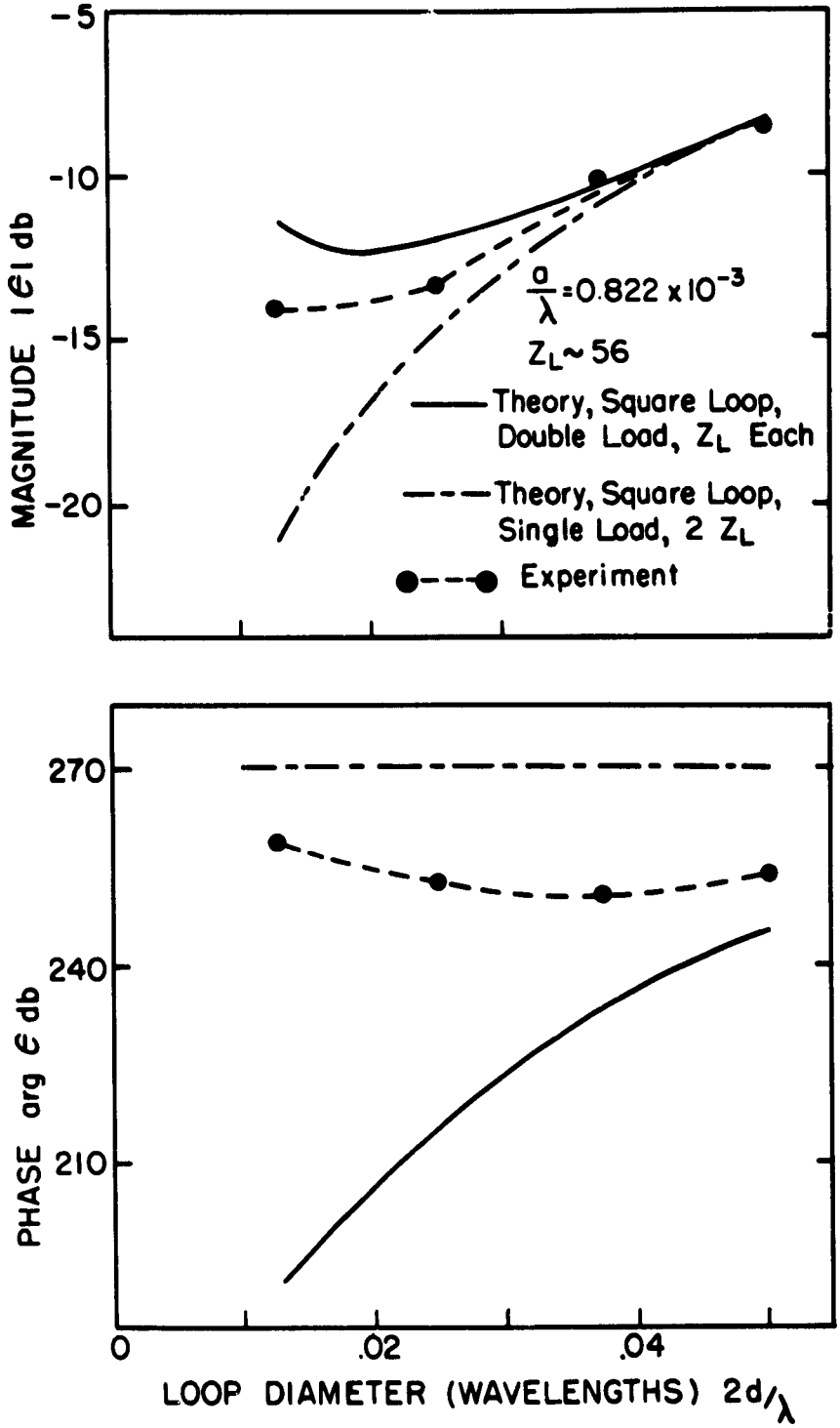

TABLE V-1 DEPENDENCE OF SENSITIVITY CONSTANTS ON LOAD POSITION

SQUARE LOOP, SINGLE LOAD, $2d = .05\lambda$, $a = 1.984 \times 10^{-3}\lambda$, $Z_L = 56$

FUNCTION	LOAD POSITION		
	#1	#2	#3
$\lvert S_B \rvert$ db*	16.6	16.8	17.2
arg S_B (DEGS)*	313	313	31.4
$\lvert S_E \rvert$*	10.6	8.7	10.7
arg S_E*	223	224	222
$\lvert \epsilon \rvert$	- 6.0	- 8.1	- 6.5
arg ϵ	270	271	268

*THESE ARE RELATIVE VALUES ONLY

TABLE V-2 MEAN DEVIATION OF SENSITIVITY CONSTANTS FOR VARIOUS LOAD POSITIONS

FUNCTION	LOAD POSITION		
	#1	#2	#3
$\bar{\delta} \lvert S_B \rvert$ db	±0.4	±0.4	±0.4
$\bar{\delta}$ arg S_B (DEG)	± 2	± 1	± 1
$\bar{\delta} \lvert S_E \rvert$	±0.2	±0.3	±0.2
$\bar{\delta}$ arg S_E	± 2	± 3	± 2

TABLE V-3 SENSITIVITY CONSTANTS, SQUARE AND BRIDGED LOOP

DOUBLE LOAD, $2d = .05\lambda$, $a = 1.984 \times 10^{-3}\lambda$, $Z_L = 100$

FUNCTION	THEORY	EXPERIMENT			
		IMAGE		FREE SPACE	
	SQUARE	SQUARE	BRIDGED	SQUARE	BRIDGED
$\lvert S_B \rvert$ db.	49.2	48.1	48.2	(50.2)	(49.8)
arg $S_{B(DEGS)}$	228	226	227	221	220
$\lvert S_E \rvert$	43.6	44.0	44.3	(46.0)	(42.1)
arg S_E	85	87	118	90	117
$\lvert \epsilon \rvert$	-5.6	-4.1	-3.9	-4.2	-7.7
arg ϵ	217	221	251	229	257

( ) THESE MAGNITUDES ARE NOT NORMALIZED WITH RESPECT TO THE IMAGE VALUES

TABLE V-4 MEAN DEVIATION OF SENSITIVITY CONSTANTS

FREE SPACE LOOPS OF TABLE V-3

FUNCTION	LOOP TYPE	
	SQUARE	BRIDGED
$\bar{\delta}$ $\lvert S_B \rvert$ (db)	± 0.2	± 0.1
$\bar{\delta}$ arg S_B (DEGREES)	± 2	± 2
$\bar{\delta}$ $\lvert S_E \rvert$	± 0.7	± 0.9
$\bar{\delta}$ · arg S_E	± 3	± 3

CHAPTER VI. ELECTROMAGNETIC FIELD MEASUREMENTS

Section A. Far-Zone Type Fields

1. Single field measurements

The measurement of fields of the far-zone type is a relatively simple matter, as shown in Fig. VI-1. The electric field is polarized in a plane normal to the direction of propagation, and its two components, E_θ and E_ϕ can be measured using a short electric dipole probe (Chapter II). The magnetic field is also polarized in the same plane, and both its components can be measured using a conventional singly-loaded loop oriented in a plane perpendicular to the desired component. The side of the loop containing the load can be oriented perpendicular to both components of the electric field so that any electric mode current has a zero at the position of the load, and the load current is proportional to the normal magnetic field alone. This simple measurement of B is possible because the radial electric field E_R is zero in the far zone.

It should also be mentioned that in the far zone corresponding magnetic and electric field components are equal:

$$c\,B_\theta = E_\phi \qquad \text{(VI-1a)}$$

$$c\,B_\phi = E_\theta\,. \qquad \text{(VI-1b)}$$

Therefore, it is not really necessary to measure the magnetic field itself. Furthermore, if the magnetic field is being measured and the probe is misoriented so that electric mode currents flow in the load, Eqs. VI-1 show that these currents will also be proportional to the magnetic field and therefore will produce no error in a relative measurement, provided only that the probe orientation remains constant with respect to spherical coordinates.

2. Universal probe

It is interesting that for any linearly polarized field with, say, only B_Φ and E_Θ present, a singly-loaded loop can be so oriented as to respond to B alone, E alone, or a combination of B and E. In Fig. VI-2 the following equations apply to the respective load currents:

$$I_L = S_B^{(1)} c B_\Phi \tag{VI-2a}$$

$$I_L = S_E^{(1)} E_\Theta \tag{VI-2b}$$

$$I_L = S_B^{(1)} c B_\Phi + S_E^{(1)} E_\Theta . \tag{VI-2c}$$

For probes of a convenient size it is quite possible to have $S_E^{(1)}$ and $S_B^{(1)}$ equal (Chapters III and IV). This is the basis of a rather interesting "universal microwave probe" proposed by Conley and Talham [1], mainly for demonstration purposes. A very similar situation can be found in certain transmission line measurements, which are discussed in Chapter VII.

3. Direction finders [2]

The direction finding loop is typically a shielded loop with the gap load at the top, free to rotate about the vertical z axis in order to determine the azimuth of an incoming vertically polarized signal. Figure VI-3 illustrates the loop response to the four possible types of incident traveling wave. I_B is the load current due to the incident B field and I_E is the load current due to the incident E field. With this type of loop the observed output is I_L:

$$I_L = I_B + I_E . \tag{VI-3}$$

The loop is rotated to the position for a null in I_L and then assumed to lie in a plane perpendicular to the direction of propagation (and to the azimuth of the distant source).

The wave incident on the loop may be a composite of all four postulated types even if the distant source is transmitting only a horizontally propagated, vertically polarized wave. This is due to various propagation effects such as scattering, refraction, and ionospheric reflection [3]. There are two types of errors introduced by these waves, antenna effect and night effect.

Antenna effect is due to the presence of electric mode currents in the load. It is normally thought of as referring to the effect of a vertical electric mode in an unshielded loop when the load is unbalanced with respect to ground, but it applies equally well to the case of the horizontal electric mode from a horizontally polarized wave, as in Figs. VI-3b, c, d. At low frequencies the loops used are electrically so small in diameter that $S_E^{(1)}$ is very small compared to $S_B^{(1)}$ and the response to the electric mode is negligible. At higher frequencies, however, it is expected that antenna effect will become quite significant if a horizontally polarized electric field is present in addition to the vertically polarized field. For example, if the loop is turned to the null position for the vertically polarized incident field of Fig. VI-3a, it will be in the position for maximum current due to any horizontally polarized field like that in Fig. VI-3b. Therefore, the null in the load current of the loop will depend upon a combination of the two currents as in Eq. VI-3 and may occur at practically any angle with respect to the direction of propagation, so that the measured direction of the source will be in error. This effect must be eliminated by making the system error ratio small. It has been shown in previous chapters that this may be accomplished by making the loop physically very small (diameter less than $.01\lambda$), or by a double loading scheme with cancellation of the undesired current.

Night effect is due to the presence of vertically propagated waves.* With a vertically polarized source the normally polarized vertically propagated wave produces no error as seen in Fig. VI-3c, but the abnormally polarized wave shown in Fig. VI-3d can produce large errors. For the abnormally polarized wave both I_B and I_E have maxima when the loop is in the usual null position and this will lead to an error in source bearing determination. Again, the value of I_E can be made negligibly small, as described above, but I_B remains as a source of error which could only be eliminated by rotating the loop to the horizontal plane, in which case it would provide no azimuth information.

4. Fields due to multiple sources

The measurement of the net field due to multiple sources reduces to the simultaneous measurement of a combination of the four field types shown in Fig. VI-3. This can be done only if the system error ratio ϵ due to electric modes is made very small. The problem is the presence of three components of electric field rather than the two present in a single far-zone field. This will be discussed further in Section B below.

- - - - - - -

*These may arise from elevation of the source in an airplane or from ionospheric reflection of radio frequency waves.

Section B. Near-Zone Fields

5. General comments

The measurement of near-zone fields is characterized by the presence of longitudinal as well as transverse components of the field vectors, so that, in general, all three components of $\mathbf{E}$ and $\mathbf{B}$ will be present. The use of an electric dipole to measure $\mathbf{E}$ is still straightforward, but the measurement of $\mathbf{B}$ is more difficult.

In the far-zone type of field it was possible to orient a loop probe so that electric modes were not excited. In rectangular coordinates, this method is only possible if the following requirements are satisfied:

To measure B_x, E_y or E_z must be zero

To measure B_y, E_z or E_x must be zero

To measure B_z, E_y or E_x must be zero.

For example, the field components B_x and B_y of a transverse wave traveling in the z direction may easily be measured by making use of the fact that E_z is zero. But the presence of the longitudinal field component, E_z, in a near-zone type of field makes it impossible to orient the probe for the desired $\mathbf{B}$ response without an $\mathbf{E}$ response being present also.

6. Methods of attack

Since, in general, undesired electric modes will be excited in a loop probe, they must be made negligibly small or canceled out. A measure of the relative response of the entire system to unit electric field as compared to its response to unit magnetic field* is the system error ratio ϵ_S.

- - - - - - -

*Here magnetic field is cB, measured in the same units as $\mathbf{E}$.

$$\epsilon_S = \frac{S_{SE}}{S_{SB}} \tag{VI-4}$$

where S_{SE} and S_{SB} are now system sensitivities. For the singly-loaded loop, S_{SE} and S_{SB} are the same as the probe sensitivities $S_E^{(1)}$ and $S_B^{(1)}$, but for the doubly-loaded loop with a balun detector (Section I-13, 14) in the difference output circuit:

$$S_{SE} = S'_{\Delta U} S_E^{(2)} \tag{VI-5a}$$

$$S_{SB} = S_B^{(2)} \tag{VI-5b}$$

where $S'_{\Delta u}$ is a mode separation constant for the entire system.* Therefore, the system error ratios are:

$$\epsilon_S^{(1)} = \epsilon^{(1)} \tag{VI-6a}$$

$$\epsilon_S^{(2)} = S'_{\Delta U} \epsilon^{(2)}. \tag{VI-6b}$$

For magnetic probe use, the system error ratio must be minimized. It has been shown in Chapters III and IV that $\epsilon^{(1)}$ can be reduced without limit by decreasing the diameter of the probe, but that the diameter must be of the order of $.01\lambda$ before the error ratio is reduced to 10% and of the order of $.001\lambda$ for an error ratio of 1%. This is the simplest method of approach and should be used if it is possible to construct a small enough probe.

At microwave frequencies it may be difficult to construct a singly-loaded loop small enough to make the electric response negligible. If this is the case, two courses are open: making two measurements with a singly-loaded loop, or making one measurement with a doubly-loaded loop [4].

- - - - - - -

*Compare with Eqs. I-2, 3 where $S_{\Delta U}$ is a scattering matrix element for the balun detector alone.

In the first method, the load currents with the loop in a given position and rotated 180 degrees from that position are:

$$I_{L0} = S_B^{(1)} (c\, B_{y0}) + S_E^{(1)} (E_{z0}) \qquad \text{(III-38b)}$$

$$I_{L\pi} = S_B^{(1)} (c\, B_{y0}) - S_E^{(1)} (E_{z0}). \qquad \text{(III-41)}$$

I_{L0} and $I_{L\pi}$ may be measured consecutively and then added to get a current proportional only to B. This method requires a probe-rotating system accurate to 0.5 degree for accuracy of 1% in the usual case with an E_x field present, but only within 8 degrees if such a field component is known to be absent.

The second method has the advantage of requiring only a single measurement at each field point. A probe-rotating system is not required except for the initial balancing of the loop system. Since this can be done at a single point in a known field, and in particular a field with $E_x = 0$, the rotating system can be very simple and need only have a relative accuracy of 8 degrees. Once the balance is adjusted (Section I-14), the probe can then be used to measure any unknown field. The accuracy of this method depends on both the error ratio and the balance adjustment. For a doubly-loaded loop of any size less than .125λ in diameter,* $|\epsilon^{(2)}|$ does not differ very greatly from 1, so that very small probe size need not be achieved. It is, however, essential to make a good balance adjustment, and it was indeed possible to reduce $S'_{\Delta U}$ to 2% without undue difficulty. Greater accuracy would probably require much more refined techniques.

- - - - - - -

*This method can be used with larger probes, too, but account must then be taken of resonance effects on the currents in the loop and the small loop analysis breaks down. Furthermore, there will be significant field averaging effects for large probes.

7. Experiment

Equations III-38b, 41 above show that the accuracy of a magnetic field measurement with an electric response present can be determined by comparing the two output currents from the probe in a given location, rotated 180 degrees in its plane between readings. Any difference in these currents is due to an error dependent on the electric field.

The experiment was conducted using the near-zone field of a unipole over an image plane in the free-space room (Chapter I). This has an elliptically-polarized electric field lying in the plane normal to the magnetic field (Fig. VI-4), so that electric modes will be excited for any usable orientation of the loop. The magnetic field, B_ϕ in confocal coordinates, was measured along the equi-phase ellipse with $k_e = 2.0$ in a plane containing the source antenna (Fig. VI-4). Four runs were taken with each probe, using the four different rotational orientations indicated in Fig. VI-5. Square loops of various diameters and with both single and double loads were used.

8. Results

The results were normalized in pairs, Right-Left and Out-In, to a magnitude of 100 and a phase of 0 degrees at the position of the image plane (arcsin $k_h = 0^o$),* and plotted against arcsin k_h in Figs. VI-6a - h.

For the singly-loaded loops, the two magnitude curves, Right and Left, are seen to differ from each other by a significant amount even for the smallest

- - - - - - -

*This point, being the point of maximum field intensity, would usually be chosen for normalization of relative measurements. The normalization was done by pairs to allow direct comparison of readings with probe orientations differing by 180 degrees.

probe, $2d = .013\lambda$, and the difference increases greatly for larger probes. In phase there is good agreement only out to a certain angle, at which point one of the measured phases jumps by 180 degrees.

The magnitudes measured using the singly-loaded loop with orientations Out and In,* and those using the doubly-loaded probe differ by only 2% of the maximum field. The phases in these instances differ by 2 to 6 degrees, with the smallest probes giving the smallest differences, and the singly and doubly-loaded loops performing equally well. Near the null in the field at $\arcsin k_h = 90^\circ$ the measured phases are seen to deviate somewhat from the theoretically expected constant value.† For present purposes, this does not matter, since it is only the difference between pairs of values that is of interest.

In absolute terms, remembering that $\tan 5^\circ \doteq 0.1$ so that 5° error corresponds to 10% error, it is found that for $\arcsin k_h \leq 85^\circ$ the magnitude and phase of B are measured within at least 10% accuracy by either the singly-loaded loop oriented Out and In or the doubly-loaded loop with any orientation. The mean deviation for a given loop over the entire range of fields is about 1%. No dependence on loop size is observed.

- - - - - - -

*It is to be noted that the field exciting the load current in the singly-loaded loop with Out-In orientation is practically identical to a far-zone field, with $E_\epsilon \doteq c\, B_\phi$, so that the electric response is proportional to the magnetic response and will introduce no error in a relative measurement, as discussed in Section VI-1.

†These deviations are due to the actual presence of scattered fields and to the difficulty of phase measurement near a null. They are discussed more fully in Appendix A.

Section C. Conclusions

9. Conclusions

The singly-loaded loop is suitable for measuring general fields only if its diameter is very small, $2d \leq .003\lambda$ for about 3% accuracy. It may be used for far-zone type fields even if its diameter is large, provided that there is no electric field parallel to the load, or, for relative measurements only, if the electric field parallel to the load is directly proportional to the magnetic field anyway. In other situations, the singly-loaded loop makes a very poor, and even inadequate, probe.

The doubly-loaded loop, with an associated balun-detector circuit can be used in all cases, provided that the balancing circuits are properly adjusted. The only limitation on probe size comes when field-averaging effects become significant (Section III-2).

It should be recalled from Chapter V that a bridged loop has a somewhat lower error ratio than a square loop of the same size, and from Chapter IV that the difference between error ratios is negligible for square and circular loops of the same magnetic sensitivity.

Bibliography, Chapter VI

1. Conley, R. E., and R. J. Talham, "A Universal Microwave Probe," American Journal of Physics, Vol. 25, p. 568 (1957).

2. Bond, Donald S., Radio Direction Finders, Chapter III, McGraw-Hill, New York (1944).

3. Terman, Frederick E., Radio Engineers Handbook, Section 10, McGraw-Hill, New York (1943).

4. King, Ronold W. P., "Quasi-Stationary and Nonstationary Currents in Electric Circuits," Handbuch der Physic, Vol. 16, p. 278, Springer-Verlag, Berlin (1958).

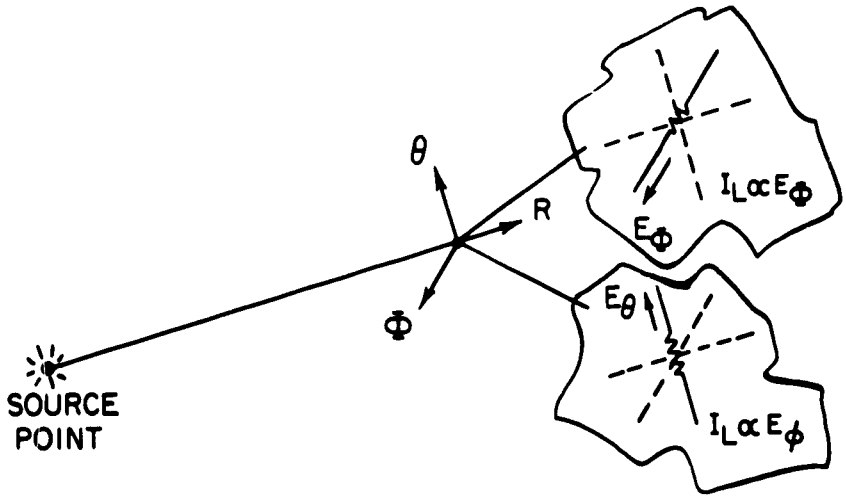

(a) ELECTRIC FIELD: PROBE ORIENTATIONS FOR MEASURING E_Φ AND E_θ

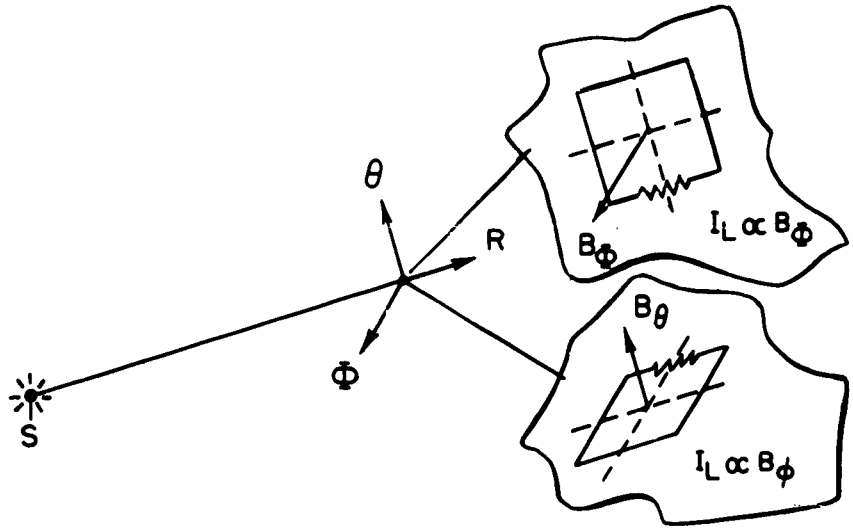

(b) MAGNETIC FIELD: PROBE ORIENTATIONS FOR MEASURING B_Φ AND B_θ

VI-1 FAR ZONE FIELD MEASUREMENTS

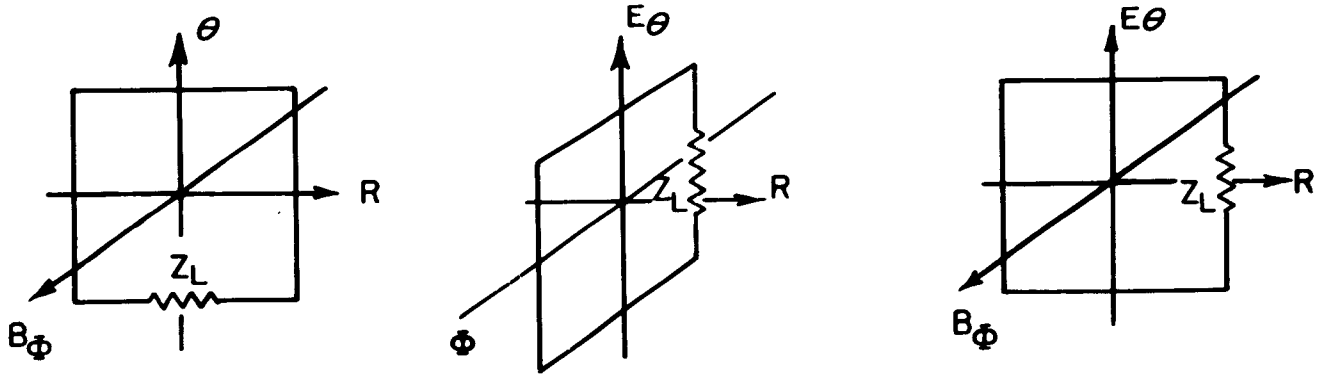

(a) MAGNETIC RESPONSE ONLY (b) ELECTRIC RESPONSE ONLY (c) COMBINED RESPONSE

VI-2 EFFECT OF PROBE ORIENTATION

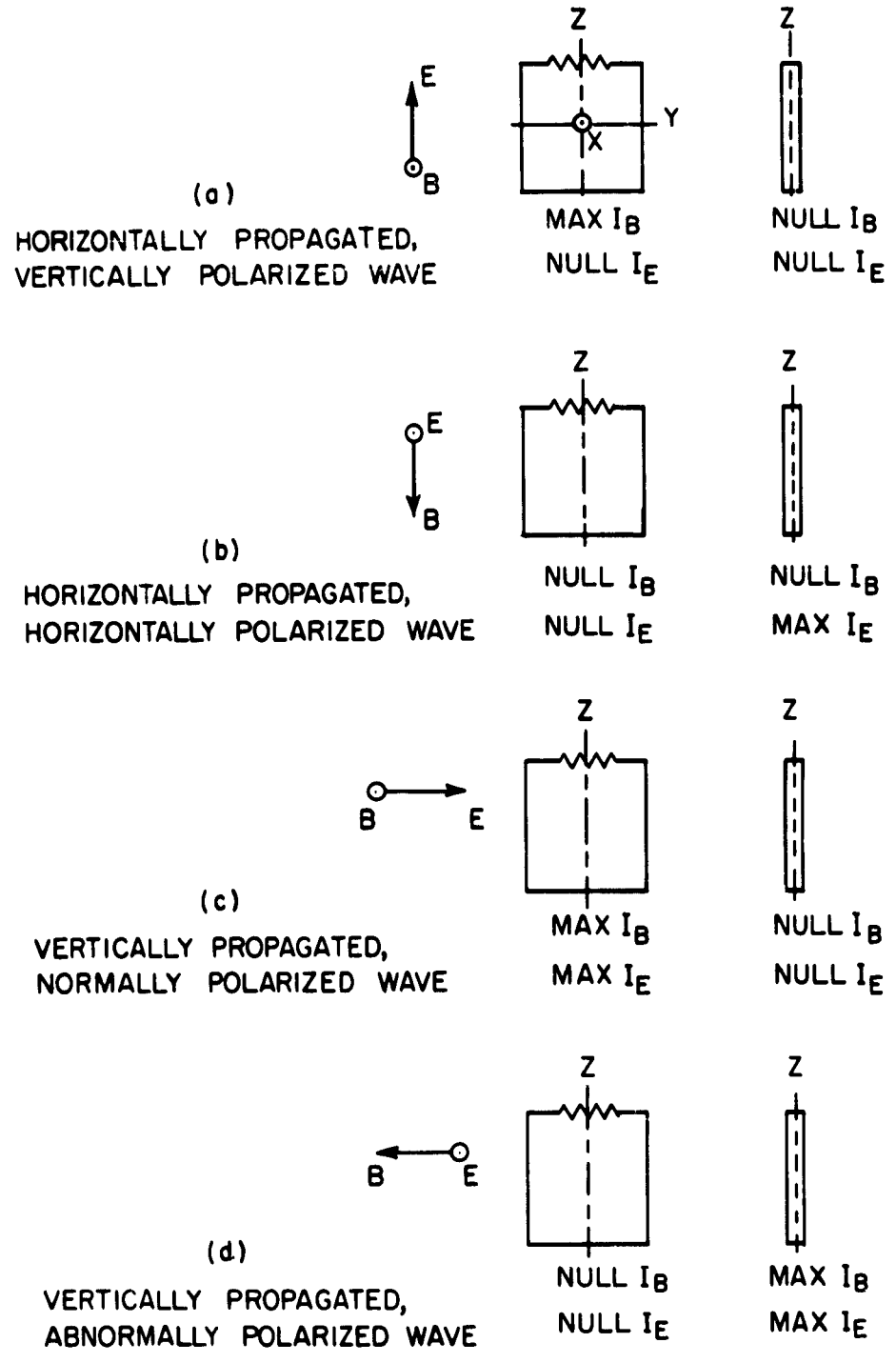

VI-3 DIRECTION FINDING LOOP

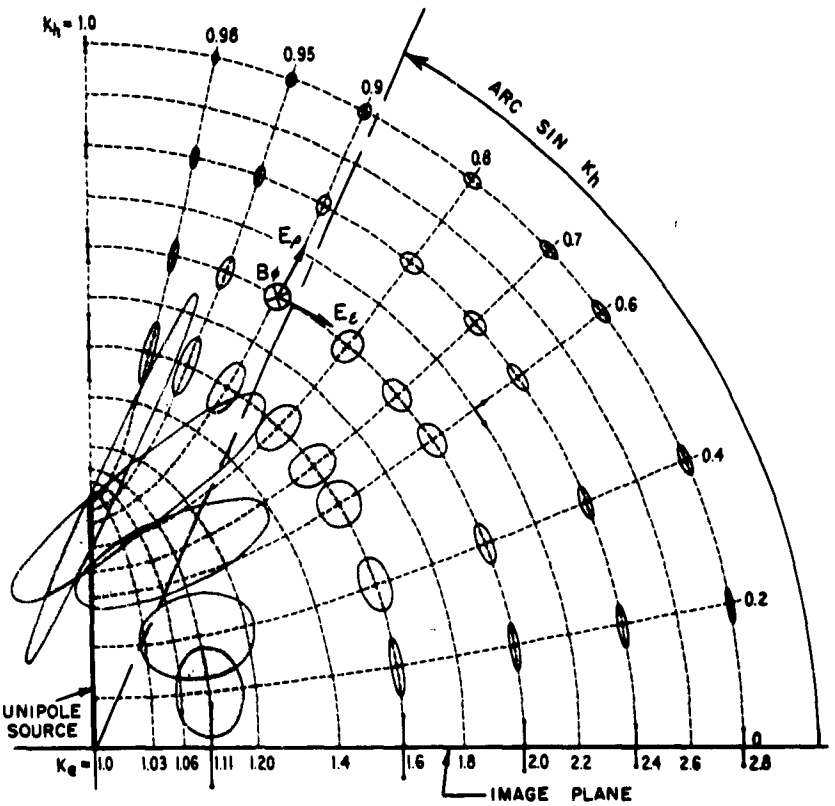

FIG VI-4 ELLIPTICALLY POLARIZED ELECTRIC FIELD NEAR A QUATER-WAVE UNIPOLE

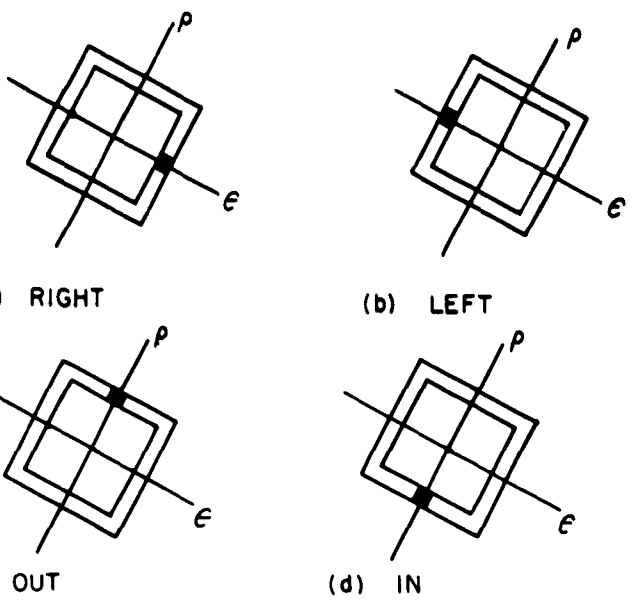

VI-5 FOUR PROBE ORIENTATIONS

VI-6a MEASURED MAGNETIC FIELD: QUARTER WAVE UNIPOLE

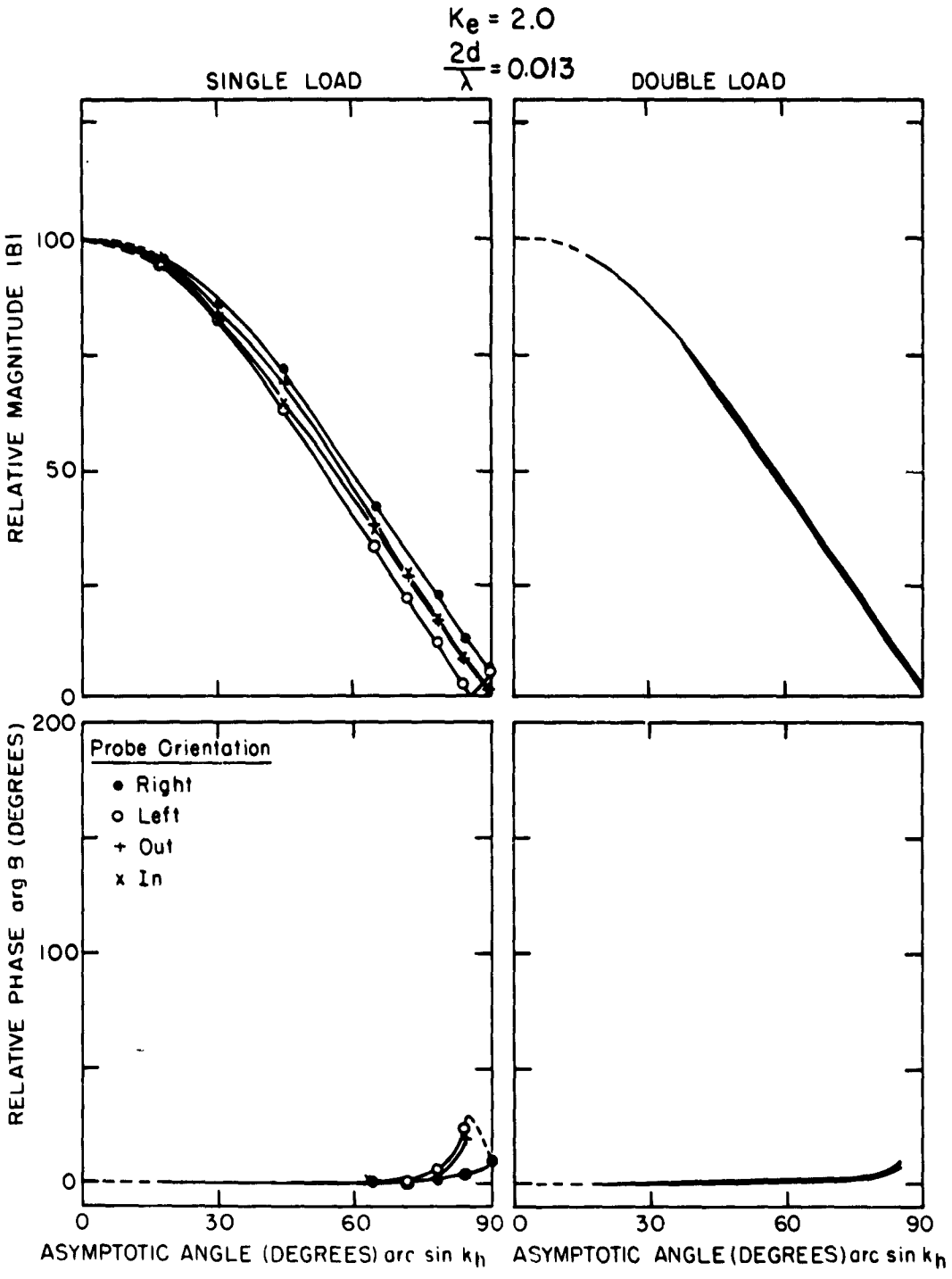

VI-6b MEASURED MAGNETIC FIELD: QUARTER WAVE UNIPOLE

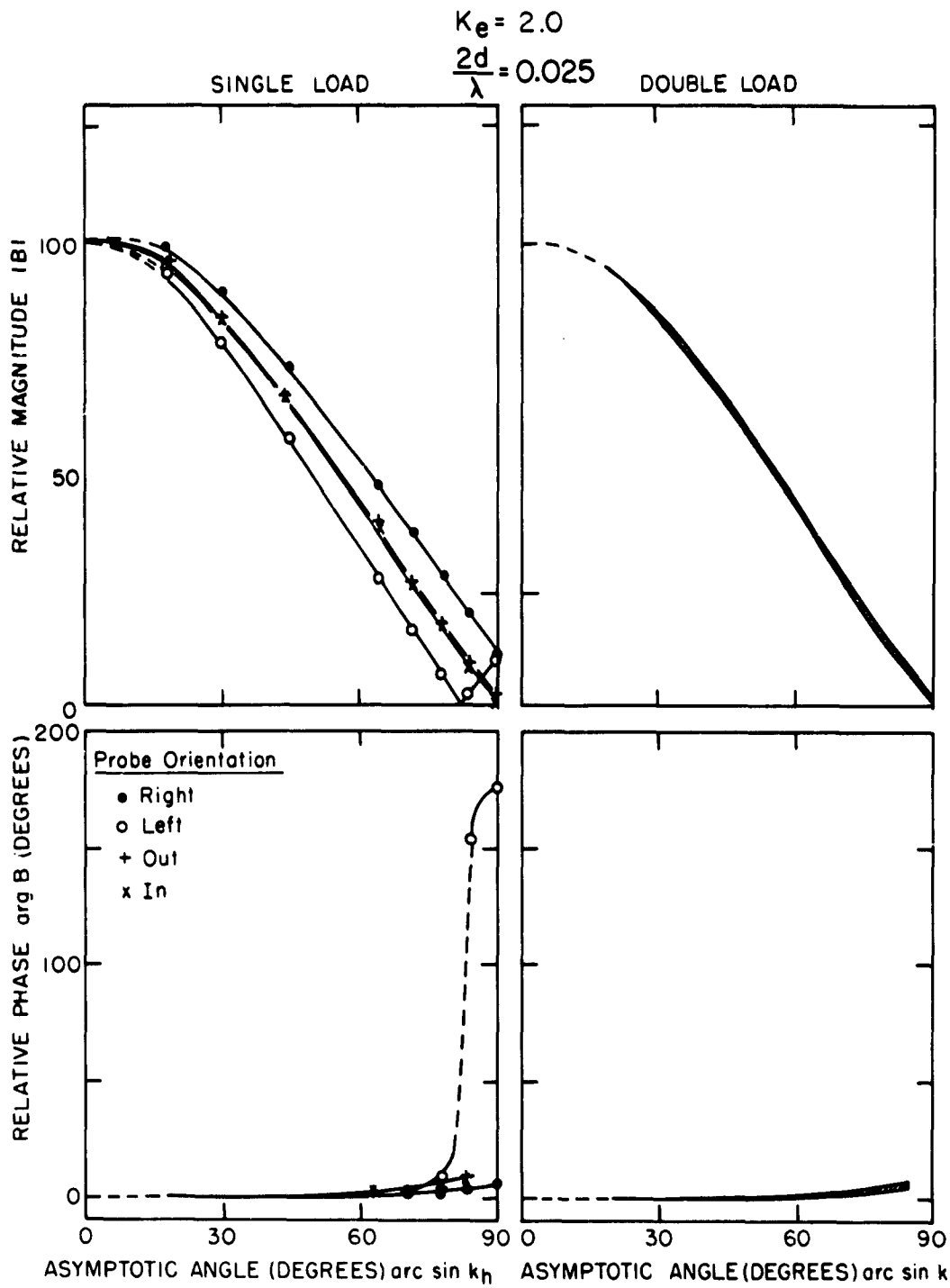

VI-6c MEASURED MAGNETIC FIELD: QUARTER WAVE UNIPOLE

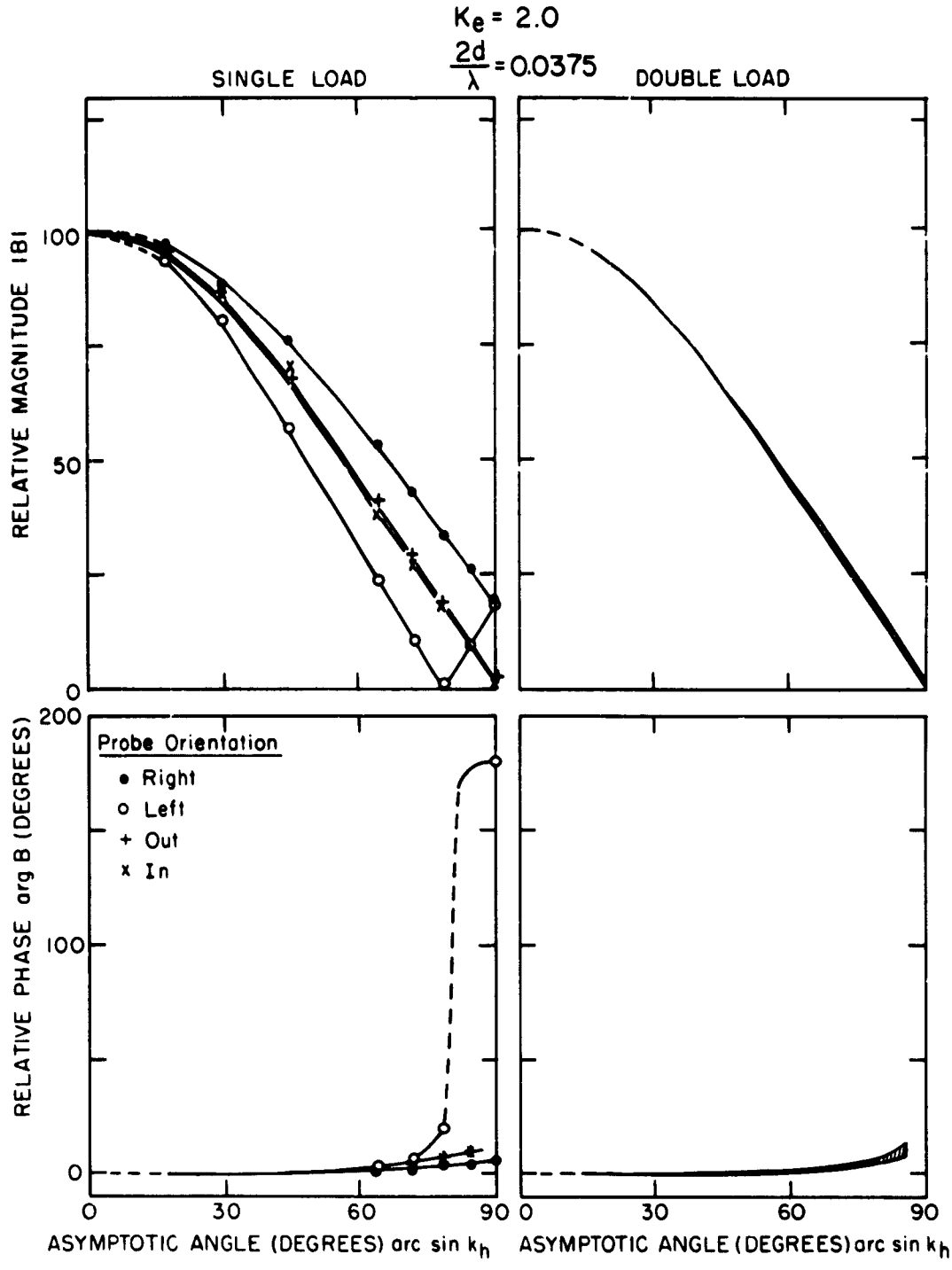

VI-6d MEASURED MAGNETIC FIELD: QUARTER WAVE UNIPOLE

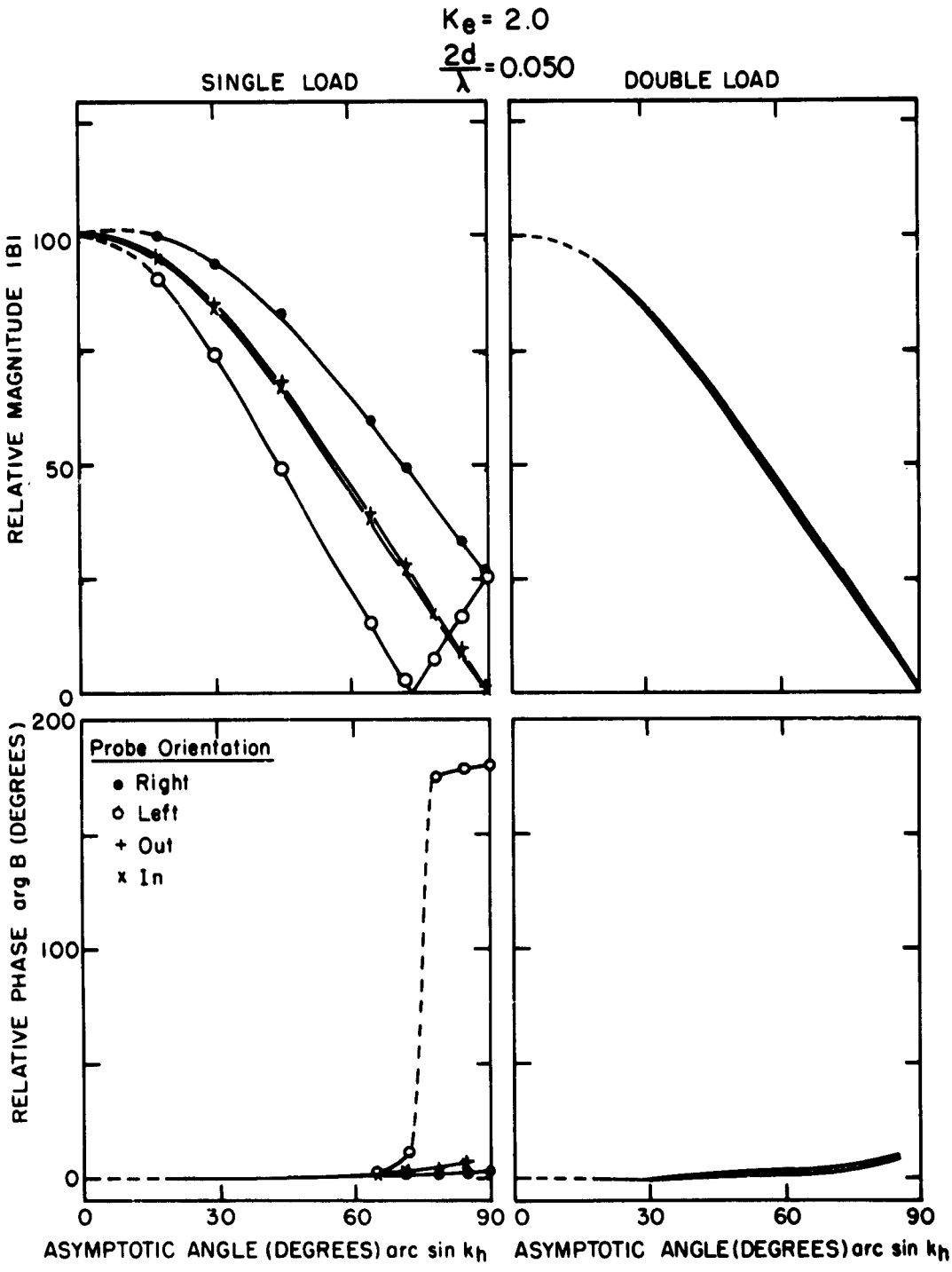

VI-6e MEASURED MAGNETIC FIELD: QUARTER WAVE UNIPOLE

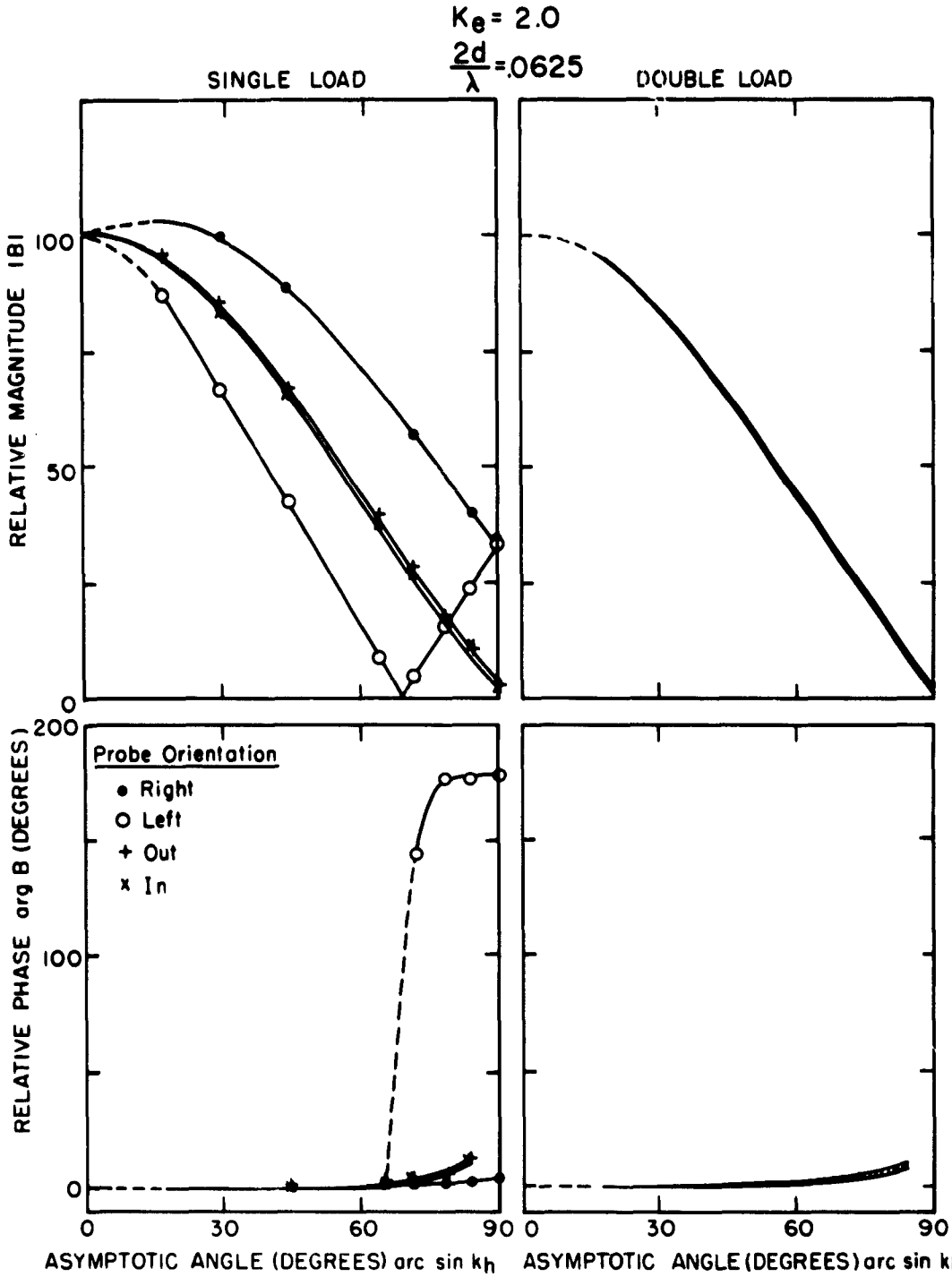

VI-6f MEASURED MAGNETIC FIELD: QUARTER WAVE UNIPOLE

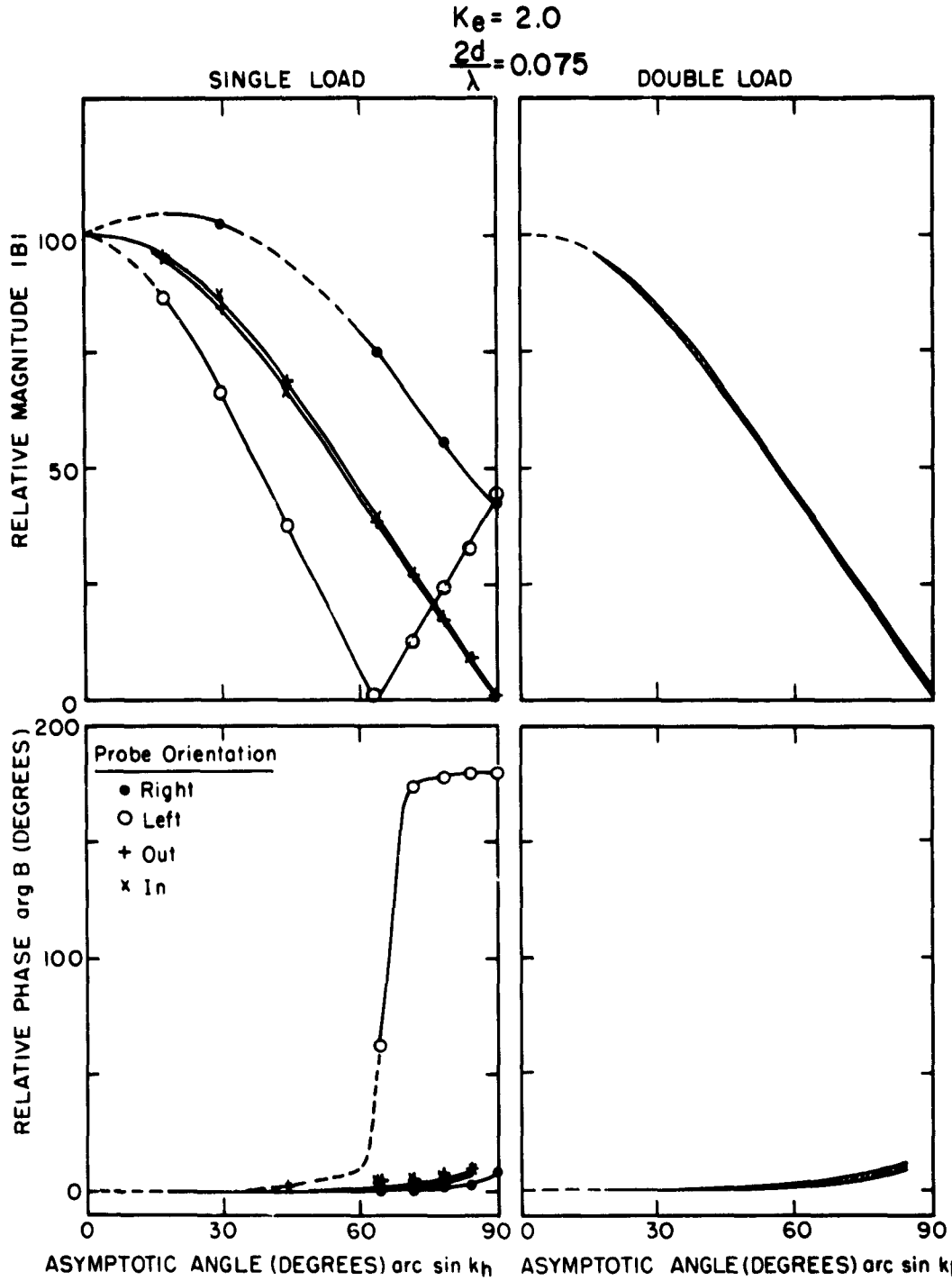

VI-6g MEASURED MAGNETIC FIELD: QUARTER WAVE UNIPOLE

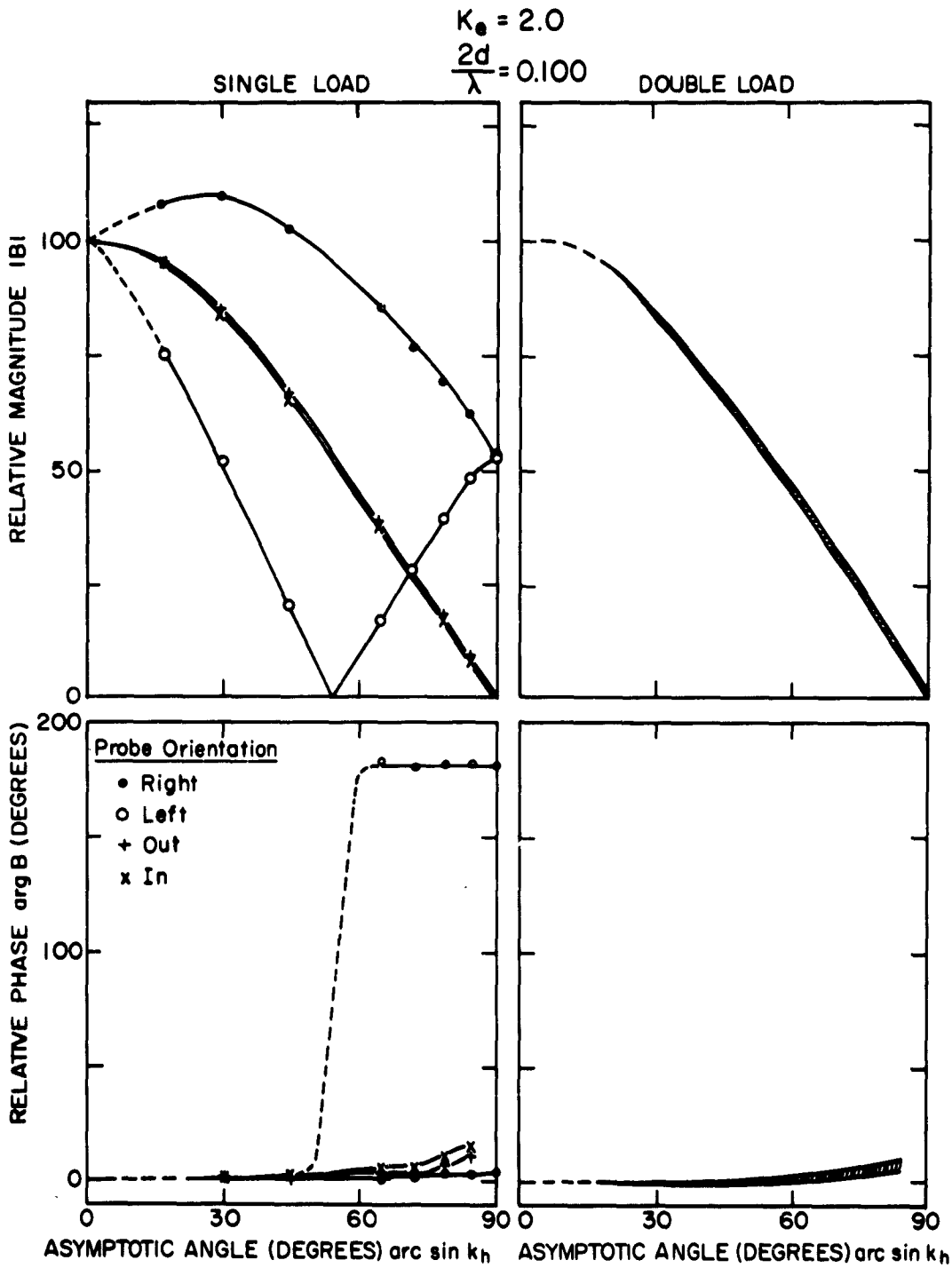

VI-6h MEASURED MAGNETIC FIELD : QUARTER WAVE UNIPOLE

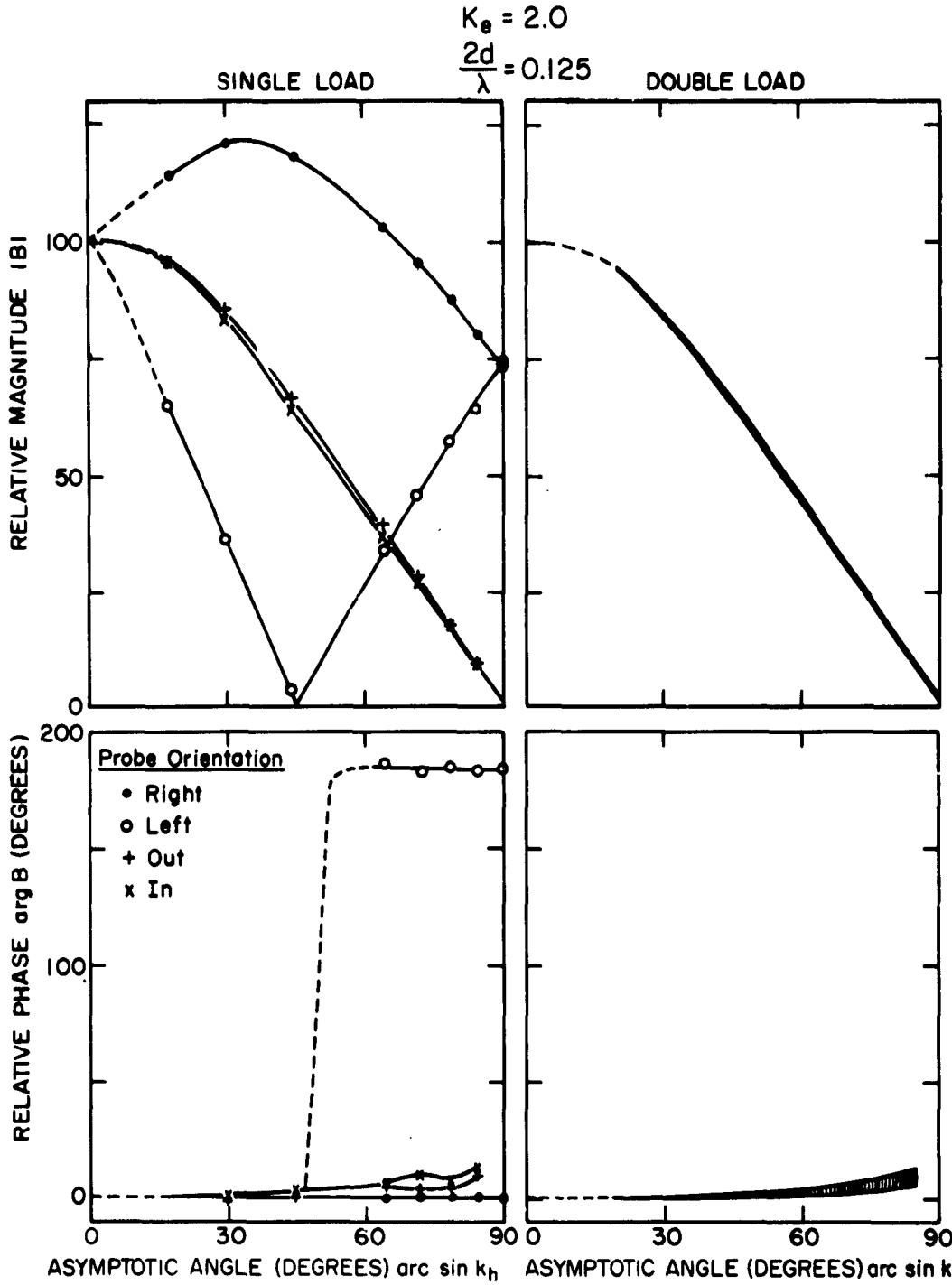

CHAPTER VII. TRANSMISSION LINE AND ANTENNA CURRENT MEASUREMENTS

Section A. Coaxial Line Currents

1. Theory

In a coaxial line it is customary to use a small movable loop protruding from the center conductor as a probe for measuring the transmission line current [1] (Fig. VII-1a). It is instructive to study the basis upon which this can be done.

The Ampere-Maxwell equation can be written in integral form for the region within the coaxial line:

$$\oint \vec{H} \cdot \vec{ds} = \int_a (\vec{J} + \frac{\partial D}{\partial t}) \cdot \vec{da} \ . \qquad \text{(VII-1)}$$

If the line integral is taken around a circle of radius r lying in the plane perpendicular to the center conductor, and it is noted that the longitudinal component of $\vec{D}$ vanishes and that H_θ is independent of θ, this equation reduces in cylindrical coordinates to:

$$2\pi r H_\theta = I_z \qquad \text{(VII-2)}$$

where I_z is the total current in the center conductor. For a simple medium filling the line this leads to:

$$c B_\theta = \frac{1}{2\pi r} \sqrt{\frac{\mu}{\epsilon}} I_z \ . \qquad \text{(VII-3)}$$

This equation shows clearly that a probe which measures B_θ at constant r can be considered to measure I_z as a function of z when it is moved along the line. Ideally the current in a loop probe lying in a plane longitudinal to the line is a measure of $c B_\theta$ at the center of the loop, so it makes a very satisfactory current probe. The only question to be asked is how well such a loop approaches the ideal.

2. Possible sources of error

In summary, the theory makes the following assumptions:

1. D_z vanishes
2. H_ϕ is independent of θ
3. The probe measures B_θ
4. The probe travels at constant r.

The first and second assumptions are equivalent to assuming that only the TEM mode is present. It can be shown [2] that all higher order modes are cut off if the average of the inner and outer radii of the line is less than about 0.16λ.

The last assumption depends only on accurate construction. The use of slotted tubing for the center conductor with the probe traveling in the slot and positioned next to the surface (where the field is greatest) fulfills this requirement very well. The introduction of a slot in the center conductor may introduce local fringing fields,but usually this is not a problem. The effect of such a slot has been discussed in some detail by Morita [3], and he concludes that its effect is a slight reduction in the magnetic field in the vicinity of the slot. Since the reduced field is directly proportional to the original field, and thus to the current I_z, this will produce no error in a relative measurement of the longitudinal distribution of current.

The main difficulty arises in connection with assumption number three. In the first place this requires that the probe be so small that it produces a negligible effect on the input impedance of the line,* that is, that probe loading

- - - - - - -

*Sometimes it is stated that the probe must not alter the field to be measured, but this is an impossible requirement. The current induced in a conducting

be negligible. It has been observed in a few cases that this requirement is satisfied by probes with dimensions smaller than the diameter of the center conductor.

In the second place, an electric field E_r is present in addition to B_θ, and this may also excite probe currents. The existence of such an electric dipole mode in a loop probe has already been discussed in some detail in previous chapters. The ratio of loop current due to unit electric field to the current due to unit magnetic field (both measured in volts/meter) has been defined as the loop error ratio, ϵ. In the present situation it is necessary either to make ϵ very small or to locate the load of the loop at a zero of the electric mode currents. In practice, it is attempted to do both of these at once.

The conventional probe shown in Fig. VII-1a has the load gap located symmetrically with respect to E_r, and since E_z is zero, no electric mode current enters the load. If the load is actually off center because of manufacturing tolerances, the currents excited by E_r will not vanish at the load and error will be introduced. The magnitude of this error can be estimated as follows: let s_t be the total perimeter of the loop and its image in the coaxial center conductor, δ the displacement of the load from the symmetric position, and ϵ the error ratio of the loop. For small loops the electric mode current can be approximated by a triangular distribution with zeros on the axis of symmetry. The electric mode current at the "center" of a side is:

- - - - - - -

probe must produce a field equal and opposite to the incident field along the probe surface in order that the boundary conditions be satisfied. The real requirement is that the field scattered by the probe be negligible except in a small region around the probe itself, so that this local perturbation will be proportional to the pre-existent field at that point. That is, the incident field must not be changed by the presence of the probe although the total field will be changed.

$$I_E = S_E E_r \tag{VII-4}$$

and therefore the electric mode current at the asymmetrically located load is:

$$I_{LE} \doteq \frac{\delta}{\frac{1}{4} s_t} S_E E_r \,. \tag{VII-5}$$

The magnetic mode current is given as usual by:

$$I_{LB} = S_B \, c B_0 \,. \tag{VII-6}$$

Therefore, the ratio of the undesired to the desired output current is:

$$\frac{I_{LE}}{I_{LB}} \doteq \frac{\delta}{\frac{1}{4} s_t} \epsilon \frac{E_r}{c B_0} \tag{VII-7}$$

and the total current in the load is:

$$I_L = I_{LB} + I_{LE} \,. \tag{VII-8}$$

In deriving this equation the actual shapes of the loop and its image have been ignored, so that it is only an order of magnitude calculation. For an incident traveling wave $E_r = c B_0$, but for a standing wave the ratio $\frac{E_r}{c B_0}$ may assume any value from zero to infinity, so that it is very desirable to make the first two factors as small as possible. The factor $\frac{\delta}{(1/4) s_t}$ can be made as small as 0.01 by good machining, but it is questionable whether it can be made much smaller for small sized probes. The loop error ratio ϵ has not been calculated for a loop with asymmetrically located loads, which would correspond to this loop with its image. It is expected that ϵ will lie somewhere between the value for the unloaded case (which corresponds to exact symmetry*) and the value for the singly-loaded case (which corresponds to complete asymmetry). But these values are equal, since the load admittance factor cancels out in the expression

- - - - - - -

*In the case of exact symmetry, the load is at a zero of the electric mode current and therefore can have no effect on it.

for $\epsilon^{(1)}$ (Eq. III-39, 40). The loop and image do not have a simple shape, but there is no reason to believe that the error ratio for such a shape will differ greatly from that for a square or circular loop of the same diameter. From these considerations it is seen that each individual probe should be tested for electric response, a procedure which will be discussed below.

The probe in Fig. VII-16 has the advantage that the load and its image are adjacent, so that it behaves essentially like a singly-loaded loop, for which the error ratio can be reduced indefinitely by reducing the loop size. On the other hand, the load is in the position for maximum response to E_r, so that the error current in the load may be very large compared to the desired current if, as in the case of standing waves in the main line, $E_r >> c B_\theta$.

In Fig. VII-1c is shown a doubly-loaded probe with two outputs which can be added at the detector in the usual way to cancel the electric mode currents I_{LE} due to E_r and leave the desired magnetic mode current I_{LB}. This probe is more complicated than that of Fig. VII-1a and the balance adjustment probably cannot be made any better than the load can be symmetrically located, so there is no practical advantage in using this style for coaxial line measurements. Despite these considerations, this probe is of interest with a view to application in antenna current measurements where E_z is not zero and the conventional loop encounters difficulties.

3. Testing the probe for error

A study of the distribution curve in a short-circuited coaxial line is adequate to determine the probe error for coaxial line measurements in general. For a lossless line and a perfect short circuit, the fields at the surface of the center conductor are given as functions of w, the distance from the load, by:

$$c B_\theta(a, w) = 2 c B_{0a} \cos kw \qquad \text{(VII-9a)}$$

$$E_r(a, w) = j 2 E_{0a} \sin kw. \qquad \text{(VII-9b)}$$

For any probe the output current is the sum of the components proportional to each of these fields:

$$I_L(w) = S_B(2 c B_{0a} \cos kw) + S_E(j 2 E_{0a} \sin kw) \qquad \text{(VII-10a)}$$

where S_B and S_E are suitably defined complex sensitivity constants. In general, $c B_{0a}$ equals E_{0a}, and for convenience these may be taken equal to 0.5, leaving:

$$I_L(w) = S_B \cos kw + j S_E \sin kw. \qquad \text{(VII-10b)}$$

Let w_0 be the position of a minimum in the magnetic field, exactly one-quarter wavelength from the load, and w_1 the position of a maximum in the magnetic field, exactly one-half wavelength from the load. Then:

$$\frac{I_L(w_0)}{I_L(w_1)} = \frac{j S_E}{S_B} = je \qquad \text{(VII-11)}$$

where e is a suitably defined error ratio which can be determined from the relative output currents at these two points. This method has the disadvantage that the calibration points must be located mechanically, assuming the load to be a perfect short citcuit. For a reactive load, it would be necessary to measure the actual load impedance, using a charge probe, and make an appropriate correction to the location of magnetic field maximum and minimum.

It has been suggested in the past [3] that the degree of balance (symmetry) of a probe may be tested by examining the symmetry of the distribution curve near the minimum. Letting $e = e' + je''$, where e' and e'' are real, the magnitude of the output current can be deduced from Eq. VII-10b:

$$|I_L(w)| = |S_B| \sqrt{\cos^2 kw + |e|^2 \sin^2 kw - 2 e'' \sin kw \cos kw} \qquad \text{(VII-12)}$$

From this equation it is seen that it is only the imaginary part of e that will cause an asymmetry of $|I_0(w)|$ near the minimum, so that examination of the symmetry will not reveal the presence of a real part in e . For this reason the previous method, using the currents at quarter and half wave points is preferred. It is also seen that the presence of a real part in e does cause the distribution curve to differ from the normal $|\cos kw|$ shape,* a condition which is easily recognized by the occurrence of a finite, non-zero value of the minimum current.

The presence of losses in the line or the load complicates the testing still further. In the case of low losses, the usual transmission line equations [4] combined with Eq. VII-8 lead to a new expression for the load current in the probe:

$$I_L(w) = S_B\left\{(1 - j\pi \frac{\alpha}{\beta}) \cos \beta w + j (e - \pi \frac{\alpha}{\beta} - \frac{Z_S}{Z_C}) \sin \beta w\right\} \quad \text{(VII-13)}$$

where α and β are the real and imaginary parts of the propagation constant (now complex), Z_S is the load impedance, Z_C is the characteristic impedance of the line, and the incident field has been normalized as in Eq. VII-10b. It is seen at once that e can be found directly using the method of Eq. VII-11 only if $\pi \frac{\alpha}{\beta} << e$, $\pi \frac{\alpha}{\beta} << 1$, and $\frac{Z_S}{Z_C} << e$. Otherwise three independent measurements would have to be made. This could be done by first measuring $\frac{\alpha}{\beta}$ and $\frac{Z_S}{Z_C}$ with a charge probe and then making a current measurement using Eq. VII-13, but this does not lend itself to a procedure for minimizing e ; it just allows its determination for a given configuration. Fortunately, in the

- - - - - - -

*An extreme example of this occurs for e = 1 , when $|I_0(w)| = |S_B|$ = constant.

great majority of instances, losses will be negligible and the simpler procedure of Eq. VII-11 can be used.

4. Directional couplers

The electric dipole mode of a loop has long been used in the construction of broadband coaxial directional couplers, although the analysis is usually couched in terms of capacitive and inductive coupling [5]. Referring to Fig. VII-2 for the forward wave the fields at the center of the loop are $E_r^f = c B_\theta^f$, but for the backward wave they are $E_r^b = - c B_\theta^b$. The current in the probe depends on both electric and magnetic modes:

$$I_{L2} = S_B \, c B_\theta + S_E \, E_r \qquad \text{(VII-14)}$$

where S_E and S_B are over-all probe sensitivities for the coupling loop, and their ratio is the error ratio e. Then:

$$I_{L2} = S_B \left[(1 + e) \, c B_\theta^f + (1 - e) \, c B_\theta^r \right] . \qquad \text{(VII-15)}$$

Reference to Figs. III-9 and IV-5 shows that for square or circular loops an error ratio $e = -1$ may be obtained. Presumably this is also possible for a loop protruding into a coaxial line through the outer shell. In this case the detector current reduces to:

$$I_{L2} = 2 S_B \, c B_\theta^r . \qquad \text{(VII-16)}$$

This shows coupling to the backward wave only, as desired in directional coupler operation. Similarly, the detector could monitor I_{L1}, in which case it would be coupled to the forward wave only.

5. Experiment, probe loading

The first experiment was designed to test for probe loading with the particular probes used. A more general study of probe loading would be a worthwhile subject for future research.

The resonance method was used to study the effects of various probes on the apparent load impedance of a coaxial line. This is illustrated schematically in Fig. VII-3. The generator V^e and its internal impedance Z_G consist of a movable feeding piston carrying a coupling loop, driven by an external generator. By moving the piston and thus varying s, and observing the output from the fixed probe, it is possible to measure the impedance Z_{sA} looking to the right at a reference plane $A - A'$, an integral number of wavelengths from the load. The complex terminal function of this impedance is [6]:

$$\theta_{sA} = \rho_{sA} + j \phi_{sA} \tag{VII-17}$$

and the impedance can be found from:

$$Z_{sA} = Z_C \coth \theta_{sA}. \tag{VII-18}$$

A loop probe protrudes through a slot in the center conductor and can be moved along it (Fig. VII-1a). The current in the probe is proportional to the line current at the probe position, which is known from transmission line theory to be [7]:

$$|I_z| = \frac{V^e}{R_C} S_x \frac{S_w}{S_s} \tag{VII-19}$$

where $\frac{V^e S_x}{R_C}$ is a constant of the generator and line, and for low-loss lines:

$$S_w \doteq [\sinh^2 \rho_{sA} + \sin^2 (\beta_w + \phi_{sA})]^{1/2} \tag{VII-20a}$$

$$S_s \doteq [\sinh^2 \rho_{sA} + \sin^2 (\beta_s + \phi_{sA} + \phi_G)]^{1/2}. \tag{VII-20b}$$

From these equations it follows directly that if w is kept constant and s is varied by moving the generator piston, the terminal functions are given by:

$$\rho_{sA} = \coth^{-1} \frac{I_{max}}{I_{min}} \tag{VII-21a}$$

$$\phi_{sA} = \frac{\pi}{2} + \frac{2\pi}{\lambda}(s_0 - s_{max}) \qquad \text{(VII-21b)}$$

where s_0 is the line length for maximum current with a pure short circuit as a load, and s_{max} is the line length for maximum current with the actual load, a short circuit with an intervening probe of significant size. The ratio I_{max}/I_{min} is the standing-wave ratio.

The actual equipment used was a coaxial line built by Andrews [8] and illustrated in Fig. VII-4. The line is filled with Styrofoam and has an inner conductor with 0.635 cm O.D. and an outer conductor with 5.16 cm I.D. The guide wavelength was approximately 50 cm.

6. Results, probe loading

The measured reciprocal standing-wave ratio and shift in maximum position are plotted in Fig. VII-5a against probe position for singly-loaded probes of two different diameters, together with the theoretical curve for zero probe loading. The terminal functions and the impedance could be calculated directly from these quantities, but this was not necessary to determine the probe size for negligible loading effects. It is seen at once that the small probe with $2d = .01\lambda_g$ was quite satisfactory, producing negligible change in the SWR and maximum current position for any location of the probe. On the other hand, the larger probe with $2d = .03\lambda_g$ produced changes in these quantities which are unacceptably large.

Figure VII-5b shows the current distribution in a short-circuited line measured with these probes, and compared with the theoretical cosinusoidal distribution. The results for the small probe agree very closely in magnitude with the theory, but the results for the large probe deviate considerably. Part of this deviation may be due to probe asymmetry and electric mode currents,

but since the null is quite sharp and located very close to $0.25\lambda_g$ from the load, it is clear from Eq. VII-12 that this is not the major effect. The main cause of this deviation is that the large probe does indeed load down the line. The discrepancies in both phase measurements near the null in current are due to the difficulty of measuring phase near a null (Section I-15) and to some extent to probe symmetry. This latter is the reason that the smaller probe shows the larger phase deviation. In any event the phase deviations are not large.

7. Experiment, electric modes

The same equipment was used for a study of the effect of electric mode probe currents on the measured values for the current in the coaxial line. For this purpose doubly-loaded loop probes, as shown in Figs. VII-1 c and VII-13b, were used. Measurement was made of the current in the front load, I_f, the current in the rear load, I_r, and of their sum, I_B, as a function of position along a short-circuited coaxial line.

In order to obtain I_B electrically, it was necessary to use a balun detector and balancing circuits very similar to those described in Sections I-13, 14. These circuits are enclosed in a shielded box, shown with the cover off in Fig. VII-4. The balance adjustment is made by locating the probe mechanically $0.25\lambda_g$ from the (short circuit) load, and adjusting for I_B equal to zero. It is seen from Eq. VII-12 that this is the condition for zero error ratio e, now referred to the measured current I_B. This method involves the assumption of negligible losses in the line and load. Andrews' data [8] give $\pi \frac{\alpha}{\beta} = 0.00065$ for the line, so that line losses are indeed negligible. A measurement of the resistance of the short-circuit termination gives $R_S / Z_C = 0.008$, which may cause 1% error in the balance adjustment. Also, the reference position is located mechanically, so that it is only accurate to about ± 0.5 mm, which is

$0.001\ \lambda_g$. Equation VII-12 shows that this may cause an adjustment of $|e|$ that differs from zero by less than 0.013.* Therefore, the value of $|e|$ actually obtained will be less than 0.023, equivalent to 33 db separation between electric and magnetic modes.

Since the current in a coaxial line is given by $I_z = \frac{2\pi r}{\zeta} c B_\theta$ and the charge by $\frac{q}{\zeta} = \frac{2\pi r}{\zeta} E_r$,† the total load current in a singly-loaded probe can be written in a manner similar to Eq. VII-8:

$$I_L = S_I I_z + S_q \frac{q}{\zeta}. \qquad \text{(VII-22)}$$

This equation illustrates explicitly the desired (current) response, and the (undesired) charge response. The electric mode in the probe could now be called a charge mode, and the magnetic mode a current mode. Now the error ratio e is given by S_q/S_I, although its value is the same as before.

Returning to the doubly-loaded probe, it is seen that the currents to be observed are:

$$I_f = S_I I_z + S_q \frac{q}{\zeta} \qquad \text{(VII-23a)}$$

- - - - - - -

*Referring to Eq. VII-12, adjustment is made for $I_L = 0$ at the point in question. If the point is δ away from $w=0.25\lambda_g$, then this condition will imply:

$$\sin^2 k\delta + |e|^2 \cos^2 k\delta - 2e'' \sin k\delta \cos k\delta = 0$$

which reduces for small $k\delta$ to

$$|e|^2 = -k^2\delta^2 + 2e'' k\delta .$$

Therefore, the error ratio is limited by:

$$|e| \leq 2k\delta$$

and for $\delta \leq 0.001\ \lambda_g$, $|e| \leq 0.013$.

†Charge is measured here in units of coulombs/ohm to agree with the units of current. $\zeta = \sqrt{\mu/\epsilon}$ is the wave impedance in the line.

$$I_r = S_I I_z - S_q \frac{q}{\zeta} \qquad \text{(VII-23b)}$$

$$I_B = I_f + I_r = 2 S_I I_z . \qquad \text{(VII-23c)}$$

Any disagreement between I_f and I_r shows the presence of electric modes, but these are canceled in the sum current, I_B.

8. Results, electric modes

Figure VII-6 shows these effects for a probe of diameter $2d = 0.03 \lambda_g$, and one of diameter $2d = 0.01 \lambda_g$. For the larger probe the currents I_f and I_r have minima separated by $0.075 \lambda_g$ and maxima separated by $0.125 \lambda_g$. These two currents are nearly exact images of each other in both magnitude and phase with respect to the point $w = 0.25 \lambda_g$. For the smaller probe, a similar effect is observed, but the minima are only separated by $0.02 \lambda_g$ and the maxima by $0.03 \lambda_g$.

The distribution measured using I_B with the electric modes canceled out is seen to resemble the theoretical cosine distribution. However, the same deviation due to probe loading observed in Fig. VII-5b for the singly-loaded loop is found again here.

9. Conclusions, transmission line measurements

It may be concluded that the conventional singly-loaded loop of Fig. VII-1a is an adequate current probe for transmission line measurements, provided that it is small enough for probe loading to be negligible. It is possible to use a balanced doubly-loaded loop of the style of Fig. VII-1c with essentially the same accuracy, but the added complication gains no advantage in transmission line measurements. In either case, the probe must be tested for the absence of electric mode output currents.

Section B. Antenna Current Measurements

10. Theory

The measurement of the current on a linear antenna is similar to the measurement of the current in the center conductor of a coaxial line, but with the important difference that the longitudinal electric field is no longer zero. This means that a singly-loaded loop with the gap load parallel to the z axis will now have an electric mode current present in the load, due to E_z (Fig. VII-7a), in addition to the desired magnetic mode current, even if the gap is symmetrically placed.

The Ampere-Maxwell equation shows that the tangential magnetic field at the surface of the antenna, $c B_\theta$,is proportional to the total axial current in the antenna, I_z , at every point just as in Section VII-1, but the presence of a non-vanishing value of E_z at points away from the antenna surface means that the magnetic field away from the surface is no longer exactly proportional to the current. Neither the radial electric field, E_r , nor the longitudinal electric field, E_z , is proportional to the current in the line at every point. For example, an infinitely thin linear dipole of half length h has a sinusoidal current distribution:*

$$I_z = I_m \sin k(h - |z|) . \qquad \text{(VII-24)}$$

For all points that are not too near the center or the ends of the antenna, as required by:

$$(h - |z|)^2 >> r^2 \qquad \text{(VII-25a)}$$

$$|z|^2 >> r^2 \qquad \text{(VII-25b)}$$

---

*This discussion is derived from an analysis by King [9].

the fields at any point (r, z) near the antenna due to this current may be approximated by the following expressions in cylindrical coordinates:

$$c B_\theta \doteq \frac{60}{r} I_m(\sin kh \cos kz - \cos kh \sin kz) \qquad \text{(VII-26)}$$

$$E_r \doteq -j \frac{60}{r} I_m(\sin kh \sin kz + \cos kh \cos kz) \qquad \text{(VII-27)}$$

$$E_z \doteq 60 \frac{h}{(h^2 - z^2)} I_m \left\{ \left[-j \left(1 + \frac{z}{h} - \frac{h}{z}\right) \cos kh - \sin kh\right] \cos kz \right.$$

$$\left. + \left[\frac{h}{z} \cos kh - j \frac{z}{h} \sin kh\right] \sin kz \right\} . \qquad \text{(VII-28)}$$

By expanding the expression for the antenna current and using the equation of continuity to derive the expression for the charge distribution it can be shown that:

$$I_z = I_m(\sin kh \cos kz - \cos kh \sin kz) \qquad \text{(VII-29)}$$

$$cq_z = -j I_m(\sin kh \sin kz - \cos kh \cos kz) . \qquad \text{(VII-30)}$$

Therefore:

$$c B_\theta \doteq \frac{60}{r} I_z \qquad \text{(VII-31)}$$

$$E_r \doteq \frac{60}{r} cq_z . \qquad \text{(VII-32)}$$

These equations actually become exact at the surface of any linear antenna,* but away from the surface they are approximations, valid only at points where Eqs. VII-25a, b are satisfied.

It should be noted that most probes measure the fields a finite distance away from the surface of the antenna and that they will therefore lose accuracy

- - - - - - -

*Equation VII-31 was derived directly from the Maxwell-Ampere equation in Section VII-1, and Eq. VII-32 can be derived directly from Gauss' theorem, both for an arbitrary current and charge distribution.

at distances of about 10r from the ends and center of the dipole. A charge probe can consist of a short radial electric unipole, which responds only to E_r. A current probe can consist of a small loop in the r_z plane which ideally would respond only to cB_θ. Electric modes will cause departures from this ideal. Finally, it is seen that E_z is not simply related to either the current or the charge at a point on the antenna.

11. Errors with various probes

The first method of current measurement uses the singly-loaded loop of Fig. VII-7a. The current in the load is:

$$I_L = S_B (cB_\theta) + S_E E_z \qquad \text{(VII-33)}$$

where S_B and S_E are suitably defined sensitivity constants. The fields cB_θ and E_z are the values at the center of the loop. The sensitivity constants are not known exactly because the problem of the semicircular loop with its image in a cylindrical antenna has not been solved. It may be estimated, however, that the constants are about the same as for a doubly-loaded (because of the image load) circular loop of the same diameter, 2d. The load current is independent of E_r. The ratio of the error current in the probe to the desired current is:

$$\frac{I_E}{I_B} = e \frac{E_z}{cB_\theta} . \qquad \text{(VII-34)}$$

The error ratio is a constant of the probe dimensions, and may be as low as 0.3 for a small probe (Fig. III-9). The ratio of the fields varies from antenna to antenna. It can be shown from Eqs. VII-26 and 28 for a half-wave dipole that this ratio is given by:

$$\left| \frac{E_z}{cB_\theta} \right| = \frac{d}{2h} \frac{\left| 1 + j \frac{z}{h} \tan kz \right|}{1 - \left(\frac{z}{h}\right)^2} . \qquad \text{(VII-35)}$$

This ratio has a nearly constant value equal to $d/2h$ over most of the antenna, but it increases very rapidly near the end, reaching a value of $10\,\frac{d}{2h}$ at a distance $0.2\,h$ from the end, as may be seen in Fig. VII-8. It is evident from these considerations that the ratio $d/2h$ must be made as small as possible for accurate measurements. It should at least be less than 0.03 to ensure accuracy within 10% out to a distance $0.2\,h$ from the end of the antenna.

The second method of current measurement uses a doubly-loaded loop probe as shown in Fig. VII-7b. The two load currents I_f and I_r are added to give I_B in the same way as for the coaxial line, described in Section VII-6. The output current is:

$$I_B = S_B(c\,B_0) + S'_{Er}\,E_r + S'_{Ez}\,E_z\,. \qquad \text{(VII-36)}$$

Here there are different electric sensitivities for the two components of electric field. The product of the electric sensitivity for a doubly-loaded loop, S_{Er}, and the cross-coupling coefficient of the adder circuit, $S_{\Sigma U}$, gives S'_{Er}. For a perfectly balanced system, S'_{Er} would vanish, but in practice it has a value of about 0.01.* This means that 10% inaccuracy will be introduced in I_B when the field ratio $E_r/c\,B_0$ becomes greater than 10. This occurs for the half-wave dipole within $0.06\,h$ of the end. The sensitivity S'_{Ez} to the longitudinal electric field E_z appears in Eqs. VII-36 because the loads are not located at zeros of the electric dipole mode due to this field. It should be observed that this type of electric mode produces a current with the same symmetry as the magnetic mode current. Therefore, the error current $S'_{Ez}\,E_z$ cannot be canceled by the adder circuit like the usual electric mode error current. A rough estimate of the magnitude of S'_{Ez} can be made by assuming that the antenna

- - - - - - -

*This is made up of $|S_{Er}| \doteq 0.3$ and $|S_{\Sigma U}| \doteq 0.03$.

surface is the closing side of the loop, giving a loop perimeter $s_t = (2 + \pi)\, d$. Assuming that the electric dipole mode in question has a triangular distribution of current with maxima at the centers of the top and bottom of the loop, and zeros $0.25\, s_t$ from these points, the current in the loads in this mode is then about 0.06 times the maximum,* and S'_{Ez} is $0.06\, S_{Ez}$, where S_{Ez} is an electric sensitivity approximated by that for an unloaded loop. Thus, S'_{Ez} may easily have a value of 0.02 or so for a probe diameter of $.05\lambda$, an order of magnitude better than S_E for the singly-loaded loop.

It is possible to vary the design of the doubly-loaded loop probe to that shown in Fig. VII-7c in an attempt to place the load gaps nearer the zeros of the longitudinal electric mode currents. Because of the appearance of "image loads," it is doubtful what success this will have, although it will be better than the probe of Fig. VII-7b for probes of moderate size. However, its error ratio, referred to the longitudinal field, is more nearly approximated by $\epsilon^{(2)}$ than by $\epsilon^{(1)}$, so that for very small sizes this style is actually poorer than the probe of Fig. VII-7c (see Fig. III-9).

Finally, the current may be measured indirectly by using a charge probe as in Fig. VII-7d. The output current is:

$$I_L = S\, E_r \,. \qquad \text{(VII-37)}$$

From Eq. VII-32 it is seen that I_L will be proportional to the charge at every point except near the base and the ends of the antenna. The equation of continuity can be integrated to give:

- - - - - - -

*The load is displaced from the current null by a distance $(0.5\,\pi d - 0.25\, s_t)$, and thus will be at a position where the current is $(0.5\,\pi d - 0.25\, s_t)/(0.25\, s_t)$ times the maximum. Substitution for s_t gives the stated value.

$$I_z(z) = I_z(0) - j\omega \int_0^z q(z)\, dz \,. \qquad \text{(VII-38)}$$

If $q(z)$ is measured, using the charge probe, the integral can be evaluated numerically at any z. The constant $I_z(0)$ is chosen to make $I_z = 0$ at the end of the antenna, and values for $I_z(z)$ may be readily derived. This method has the disadvantage of being indirect and, therefore, more prone to experimental errors, but it has the advantage of using a probe which responds to only a single field component.

12. Experiment

The measurements of the current along a linear antenna were made on a quarter-wave unipole over a conducting screen. By the theorem of images this is equivalent to a half-wave dipole in free space, as has been discussed in Section II-4. The equipment consists of a coaxial feed line, with the center conductor extending through the image plane to form the antenna (Figs. VII-9, 10). The center conductor is slotted, with a traveling probe protruding through the slot just as in the experiment on probe loading (Section VII-5) (Fig. VII-11). The coaxial line is the one built by Andrews [8], slightly modified to allow connection of a doubly-loaded probe if desired. The image plane and the transmitter are also the same as Andrews', but a different receiver system was used. The receiver system is basically the same as that described in Section I-C with a heterodyne detector, a phase measuring bridge, and a balun detector for adding and subtracting the two load currents from a doubly-loaded loop (Figs. VII-4, 12).

Two singly-loaded probes with diameters $2d = 0.01\lambda$ and 0.004λ, as illustrated in Figs. VII-7a, 13c were used in the first method of current

determination. The second method made use of the improved doubly-loaded probe with $2d = 0.01\lambda$, shown in Figs. VII-7c, 11. The measurement of the charge distribution, for current determination by integration, made use of the charge probe of Figs. VII-7d, 13a, with $h = 0.02\lambda$.

13. Results

Figure VII-14 shows the measured current along a unipole with $h = 0.25\lambda$ and $\Omega = 8.6$.* The magnitudes measured with the four different probes show differences which are systematic, but very small, about 2% of the maximum current, except near the end of the antenna where the charge probe gives values about 6% of the maximum current below the others. When referred to the current at each point the maximum deviations are less than 4% for all the loop probes and 13% for the charge probe. The magnitudes are each normalized to a maximum value of one.

The phases all agree within 1 degree for half of the antenna length and then diverge somewhat, with values for the singly-loaded loops and the charge probe differing by 4 degrees near the end, and the value for the doubly-loaded loop differing by 7 degrees from them.

In all cases, the measured currents differ considerably from the zeroth-order theoretical current which is a cosinusoidal amplitude distribution with uniform phase. They agree somewhat better, especially in phase, with the quasi-zeroth order theory proposed by King [10] and calculated by Mack [11].

14. Probe loading

As described in Section VII-6, the effect of probe loading can significantly

---

* $\Omega = 2\ln\frac{2h}{a}$, $\frac{a}{\lambda} = .0032$.

distort current measurements on a coaxial line, especially for large probes, so it must be expected to be important in antenna current measurements also.

The loop probes used were small enough ($2d \leq 0.01\lambda$) for the expected probe loading to be negligible, and this was verified experimentally. The current distribution was measured with a fixed dummy probe near the end of the antenna and compared with the current neasured without the dummy. There was negligible (less than 1%) change in the current. This would suggest that probe loading was negligible, but a complete study would have to load the antenna at various points and measure the input impedance. This would require a setup with two probes, traveling independently.

15. Conclusions

From the discussion of Section VII-11, it was expected that a singly-loaded loop probe would be accurate within 3% out to a distance of 0.2h from the end of the antenna. This was borne out experimentally by the fact that the results for the small probe ($2d = .004\lambda$) agreed with those for the larger probe ($2d = .01\lambda$). If error was present, it would be at least twice as great for the larger probe, and thus there would have been a difference between these two results.*

The doubly-loaded loop was expected to be accurate out to about the same point, with an inaccuracy due to the slight error in balancing the probe circuits. The error signal in this case would be proportional to the radial electric field, and it may well be in quadrature with the desired signal. This would explain the deviation in the phase curve for the doubly-loaded loop as the end of the antenna is approached.

- - - - - - -

*A probe of still larger dimensions could not readily be used to illustrate this type of error because probe-loading effects would also have become prominent.

The accuracy of the charge-probe method is hard to estimate because of the integration of the experimental errors, but it was expected that these would not be very large, and that is borne out by the close agreement of these results with the others. The fact that the amplitudes determined by the charge-probe method are a bit lower than the others near the end of the antenna is due to the evaluation of the integration constant in Eq. VII-38 by requiring $I = 0$ at the end of the antenna. The currents measured with the loop probes do not approach zero at the end because the magnetic field, unlike the current, has a finite value there.

It was concluded, therefore, that the best probe for antenna current measurements is the simple singly-loaded loop, but that it must be quite small ($2d \backsim .01\,\lambda$) to avoid probe loading and electric mode errors. If a larger probe must be used, the doubly-loaded style should be somewhat the better, but neither will be very good.

Finally, it must be remembered that no field probe will be accurate in determining the current (or charge) within a distance $5d$ from the ends or (except in special cases) from the base, where d is the probe height. This is a consequence of the fact that the fields near the ends (and base) are not strictly proportional to the current and charge except at the very surface of the antenna (Eq. VII-25).

Bibliography, Chapter VII

1. Morita, Tetsu, "The Measurement of Current and Charge Distributions on Cylindrical Antennas," Cruft Laboratory Technical Report No. 66, Harvard University, pp. 7 and 13-15 (February 1949).

2. Ramo, S., and J. R. Whinney, Fields and Waves in Modern Radio, Second Edition, pp. 364-366, Wiley, New York (1953).

3. Morita, op. cit., pp. 46, 41.

4. King, Ronold W. P., Transmission Line Theory, pp. 83, 93, 95, McGraw-Hill, New York (1955).

5. King, Donald D., Measurements at Centimeter Wavelength, pp. 95-98, Van Nostrand, New York (1952).

6. King, Ronold W. P., op. cit., p. 102.

7. Ibid., p. 249.

8. Andrews, Howard W., "Image-Plane and Coaxial-Line Measuring Equipment at 600 MC," Cruft Laboratory Technical Report No. 177, Harvard University (July 1953).

9. King, Ronold W. P., The Theory of Linear Antennas, pp. 523-528, Harvard University Press, Cambridge (1956).

10. King, Ronold W. P., "Linear Arrays: Currents, Impedances, and Fields, I," Cruft Laboratory Scientific Report No. 1 (Series 2), Harvard University, p. 25 f. (May 1959).

11. Mack, Richard B., forthcoming thesis, Harvard University.

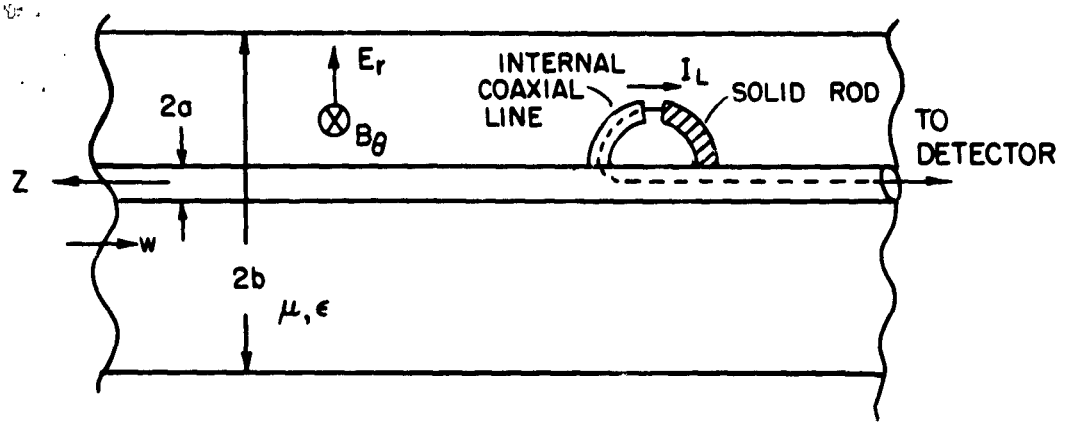

(a) SINGLE GAP PARALLEL TO E_z

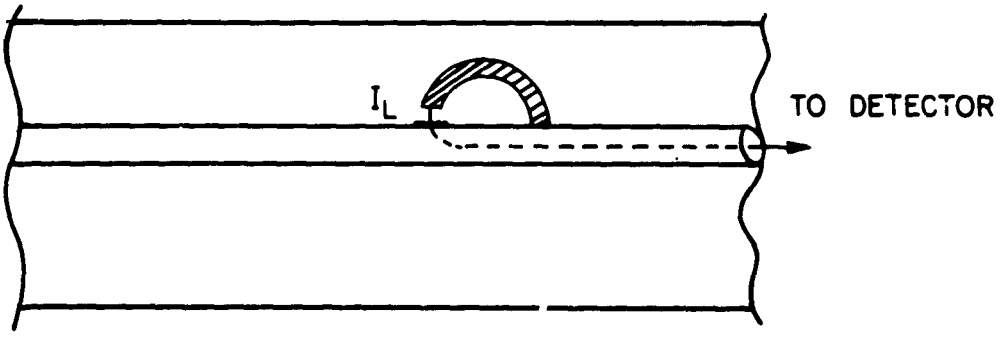

(b) SINGLE GAP PARALLEL TO E_r

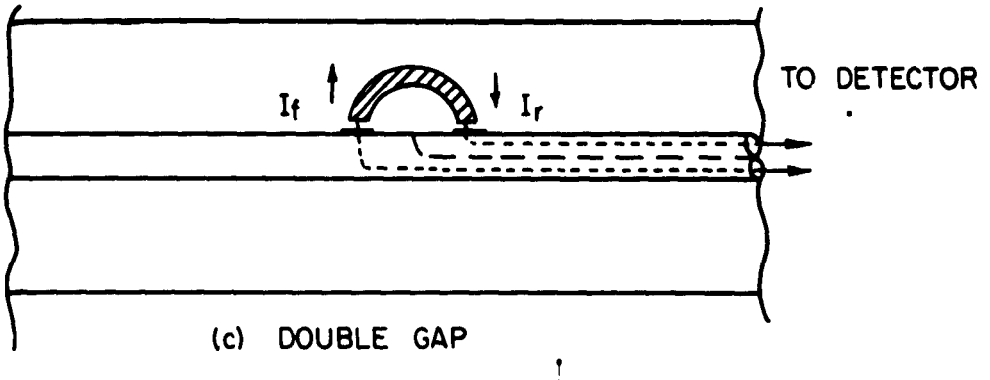

(c) DOUBLE GAP

VII-1 COAXIAL LINE WITH CURRENT PROBES

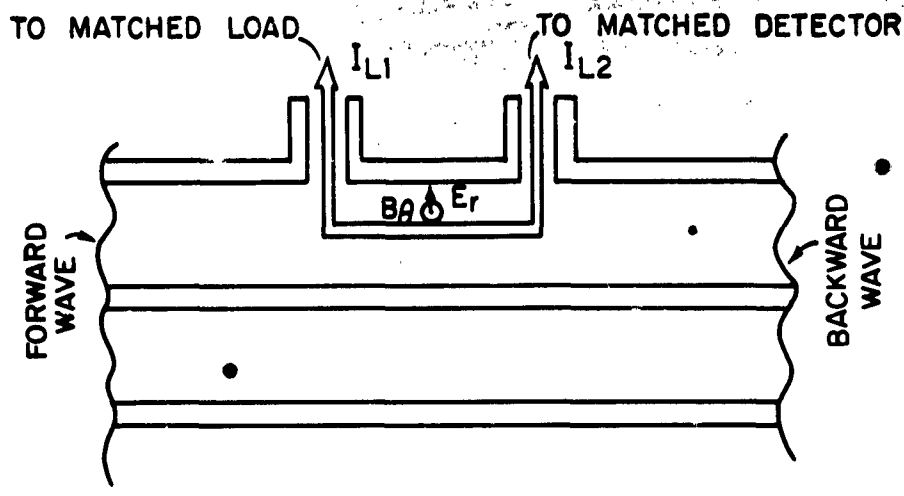

VII-2 DIRECTIONAL COUPLER, COUPLING TO BACKWARD WAVE ONLY

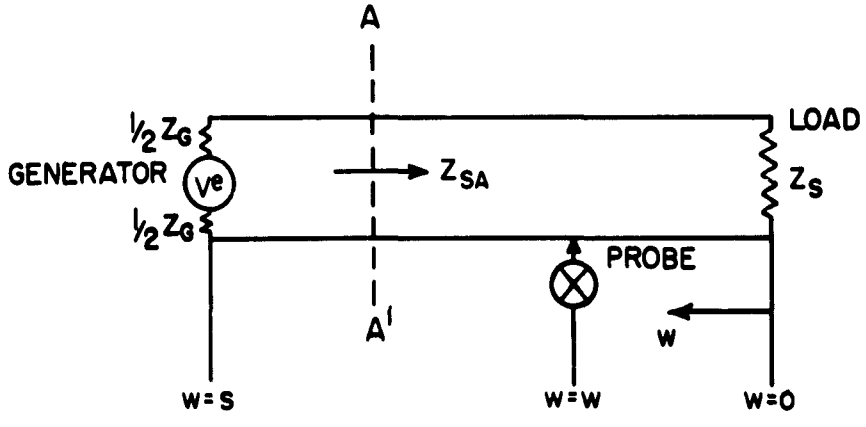

VII-3 RESONANCE METHOD OF IMPEDANCE MEASUREMENT

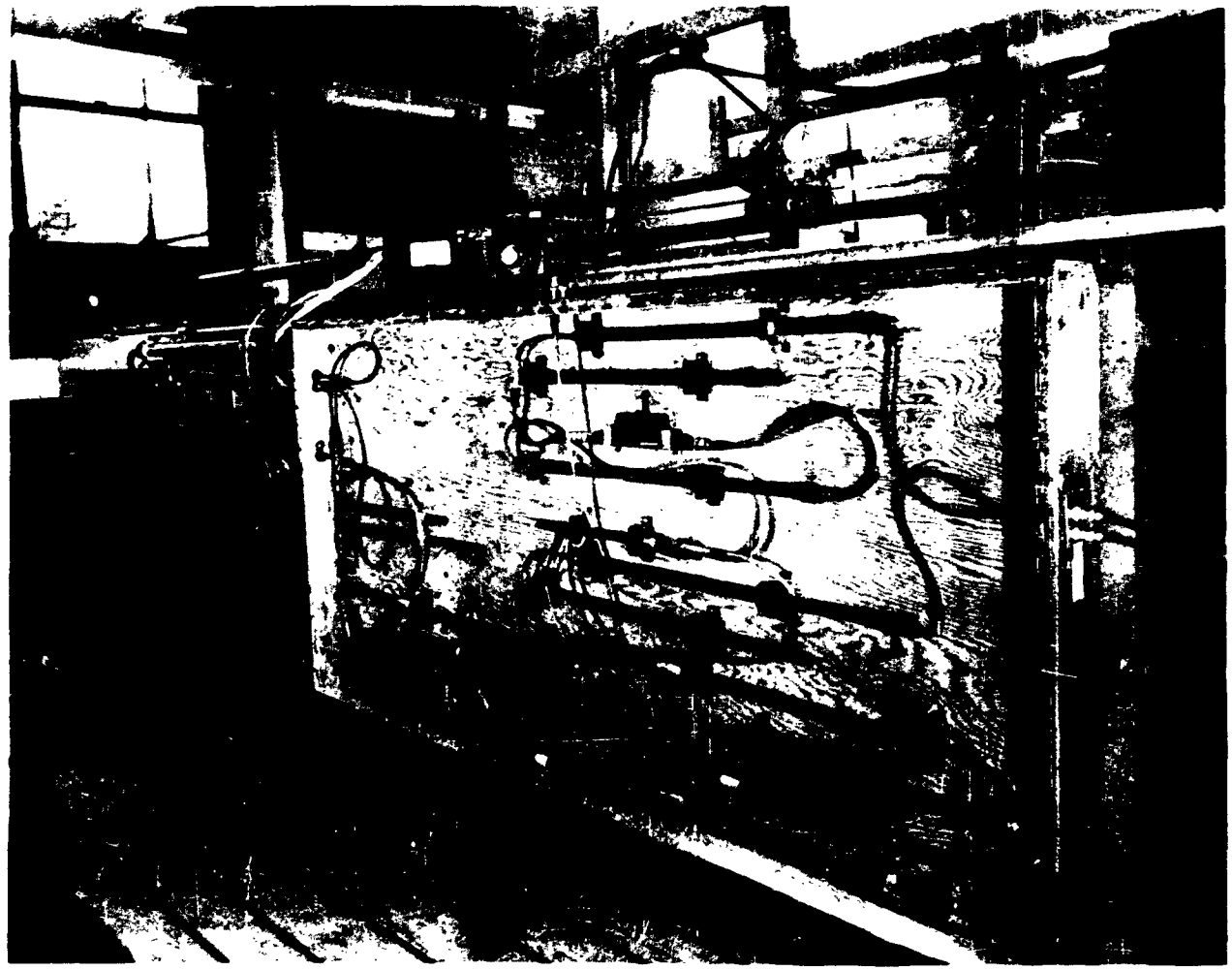

Fig. VII-4. COAXIAL LINE AND RECEIVER SYSTEM FOR CURRENT MEASUREMENTS

VII-5 PROBE LOADING; SHORT CIRCUITED COAXIAL LINE; EXPERIMENT

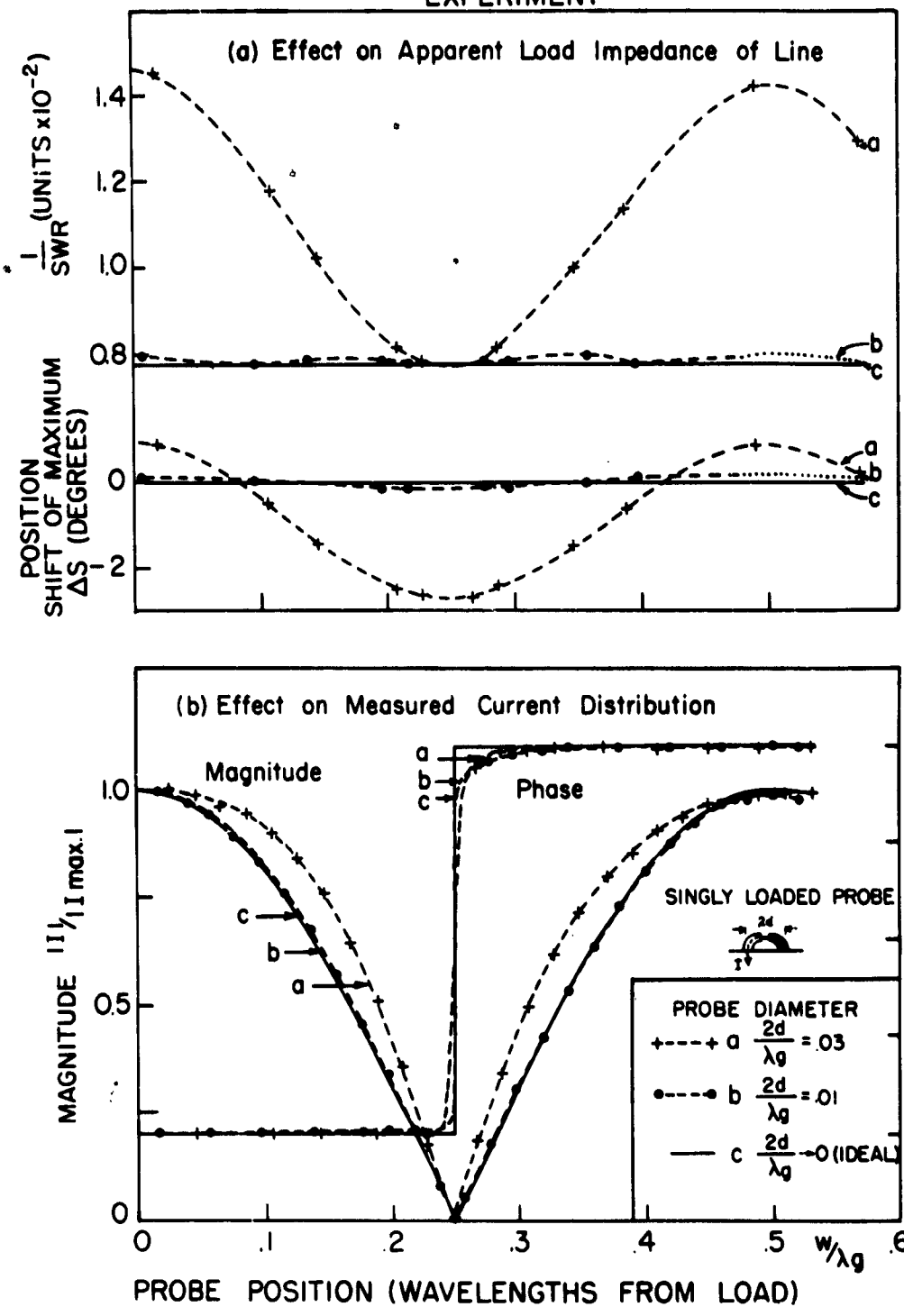

VII-6 MEASURED EFFECT OF ELECTRIC MODE ON CURRENT MEASUREMENT, SHORT CIRCUITED COAXIAL LINE

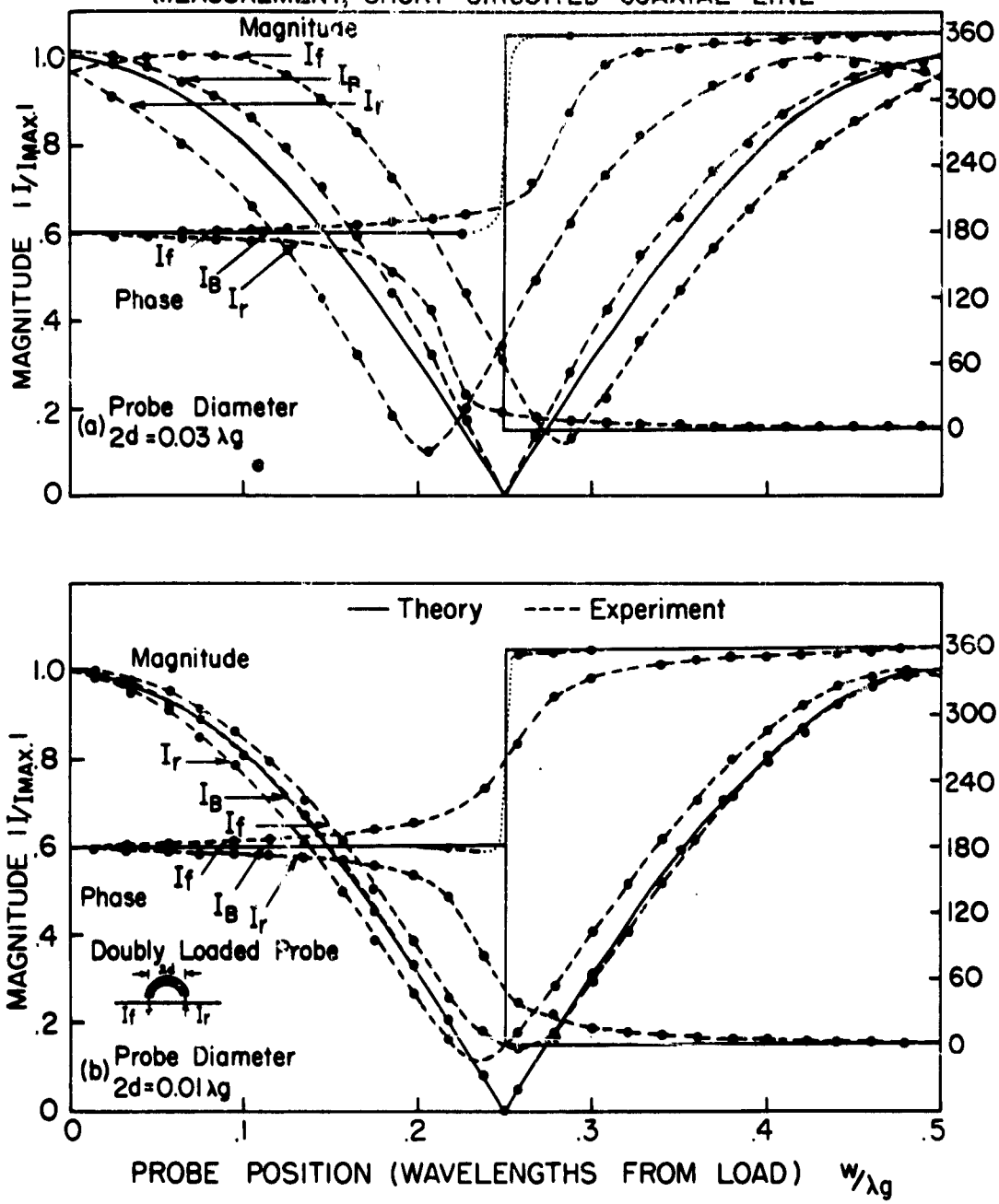

VII-7 PROBES ON A LINEAR ANTENNA

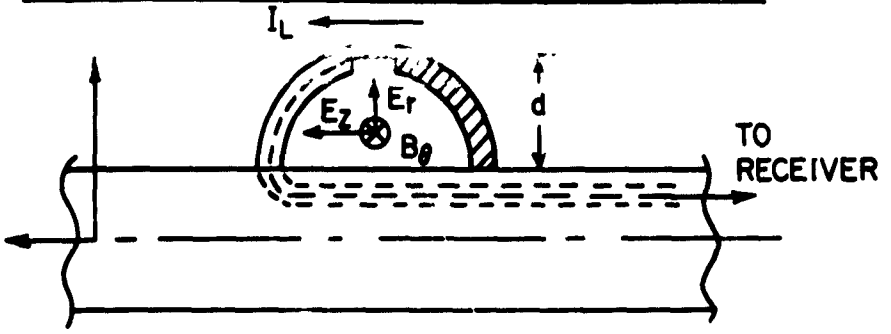

VII-7a SINGLY LOADED LOOP

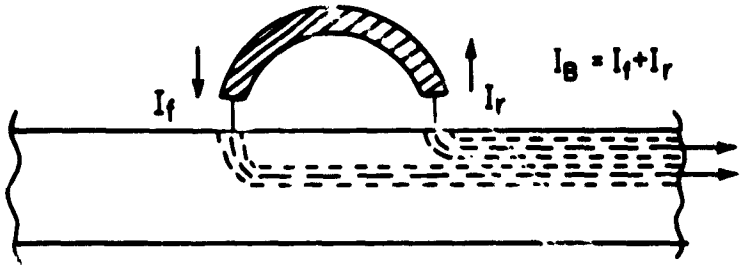

VII-7b DOUBLY LOADED LOOP

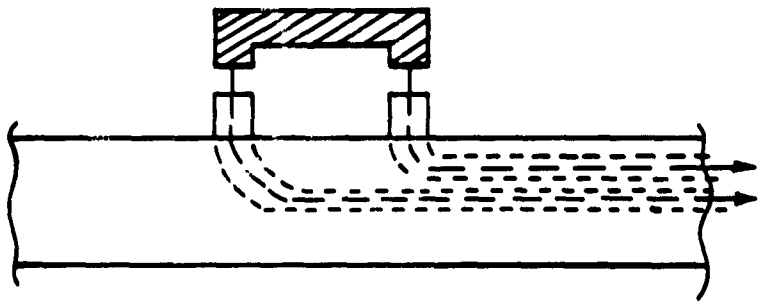

VII-7c DOUBLY LOADED LOOP, IMPROVED SYMMETRY

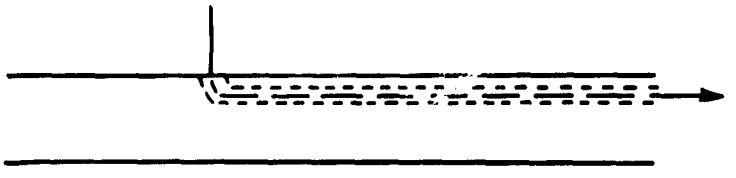

VII-7d CHARGE PROBE

FIELD RATIO NEAR A HALF-WAVE DIPOLE

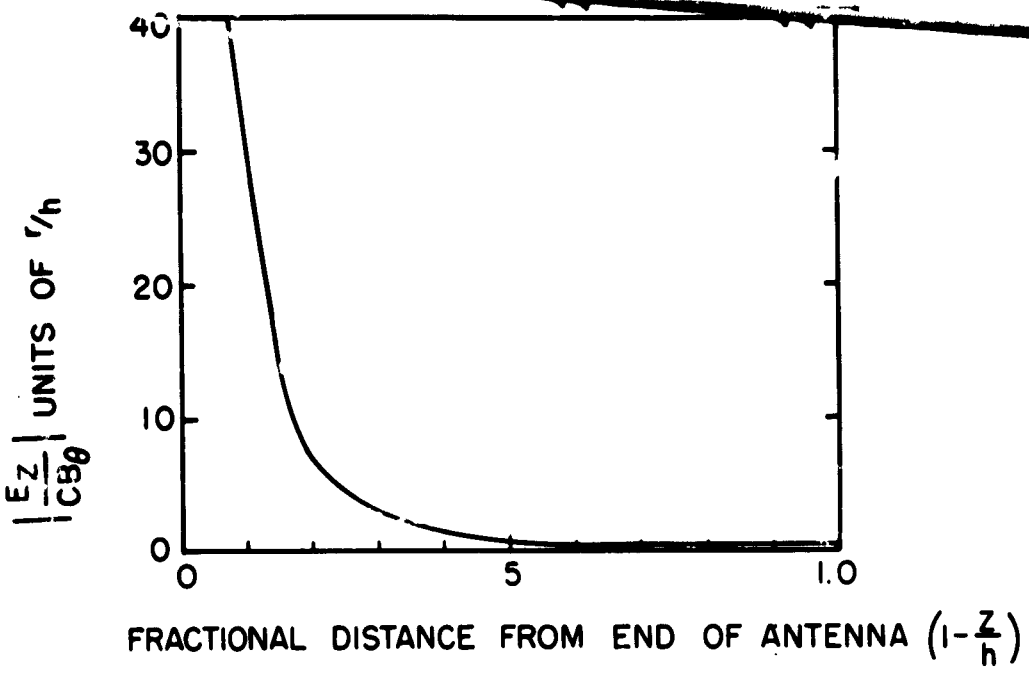

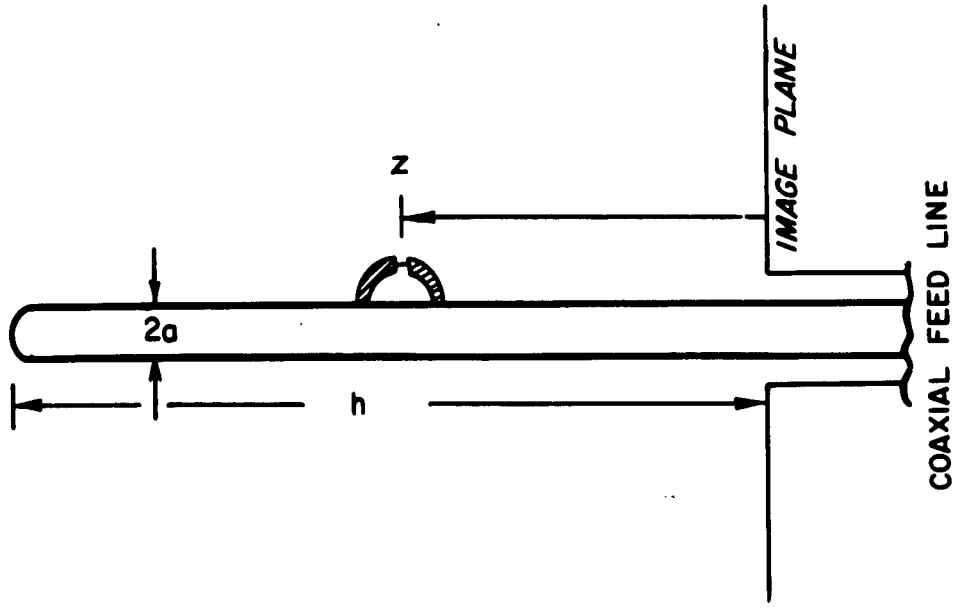

VII-9 CURRENT MEASUREMENT ALONG A UNIPOLE

Fig. VII-10. IMAGE PLANE WITH UNIPOLE ANTENNA

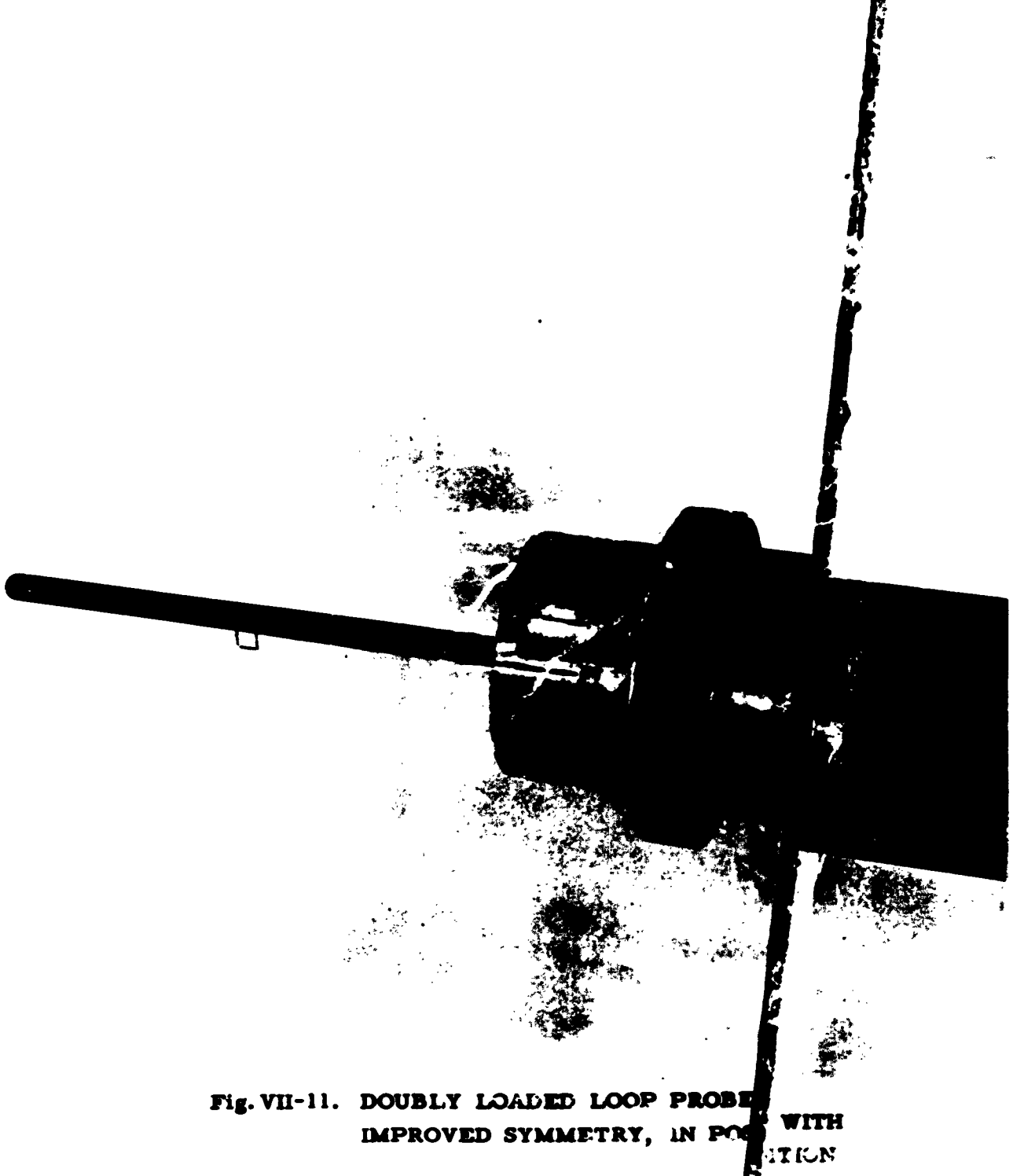

Fig. VII-11. DOUBLY LOADED LOOP PROBE WITH IMPROVED SYMMETRY, IN POSITION

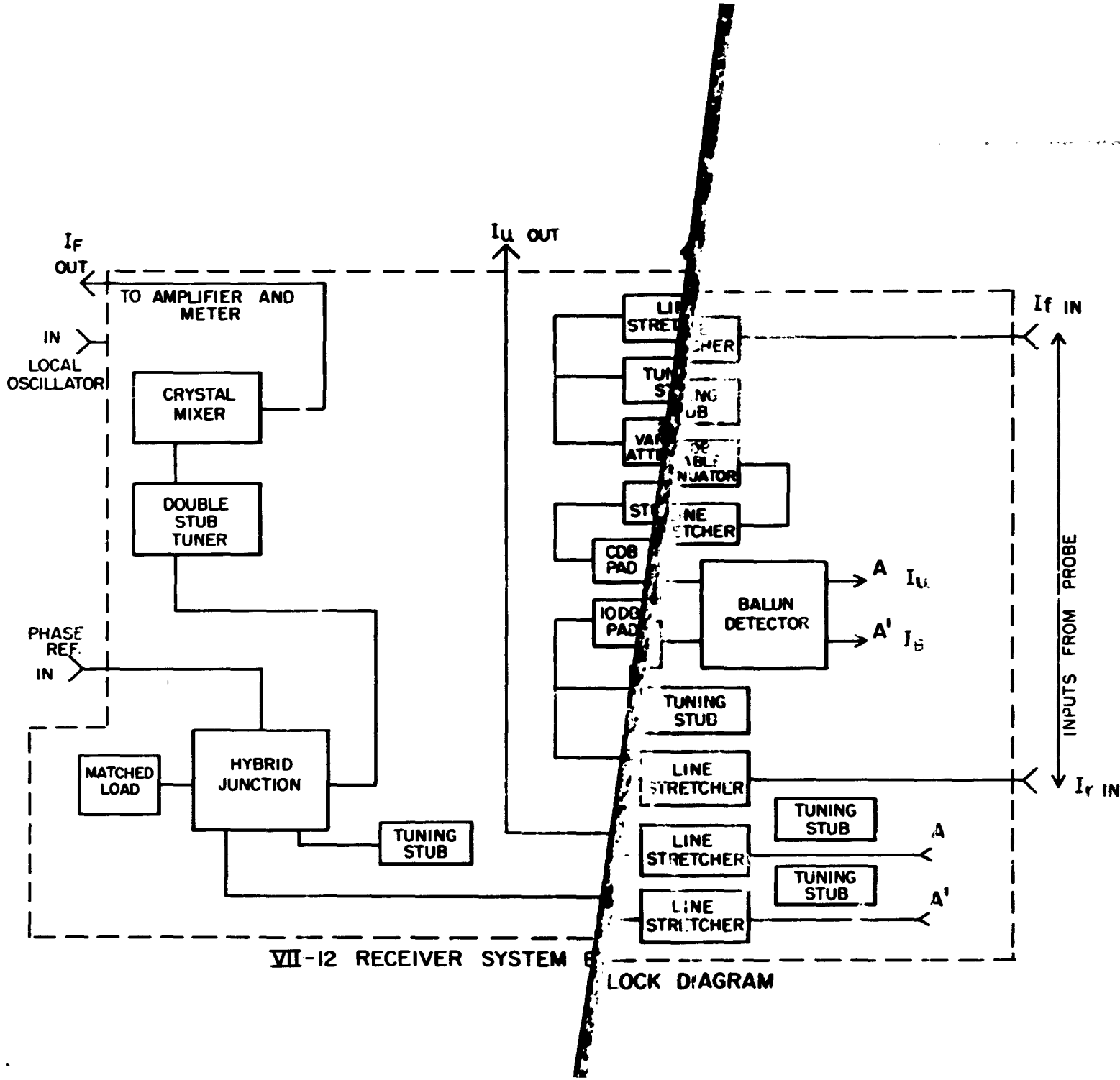

VII-12 RECEIVER SYSTEM B LOCK DIAGRAM

Fig. VII-13a. CHARGE PROBE

Fig. VII-13b. DOUBLY LOADED LOOP PROBES

Fig. VII-13c. SINGLY LOADED LOOP PROBES

VII – 14 CURRENT DISTRIBUTION, QUARTER WAVE UNIPOLE

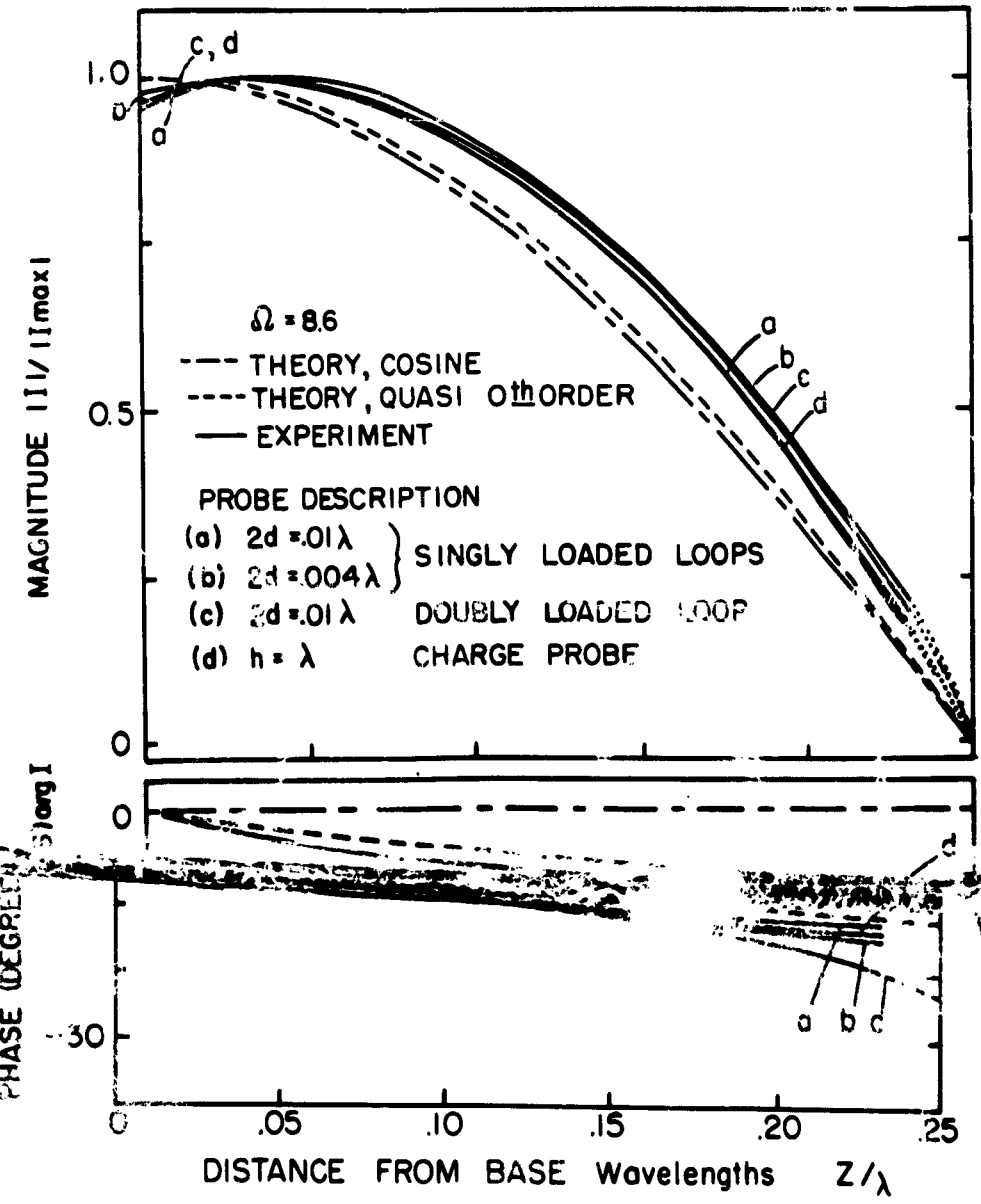

CHAPTER VIII. GENERAL CONCLUSION

Section A. Review of Findings

The purpose of this study was to investigate the behavior of various probes used in the measurement of an electromagnetic field.

Chapter I is a discussion of the experimental apparatus, which describes in some detail the specialized equipment involved: particularly the free-space room, designed to allow free-space measurements to be made indoors; the balancing circuits, which provide accurately the sum and difference of two currents; and the phase-measuring system, which was somewhat more accurate than existing systems, especially for large variations in signal level.

The unipole probe over an image plane, which corresponds to a dipole in free space, is studied in Chapter II. Very good agreement is found between the theoretical and the experimental values of the probe sensitivity* for a range of wire diameters and lengths. These measurements differed from those previously made by Morita and Taylor (Reference II-15) in that an absolute magnitude was obtained for the probe sensitivity, while they found only a relative value. Otherwise, these results agree with theirs except for a discrepancy at short lengths which is probably due to one of the assumptions made in their calculation. The main value of this work was to confirm generally their results and to establish a procedure for the measurements.

In Chapters III and IV, the behavior of circular and square-loop probes is studied in considerable detail. It was shown that these probes can respond to both the normal magnetic field and the tangential electric field, so that both magnetic and electric sensitivities are defined. The effects of probe diameter,

- - - - - - -

*Probe sensitivity is output current per unit incident field.

wire size, and load impedance on the sensitivities and error ratios* were studied both theoretically and experimentally, and agreement was generally quite satisfactory, except that all the measured magnetic sensitivities were about 10% lower than expected, and therefore, the error ratios were about 10% higher than expected. It was found that the error ratio decreases with loop size and is independent of wire size and load impedance for a singly-loaded loop.

Doubly-loaded loops were then tested in the same way. Following a suggestion by King [1], the currents from the two loads were added in a balanced detector to cancel the electric mode currents and enhance the magnetic mode currents. This resulted in an improvement of 20 to 30 db in the system-error ratio, referred to the currents in the detector, as shown in Fig. VIII-1. The amount of improvement for the doubly-loaded loops depends on the accuracy of the balance adjustment since the error ratio for the currents in the loop itself is actually worse than in the singly-loaded case. It was determined that the doubly-loaded loops have an optimum diameter of about $2d = .04\lambda$ for which the error ratio reaches a minimum value of about 0.5. It was also found that reduction of wire size and load impedance reduces the error ratio for the doubly-loaded loops.

When a balun detector is used with the doubly-loaded loops of Chapters III and IV, the sum and the difference of the two load currents can be measured simultaneously. Since the sum current is proportional to the normal magnetic

- - - - - - -

*The error ratio is the ratio of the electric sensitivity to the magnetic sensitivity, and is equal to the ratio of the (undesired) electric mode current to the (desired) magnetic mode current in a plane wave field with the probe oriented for maximum excitation of both modes.

field and the difference current is proportional to the tangential electric field, it was shown that both fields can be determined at once using a single probe.

It was found in Chapter IV that the presence of the transmission line caused an increase in the error ratio of the doubly-loaded loop. It was felt that this was due to the asymmetrical connection of the line, and the experiments of Chapter V verified this hypothesis. Then a new bridge-style loop was developed which allows the transmission line to be connected at the geometrical center of the loop and removes this increase in error ratio without changing the magnetic sensitivity of the loop.

Chapter VI contains a discussion of the use of loop probes in field measurements in terms of the loop constants studied in previous chapters. The application of these principles to radio direction finders is discussed in some detail. Finally, a demonstration of the need for the doubly-loaded probe is made, using the near-zone field of a unipole as the field to be investigated. This field has both a longitudinal and a transverse component of $\vec{E}$ present, so that there will always be an electric mode current in the load when $\vec{B}$ is being measured. The conventional loop probe must be made exceedingly small ($2d \leq .003\lambda$) to make the output current independent of the electric field (within 3%), but the new doubly-loaded probe may be quite large ($2d \sim .13\lambda$) without the electric mode current becoming more than 3% of the sum output. This allows the accurate measurement of the magnetic component of fields for much smaller wavelengths than possible with ordinary probes.

Finally, Chapter VII is an investigation of the use of loop probes in a coaxial line and along a linear antenna. An interesting sidelight is the appearance of the electric modes of a loop in the theory of the coaxial directional coupler, a very useful device which allows the independent measurement of

either the forward or the reflected wave in a transmission line. It is concluded that a conventional loop probe is adequate for measurement of the current within a coaxial line because of the absence of a longitudinal electric field, but that a doubly-loaded loop may be a somewhat superior probe for current measurement along a linear antenna, where this field does not vanish.

Section B. Suggestions for Further Research

A discrepancy of 10% between all the experimental and theoretical values of magnetic sensitivity remains unexplained, as mentioned above, and although this does not destroy the usefulness of the general results of this study, it would be very interesting to determine the source of this disagreement.

It would be particularly desirable to use these probe techniques in explaining discrepancies in existing measurements of various kinds where a significant electric mode current may be present. Such a situation is the measurement of surface current on a scattering cylinder [2], for which measurements have been started in this laboratory.

It would also be desirable to investigate other aspects of probe behavior, such as ways to reduce the physical size of the probe while maintaining sufficient output power. A possible method would use a core of magnetic material within the loop, and this would involve finding the proper material for a given frequency [3].

The possibility of making free-space measurements without using a transmission line is an intriguing one. Recent work by Hu [4] and by Iizuka [5] on a reaction type of measurement similar to that used in cavities is promising in this regard.

Further study of the behavior of a probe near, but not against, a metal boundary surface or edge would also be of considerable interest. Some theoretical work has already been done on this problem [6], but only meager experimental results are known to be available, and the existing theory is not complete.

Bibliography, Chapter VIII

1. King, Ronold W. P., "The Loop Antenna as a Probe in Arbitrary Electromagnetic Fields," Cruft Laboratory Technical Report No. 262, Harvard University (May 1957).

2. Wetzel, Lewis and Donald B. Brick, "An Experimental Investigation of High Frequency Current Distribution on Conducting Cylinders," Cruft Laboratory Scientific Report No. 4, Harvard University (December 1955), cited in King, Ronold W. P., and Tai Tsun Wu, The Scattering and Diffraction of Waves, p. 39, Harvard University Press, Cambridge (1959).

3. Steward, J. L., "Research in Magnetic Antennas," Final Reports of Contract No. DA-36-039-SC73189 (Signal Corps, Department of the Army), California Institute of Technology, Pasadena, California (September 1957).

4. Hu, Ming-Kuei, "On Measurements of Microwave E and H Field Distributions by using Modulated Scattering Methods," Institute of Radio Engineers, Transactions on Microwave Theory and Techniques, pp. 295-300 (May 1960).

5. Iizuka, Keigo, "A New Technique for Measuring an Electromagnetic Field by a Coil Spring," Cruft Laboratory Technical Report No. 365, Harvard University (June 1962).

6. Hsu, Hwei-Piao, "Analysis of the Interaction between a Measuring Probe and a Reflector," Scientific Report No. 22, Case Institute of Technology (February 1961).

VIII-1 TYPICAL SYSTEM ERROR RATIO, SQUARE LOOP

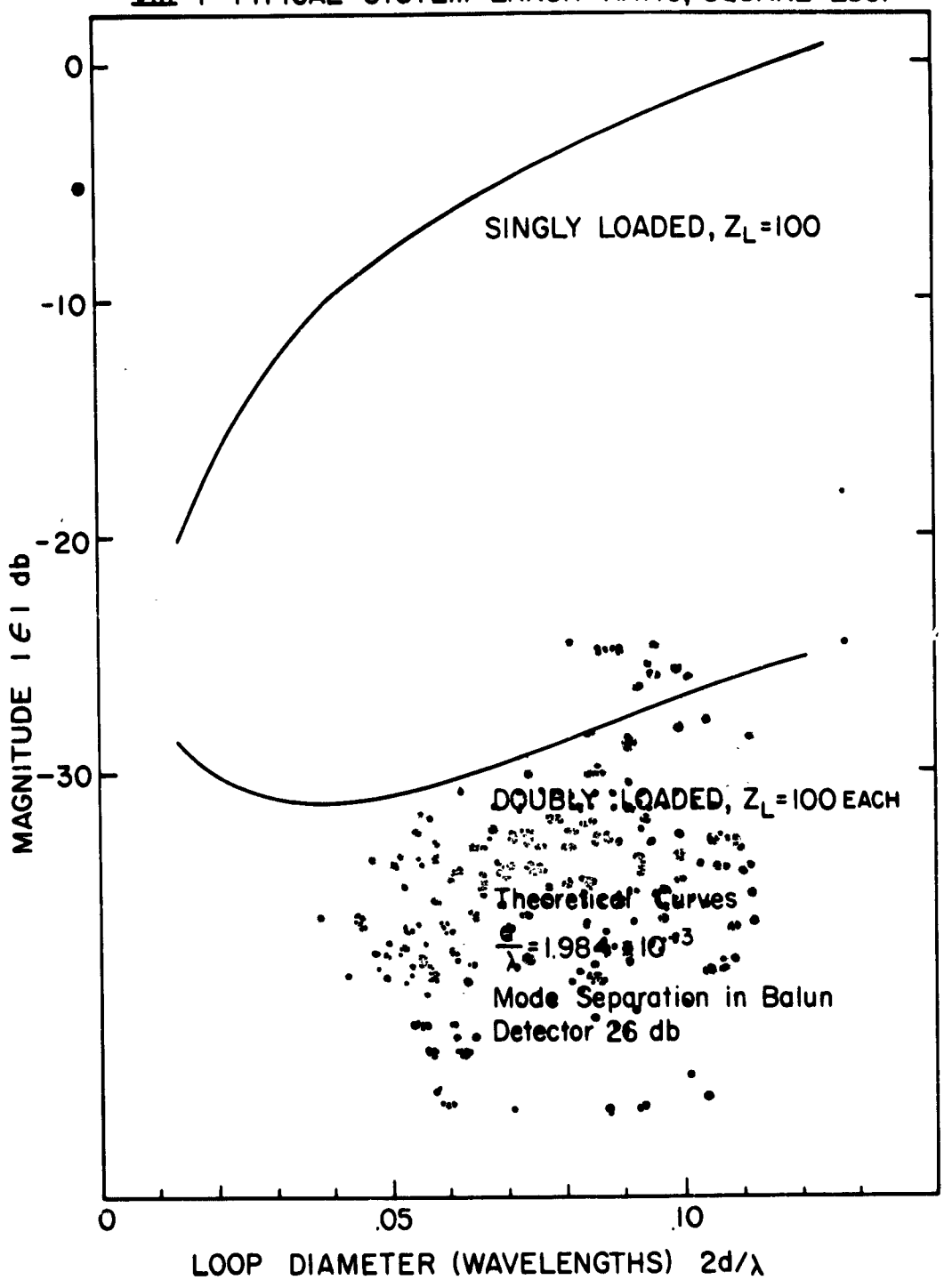

Appendix A. The Near-Zone Field of a Dipole

1. Current on a dipole

The current distribution on a dipole (or a unipole) is usually assumed to have uniform phase and a cosinusoidal amplitude. This is, in fact, only a zeroth-order approximation. A new analysis of the problem by King [1] gives a quasi-zeroth order solution that is considerably better for lengths near anti-resonance, and somewhat better for all lengths. A more exact solution to the problem can be represented as the ratio of two convergent infinite series, but at best only second-order values have been calculated [2].

The current distribution on a half-wave dipole (or a quarter-wave unipole) has been measured by various people for various antenna thicknesses, and the results agree in showing a bulge in the measured current so that it is considerably larger than the zeroth-order (or even the second-order) theory predicts over much of the length of the antenna. There is also a phase lag towards the end of the antenna, but this is fairly well predicted by the quasi-zeroth order theory. Figure VII-14 shows a comparison between theory and experiment, for $\Omega = 8.6$, where the accuracy of the various experimental curves is discussed in Sections VII-13-15.

The quarter-wave unipole source used in most of the measurements described in this paper has a thickness parameter $\Omega = 11.4$. Since the diameter of this source was only 1/16 inch, the current could only be estimated and not measured directly. The current in the infinitely thin antenna is known from the series expansion to approach the zeroth-order value, so it is to be expected that the current in a thin antenna will lie somewhere between the cosinusoidal current with constant phase and the actual measured current for the thick antenna of Fig. VII-14.

2. Near-zone field of a dipole, theory

The integrals for the near-zone field of a half-wave dipole can be performed analytically for a thin antenna with the zeroth-order current distribution [3]. They are readily expressed in confocal spheroidal coordinates as (Fig. VI-4):

$$c B_\phi = j \frac{2 \zeta_0 I_m \cos \frac{\pi}{2} k_h}{\pi \lambda \sqrt{(k_e^2 - 1)(1 - k_h^2)}} e^{-j \frac{\pi}{2} k_e} \qquad \text{(A-1)}$$

$$E_\epsilon = j \frac{2 \zeta_0 I_m \cos \frac{\pi}{2} k_h}{\pi \lambda \sqrt{(k_e^2 - k_h^2)(1 - k_h^2)}} e^{-j \frac{\pi}{2} k_e} \qquad \text{(A-2)}$$

$$E_\rho = \frac{2 \zeta_0 I_m \sin \frac{\pi}{2} k_h}{\pi \lambda \sqrt{(k_e^2 - k_h^2)(k_e^2 - 1)}} e^{-j \frac{\pi}{2} k_e} . \qquad \text{(A-3)}$$

These expressions have been used for calculation of the theoretical fields in Chapter VI and the reference fields in the earlier chapters.

In order to estimate the accuracy of these field calculations, a numerical calculation was made of the magnetic field at various points due to the (normalized) current actually measured for the antenna with $\Omega = 8.6$ (Fig. VII-14) and compared with the magnetic field due to a cosinusoidal current distribution with unit amplitude. Both calculations were made by using Simpson's rule with sixteen panels to evaluate the integral expression for the field from the axial current distribution $i(z')$. The appropriate integral is:

$$\vec{B} = -\frac{\mu_0}{4\pi} \int_{-h}^{h} (\hat{R} \times \hat{z})\, i(z')\, e^{-jkR} \left(\frac{1}{R^2} + \frac{jk}{R}\right) dz' \qquad \text{(A-4)}$$

which can be reduced in cylindrical coordinates to:

$$c B_{\phi} = 30r \int_{-h}^{h} i(z') (\cos \gamma + j \sin \gamma) \frac{\sqrt{1 + k^2 R^2}}{R^3} dz' \qquad \text{(A-5)}$$

where

$$R = \sqrt{r^2 + (z - z')^2}$$

$$\gamma = \arctan kR - kR .$$

Table A-1 gives a comparison of the results for each source current at certain field points, and Table A-2 gives their differences, as calculated from Table A-1. The numerical integration was accurate within 0.1 db and 0.5 degree.* It is seen from these tables that the primary effect of the changed current distribution is to increase the fields by a constant factor and retard the phases by a constant angle at all points.

The source antenna actually used in Chapter VI and elsewhere had $\Omega = 11.4$ and was thus much thinner than the antenna for which a measured current distribution was obtained in Chapter VIII. Therefore, it is assumed that the actual magnetic field was somewhere between the two values given in Table A-1. The actual field will then vary in the same way as the zeroth-order field, within the limits of experimental error. However, there may be a change in the normalization factor of the order of 0.5 db and 3 degrees due to the deviation of the actual source current from the zeroth-order distribution. In a relative measurement this would not be significant.

- - - - - - -

*It is readily shown that the error in a calculation by Simpson's rule decreases by a factor of about 16 when the number of panels is doubled. Therefore, the error in a given calculation is estimated at 0.1, the difference between a calculated value and that calculated using half the number of panels [4].

Furthermore, except very near the antenna, the transverse electric field will be changed by a change in source current in much the same way as the magnetic field.* Therefore, the type of deviation suggested here may produce a general normalization error of the order of 0.5 db and 3 degrees in the measured values of both the probe sensitivity constants, S_B and S_E. Such an error would cancel in the measurement of the loop error ratio ϵ, and could not be the source of the measured deviation which was found only in S_B.

3. Near-zone field of a dipole, experiment

Previous measurements of the near-zone field of a dipole use a modeling technique based on Babinet's principle and measure the near-zone field of a slot [5]. It was, therefore, desirable to measure this field directly, even though there is no reason to doubt the validity of the modeling procedure in this instance.

The measurement of the electric field was a relative measurement, normalized for best mean fit, using an electric dipole probe of length $2\ell = 0.08\lambda$.† The setup uses a unipole source with $\Omega = 11.4$ and $h = 0.25\lambda$ over an image plane in the free-space room, as described in Chapter I. The results are plotted in Figs. A-1, 2 against arcsin k_h (approximately the angle from the image plane) for various values of k_e (approximately proportional to the distance of

- - - - - - -

*At distances greater than about 0.2λ from the source, the far-zone terms become dominant in both electric and magnetic fields. These terms are identical in magnitude and phase.

†This probe was left fairly long to get good discrimination against the cross-polarized field.

the field point from the origin). Agreement between theory* and experiment is very good, except near the image plane where coupling to the image probe becomes significant, and near the axis of the source, where the tangential electric field theoretically has a zero, but only a minimum is measured.

The measurement of the magnetic field was also a relative measurement, normalized for best mean fit. A bridged square loop of diameter $2d = 0.038\lambda$ was used as a probe, and the results are plotted in Fig. A-3. Again the agreement is very good, with significant departures only in the region of small B_ϕ where the effect of scattered fields and coupling to electric fields would produce the greatest change in the measured field.

The fields were also measured along the image plane by inserting probes through small holes in the plane. The electric probe was a unipole of length $\ell = 0.04\lambda$, and the magnetic probe was a half-square loop of diameter $2d = .038\lambda$. Since no transmission line is present in the field, these are the most accurate measurements of all. The results are plotted in Fig. A-4, and are seen to agree closely with the theory. The deviations are periodic and give a measure of the standing waves in the room. The calculated standing-wave ratio is one plus twice the maximum percentage deviation in field. Therefore, the SWR is about 1.07 for both the electric and the magnetic fields along the image plane.

- - - - - - -

*The theory referred to is the zeroth-order theory, which assumes a cosinusoidal source current distribution.

4. Near-Zone field of a dipole, conclusion

It is concluded that the actual near-zone field of a thin dipole is very close to that predicted by the zeroth-order theory. Departures in the measured values are small and of such a nature that they can be attributed to experimental error, especially to the presence of small standing waves in the "free-space" room.

Bibliography, Appendix A

1. King, Ronold W. P., "Linear Arrays: Currents, Impedances and Fields, I," Cruft Laboratory Scientific Report No. 1 (Series 2), Harvard University, p. 25 f. (May 1959).

2. King, Ronold W. P., The Theory of Linear Antennas, pp. 86-140, Harvard University Press, Cambridge (1956).

3. Ibid., pp. 532-560.

4. Kunz, Kaiser S., Numerical Analysis, p. 146, McGraw-Hill, New York (1957).

5. Reynolds, Donald K., "Surface-Current and Charge Measurements on Flat Metal Sheets," Cruft Laboratory Technical Report No. 53, Harvard University, pp. 59-63 (August 1948).

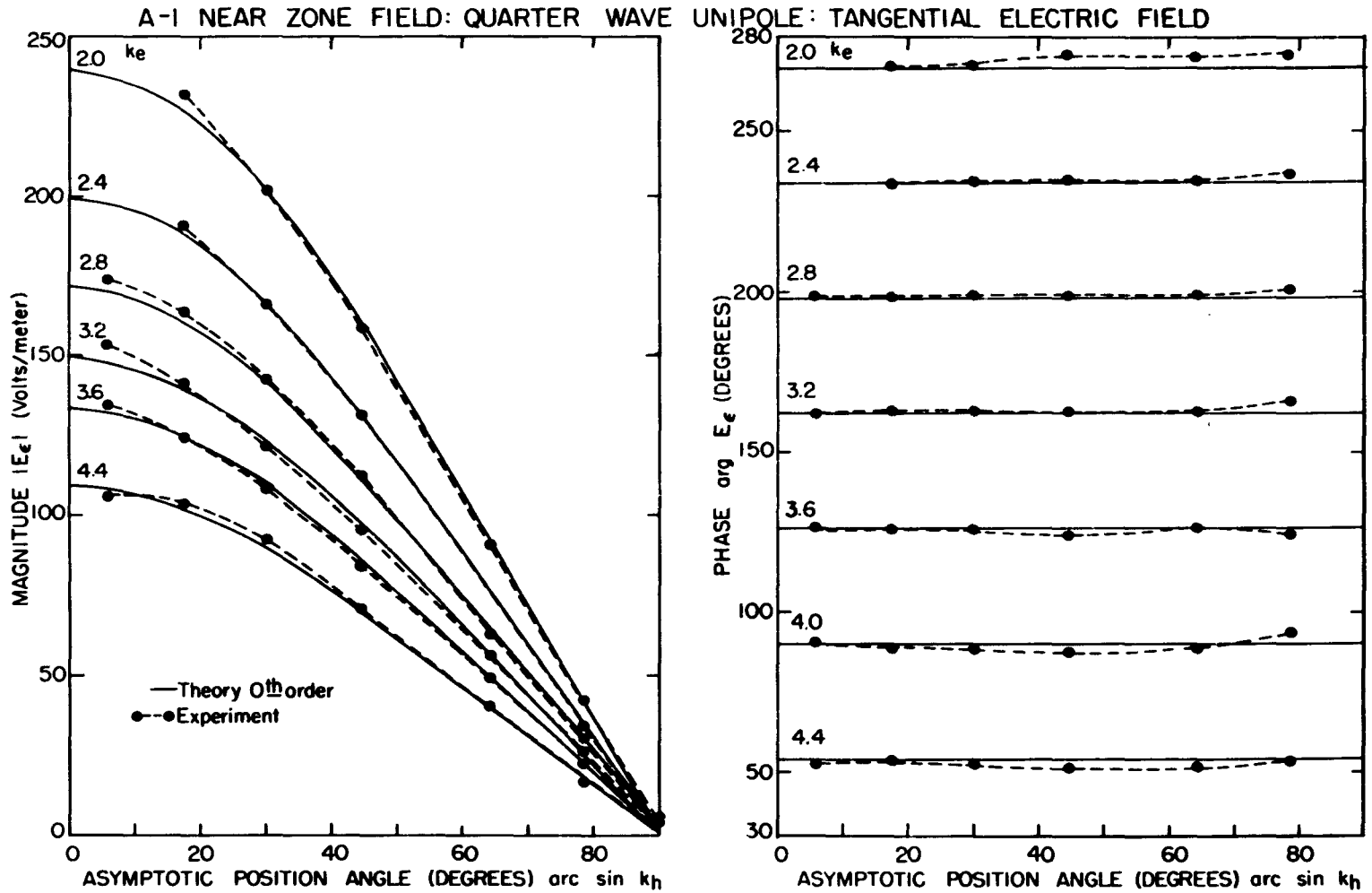
A-1 NEAR ZONE FIELD: QUARTER WAVE UNIPOLE: TANGENTIAL ELECTRIC FIELD
MAGNITUDE |Eϕ| (Volts/meter)
PHASE arg Eϕ (DEGREES)
2.0 ke
2.4
2.8
3.2
3.6
4.4
4.0
—Theory 0th order
●--●Experiment
ASYMPTOTIC POSITION ANGLE (DEGREES) arc sin kh
ASYMPTOTIC POSITION ANGLE (DEGREES) arc sin kh

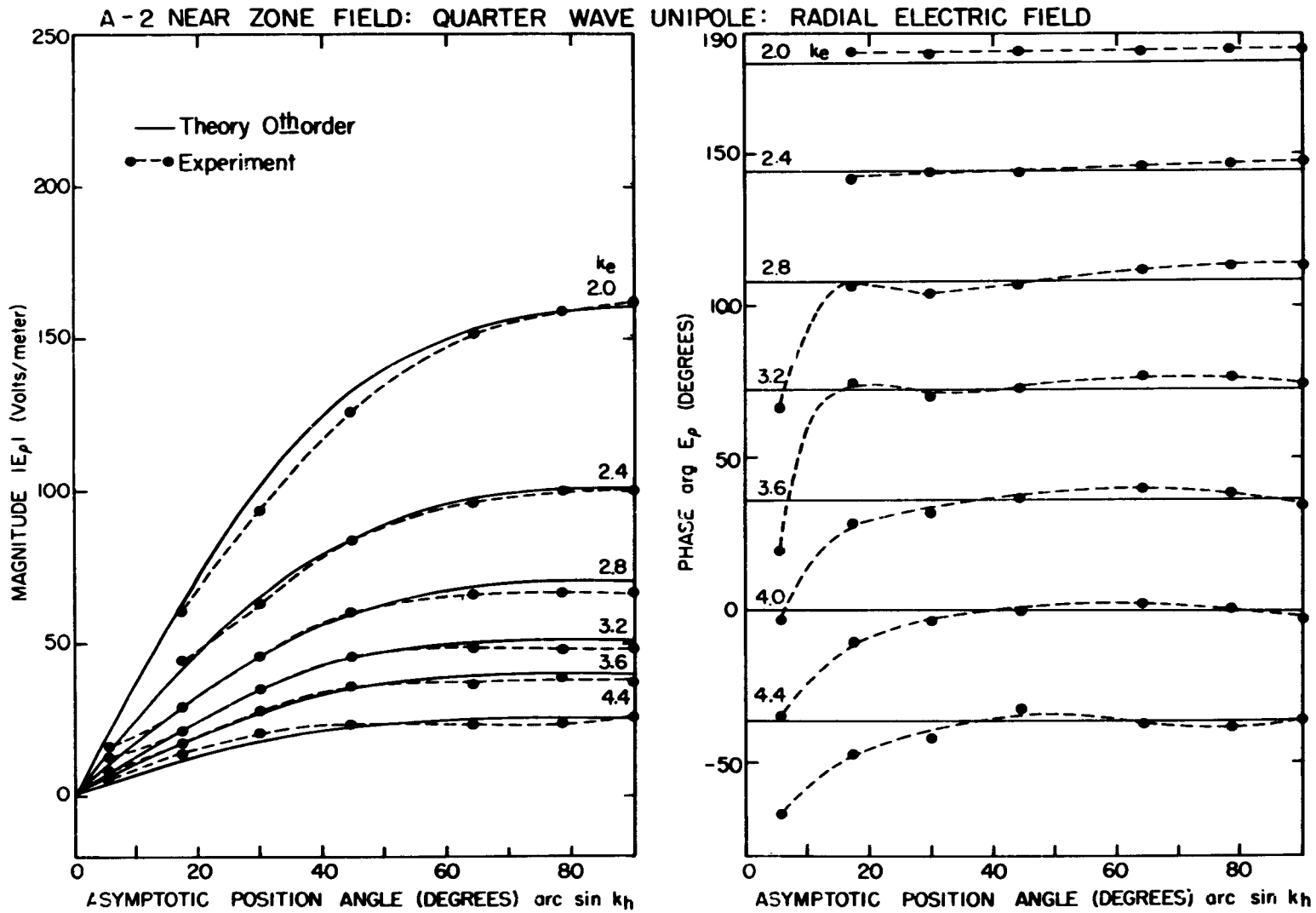
A-2 NEAR ZONE FIELD: QUARTER WAVE UNIPOLE: RADIAL ELECTRIC FIELD
Theory 0th order
Experiment
MAGNITUDE |Eρ| (Volts/meter)
PHASE arg Eρ (DEGREES)
ke
2.0
2.4
2.8
3.2
3.6
4.0
4.4
ASYMPTOTIC POSITION ANGLE (DEGREES) arc sin kh
ASYMPTOTIC POSITION ANGLE (DEGREES) arc sin kh

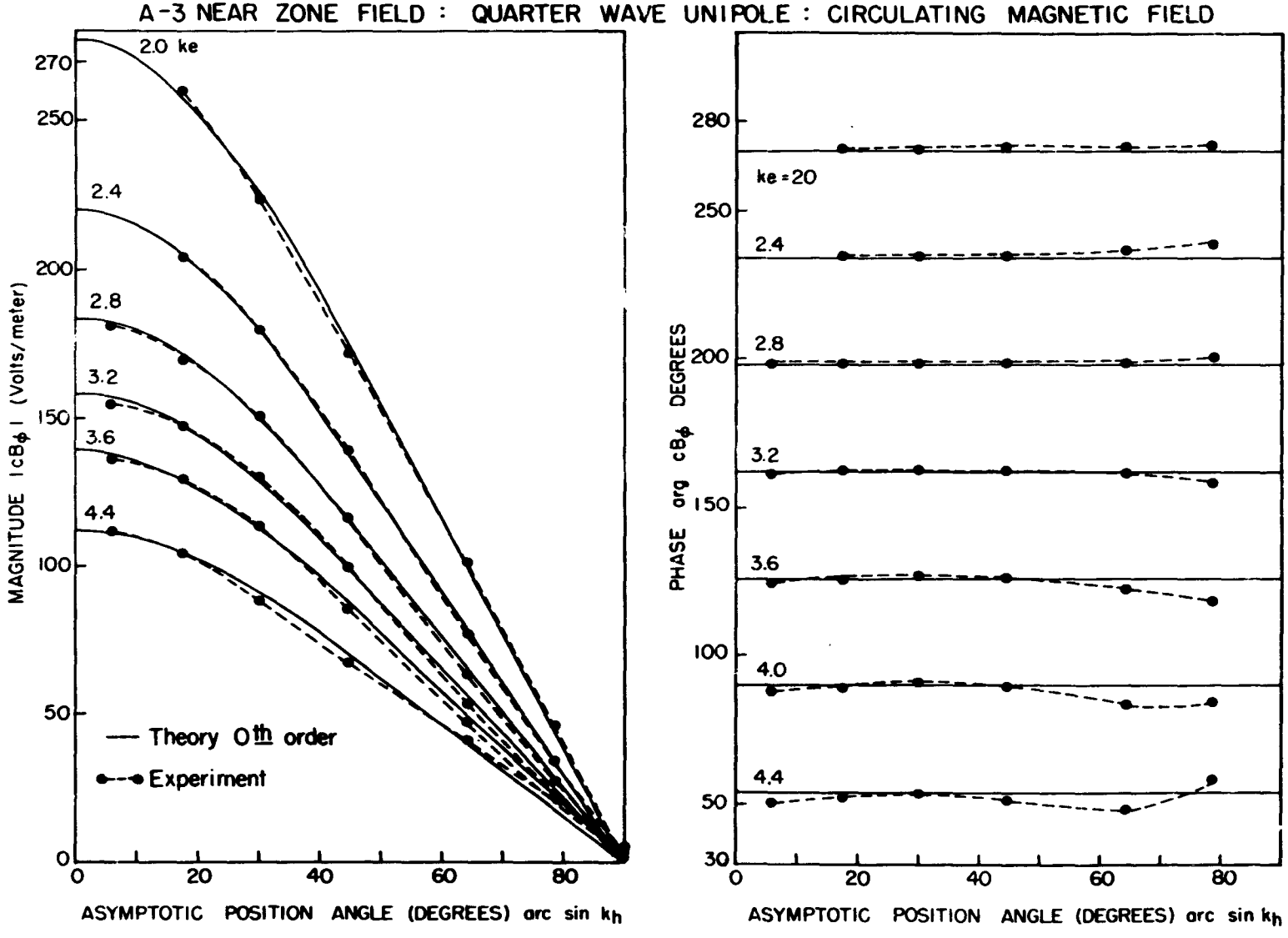
A-3 NEAR ZONE FIELD : QUARTER WAVE UNIPOLE : CIRCULATING MAGNETIC FIELD
MAGNITUDE |cBφ| (Volts/meter)
2.0 ke
2.4
2.8
3.2
3.6
4.4
Theory 0th order
Experiment
ASYMPTOTIC POSITION ANGLE (DEGREES) arc sin kh
PHASE arg cBφ DEGREES
ke=20
2.4
2.8
3.2
3.6
4.0
4.4
ASYMPTOTIC POSITION ANGLE (DEGREES) arc sin kh

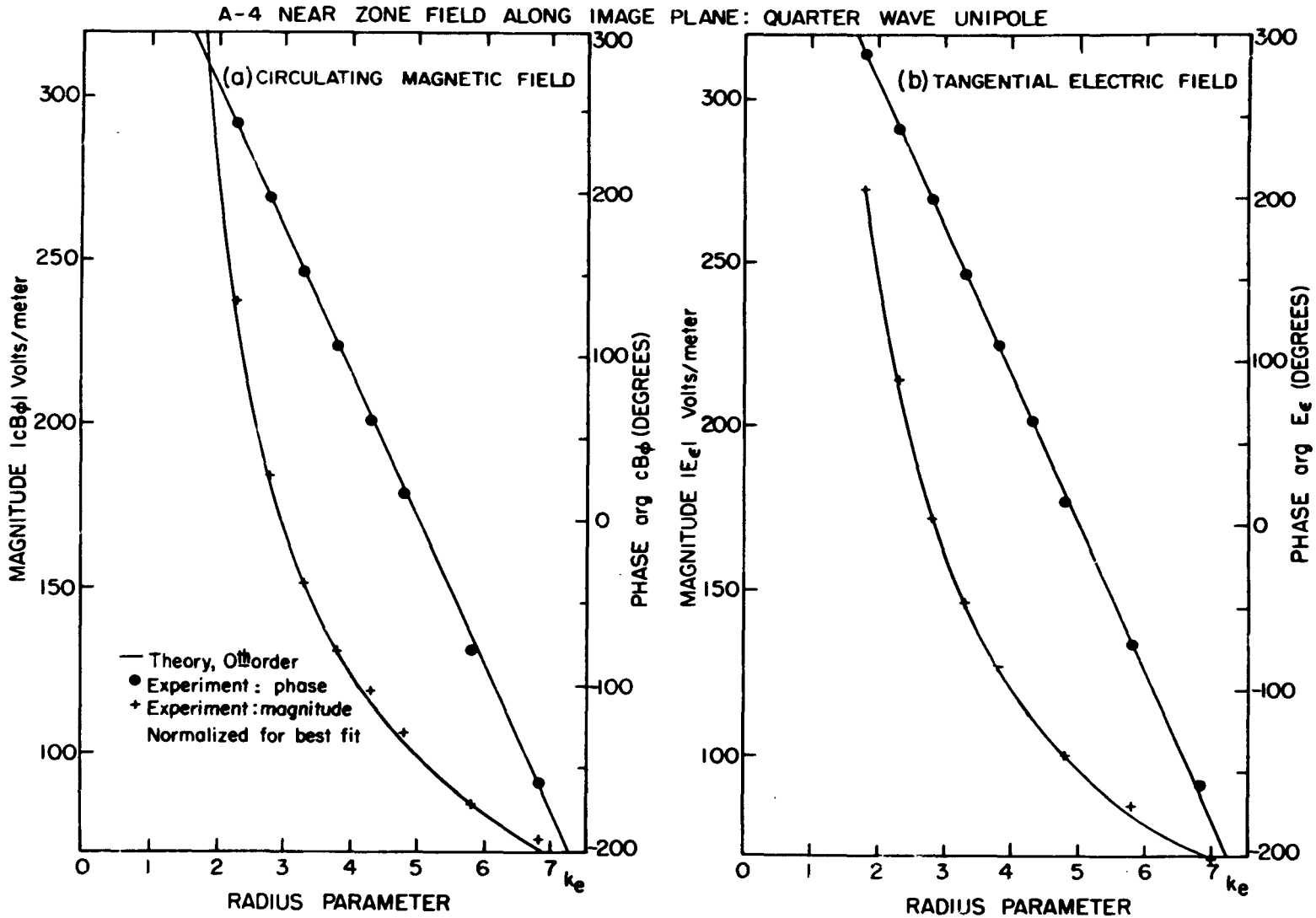
A-4 NEAR ZONE FIELD ALONG IMAGE PLANE: QUARTER WAVE UNIPOLE
(a) CIRCULATING MAGNETIC FIELD
(b) TANGENTIAL ELECTRIC FIELD
MAGNITUDE |cBφ| Volts/meter
PHASE arg cBφ (DEGREES)
MAGNITUDE |Eε| Volts/meter
PHASE arg Eε (DEGREES)
RADIUS PARAMETER
ke
Theory, 0th order
Experiment : phase
Experiment : magnitude
Normalized for best fit

Table A-1 Magnetic Field due to the Current on a Dipole

Position		Magnetic Field (cosinusoidal current)		Magnetic Field (measured current)	
		magnitude	phase	magnitude	phase
k_e	k_h	$\lvert c B_\phi \rvert$ (db)	arg $c B_\phi$ (degrees)	$\lvert c B_\phi \rvert$ (db)	arg $c B_\phi$ (degrees)
2.0	0	48.9	-90.1	49.7	-97.6
	0.5	47.1	-90.0	47.8	-97.3
	0.9	40.0	-90.0	41.1	-95.7
	0.98	32.8	-90.0	34.0	-95.3
	1.0	-	-	-	-
5.8	0	38.5	-72.0	39.2	-79.2

Magnitudes are in db referred to 1 volt/meter.

Phases are in degrees referred to the phase of the current at the base of the antenna.

Table A-2 Change in Magnetic Field due to a Change in Current

Position		Field Ratio: $\frac{c B_\phi \text{ (measured current)}}{c B_\phi \text{ (cosinusoidal current)}}$	
k_e	k_h	magnitude (db)	phase (degrees)
2.0	0	0.8	-7.5
	0.5	0.7	-7.3
	0.9	1.1	-5.7
	0.98	1.2	-5.3
	1.0	-	-
5.8	0	0.7	-7.2
	Average Values	0.9	-6.6

Activity Supply Officer
Building 2504, Charles Wood Area
Fort Monmouth, New Jersey (50)
Attn: Director of Research

Commanding Officer
Office of Naval Research
Navy 100, Box 39 (25)
Fleet Post Office
New York, New York

Armed Services
Technical Information Agency
Arlington Hall Station (10)
Arlington 12, Virginia
Attn: TIPDR

The Director
Naval Research Laboratory
Washington 25, D. C. (6)
Attn: Technical Information Office

Commander, AF CRL
AFRD, ARDC, CRRLC
Laurence G. Hanscom Field (6)
Bedford, Massachusetts
Attn: Electronics Research Directorate

Commanding General
Air Research and Development Command
P. O. Box 1395 (3)
Baltimore 3, Maryland
Attn: RDTRRP

Chief of Naval Research
Department of the Navy (2)
Washington 25, D. C.
Attn: Dr. A. Shostak, Code 427

Chief of Naval Research
Department of the Navy (2)
Washington 25, D. C.
Attn: Code 427

Commanding Officer
Office of Naval Research
495 Summer Street (2)
Boston, Massachusetts

Chief, Bureau of Ships
Department of the Navy (2)
Washington 25, D. C.
Attn: Code 810

Director, Air University
Library (2)
Maxwell Air Force Base
Alabama

Chief of Naval Research
Department of the Navy
Washington 25, D. C.
Attn: Code 421

Commanding Officer
Office of Naval Research
495 Summer Street
Boston, Massachusetts

Commanding Officer
Office of Naval Research
John Crerar Library Building
86 East Randolph Street
Chicago 1, Illinois

Commanding Officer
Office of Naval Research
346 Broadway
New York 13, New York

Commanding Officer
Office of Naval Research
1030 East Green Street
Pasadena, California

Commanding Officer
Office of Naval Research
1000 Geary Street
San Francisco 9, California

Head, Document Section
Technical Information Division
Naval Research Laboratory
Washington 25, D. C.

Martin A. Garstens
Magnetism Branch, Code 6450
Solid State Division
Naval Research Laboratory
Washington 25, D. C.

Commanding Officer
U. S. N. Air Development Center
Johnsville, Pennsylvania
Attn: NADC Library

Commander
U. S. N. Air Development Center
Johnsville, Pennsylvania
Attn: AAEL

Chief, Bureau of Aeronautics
Department of the Navy
Washington 25, D. C.
Attn: EI-1

Engineering Librarian
Convair
San Diego 12, California

Dr. John E. Pippin
Applied Physics and Ferrite Devices
Sperry Microwave Electronics Co
P. O. Box 1828
Clearwater, Florida

Engineering Library
Sperry Microwave Electronics Co
Clearwater, Florida

Dr. Tajee Ramal
Research Division
Raytheon Company
Waltham 54, Massachusetts

Elizabeth Weeks, Librarian
Raytheon Company
28 Seyon Street
Waltham 54, Massachusetts

Report Librarian
Sylvania Electric Products Inc
Electronic Systems Division
100 First Avenue
Waltham, Massachusetts

Document Control Center
Wayland Library
Raytheon Manufacturing Co
Wayland, Massachusetts

J. E. Goldman
Scientific Laboratory
Ford Motor Company
Engineering Staff
P. O. Box 2053
Dearborn, Michigan

Charles C. H. Tang
Bell Telephone Labs.
Murray Hill, New Jersey

Librarian
RCA Laboratories
Princeton, New Jersey

Dr. A. Arnold
RCA
Princeton, New Jersey

Commander (2)
U. S. Naval Electronics Lab.
San Diego, California

Commanding General, RCRW
Rome Air Development Center
Griffiss Air Force Base (2)
Rome, New York

Commanding General
Air Research and Development Command
P. O. Box 1395 (2)
Baltimore, Maryland
Attn: RDDDE

Commander
Air Force Cambridge Research Labs.
Laurence G. Hanscom Field (2)
Bedford, Massachusetts
Attn: CROTLS

Commander
Wright Air Development Center
Wright Patterson Air Force Base
Ohio (2)
Attn: WCLRA Library

National Security Agency
Physical Sciences Division (2)
Fort George Meade, Maryland
Attn: Dr. Alvin Meckler

Associate Prof. A. Kaprielian
Department of Electrical Engineering
University of Southern California
University Park
Los Angeles 7, California

Assistant Secretary of Defense
(Research and Development)
Research and Development Board
Department of Defense
Washington 25, D. C.

Chief of Naval Operations
Department of the Navy
Washington 25, D. C.
Attn: Op-30

Chief of Naval Operations
Department of the Navy
Washington 25, D. C.
Attn: Op-32

Chief of Naval Operations
Department of the Navy
Washington 25, D. C.
Attn: Op-413

Chief, Bureau of Aeronautics
Department of the Navy
Washington 25, D. C.
Attn: EL-4

Technical Library
U. S. Naval Proving Ground
Dahlgren, Virginia

Director
Naval Ordnance Laboratory
White Oak, Maryland

Librarian
U. S. Naval Post Graduate School
Monterey, California

Air Force Office of Scientific Research
Air Research and Development Command
Washington 25, D. C.
Attn: SRY, Physics Division

Commanding General
Rome Air Development Center
Griffiss Air Force Base
Rome, New York
Attn: RCREC-4C

Commanding General
Rome Air Development Center
Griffiss Air Force Base
Rome, New York
Attn: RCR

Commander
Air Force Cambridge Research Center
230 Albany Street
Cambridge 39, Massachusetts
Attn: CRZL

Commander
Air Force Cambridge Research Center
230 Albany Street
Cambridge 39, Massachusetts
Attn: CRZM

Commander
AF Cambridge Research Laboratories
Laurence G. Hanscom Field
Bedford, Massachusetts
Attn: Dr. Hollingsworth

Commander
Wright Air Development Center
Wright Patterson Air Force Base
Ohio Attn: WCRR

Sandia Corporation
Org. 1424, Sandia Base
Albuquerque, New Mexico
Attn: Dr. C. W. Harrison, Jr

Sandia Corporation
Sandia Base
Albuquerque, New Mexico
Attn: Library Division 1922-1

Mr. Robert Turner
General Electric Company
Advanced Electronics Center
Cornell University
Ithaca, New York

Library
Airborne Instruments Lab.
Walt Whitman Road
Melville, Long Island, New York

Secretary, Working Group
Semiconductor Devices
346 Broadway, 8th Floor
New York 13, New York
Attn: AGET

Metals Research Laboratories
Electro Metallurgical Company
Box 580, Niagara Falls, New York
Attn: Mr. R. J. Gladieux

Librarian
General Electric Research Lab
P. O. Box 1088
Schenectady, New York

Westinghouse Electric Corp
Research Laboratories
Beulah Road, Churchill Boro
Pittsburgh 35, Pennsylvania

Prof. O. E. H. Rydbeck
P. O. Box 266
Belmar, New Jersey

Dr. Melvin W. Aarons
811 East Genesee Street
Fayetteville, New York

Laboratory
Airborne Instruments
Mineola, New York

Commander
Wright Air Development Center
Wright Patterson Air Force Base
Ohio
Attn: WCRRH

Commandant
Air Force Institute of Technology
Wright Patterson Air Force Base
Ohio
Attn: MCLI Library

AF Special Weapons Center
Kirtland Air Force Base
Albuquerque, New Mexico
Attn: SWOI

Headquarters
AF Missile Test Center
MU-135, ARDC
Patrick Air Force Base
Florida

U. S. Coast Guard
1300 E Street, N. W.
Washington 25, D. C.
Attn: EEE

M. A. Krinsnich, Chief
Systems Component Branch
Electronic Warfare Division
Signal Corps Agency
White Sands Proving Ground
New Mexico

Mr. A. D. Bedrosian
Signal Corps Liaison Office
Mass. Institute of Technology
Building 26, Room 131
Cambridge 39, Massachusetts

Chief, European Office
ARDC Command
Shell Building
60 Rue Ravenstein
Brussels, Belgium

Dr. J. Anton Hofman
Ordnance Materials Res. Office
Watertown Arsenal
Watertown, Massachusetts

Acquisitions Officer
ASTIA Reference Center
Arlington Hall Station
Arlington 12, Virginia

Stanford Research Institute
Documents Center
Menlo Park, California
Attn: Mary Lou Fields

Dr. C. H. Papas
Dept. of Electrical Engineering
California Institute of Technology
Pasadena, California

Stanford Electronics Lab
Stanford University
Stanford, California
Attn: Document Library
Applied Electronics Lab.

Department of Electrical Engineering
Yale University
New Haven, Connecticut

Librarian
Johns Hopkins University
1315 St. Paul Street
Baltimore 2, Maryland

Radiation Laboratory
Johns Hopkins University
1315 St. Paul Street
Baltimore 2, Maryland

Director, Lincoln Laboratory
Mass. Institute of Technology
Bedford, Massachusetts

Mr. John Hewitt
Document Room
Research Lab. of Electronics
Mass. Institute of Technology
Cambridge 39, Massachusetts

Professor A. Von Hippel
Mass. Institute of Technology
Lab. for Insulation Research
Cambridge 39, Massachusetts

Library, Room A 229
Lincoln Laboratory
P. O. Box 73
Lexington 73, Massachusetts

K. M. Siegel, Head
Theory and Analysis Department
Willow Run Laboratories
University of Michigan
Willow Run Airport
Ypsilanti, Michigan

Librarian
National Bureau of Standards Library
Room 301, Northwest Building
Washington 25, D. C.

Librarian
U. S. Department of Commerce
National Bureau of Standards
Boulder, Colorado

Dr. Earl Callen
National Security Agency
Physical Sciences Division
Fort George Meade, Maryland

Dr. H. Campaigne
National Security Agency
Physical Sciences Division
Fort George Meade, Maryland

Cheng Kung University
Electrical Engineering Department
Tainan, Taiwan
Republic of China
Attn: Professor Chao-Hai Chou
Head, Eng. Department

Mr. D. S. Jones
Department of Mathematics
Univ. College of No. Staffordshire
Keele, Staffordshire, England

Professor Paul Ichel Mito
Osaka City University
Dept. of Engineering Sciences
12 Nishi Ogimachi Kitaku
Osaka, Japan

Donald C. Stinson
Dept. of Electrical Engr.
University of Arizona
Tucson 25, Arizona

Professor Jerome R. Singer
Div. of Electrical Engineering
University of California
Berkeley 4, California

Professor Charles Kittel
Department of Physics
University of California
Berkeley 4, California

Serials Library
Brandeis University
Waltham, Massachusetts

Professor H. G. Booker
School of Electrical Engineering
Cornell University
Ithaca, New York

Library, College of Engineering
University Heights Library
University Heights
New York University
New York 53, New York

E. A. Chapman, Librarian
Rensselaer Polytechnic Institute
Amos Eaton Hall
Troy, New York

Robert Plonsey
Department of Engineering
Case Institute of Technology
University Circle
Cleveland 6, Ohio

Dept. of Electrical Engineering
Case Institute of Technology
University Circle
Cleveland 6, Ohio
Attn: S. Seely, Head

Dr. C. J. Falkenbach
Battelle Memorial Institute
Columbus, Ohio
Attn: Electrical Engineering Division

Librarian
Engineering Library
Brown University
Providence, Rhode Island

Professor A. W. Straiton
Dept. of Electrical Engineering
University of Texas
Austin 12, Texas

Mr. William Way
Research Librarian
Tasker Instruments Corp.
1861 Cahuenga Boulevard
Hollywood 28, California

SOLID STATE ONLY

Martin A. Garstens, Head
Paramagnetic Section
Magnetism Branch
Solid State Division
Naval Research Laboratory
Washington 25, D. C.
Attn: Code 6451

Dr. Rosaler Descubes, Jr
Ordnance Materials
Research Laboratory
Watertown Arsenal
Watertown, Massachusetts

Mr. A. Saito
Himeji Technical College
Himeji, Japan

Electronics Research Laboratory
Division of Electrical Engineering
University of California
Berkeley 4, California
Attn: Librarian

Johns Hopkins University
34th and Charles Street
Whitehead Hall
Baltimore 18, Maryland
Attn: Mr. J. O. Artman

Librarian
Physics Department
Amherst College
Amherst, Massachusetts
Attn. Mr. Romer

Professor I. Lowe
Department of Physics
University of Minnesota
Minneapolis, Minnesota

Professor R. E. Norberg
Department of Physics
Washington University
St. Louis, Missouri

Microwave Research Institute
Polytechnic Institute of Brooklyn
55 Johnson Street
Brooklyn, New York
Attn: Librarian

Dr. Sidney Shapiro
Arthur D. Little, Inc.
15 Acorn Park
Cambridge 40, Massachusetts

Dr. Simon Foner
Lincoln Laboratory
Box 73
Lexington, Massachusetts

Mr. William H. [illegible]
Ewen Knight Corporation
206 A Street
Needham, Massachusetts

Dr. Edward U. C[illegible]
6604 Waterman Avenue
St. Louis, Missouri

Dr. W. M. Wal[illegible]
Bell Telephone Laboratories, Inc.
Murray Hill, New Jersey

Library
[illegible] Laboratories
[illegible] Street
New York 27, New York

ELECTROMAGNETIC RADIATION ONLY

Michigan State College
Department of Mathematics
East Lansing, Michigan

Microwave Research Institute
Polytechnic Institute of Brooklyn
55 Johnson Street
Brooklyn, New York

Mr. [illegible] R. [illegible], Jr.
Box [illegible] 14, [illegible] 2617
Hughes Research Laboratories
Culver City, California

Professor O. E. H. Rydbeck
P. O. Box 26
Belmar, New Jersey

One Copy Unless Otherwise Specified